DOCTORAL THESIS

# CFRP Strengthening of Cut-Out Openings in Concrete Walls – Analysis and Laboratory Tests

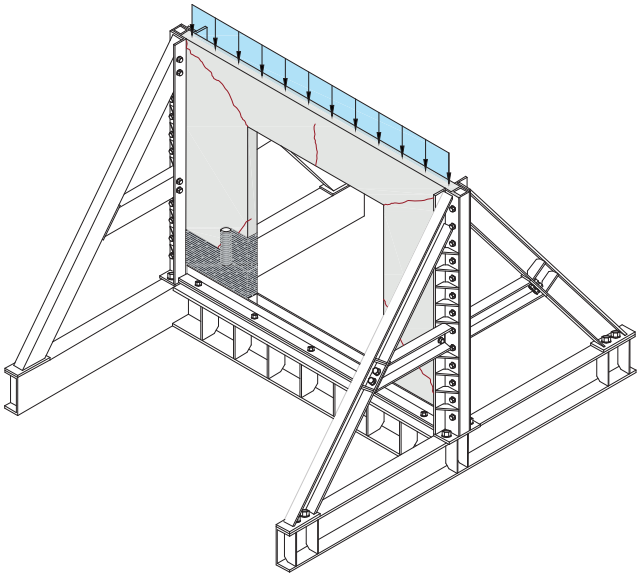

Cosmin Popescu

Structural Engineering

LULEÅ UNIVERSITY OF TECHNOLOGY

DOCTORAL THESIS

# CFRP Strengthening of Cut-Out Openings in Concrete Walls – Analysis and Laboratory Tests

**Cosmin Popescu**

Luleå University of Technology
Department of Civil, Environmental and Natural Resources Engineering
Division of Structural and Fire Engineering
SE-971 87 Luleå, Sweden
www.ltu.se

Front page: The illustration shows a pre-cracked concrete wall with an opening strengthened with CFRP sheets in the test rig ready to be tested under uniform axial loading.

Printed by Luleå University of Technology, Graphic Production 2017

ISSN 1402-1544
ISBN 978-91-7583-794-9 (print)
ISBN 978-91-7583-795-6 (pdf)

Luleå 2017

www.ltu.se

**Cosmin Popescu**
Division of Structural and Fire Engineering
Department of Civil, Environmental and Natural Resources Engineering
Luleå University of Technology

## Academic thesis

For the degree of Doctor of Philosophy (Ph.D.) in Structural Engineering, which by due permission of the Technical Faculty Board at Luleå University of Technology will be publicly defended in:

Room F1031, Luleå University of Technology,

Thursday, February 23rd, 2017, 10:00

| | |
|---|---|
| Opponent: | Professor **Stijn Matthys**, Magnel Laboratory for Concrete Research, Department of Structural Engineering, Ghent University, Ghent, Belgium |
| Examining Committee: | Professor **Karin Lundgren**, Division of Structural Engineering, Department of Civil and Environmental Engineering, Chalmers University of Technology, Gothenburg, Sweden |
| | Professor **Henrik Stang**, Section for Structural Engineering, Department of Civil Engineering, Technical University of Denmark, Lyngby, Denmark |
| | Professor **Mats Oldenburg**, Division of Mechanics of Solid Materials, Department of Engineering Sciences and Mathematics, Luleå University of Technology, Luleå, Sweden |
| Chairman, Principal supervisor | Professor **Björn Taljsten**, Division of Structural and Fire Engineering, Department of Civil, Environmental and Natural Resources Engineering, Luleå University of Technology, Luleå, Sweden |
| Assistant supervisor | Researcher, Ph.D. **Gabriel Sas**, Infrastructure, Materials, Structural Engineering, Northern Research Institute—NORUT, Narvik, Norway<br>Division of Structural and Fire Engineering, Department of Civil, Environmental and Natural Resources Engineering, Luleå University of Technology, Luleå, Sweden |
| | Assoc. Professor **Thomas Blanksvärd**, Skanska Sverige AB, Teknik<br>Division of Structural and Fire Engineering, Department of Civil, Environmental and Natural Resources Engineering, Luleå University of Technology, Luleå, Sweden |

## PREFACE

This PhD programme was jointly managed under a cooperative agreement between the Northern Research Institute – Norut Narvik – and Luleå University of Technology (LTU).

Many people have contributed to this thesis, the research it is based upon, and my professional development. First and foremost, I would like to thank the supervisory team from LTU and Norut Narvik consisting of my main supervisor Prof. Björn Täljsten, and assistant supervisors Dr. Gabriel Sas and Assoc. Prof. Thomas Blanksvärd, who gave me the freedom to explore while always guiding me. Dr. Gabriel Sas provided me with valuable advice and fruitful discussions almost every day. His constant enthusiasm, encouragement and optimism have always motivated me. Dr. Thomas Blanksvärd is acknowledged for his support throughout my studies and for critically reviewing my work. Besides scientific guidance, Prof. Björn Taljsten is a visionary who taught me valuable lessons about project management and thinking ahead. Once again I am deeply grateful for your assistance and suggestions throughout my studies.

I would also like to express thanks to those who provided help during this research programme. Special thanks are due to the technicians at CompLab, the structural engineering laboratory at LTU, Dr. Dan Diaconu from Politehnica University Timisoara for the help provided with the strengthening work and PhD student Cristian Sabău and Dr. Mohammed Salih from LTU for providing help with optical measurements. During the last year of my PhD studies, I had the opportunity of spending three excellent months at Technical University of Denmark (DTU). I need to express my gratitude to Assoc. Prof. Jacob W. Schmidt and Prof. Per Goltermann, both from DTU, who made my stay there pleasant and fruitful.

My first steps into the research started at Politehnica University of Timisoara under the supervision of Prof. Valeriu Stoian, to whom I am eternally grateful. My former colleagues and dear friends from the same university, Dr. Tamás Nagy-György, Dr. Sorin-Codruț Floruț, and Dr. Cosmin Dăescu are also acknowledged for the fruitful collaboration we had during my PhD studies. I look forward to our continued collaboration.

A big thank you to my colleagues at the Division of Structural and Fire Engineering at LTU is also due for making the working days enjoyable. Special thanks to Tech. Lic. Niklas Bagge, Tech.Lic. Jens Häggström, PhD student Cristian Sabău and Dr. Jonny Nilimaa for all the time we spent together. All my colleagues from Norut Narvik are appreciated for kind hospitality during my visits. My appreciation also extends to MSc. Bård Arnsten from Norut Narvik for all the support I received. The administrative support received from Ms. Carina Hannu from LTU is greatly appreciated; her kindness and continuous encouragement to improve my Swedish skills have always motivated me.

I gratefully acknowledge the funding sources that made my Ph.D. studies possible. In particular, The Research Council of Norway (RFF), Development Fund of the Swedish Construction Industry (SBUF) and Skanska for largely financing the presented work. Other financial contributions from LTU, Norut Narvik, Elsa and Sven Thysells' Foundation, Nordea Bank, Wallenberg

Foundation, Åforsk Foundation and the Norwegian Concrete Association (Norsk Betongforening) are also gratefully acknowledged as they offered me the opportunity to present my research work at international conferences.

Above all I would like to thank my family: my wife Adriana for her love, endless support and encouragement and my son Albert for giving me the strength to finalise this work.You are the force behind me always pushing me forward.

Cosmin Popescu
Luleå, February 2017

**SUMMARY**

Redesigning buildings to improve their space efficiency and allow changes in use is often essential during their service lives to comply with shifts in living standards and functional demands. This may require the introduction of new openings in elements such as beams, walls, and slabs, which inevitably reduces their structural performance and hence requires repair or strengthening. However, there are uncertainties regarding both the effects of openings and the best remedial options for them. Traditionally, two methods have been used to strengthen reinforced concrete (RC) walls with openings, these being either to create a frame around the opening using RC/steel members or to increase the cross-sectional thickness. Currently, intervention in existing buildings must be minimal in order to minimise inconvenience caused by limiting the use of the structure during repairs. One option is to use externally-bonded fibre-reinforced polymers (FRPs).

In this study, the author reports on an experimental investigation of the effectiveness of carbon FRP (CFRP)–based strengthening for restoring the axial capacity of a solid reinforced concrete wall after cutting openings. Nine half-scale specimens, designed to represent typical wall panels in residential buildings with and without door-type openings, were tested to failure. The walls were tested in two-way action and subjected to axial loading with low eccentricity (defined as one sixth of the wall's thickness) along the weak axis to represent imperfections due to thickness variation and misalignment of the panels during the construction process. An extensive instrumentation scheme was used to monitor the specimen's behaviour during the loading cycles. In addition to classical approaches for measuring strains and displacements, optical 3D measurements were also acquired using the digital image correlation (DIC) technique. These provided better overviews of the failure mechanism by recording the crack pattern development and deformation of the walls throughout the loading history.

Reducing the cross-sectional area by cutting out openings i.e. 25% (hereafter referred to as small opening) and 50% (hereafter referred to as large opening) led to 36% and 50% reductions in peak loads, respectively. In both situations the failure was brittle due to crushing of concrete with spalling and reinforcement buckling. The CFRP strengthening increased the axial capacity of walls with small and large openings by 34 – 50% and 13 – 27%, respectively. This partially restored their capacities to 85 – 95% and 57 – 63% of their precutting capacity (i.e. solid wall), respectively. A procedure based on a rigid-plastic approach for evaluating the ultimate load of walls with cut-out openings that have been strengthened with FRPs was also proposed in this study. Predictions made using the proposed method agree closely with experimental results.

**Keywords**: Strengthening, Fibre-reinforced polymers, Concrete walls, Openings, Axial load, Eccentricity, Two-Way

**SAMMANFATTNING** (summary in Swedish)

Ombyggnation av byggnader är väsentligt för att förbättra platseffektivitet och möjliggöra förändringar under dess brukstid för att till exempel uppfylla ändrade levnadsstandarder och funktionskrav. Detta kan innebära att nya behov uppstår, exempelvis nya öppningar i element såsom balkar, väggar och plattor. Den här typen av åtgärder innebär oundvikligen att den strukturella prestanda reduceras och följaktligen erfordras reparation och förstärkning. Däremot förekommer osäkerheter med avseende på inverkan av öppningar samt vilken åtgärd som är bäst lämpad. Traditionellt sett har två metoder använts för att förstärka armerade betongväggar med öppningar, antingen genom att skapa en ram av armerade betongelement, alternativt stålelement, runt öppningen eller genom att öka tvärsnittets tjocklek. Ingripanden i befintliga byggnader bör vara minimal för att reducera olägenheter som orsakas av begränsad tillgång till konstruktionen i samband med reparation. En alternativ metod är att använda externt applicerade fiberarmerade polymerer.

I denna studie rapporterar författaren en experimentell undersökning om i vilken omfattning den axiella kapaciteten kan återskapas hos en armerad betongvägg efter håltagning/öppning genom förstärkning baserat på kolfiberarmerade polymerer. Nio väggmodeller, i halvskala, belastades till brott. Dessa var utformade med åtanke att representera typiska väggelement i bostadshus med respektive utan dörrliknande öppningar. Väggarna provades dubbelspända och utsattes för en belastning med liten excentricitet (definierad som en sjättedel av väggtjockleken) längs den veka axeln för att motsvara imperfektioner på grund av t ex felplacering av element i byggskedet. Ett omfattande mätprogram utformades för att övervaka väggmodellens beteende under lastcyklerna. Utöver klassiska tillvägagångssätt för mätning av töjningar och förskjutningar användes optiska 3D mätningar baserat på digital bildkorrelationsteknik. Dessa tillhandahöll bättre information av brottmekanismen genom att sprickbildningen och deformationer registrerades över ett större område under hela belastningsförfarandet.

Håltagningen motsvarande en reduktion med 25% (härefter benämnd som liten öppning) och 50% (härefter benämnd som stor öppning) av tvärsnittsarean. Dessa areareduktioner ledde till 36% respektive 50% minskning i maximal last. I båda fallen inträffade ett sprött bott på grund av krossning av betong samt spjälkning och buckling av armering. Kolfiberförstärkningen ökade den axiella kapaciteten med 34 – 50% för väggar med liten öppning och 13 – 27% för väggar med stor öppning, vilket innebär att 85 – 95% respektive 57 – 63% av den ursprungliga kapaciteten återskapades (d.v.s. kapacitet för solid vägg utan håltagning). I denna studie förslogs även en metod baserat på plasticitetsteori för att utvärdera bärförmågan hos väggar med uttagna öppningar som har förstärkts med fiberarmerade polymerer. Beräkningar baserad på den förslagna metoden påvisar god överrensstämmelse med de experimentella resultaten.

**Nyckelord**: Förstärkning, Fiberarmerade polymerer, Betongväggar, Öppningar, Axiallast, Excentricitet, dubbelspänd

**SAMMENDRAG** (summary in Norwegian)

For å imøtekomme endrede brukskrav vil det ofte være behov for å endre planløsninger gjennom levetiden til bygninger. Dette kan bety innføring av nye åpninger (hulltagning) i bygningselementer som bjelker, vegger og plater. Hulltagning betyr uunngåelig nok at den konstruksjonsmkaniske kapasiteten reduseres, og som et resultat kreves reparasjon eller forsterkning. Det er imidlertid usikkerhet knyttet til virkningene av hulltagning, og hvordan man skal gjennomføre kompenserende tiltak. Tradisjonelt benyttes to fremgangsmåter for å forsterke armerte betongvegger med hulltagning; det etableres en ramme ved hjelp av armert betong eller stål rundt åpningen. Alternativet er tradisjonelt å øke veggens tverrsnitt. Begge metoder innebærer redusert utnyttelse av bygning under gjennomføring, noe som er med på å redusere ombyningen. En alternativ mulighet er å benytte eksternt pålimte fiberarmerte polymerer (FRPs).

I avhandlingen presenterer forfatteren resultater fra eksperimentelle forsøk hvor effekten av å anvende eksternt pålimte karbonfiberarmerte polymerer (CFRP) for å gjenopprette den aksiale kapasiteten til en armert betongvegg som det er tatt hull i undersøkes. Ni prøver i halv skal, designet for å representere typiske veggskiver i boliger med og uten dør-type åpninger, ble testet til brudd. Veggene ble utsatt for aksiell belastning med lav eksentrisitet (definert som en sjettedel av veggens tykkelse) langs den svake aksen. Dette for å simulere ujevnheter på grunn av variasjoner i tykkelse og forskyvning av platene under byggeprosessen. Omfattende instrumentering ble brukt til å overvåke skivenes oppførsel under de ulike lastsyklene. I tillegg til klassiske metoder for måling av spenninger og deformasjoner, ble også optisk 3D-målinger ved hjelp av digitale bildekorrelasjon (DIC) anvendt. Disse målingene gir bedre oversikt over bruddmekanismen gjennom at man kan følge utvikling av riss og deformasjoner gjennom hele forsøket.

Ved å skjære ut åpninger på ble tverrsnittsarealet redusert med 25% (heretter kalt liten åpning) og 50% (heretter kalt stor åpning). Dette førte til henholdsvis 36% og 50% reduksjon i kapasitet for veggene. For begge tilfeller ble det registrert sprøbrudd på grunn av knusing av betong og avskalling og knekking av armering. Forsterking med CFRP økte den aksiale kapasitet til veggene med store og små åpninger med 34 - 50% og 13-27%, respektivt. Dette gjenopprettet delvis deres kapasitet dvs henholdsvis 85 - 95%, og 57-63% av opprinnelige kapasitet.

Som en del av studien ble det også foreslått en metode som kan anvendes for å beregne kapasiteten til vegger hvor det er skjært ut åpninger og gjennomført påfølgende forsterkning med FRPs. Metoden som er basert på plastisitetsteori gir svært godt samsvar med eksperimentelle resultater.

**Nøkkelord**: Forsterkning, Fiberarmerte polymerer, betongvegger, åpninger, aksial belastning, eksentrisitet, Toveis

## TABLE OF CONTENTS

## NOTATION AND SYMBOLS

**Roman letters**

| | | |
|---|---|---|
| $A_c$ | cross-sectional area of concrete | [mm$^2$] |
| $A_e$ | effective confinement area | [mm$^2$] |
| $A_g$ | the gross area of the column section with rounded corners | [mm$^2$] |
| $D'$ | diameter of equivalent circular column | [mm] |
| $E_d$ | energy dissipation | [kNm] |
| $H$ | height of the wall | [mm] |
| $H_{eff}$ | effective height of the wall | [mm] |
| $N_{I\text{-}C}$ | failure load of the solid wall | [kN] |
| $L$ | length of the wall | [mm] |
| $L_{pier}$ | length of the wall pier | [mm] |
| $N_{exp}$, $N_u$ | experimental/predicted ultimate load for walls under axial loading | [kN] |
| $R$ | corner radius | [mm] |
| $S_{exp}$, $S_u$ | experimental/predicted ultimate load for slabs under transverse loading per unit area | [kN/m$^2$] |
| $b$ | width of the vertical strip cross-section | [mm] |
| $e$ | test eccentricity | [mm] |
| $e_a$ | additional eccentricity | [mm] |
| $f_c$ | compressive strength of unconfined concrete | [N/mm$^2$] |
| $f_{cc}$ | compressive strength of confined concrete | [N/mm$^2$] |
| $f_{ct}$ | tensile strength of concrete | [N/mm$^2$] |
| $f_{frp}$ | tensile strength of a FRP jacket | [N/mm$^2$] |
| $f_l$ | confining pressure | [N/mm$^2$] |
| $f_y$ | yield strength of reinforcement | [N/mm$^2$] |
| $h$ | height of the vertical strip cross-section | [mm] |
| $k_1$ | confinement effectiveness coefficient | [-] |
| $k_{s1}$ | shape factor for strength enhancement | [-] |
| $l$ | length of the yield line | [mm] |
| $m_b$ | moment resistance per unit length of the yield line | [kNm/m] |
| $m_c$ | membrane moment | [kNm/m] |
| $m_x$, $m_y$ | moment capacities per unit width in the x and y directions, respectively | [kNm/m] |
| $n_{ux}$, $n_{uy}$ | uniform in-plane compressive force per unit length applied in the x and y direction, respectively | [kN/m] |
| $t$ | wall thickness | [mm] |
| $t_{frp}$ | thickness of a FRP jacket | [mm] |

**Greek letters**

| | | |
|---|---|---|
| $\alpha$ | yield line's inclination relative to the reinforcement | [°] |
| $\beta$ | effective height factor | [-] |
| $\delta$ | virtual displacement | [-] |
| $\delta_1$, $\delta_2$ | out-of-plane displacements at indicated positions | [mm] |
| $\delta_{peak}$ | out-of-plane displacements at peak load | [mm] |
| $\varepsilon_c$ | strain in concrete | [mm/m] |
| $\varepsilon_f$ | strain in fibre-reinforced polymers | [mm/m] |
| $\varepsilon_s$ | strain in steel reinforcement | [mm/m] |
| $\mu_\Delta$ | ductility factor | [-] |

| | | |
|---|---|---|
| $\nu_1$, $\nu_2$ | effectiveness factor | [-] |
| $\theta$ | angle of disc rotation | [°] |
| $\rho_{sc}$ | cross-sectional area ratio of longitudinal steel | [-] |
| $\sigma_c$ | stress in concrete | [N/mm$^2$] |
| $\sigma_f$ | stress in fibre-reinforced polymers | [N/mm$^2$] |
| $\sigma_s$ | stress in steel reinforcement | [N/mm$^2$] |
| $\Phi$ | factor taking into account eccentricity, including second order effects and normal effects of creep | [-] |

**Abbreviations**

| | |
|---|---|
| RC | Reinforced Concrete |
| FRP | Fibre-Reinforced Polymers |
| CFRP | Carbon Fibre-Reinforced Polymers |
| GFRP | Glass Fibre-Reinforced Polymers |
| AFRP | Aramid Fibre-Reinforced Polymers |
| BFRP | Basalt Fibre-Reinforced Polymers |
| FE | Finite Element |
| DoE | Design of Experiments |
| OW | One-Way |
| TW | Two-Way |
| DAT | Design Assisted by Testing |
| DIC | Digital Image Correlation |
| 3D-DIC | Three-Dimensional Digital Image Correlation |

# Chapter 1

# Introduction

## 1.1 Background

At present, one of the most significant discussion points relating to sustainable development of our society is that such development must always be supported by a safe, functional and durable built environment. It is widely acknowledged that our building stock requirements (e.g. maintenance) are enormous, due to the ever-increasing demands of society, with continual wear and degradation on structures potentially leading to large monetary and social losses. For example, the need for repair and refurbishment in the housebuilding sector increases annually (FIEC 2014); figures indicate an estimated 270 billion Euros were spent in 2014 in the E.U., of which more than 6.9 billion Euros were spent in Sweden (see Table 1.1). Many civil infrastructure facilities (e.g. buildings, bridges, tunnels) operate in harsh environmental conditions, and are thus susceptible to ageing. This challenge have prompted numerous research programmes that address the following problems: material degradation models (Vu and Stewart 2000, Hanjari et al. 2011), repair and upgrading methods (Silfwerbrand 2010, Puurula et al. 2015), life-cycle cost solutions (Frangopol and Liu 2007, Safi et al. 2015) and maintaining the desired levels of reliability (Schlune et al. 2012, Plos et al. 2016).

The abovementioned studies were focused *in toto* on improving our understanding of how the existing structures behave over the long term. Hence, improved assessment procedures and new strengthening methods have been proposed as a result of intense research over the last few decades. The focus was, however, on infrastructure (e.g. bridges) as that is subjected to arguably more intense load effects and harsh environmental exposure than residential buildings, and the burden on society is somewhat more evident. However, the global population is continuously growing and so new structures are being built while existing ones still need to be used.

**Table 1.1** Investment trends in rehabilitation and maintenance in Europe (FIEC 2014)

| Country | Mln. € fixed prices | Percent variation of production in real terms on previous year | | | | |
|---|---|---|---|---|---|---|
| | **2013** | **2010** | **2011** | **2012** | **2013** | **2014** |
| Sweden | 6931 | 18.0 | -2.2 | -3.3 | -1.3 | 1.4 |
| Norway | 3763 | 2.1 | 1.9 | 5.1 | 3.1 | 3.0 |
| Denmark | 3995 | 0.2 | 13.2 | -1.4 | -2.2 | 3.5 |
| Finland | 5441 | 5.7 | 3.0 | 3.1 | 3.0 | 3.0 |
| European Union | 266201 | 2.1 | 1.2 | 2.1 | -0.1 | 1.9 |

The majority of structures around the world are made of reinforced concrete (RC), most of which were built between 1946 and 1980 (Dol and Haffner 2010). A high proportion of these buildings are multi-dwelling buildings made of prefabricated sandwich panels. The system, called large panel building, was developed in the West and used for the first time in Denmark, England and France (Csoknyai et al. 2016), later expanding across the whole of Europe. The block of flats shown in Fig. 1.1a consists of large panels and is "an important, almost iconic, common element of the building stock in Eastern Europe" (Csoknyai et al. 2016). For example, in Slovakia, Poland and Estonia, such buildings represent 40%, 49% and 45% of the residential building stock, respectively (Csoknyai et al. 2016). In Sweden, this type of building can be divided into three main subgroups as seen in Fig. 1.1b – d, with the most widely used type consisting of load-bearing cross-walls (Fig. 1.1b) (Eriksson 1978).

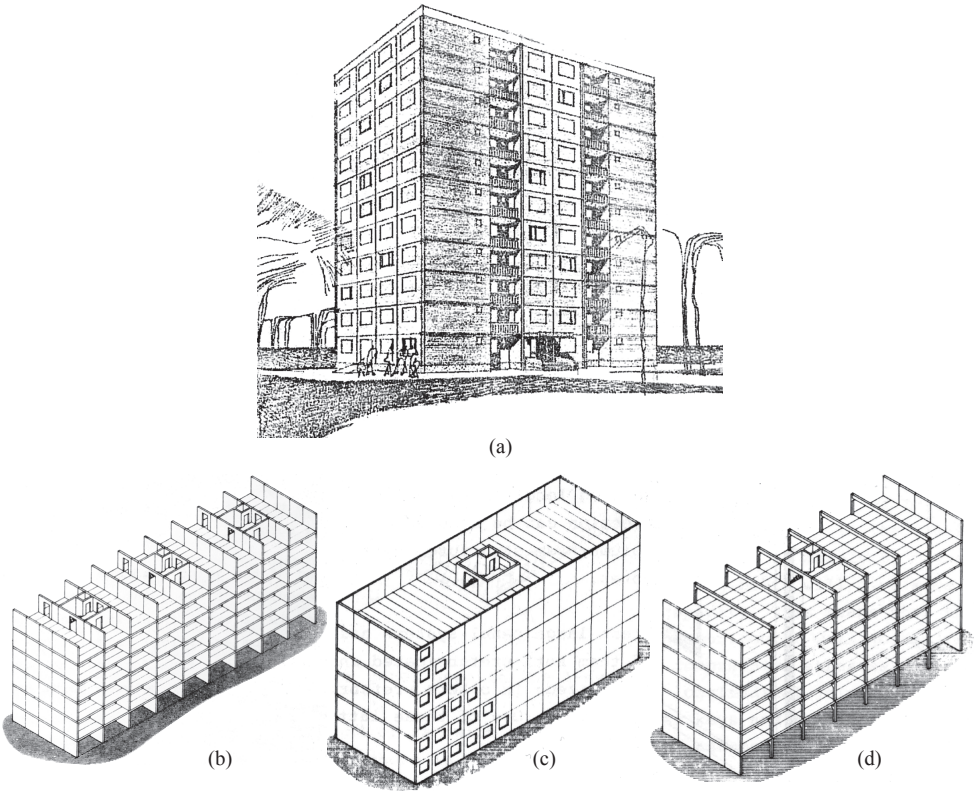


**Figure 1.1** Typical large panel buildings: (a) Perspective view of a large panel building in Romania (ISART 1973); (b – d) large panel buildings in Sweden (Eriksson 1978) with (b) load-bearing cross-walls; (c) load-bearing longitudinal walls, gable walls and a core

The structure of these buildings consists of an integral wall system in which load-bearing walls run along both longitudinal and transversal directions of the building. Structural simplicity is usually achieved by a regular floor layout which runs from the foundation to the top of the building. Such simplification has some disadvantages, in the sense that partitioning becomes more rigid and available spaces are small. Studies have shown an upward trend in the average size of homes over the last 20 years (Econometrica Inc. 2007). While these needs can safely be accommodated by architects/engineers for newly-designed buildings, not much can be done for old buildings where the available useful space is rather small. Of course, in such cases the available space cannot be enlarged but, in recent years, there has been a growing interest in enlarging spaces by connecting adjacent rooms using openings created in existing solid walls. Thus, greater flexibility and better use of spaces can be achieved.

As previously stated, improving the space efficiency and flexibility of buildings by redesigning them is often essential. Such modifications may well involve cutting openings into structural walls to allow for new windows, doors or ventilation systems. In an existing RC building, the addition of new openings (introduced to meet the requirements mentioned above) should be avoided whenever possible, in order to reduce unfavourable effects due to discontinuous regions. This is because the special structural detailing around openings (a strict requirement found in all design codes) cannot be fulfilled when openings have to be introduced in structures that have already been built. Consequently, such openings can reduce the stiffness and load-bearing capacity of a structure, in proportion to their size. Hence, this action usually requires repair or strengthening work.

Two methods have, traditionally, been employed to strengthen RC walls with openings. One is to create a frame using RC/steel members around the opening (Engel n.d.), the other is to increase the cross-sectional thickness (Delatte 2009). Currently, work to existing structures must be minimised in order to reduce inconvenience to those users of the building. One option is to use externally-bonded fibre-reinforced polymers (FRPs), a technique successfully tested by a number of authors in seismic retrofitting scenarios (Demeter 2011, Li et al. 2013, Mosallam and Nasr 2016, Todut et al. 2015). As the contexts of these tests were seismic retrofits, the strengthening schemes they used may not be appropriate for repairing gravitationally-loaded walls, and more research into their effects on the responses of elements to vertically applied loads is necessary. Cases where the gravitational load governs the design are usually structures built in non-seismic regions and are, therefore, the focus of this study.

## 1.2 Hypothesis, aim and research questions

Hypothesis: Strengthening axially-loaded concrete walls with cut-out openings using carbon-FRP (CFRP) enhances their structural performance i.e. axial strength, stiffness and energy dissipation.

Aim: To develop a system for strengthening concrete walls with newly created openings using CFRP materials. The three immediate objectives were:

a) Assess the current research level carried out worldwide on concrete walls with and without openings;

b) Experimental investigation of the structural behaviour of RC walls with cut-out openings and the contribution from the CFRP-based strengthening solution;

c) Derive a theoretical model for estimating the capacity of CFRP-strengthened RC walls with openings.

Research questions: In order to comply with the aims of this research project, the following research questions are stated:

I. Do existing models accurately predict the ultimate capacity of axially-loaded concrete walls with and without openings?

II. What are the effects when cut-out openings are introduced into solid walls?

III. Does the failure mechanism of a concrete wall with an opening change after strengthening with CFRP?

IV. Is it possible to adapt the rigid-plastic approach in order to devise a new model for RC walls strengthened using CFRPs?

### 1.3 Scientific approach

The research was carried out by following the conventional methodological approach in order to accomplish the research objectives. The process started with a critical literature review of the existing knowledge of concrete walls with and without openings, with an emphasis on the latter. The study indicated areas where further testing is required in order to enhance the reliability of current design models. Moreover, research questions were formulated in accordance with the research gaps identified in the literature.

Previous experience from experimental tests was used to calibrate a finite element (FE) model used for finding important information such as crack development, strain/stress patterns for steel reinforcement and concrete, deformation behaviour, failure mode and ultimate capacity. The information gathered was used to answer the question: *What needs to be measured in order to obtain reliable data that would form the basis of answering the research questions?* The instrumentation design was the first important outcome from this investigation. The second outcome was the design of a test rig able to reproduce the as-built boundary conditions and to facilitate the desired loading regime. The third outcome was to design a reliable test matrix using the design of experiments (DoE) technique (Box et al. 1978).

Existing design methods found in the research literature were used to analyse the effects of cut-out openings and to design the strengthening system. The results obtained were then verified using laboratory experiments. However, the theoretical work had to be revisited because of the findings from experimental tests and a new design strategy was proposed.

## 1.4 Limitations

The literature study considered the performance of design models found in scientific articles published from 1990 onwards and indexed in databases such as Scopus and Web of Science. Therefore, it is possible that some reported research may have been unintentionally overlooked.

The experimental study involved short-term tests and newly cast specimens, therefore the results may not be fully representative for walls in existing structures, which are always subject to heavy sustained loads and effects of degradation due to aging.

In an attempt to carry out all the strengthening work at once, the pre-cracked specimens (pre-cracking being a test variable) were removed from the test-rig, thus, the cracks formed were nearly closed before strengthening was applied.

Indeed, some choices made by the author such as the number of specimens, degree of eccentricity, the aspect and slenderness ratios, boundary conditions or the loading protocol, may all be regarded as limitations. However, these choices were imposed by the study proposal and, more obviously, financial considerations.

## 1.5 Outline of the thesis

This thesis is article-based, in which printed or reprinted journal articles are appended to an overall summary of their content. This summary consists of *Chapters 1 – 5*, briefly described below:

*Chapter 1* sets out the general research focus and the aim and research questions are described. It also introduces the appended papers and their original contributions.

*Chapter 2* summarises previous work related to the research subject. Key paper: *Paper I*

*Chapter 3* defines the research design and presents an overview of the laboratory-based experimental programme and analysis of the results. Key papers: *Papers II* and *III*

*Chapter 4* introduces the rigid-plastic approach and the assumptions made for the current research in order to provide an alternative design method. Key paper: *Papers IV* and *V*

*Chapter 5* presents the conclusions based on findings related to the aim of the research and answers the research questions. In addition, future research areas are also identified and discussed.

## 1.6 Appended papers

The core of this thesis incorporates five journal papers. For a better understanding, the reader is referred to these publications summarised below.

### PAPER I

**Popescu, C.**, Sas, G., Blanksvärd, T., & Täljsten, B. (2015). "Concrete walls weakened by openings as compression members: A review." *Engineering Structures, 89*, 172-190.

Paper I is a review of the advances that have been made in the design of concrete walls, both with and without openings, subjected to eccentric axial loads. A statistical analysis of available models from design codes and research studies from around the world was carried out using a database covering 253 tests.

*My contribution was gathering all the previous test results and building the database. Furthermore, I analysed all the design models included in the paper, formulated the conclusions and wrote the manuscript.*

### PAPER II

**Popescu, C.**, Sas, G., Sabău, C., & Blanksvärd, T. (2016). "Effect of cut-out openings on the axial strength of concrete walls." *Journal of Structural Engineering*, 142(11), 04016100.

In Paper II, the experimental results of tests on unstrengthened walls with and without openings are presented. The effect of the cut-out openings on the axial strength of concrete walls is evaluated in terms of ultimate capacity, failure mechanism, ductility and energy release at failure. The results were also used to assess the accuracy of the most reliable design models found in *Paper I*.

*My contributions were the design of the experiments including the test set-up design, carrying out the experiments and analyses, drawing conclusions and finally writing the manuscript.*

### PAPER III

**Popescu, C.**, Sas, G., Blanksvärd, T., & Täljsten, B. (2016). "Concrete walls with cutout openings strengthened by FRP confinement." *Journal of Composites for Construction,* 04016106

In Paper III, the investigation into the effectiveness of CFRP confinement to increase the axial strength of concrete walls damaged by cut-out openings is described. Comparisons were made between unstrengthened and strengthened elements in order to evaluate the global and local performances such as cracking, demands on the steel reinforcement and utilisation of the composite fibres.

*My contributions were the design of the experiments including the test set-up design, carrying out the experiments and analyses, drawing conclusions and finally writing the manuscript.*

**PAPER IV**

Floruț, S.-C., Sas, G., **Popescu, C.**, and Stoian, V. (2014). "Tests on reinforced concrete slabs with cut-out openings strengthened with fibre-reinforced polymers." *Composites Part B: Engineering*, 66, 484–493.

In Paper IV, the results of experimental and theoretical investigations on RC slabs, with and without cut-out openings, strengthened using FRPs, are described. Using the yield line method, both pre-test and post-test analytical predictions were made and compared against experimental values.

*For this publication, my contribution was writing chapter 1. Introduction, deriving the equations for the yield line predictions and writing chapter 3.3 Test predictions by yield line theory.*

**PAPER V**

**Popescu, C.**, Schmidt, J.W., Goltermann, P. and Sas, G. (2014). "Assessment of RC walls with cut-out openings strengthened by FRP using a rigid plastic approach." *Engineering Structures*

In Paper V, a proposal is described for a new procedure based on the rigid-plastic approach for evaluating the ultimate load of walls with cut-out openings that have been strengthened using CFRP. The approach is verified against transverse (out-of-plane) and axial (in-plane) loading. Predictions made using the new method were compared with experimental results obtained from tests carried out at Technical Univ. of Denmark and Luleå Univ. of Technology, respectively.

*My contributions were the description of the experimental tests, proposal and derivation of the theoretical model and writing the paper.*

## 1.7 Additional publications

Apart from the research project described in this thesis, the author had the opportunity to collaborate with other researchers on different projects that are related, directly or indirectly, to the current research project. This work was published in several journals, reports and conference papers. These papers are listed here, but not appended to the thesis.

### Licentiate thesis

**Popescu C.** (2015). "FRP strengthening of concrete walls with openings." Luleå University of Technology, Luleå, Sweden.

### Journal papers

**Popescu, C.**, & Sas, G. (2014). "The development of an experimental program through design of experiments and FEM analysis: A preliminary study." *Nordic Concrete Research,* 51(3), 29-42.

Sas, G., Dăescu, C., **Popescu, C.**, & Nagy-György, T. (2014). "Numerical optimization of strengthening disturbed regions of dapped-end beams using NSM and EBR CFRP." *Composites Part B: Engineering, 67*, 381-390.

**Popescu, C.**, Dăescu, C., Tamás, N-G. & Sas, G. (2013). "Disturbed regions in dapped-end beams: numerical simulations of strengthening techniques." *Nordic Concrete Research*, 48(2), 13-25.

**Conference papers**

**Popescu, C.**, Sas, G., Blanksvärd, T. & Täljsten, B. (2016). "Two-way walls with cut-out openings strengthened by fiber-reinforced polymers." *19th IABSE Congress: Challenges in Design and Construction of an Innovative and Sustainable Built Environment*, Stockholm, Sweden. (Presented by Blanksvärd, T.)

Sabău, C., **Popescu, C.**, Sas, G., Blanksvärd, T. & Täljsten, B. (2016). "Monitoring structural behavior of reinforced concrete walls with openings using digital image correlation." *19th IABSE Congress: Challenges in Design and Construction of an Innovative and Sustainable Built Environment*, Stockholm, Sweden. (Presented by Sabău, C.)

**Popescu, C.**, Sas, G., Sabău, C., Blanksvärd, T. & Täljsten, B. (2015). "Experimental tests on RC walls with openings strengthened by FRP." *The 12th International Symposium on Fiber Reinforced Polymers for Reinforced Concrete Structures (FRPRCS-12) & The 5th Asia-Pacific Conference on Fiber Reinforced Polymers in Structures (APFIS-2015),* Joint Conference, Wu, Z., Wu, G. & Wang, X. (eds.) Nanjing, China. (Presented by Popescu, C.)

**Popescu, C.**, Sas, G., Täljsten, B. & Blanksvärd, T. (2014). A state of the art review on walls with openings strengthened by use of fiber reinforced polymers. *Proceedings of The 7th International Conference on FRP Composites in Civil Engineering (CICE 2014)*. El-Hacha, R. (ed.). Vancouver, British Columbia, Canada: International Institute for FRP in Construction. (Presented by Popescu, C.)

**Popescu, C.**, Sas, G., Täljsten, B. & Blanksvärd, T. (2014) Experimental Program for Axially Loaded RC Walls with Openings Strengthened by FRP. *XXIIth Symposium on Nordic Concrete Research & Development*, Reykjavik, Iceland. (Conference paper published in Proceedings of Nordic Concrete Research), 50(2), 285-288. (Presented by Popescu, C.)

Dăescu, C., Nagy-György, T., Sas, G., Barros, J. & **Popescu, C.** (2013) Numerical Assessment of Dapped Beam Ends Retrofitted with FRP Composites. *FRPRCS-11: 11th International Symposium on Fiber Reinforced Polymer for Reinforced Concrete Structures*. Barros, J. & Sena-Cruz, J. (eds.). Guimarães, Portugal. (Presented by Popescu, C.)

**Technical reports**

Sas, G., Daescu, C., Sæther, I., **Popescu, C.**, Arntsen, B. (2013). MÅLSET DAM - Finite element analysis assisted by tests, Technical report no.: 2013/3

**Popescu, C.**, Sas, G., Sand, B. (2013) Composite slabs with profiled steel decking - numerical simulations, Technical report no.: 2012/12

# Chapter 2

# Literature review

## 2.1 An overview

The terminology used in this study is now briefly explained. In the research literature (Saheb and Desayi 1989, 1990a), walls subjected to axial loads are described as being one-way (OW) or two-way (TW). Walls restrained along their top and bottom edges are referred to as OW action panels. They tend to develop a single out-of-plane curvature in parallel to the load direction; such walls are often found in tilt-up concrete structures. Panels restrained along three or four sides are referred to as TW action panels. They generally deform along both the horizontal and vertical directions; such walls are often found in monolithic concrete structures. Typical crack patterns and deformation profiles for walls both with and without openings are shown in Fig. 2.1.

In all major design codes, a distinction is made between reinforced and unreinforced walls. It should be noted that the term unreinforced member does not only refer to plain concrete but also when the reinforcement provided does not fulfil the minimum requirements (both in terms of quantity and detailing). In Eurocode (EN1992-1-1 2004), for example, structural concrete members having less reinforcement than the minimum amount required are defined as lightly reinforced members. These members are allowed to be used in structures, as walls, columns, arches for example, where compressive normal forces are predominant. Combined axial and flexural stresses occur when, due to thickness variations and misalignment of the panels in the construction process, the vertical load acts eccentrically along the weak axis. These deficiencies can cause offsetting of the front or rear faces of the panels, thus affecting the eccentricity. The recommended tolerance limits for the accumulated misalignment and thickness variation in published guidelines (Ascent 2012) are one twelfth of the wall's thickness. When the walls are subjected to axial loads with small eccentricities (less than one sixth of the wall thickness), the recommendations for unreinforced members can be applied. Even in this case, a minimum amount of reinforcement is recommended, primarily to control cracking due to shrinkage, creep and temperature stresses. The threshold value for what design codes [ACI 318 (2011), AS3600 (2009), CAN/CSA-A23.3 (2004)] define as *small* eccentricity is $t/6$, where $t$ is the wall thickness, so that the resultant axial load acting on the wall must be located within the middle third of its overall thickness. Results obtained from the empirically developed design models may deviate from real values in cases where there is greater eccentricity.

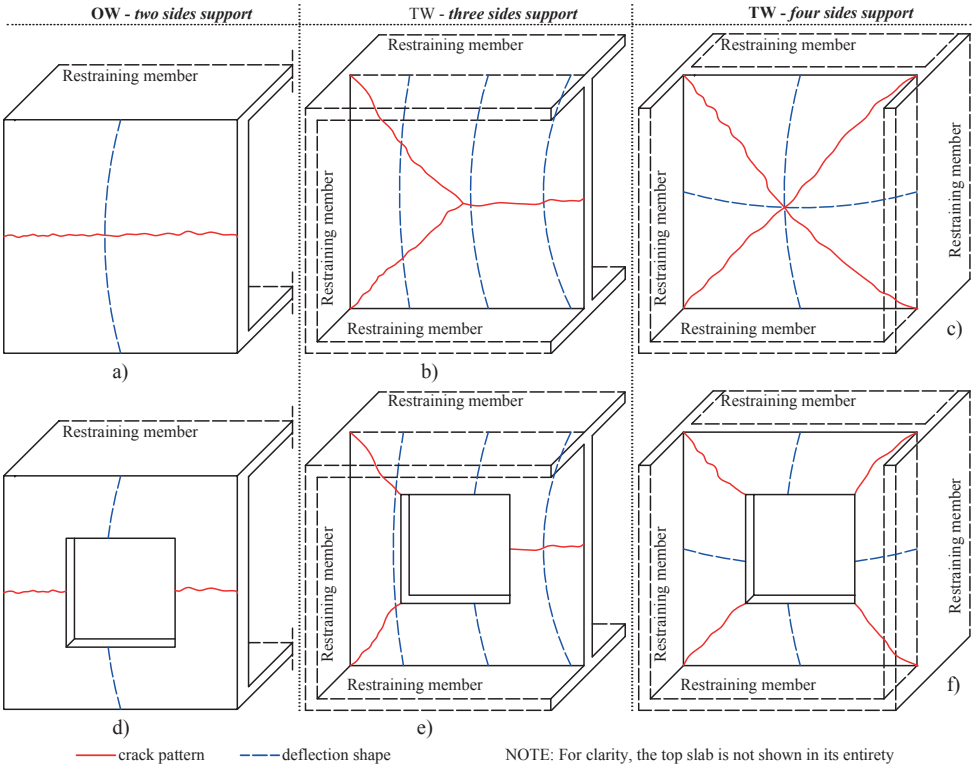


**Figure 2.1** Typical crack pattern and deflection shape of axially-loaded RC walls (Popescu et al. 2015)

As far as the author can ascertain, practical design of axially-loaded concrete walls is generally based on column theory that accounts for the equilibrium of forces over their cross-sections, and stress-strain compatibilities. A simplified procedure is described in design codes such as ACI 318 (2011), AS3600 (2009), CAN/CSA-A23.3 (2004) and EN1992-1-1 (2004). However, there are differences, mostly regarding distributions of compressive forces, slenderness and restraints. A detailed description can be found in *Paper I*. Design codes do not consider walls with openings in much detail. European (EN1992-1-1 2004) and Australian (AS3600 2009) design codes provide some guidance regarding the design of walls with openings subjected to vertical loads. If the walls are restrained on all sides, and enclose an opening with an area less than one tenth of the total and a height less than one third of the wall height, the effects of this opening on the axial strength can be neglected. If these conditions are not met, the portion between the restraining member and opening has to be treated as a separate member being supported on three sides, and the area between the openings (if more than one) has to be treated as being supported on two sides.

## 2.2 Previous tests on concrete walls under axial loads

Several researchers have spent a good deal of effort on understanding the behaviour of concrete walls treated as compression members. Both experimental and theoretical aspects have been

examined and presented in the research literature. The focus in this thesis was more on studies after 1970, partly because access to these documents was somewhat easier and partly because some pre-1970 studies were not in English. A summary of all these studies is presented herein and described in more detail in *Paper I*.

Investigations into the behaviour of axially-loaded members e.g. columns, started early in the 1900s and the outcome was applied to walls as well (Larsson 1959). As differences may exist between columns and walls, a growing interest was shown into testing concrete walls. According to a review by Larsson (1959), in 1935 Richart and Newmark (1935) and Svenska Cementföreningen (1935) reported one of the first investigations into concrete walls. These tests were later complemented by others, such as Bengtsson (1946), Seddon (1956a, 1956b), Glarbo (1951) and Johnson (1957).

Swartz et al. (1974) pointed out that RC panels are usually simply supported along all sides on which biaxial buckling may occur. Therefore, the buckling loads were monitored in several panels under test, in which the steel reinforcement ratio and the number of steel mesh layers were varied. A formula predicting the average stress in concrete at the onset of buckling was derived.

Oberlender and Everard (1977) carried out investigations into solid walls in OW action and derived an empirical design model. The reinforcement layers were arranged at different depths in order to determine the effect of reinforcement location in response to either concentric or eccentric loading conditions. Another purpose of that research was to determine the load capacities of the OW panels with respect to their aspect and slenderness ratios.

In an attempt to observe any differences from varying the steel reinforcement ratio as well as slenderness ratios, Pillai and Parthasarathy (1977) developed an experimental programme for testing OW walls and provided a new empirical design equation.

The first systematic study of concrete walls with and without openings, tested in OW and TW action, was reported by Saheb and Desayi (1989), (1990b, a). The study investigated the influence of aspect ratio, thickness and slenderness ratio as well as vertical and horizontal steel reinforcement ratio on the ultimate load. For OW action, the authors combined their own experimental results with those reported by Oberlender and Everard (1977), Pillai and Parthasarathy (1977) and Zielinski et al. (1982) to suggest modifications to existing design equations. Up to that time, no equations for predicting the ultimate strength of TW wall panels were available. Hence, the authors suggested two methods to overcome this: (1) the empirical method based on their own data and the one published by Swartz et al. (1974); (2) a semi-empirical method developed from a modification of the buckling strength theory of thin rectangular metal sheets proposed by Timoshenko and Gere (1961) (see *Paper I* for further details). For the specimens with openings, all the above parameters were kept constant in order to allow the study to account for the influence of type and location of opening(s). Saheb and Desayi (1990b) also proposed an equation for predicting the ultimate load-bearing capacity of such walls.

The experimental programme undertaken by the Fragomeni (1995) focused on investigating the axial load capacity of OW normal and high-strength concrete walls. The author suggested a change to the design formula to account for the increase in wall strength when high-strength concrete is used. Following the suggestions made by Fragomeni (1995), where the high concrete strength values are taken into account in order to increase the wall strength, Doh (2002) carried out

extensive experiments on OW and TW concrete walls in order to modify the existing equation in the design codes. Later, Doh and Fragomeni (2006) supplemented their experiments by also testing concrete walls with openings. Based on the equation proposed for solid walls (Doh and Fragomeni 2005), and following the same methodology for walls with openings proposed by Saheb and Desayi (1990b), the authors developed a new formula for concrete walls with openings. In order to provide useful information for further improvement of the code equation, an extensive experimental regime was undertaken by Lee (2008). Both OW and TW walls with openings having different slenderness ratios and concrete compressive strength were investigated. The experimental results were used to validate the design model developed by Doh and Fragomeni (2006).

In two recent studies (Ganesan et al. 2012, Ganesan et al. 2013), the axial strength of OW wall panels made from steel fibre reinforced concrete and geo-polymer concrete was studied. The key parameters in these studies were the slenderness and aspect ratios. The findings were used to modify the equation proposed by Saheb and Desayi (1989).

Robinson et al. (2013) proved that current methodologies (ACI 318 2011, AS3600 2009, EN1992-1-1 2004) have a significant conservatism when assessed using experimental results obtained from a series of tests on OW slender wall panels. Therefore, they devised a new theoretical model by using the application of "lumped plasticity" through the semi-empirical semi-probabilistic DAT (Design Assisted by Testing) methodology, allowed within the European design code (EN1990 2004).

Huang et al. (2015) tested high-strength concrete OW panels to investigate the effect of reinforcement ratio and location, eccentricity and slenderness ratio. In addition, extensive nonlinear analyses were carried out to investigate the failure mechanism of slender concrete walls. It was concluded that, within a typical slenderness range, the specimens failed by buckling. A recommendation was made to avoid this brittle failure mode by increasing the reinforcement ratio in the panel.

As can be seen, a considerable amount of literature has been published about the behaviour of solid wall panels. An up-to-date database (253 tests – see *Paper I*) collected by the author showed that 41.1% and 26.1% from the tests included in the database referred to OW and TW solid walls, respectively. Little attention has yet been given to the study of walls with openings: 19.4% and 13.4% from the tests included in the database referred to OW and TW walls with openings, respectively. The majority of all studies carried out to date concerned walls with designed openings (i.e. with diagonal bars around the opening corner to avoid premature cracking). Walls with cut-out openings (i.e. openings sawn in a solid panel) under axial load remain predominantly unresearched; as far as the author knows, just one research study (Mohammed et al. 2013) has focused on this type of problem. The findings showed that the presence of an opening in a solid OW panel led to disturbance zones. The discontinuities causing high stresses force the cracks to occur first at the corners due to inadequate reinforcement.

In addition to experimental tests, numerous design-oriented models have been developed by researchers; their performances were reviewed by Fragomeni et al. (1994) (studies up to 1990) and by Popescu et al. (2015) – *Paper I* – (studies since 1990). Both of these reviews concluded that the behaviour of walls with openings has not been thoroughly examined, with some conflicting results; more experimental tests are therefore needed. Fewer tests have been carried out on walls under TW

action, walls with openings or different load eccentricities, and more tests are required under these conditions to facilitate the development of appropriate design models. A description of the performance of current design models, using a statistical analysis of information in a database collected by the author, was published in *Paper I*.

## 2.3 Use of FRP for strengthening of concrete walls under axial loads

There are many reasons for repair and/or strengthening. However, one can identify a number of common causes for these actions such as changes in use combined with an increase in imposed load, structures ageing due to material degradation, and structural alterations which require openings to be cut into structural elements. The traditional strengthening methods (i.e. RC/steel frame or RC jacketing) may not be architecturally convenient, may result in increases in the weight of the elements strengthened and are time-consuming. As a consequence, an alternative that has been used successfully over the last few decades is the use of FRP materials as the externally-bonded material. These advanced composite materials have been increasingly used in the construction industry over the last few decades because of their excellent properties – high strength and/or stiffness, lower density, fatigue endurance, high chemical resistance to corrosion, and excellent resistance to humid environments.

The technique involves thin composite sheets, plates or bars being bonded through an adhesive to the concrete surface or inside the concrete cover (near-surface) to improve the strength and behaviour of the structural element (Täljsten et al. 2003). FRP composites are comprised of fibres with high tensile strength within a polymer matrix. The fibres are generally made from carbon (CFRP), glass (GFRP), aramid (AFRP) and basalt (BFRP). The FRP products can be found in different shapes, such as sheets, bars, plates and grids (Fig. 2.2). FRP bars are only unidirectional while FRP sheets, plates and grids can be produced as unidirectional, bidirectional or multi-directional fibres. These fibres are aligned parallel to the principal tensile stresses when structural elements are shear or flexural deficient. Axial strength can also be enhanced by wrapping the fibres transversally, a method known as FRP confinement. Some specific cases in which FRPs are successfully employed can be seen in Fig. 2.3.

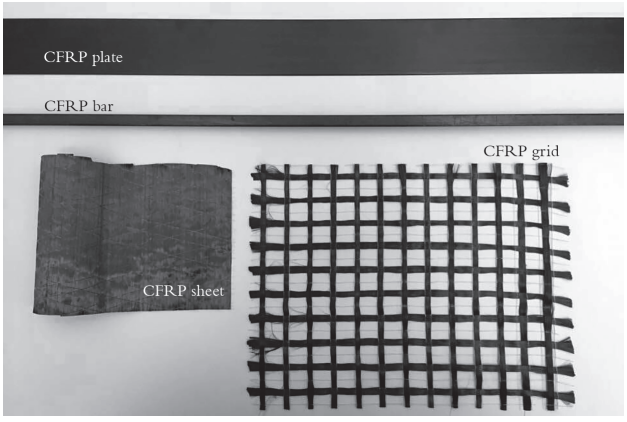


**Figure 2.2** Typical FRP products

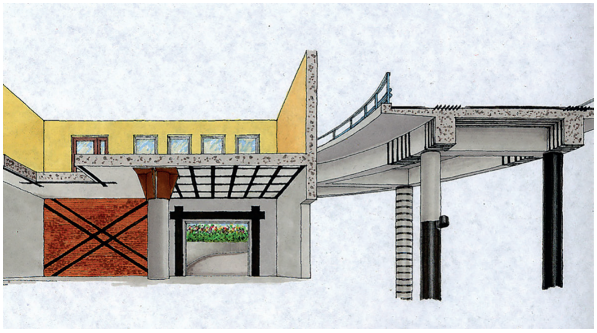

**Figure 2.3** FRP strengthening configurations in different contexts (Täljsten et al. 2012)

The adhesives used for supporting the fibres can be of organic or inorganic nature. Organic adhesives, such as epoxy, are the most common type and they have behaved well in terms of strength, bond and creep properties (Blanksvärd 2009). However, there are some drawbacks such as diffusion tightness, poor thermal compatibility with concrete and a lack of regulations for the handling of epoxy bonding agents (Blanksvärd et al. 2009). Moreover, the low fire resistance of FRP-strengthened structural elements may also be seen as poor behaviour. Thus, more recently, inorganic (mineral) binders have started to attract more attention from the research community as they may be a better alternative in terms of compatibility with the base layer i.e. concrete. One example is the so-called textile-reinforced mortar.

The research conducted so far on strengthening large structural members with openings, such as slabs or walls, using FRPs is promising (Mosallam and Nasr 2016, Todut et al. 2015, Floruț et al. 2014, Li et al. 2013, Demeter 2011, Enochsson et al. 2007). The alignment of the fibres was based on observations of the failure modes of the unstrengthened elements added in order to restore either flexural and/or shear capacity. Usually the FRP material is placed around openings in a vertical, horizontal or inclined position, or a combination of these. In general, the amount of FRPs was chosen intuitively, or by converting the amount of steel reinforcement removed into FRP material. Hansen and Stang (2012) used a fracture mechanical approach to describe strengthened RC shear walls with openings. Li et al. (2013) demonstrated that the optimisation of the direction, width and number of layers of FRP strips by using a strut-and-tie model can yield robust results.

For non-seismically designed walls with openings, Mohammed et al. (2013) was the first who investigated their behaviour when FRP-strengthened. One-way, one third scale RC walls with openings varying from 5% to 30% of the total wall area were strengthened using CFRP sheets. The CFRP sheets were placed around opening edges in two different configurations and the capacity was increased as the principal stresses on the opening corners were reduced. Given the failure mode (i.e. concrete crushing) observed in experimental tests – *Paper II* (Popescu et al. 2016a) for unstrengthened TW walls with openings, the strengthening configuration proposed by Mohammed et al. (2013) was not suitable. It is believed that a better configuration would be to strengthen the walls by confinement.

Confinement has proved to be a viable solution where ductility and/or axial strength are concerned (Matthys et al. 2006). The method is highly dependent on the cross-section geometry:

a uniform confinement effect is obtained for circular cross-sections whereas only part of the cross-section is effectively confined for rectangular cross-sections (Mirmiran 1998, Pessiki 2001, Wu and Wei 2010, Liu et al. 2015). Numerous design/analysis-oriented models have been developed by researchers; the models' performances were reviewed by Lam and Teng (2003), Rocca et al. (2008). These studies showed that as the aspect ratio of the cross-section increased, the enhancement in compressive strength decreased. Members with aspect ratios higher than 3:1 are usually treated as wall-like columns. Creating a new opening in a concrete wall inevitably increases the aspect ratio of the remaining portions, hereafter referred to as piers (or wall-like columns), reducing the effectiveness of the FRP confinement. Therefore, for high aspect ratios, simply wrapping the element in FRP will not significantly increase the axial strength. To overcome this problem, one can either increase the cross-section by adding additional material (i.e. high-strength mortar) or use FRP/steel anchors. Several methods were studied and described in the literature and these are summarised now.

The axial strength and ductility of short (1.5 m) columns with an aspect ratio of 3.65 to 1 can be increased by confinement using longitudinal and transversal FRP sheets in combination with fibre anchor spikes placed along the wider faces of the column (Tan 2002). Adding semi-cylindrical attachments (high-strength mortar) to increase the cross-sectional area (Tanwongsval et al. (2003) is another way of achieving this. According to Prota et al. (2006), quadri-directional CFRPs can improve seismic performance, but not other strength parameters. Triantafillou et al. (2015) discovered that adding heavy anchor spikes or cross-sectional enlargement with high-strength mortar can also double the confining effect of circumferential FRP, but excessively light fibre anchor spikes tend to fail prematurely and thus have little effect on strength. In contrast, De Luca et al. (2013) found that confining wall-like columns with an aspect ratio of 2.92 to 1 using FRP (but no longitudinal or anchor fibres) enhanced the axial ductility, but not the axial capacity. This all suggests that a hybrid method (FRP confinement and longitudinal FRP fibres, anchors or increasing the cross-section) is required when the axial strength and ductility of wall-like columns needs to be increased. Increasing the cross-section cannot always be a viable solution, for reasons such as spatial, esthetical or structural limitations and, therefore, using anchors remains the only available course of action. The anchors are introduced to create shorter distances which are confined between bolts (Karbhari and Seible 1998). Before this approach can be used, however, a better understanding of the response of the overall system is necessary. To this end, an experimental investigation of the effectiveness of CFRP–based strengthening for restoring the axial capacity of a solid RC wall after cutting openings was carried out at Luleå University of Technology and is described in this thesis.

# Chapter 3

# Experimental programme

## 3.1 Materials and methods

This section briefly summarises how the test specimens were designed, constructed and tested. The design and process of strengthening are also described. Specific details and results not given in this chapter can be found in *Papers II* and *III*, respectively.

### *3.1.1 Design of experiments and test matrix*

The specimens were designed to represent typical wall panels in residential buildings. In total, nine half-scale specimens were tested to failure. The walls were 1800 mm long, 1350 mm high and 60 mm thick.

A quantitative approach was used to plan the laboratory investigation, based on the DoE method (Box et al. 1978). This technique was used in order to develop a test matrix such that the response of the CFRP-strengthened concrete walls with openings could be evaluated effectively. According to the theory behind DoE, past experience should contribute to the choice of the right parameters and these should only be set at two levels, minimum and maximum. From the literature review and own experience, the size of opening and structural condition of the wall were selected as the two most influential parameters.

For the first parameter, namely size opening, *small* (450 mm x 1050 mm) and *large* openings (900 mm x 1050 mm) were set as the minimum and maximum levels. The minimum level represents the width of a typical door opening in a residential building whereas the maximum level corresponds to a double-door opening. Note that the terms *small* and *large* carry no meaning other than being a useful way of labelling the opening sizes.

For the second parameter, pre-cracked and uncracked conditions were established as the minimum and maximum levels. The minimum level represents the wall in a pre-cracked state (loaded until 75% of the peak load) whereas the maximum level corresponds to the uncracked condition. The 75% level was obtained based on nonlinear FE analyses (Popescu and Sas 2014) and observations of when the reference specimens developed a significant crack width. Whether a crack is significant or not depends on many factors, including functionality of the building and environmental exposure class. However, according to ACI 224R-01 (2001), a crack width that exceeds 0.15 mm may require repair; therefore, this value was used to record the corresponding cracking load. In order

to carry out all the strengthening work together, the pre-cracked specimens were removed from the test set-up, so the pre-cracks were nearly closed during this operation.

In addition to the tests derived from DoE, three unstrengthened specimens were loaded to failure to evaluate the opening's effect on the axial strength and the strengthening effectiveness. The designed test matrix is shown in Fig. 3.1 and divided into stages I, II and III, relating to reference specimens, pre-cracked and uncracked specimens strengthened with CFRP, respectively. For convenience, the naming system adopted consists of the test stage described above (I, II or III) and the type of wall C, S, L (where C refers to a solid wall, S and L refers to a wall with a small and large opening, respectively). In addition, the tests from the third stage were repeated and thus, the specimen's name contains a serial number. For example, II-S refers to a pre-cracked wall with a small opening, strengthened with CFRP.

### *3.1.2 Specimen preparation*

The specimens were solid panels (i.e. constant thickness) with no voids or insulating layers. They were reinforced with a single, centrally placed, welded wire mesh. The welded fabric consisted of 5 mm diameter deformed bars, spaced at 100 mm in both orthogonal directions. Before casting, electrical resistance strain gauges (KFG-5-120-C1-11L1M2R, Kyowa Electronic Instruments, Chofu, Tokyo) with pre-attached wires were bonded to the reinforcement. The reinforcement was marked and sent to the precasting plant (Br Hedmans Cementgjuteri, Älvsbyn) where the walls were fabricated. The walls were long-line cast, laid down on a steel platform (Fig. 3.2). A batch line can accommodate up to five specimens.

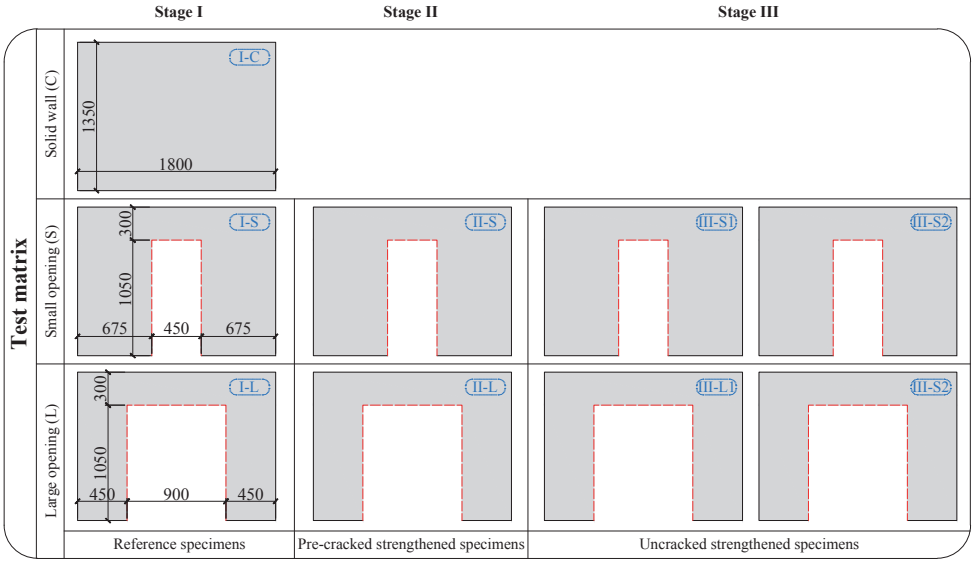


**Figure 3.1** Test matrix (dimensions in millimetres)

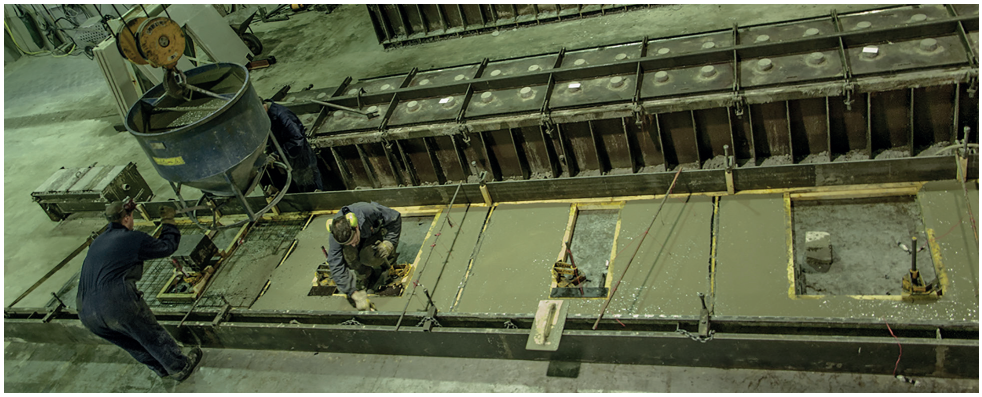

**Figure 3.2** Long-line casting of walls

### *3.1.3 CFRP strengthening – pre-test design analysis*

A suitable FRP configuration was found after analysing the failure modes of unstrengthened walls (see *Paper II*). Two methods were available to restore the capacity to that of a solid wall. One was to increase the specimen's thickness (e.g. RC jacketing, textile-reinforced mortars), the other was to increase the concrete compressive strength through confinement. The latter was the focus of interest for the work presented here.

The next step was to consider the EC2 (EN1992-1-1 2004) design model for TW walls [Eq. (3.1)] to find the confined compressive strength ($f_{cc}$) needed to regain the capacity of the solid wall:

$$N_{1-C} = 2 f_{cc} L_{pier} t \Phi \tag{3.1}$$

where the terms on the left-hand and right-hand sides represent the experimental load of the solid wall and theoretically-predicted value of a wall with an opening, respectively.

$$\Phi = 1.14\left(1 - 2\frac{e + e_a}{t}\right) - 0.02 \cdot \frac{H_{eff}}{t} \leq \left(1 - 2\frac{e + e_a}{t}\right) \tag{3.2}$$

Here, $t$ is wall thickness, $L_{pier}$ is length of the wall pier, $e$ is initial eccentricity, equal to $t/6$ and $e_a$ is additional eccentricity due to lateral deflection of the wall.

The additional eccentricity, $e_a$, accounts for the effect of slenderness, also known as second order (or P–Δ) effects and according to EN1992-1-1 (2004) is given by:

$$e_a = \frac{H_{eff}}{400} \tag{3.3}$$

with $H_{eff}$=β$H$ being the effective height. Values for the effective height factor β are given for the most commonly encountered restraints. For walls restrained along all their sides, the European code provides the following equations:

$$\beta = \begin{cases} \dfrac{1}{1+\left(\dfrac{H}{3L}\right)^2} & \text{three sides} \\ \dfrac{1}{1+\left(\dfrac{H}{L}\right)^2} & \text{four sides with} \quad L \geq H \\ \dfrac{L}{2H} & \text{four sides with} \quad L < H \end{cases} \tag{3.4}$$

By solving Eq. (3.1), it was possible to find the confined compressive strength that would be needed to restore the axial capacity to that of a solid wall. This yields a ratio between the confined and unconfined compressive strengths, $f_{cc}/f_c$, of about 1.26 and 1.44 for walls with small and large openings, respectively. The resulting value was then used in conjunction with the model presented by Lam and Teng (2003) to estimate the required thickness of the CFRP jacket. The analytical formulation proposed by Lam and Teng considered the effect of non-uniformity of confinement using a shape factor ($k_{s1}$):

$$\frac{f_{cc}}{f_c} = 1 + k_1 k_{s1} \frac{f_l}{f_c} \tag{3.5}$$

where $f_c$ is the compressive strength of the unconfined concrete, $f_{cc}$ is the compressive strength of the confined concrete, $k_1 = 3.3$ is the confinement effectiveness coefficient and $f_l$ is the confining pressure.

The shape factor, $k_{s1}$, is defined as

$$k_{s1} = \left(\frac{b}{h}\right)^2 \frac{A_e}{A_c} \tag{3.6}$$

The effective confinement area ratio $A_e/A_c$ is calculated as:

$$\frac{A_e}{A_c} = \frac{1 - \left[(b/h)(h-2R)^2 + (h/b)(b-2R)^2\right]/3A_g - \rho_{sc}}{1-\rho_{sc}} \tag{3.7}$$

where $b$ and $h$ are the width and height of the cross-section, respectively, $A_e$ is the effective confinement area, $A_c$ is the total area of the cross-section, $R$ is the corner radius, $\rho_{sc}$ is the cross-sectional area ratio of longitudinal steel and $A_g$ is the gross area of the column section with rounded corners.

The confining pressure, $f_l$, is given by

$$f_l = \frac{2 \cdot f_{frp} \cdot t_{frp}}{D'} = \frac{2 \cdot f_{frp} \cdot t_{frp}}{\sqrt{h^2 + b^2}} \tag{3.8}$$

where $f_{frp}$ and $t_{frp}$ are the tensile strength and thickness of the CFRP jacket, respectively.

Allowing for the limitation of the model (not valid for high cross-section aspect ratios), the following procedure was employed. The transverse fibre sheets were fixed using steel bolts so as to create virtual cross-sections with an aspect ratio limited to 2 (60 x 120 mm$^2$ starting from the opening edge, see Fig. 3.3). Tan (2002) assumed that the internal transverse links provide additional anchor points for the CFRP jacket. Using the same idea, the effectively confined area for pure compression

is shown in Fig. 3.3. One virtual column strip was isolated so that Eq. (3.7) would be applicable; the results were then extrapolated to the rest of the wall pier. Based on the required thicknesses of CFRP layers under these conditions back-calculated from Eq. (3.8), two and three 0.17 mm thick FRP layers were used to strengthen the specimens with small and large openings, respectively.

Prior to the application of the CFRP strengthening, 8 mm holes were drilled through the wall at positions marked on the concrete surface to help the installation of the mechanical anchorages. The concrete surfaces were then prepared by grinding – to remove the irregularities and cement paste layer, and thus, exposing the aggregates – and cleaning with compressed air. The CFRP sheets were applied using the wet lay-up procedure. First, a two-component epoxy primer (StoPox 452 EP) was applied to the specimens, followed by the application of the impregnated fibres on the concrete surface after approximately 6 hours. They were wrapped around the piers in a U-shape; full wrapping was not possible due to the existing boundary conditions (Fig. 3.4). High-strength CFRP (StoFRP Sheet IMS300 C300, Sto Scandinavia, Linköping) was used as the bonded material, and impregnated using a two-component epoxy resin (StoPox LH). A week later, when the epoxy had cured, the anchorage bolts were inserted into predrilled holes and prestressed with a torque estimated from the clamp load (i.e. 8.7 kN) as 75% of the proof load, as specified in SS-EN ISO 898-1 (2013).

### *3.1.4 Material properties*

In order to determine mechanical characteristics of the concrete (compressive strength and fracture energy), cubes and beams with standardised sizes were cast and cured under identical conditions to the specimens. The average cubic compressive strength of the concrete was determined in accordance with (SS-EN 12390-3:2009 2009). The fracture energy was determined following the RILEM TC 50-FMC (1985) standard's recommendations. Coupons were taken from the reinforcing steel meshes and tested in accordance with SS-EN ISO 6892-1:2009 (2009) in order to determine their stress-strain properties. Average values and their corresponding coefficients of variation can be found in *Paper II* and *III*, respectively.

No material tests were carried out on the CFRP system (fibres + epoxy) and their nominal properties are given here according to the tests undertaken by the supplier. The fibres of the CFRP sheets were unidirectional with an areal weight of about 300 g/m$^2$, tensile strength of 5500 MPa and elastic modulus of 290 GPa. The epoxy resin had an elastic modulus of about 2 GPa.

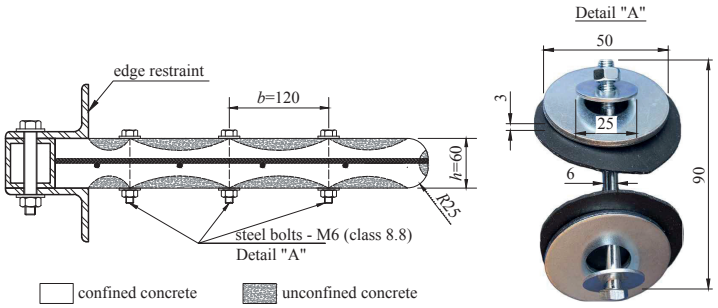


**Figure 3.3** Effectively confined area of a wall pier and the mechanical anchorage (dimensions in millimetres)

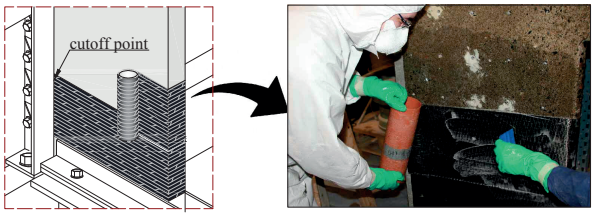


(a) (b)

**Figure 3.4** Wrapping of the CFRP sheets around the wall pier: from design (a) to fabrication in the laboratory (b)

### *3.1.5 Test set-up and instrumentation*

Attempting to duplicate the as-built conditions of the wall from a real structure for a test regime was not without some merit. A test rig had to be designed and built to fulfil the following conditions:

1. Restraints

   *a.* *Side* restraints: had to simulate the TW effect for real transverse walls that permitted rotation and prevented translation.

   *b.* *Top* and *bottom* restraints: had to simulate a hinge connection that allowed full free rotation.

2. Load application: the forces would be applied uniformly along the wall's length at an eccentricity – equal at both ends – of about one sixth of the wall thickness.

This process started with a study in which existing experimental tests described by Lee (2008) were used to calibrate a nonlinear FE model (Popescu and Sas 2014). After calibration, the model was able to describe the structural behaviour of such walls and to provide important information to the current experimental programme such as the reactions along bottom and side edges of the solid wall, maximum displacements and their location, strains in reinforcement/concrete, and crack patterns. The information was used to determine the number (and their capacity) of hydraulic jacks required to break the walls, design the test rig and build an instrumentation scheme.

Technical drawings used to build the test rig can be found in the author's Licentiate thesis (Popescu 2015). All reactions were transmitted to a reaction frame fixed to a strong floor. The reaction frame's load-carrying capacity was found to be inadequate for the whole set of forces and thus, it had to be strengthened with three additional pairs of high-strength prestressed steel rods (Fig. 3.5). An extensive instrumentation scheme was devised in order to monitor the behaviour of the walls during the loading cycles. Linear displacement sensors were used to measure out-of-plane and in-plane displacements, with strain gauges placed on steel reinforcement and on the compression side of the concrete surface. These measurements were supplemented by measuring full-field strain distributions using the three-dimensional digital image correlation (3D-DIC) technique. This is a non-contact optical measurement technique based on imaging specimens' surfaces in initial undeformed and later deformed stages to obtain deformation (strain) data. The specimens' surfaces are prepared by applying a black dot pattern, ideally stochastic, onto a white base layer (and sometimes directly onto the natural surface) in order to create a good contrast.

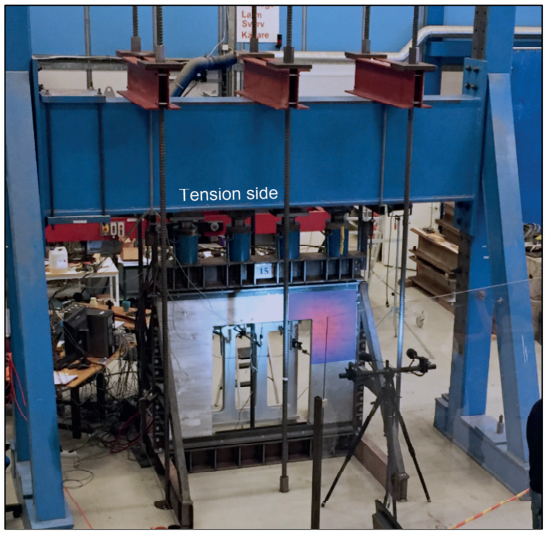


**Figure 3.5** General overview of the test set-up (reprinted from Popescu et al. 2016a)

Comparable to FE simulations, a software divides the image into multiple facets for analysis (Reu 2012). These facets defined on the reference image (i.e. undeformed state) are tracked in all the subsequent images (i.e. deformed). The images are then "compared" and the deformation is calculated. For the investigations presented herein, a commercial DIC code with 3D measuring capabilities, ARAMIS (GOM mbH, Brunswick, Germany) (GOM mbH), was used to monitor the strain and displacement fields. The right-upper corner on the tension side of the specimen (780 × 660 mm, highlighted in Fig. 3.5) was monitored since it is a particularly interesting area to observe the strain and crack development in discontinuous regions. The complete instrumentation scheme is described in *Papers II* and *III*. A general view of the test set-up is shown in Fig. 3.5.

## 3.2 Effect of cut-out openings on the axial strength of concrete walls

In order to investigate the effect of the cut-out on the axial strength, three specimens were loaded to failure in stage I: one was a solid panel, one had a symmetric half-scaled single door-type opening and the third had a symmetric half-scaled double door-type opening. The small and large openings represented a 25% and 50%, respectively, reduction in the cross-sectional area of the solid wall. In this way, it was possible to evaluate the effect of introducing new openings in a solid wall first. The damage level was evaluated in terms of ultimate load, crack pattern, displacement profiles, strains in concrete and steel reinforcement and ductility and energy release at failure. Only selected results are given here and the reader is referred to *Paper II*.

The walls behaved as predicted by the numerical analysis, showing a TW behaviour by deflecting in both vertical and horizontal directions. This aspect was also captured by the ARAMIS system in addition to strain development and distribution around the openings during loading cycles, as shown in the images in Fig. 3.6.

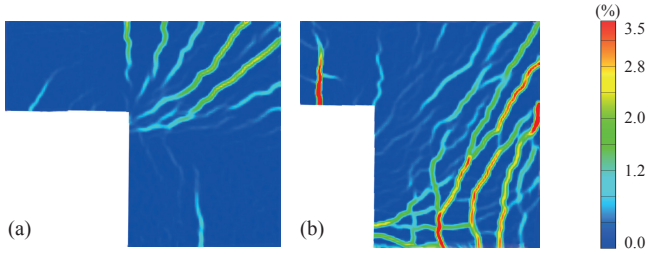


**Figure 3.6** Principal plane strain development on the tension side of the specimens at peak load: (a) specimen I-S; (b) specimen I-L

The tensile and compressive strains that developed in the reinforcement were significant at higher loads, with yielding of some bars occurring at failure. Recorded strains in the steel reinforcement indicate that the reinforcement makes no significant contribution at serviceability limit states, but yielding may occur close to failure when second-order effects start to be more active, thus contributing to the overall ductility. Yielding at ultimate also indicates that reinforcement might contribute to the ultimate capacity; however, this preliminary conclusion should be further verified with tests on walls without any reinforcement.

In all cases, the walls had a brittle failure due to crushing of concrete with spalling and reinforcement buckling along the line between the corner of the wall and opening corner of one pier. The crack pattern at failure of both tension and compression sides is shown in Fig. 3.7. The peak loads are given in Table 3.1 and effects of opening size are shown in Fig. 3.8, in which load-displacement curves of all three specimens (recorded at the same position on both piers) are plotted on the same graph.

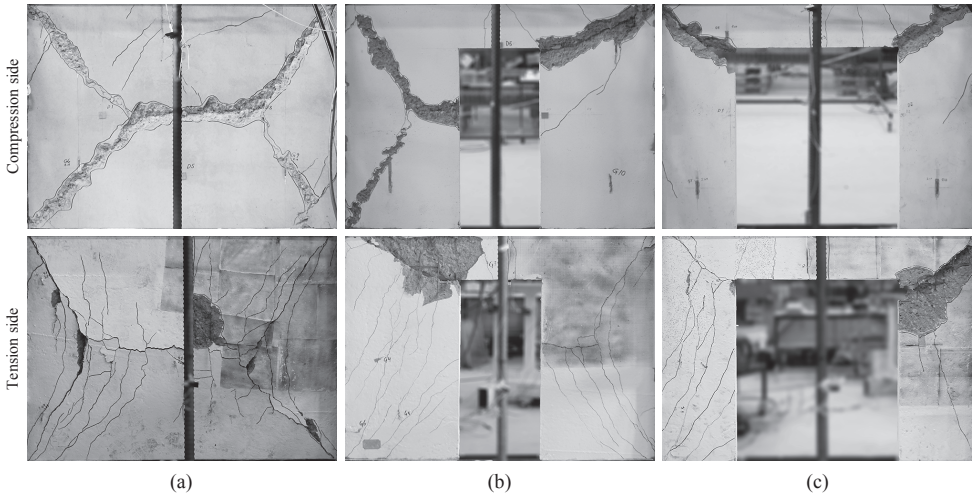


**Figure 3.7** Crack patterns and failure modes of the tested specimens: a) specimen I-C; b) specimen I-S and c) specimen I-L (reprinted from Popescu et al. 2016a)

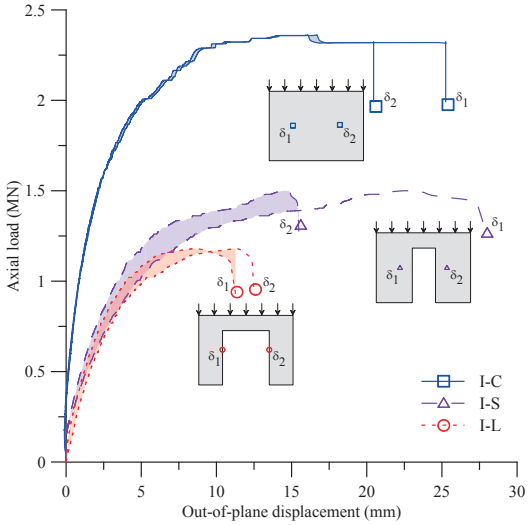


**Figure 3.8** Load-displacement responses for reference specimens; $\delta_1$ and $\delta_2$ refer to displacement sensors at indicated positions (Paper II for details)

The performances of existing design models were verified (see *Paper II*) against the experimental results in terms of ultimate capacity. Here, only the results obtained using the European (EN1992-1-1 2004) design model are presented. The equation used to predict the axial capacity of a solid wall was:

$$N_u = f_c \cdot L \cdot t \cdot \Phi \tag{3.9}$$

The above equation is valid for constant cross-sections along the height of the wall i.e. no openings. When openings with a considerable size (limits are given in Section 2.1) are created, the remaining portions are treated in accordance with the newly created boundary conditions i.e. restrained on two or three sides, in which case a different effective height factor β has to be used as defined in Eq. (3.4). This procedure helps to evaluate the ultimate capacity of individual elements, independently of the others. However, when openings exist, it is important to evaluate the strength of the entire system (in this context, walls with openings), but design codes do not provide such information. A simplified procedure is presented in *Paper II* (Popescu et al. 2016a) and the results are summarised in Table 3.1.

**Table 3.1** Summary of test results

| Specimen | $N_{exp}$ (kN) | $\mu_\Delta$ | $E_d$ (kNm) | $N_u/N_{exp}$ |
|---|---|---|---|---|
| I-C | 2363 | 4.05 | 39.37 | 0.93 |
| I-S | 1500 | 3.21 | 31.21 | 1.01 |
| I-L | 1180 | 2.78 | 10.88 | 1.12 |
| II-S | 2241 | 1.97 | 31.23 | 1.05[a)] |
| II-L | 1497 | 1.23 | 4.66 | 1.57[a)] |
| III-S1 | 2178 | 1.94 | 26.61 | 1.08[a)] |
| III-S2 | 2009 | 3.38 | 29.89 | 1.18[a)] |
| III-L1 | 1334 | 1.05 | 6.60 | 1.77[a)] |
| III-L2 | 1482 | 2.18 | 9.66 | 1.59[a)] |

[a)] The theoretical value equals peak load of the solid wall in accordance with the assumptions made in Section 3.1.3.

### 3.3 Concrete walls with cut-out openings strengthened by FRP confinement

The effectiveness of the selected strengthening method was investigated in two scenarios (Stages II and III as described in Section 3.1.1). First, the CFRP strengthening was applied to specimens that were already cracked which replicates situations where the addition of openings, and a subsequent sustained load, damages the wall. In the second scenario, unmodified specimens were strengthened with the CFRP system and then loaded to failure. The performance of the strengthening method was evaluated in terms of axial strength increase, ductility and energy release at failure, and steel reinforcement and CFRP strain utilisation. Only selected results are given here and the reader is referred to *Paper III* for more detailed results and analysis.

The strengthened specimens had lower deformations (thus increasing the stiffness) and higher capacity when compared with the unstrengthened ones, as can be seen in Fig. 3.9. The increase in capacity was in the range of 34 – 50% and 13 – 27% for specimens with small and large openings, respectively. However, the CFRP strengthening method did not fully restore the axial strength of a solid wall in any of the tests. It partially restored their capacities to 85 – 94.8% (for small opening) and 56.5 – 63.4% (for large opening) of that of a solid wall.

During the loading cycles, no cracks could be seen due to the fact that specimens were fully covered by FRP sheets. Therefore, the sound of cracking provided warning of imminent failure of the strengthened specimens rather than clear visual indications, such as deformation and cracking, as with the reference specimens. The strengthened walls failed due to crushing of concrete followed by debonding of the CFRP (Fig. 3.10). The failure was concentrated in smaller regions compared to reference specimens i.e. at the bottom of one of the piers. This was verified by stripping off the CFRP jacket upon completion of the testing.

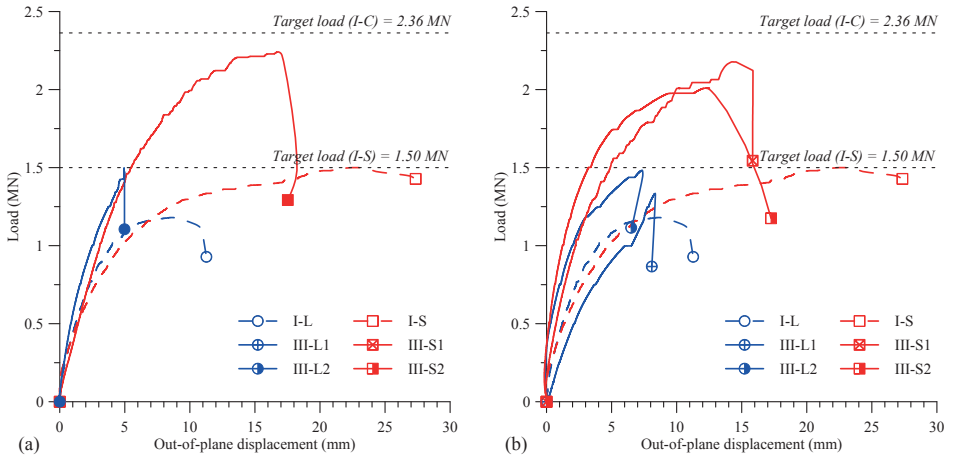


**Figure 3.9** Load-displacement curves for reference (Stage I) specimens: (a) pre-cracked strengthened (Stage II) specimens; (b) uncracked strengthened specimens (Stage III) (reprinted from Popescu et al. 2016b)

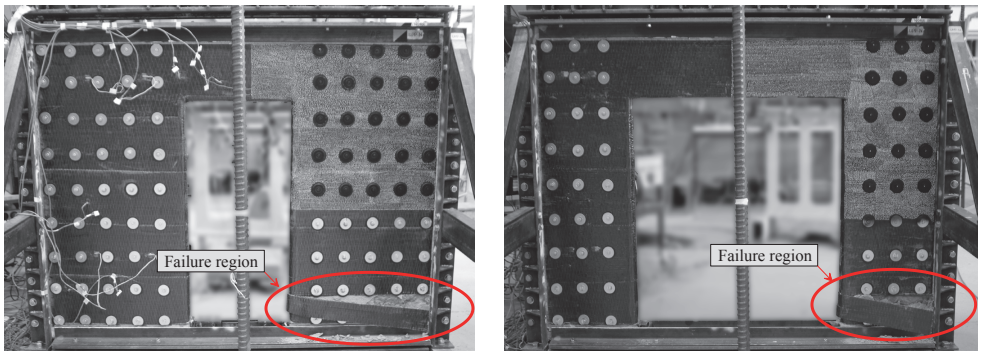


**Figure 3.10** Typical failure mode of strengthened walls

Strain readings were taken on the steel reinforcement and also on the CFRP sheets, at selected locations (see the instrumentation scheme in *Paper II* and *Paper III*). It was noted that the CFRP strengthening reduced strain on the steel reinforcement and no yielding or buckling of the reinforcement at failure was observed. Strains on the CFRP sheets recorded at peak load were recorded on both the tension and compression sides of the specimens. The strain gauges measured considerably lower strains than the ultimate strain specified by the manufacturer of the CFRP sheets (i.e. 19 ‰) with the highest value being recorded at the midspan of the spandrel, peaking at about 1.89 ‰. It should be noted that these values are measured strains and not necessarily the highest present in the specimens. Therefore, surface strain fields were determined using the ARAMIS system; these are not shown here but are plotted in *Paper III*. Since the test protocol was complex, one test for strengthened specimens took two hours. This could have affected the data collected by the ARAMIS system since the ambient light – subject to fast changes – may have influenced the readings. Displacement-based ductility ($\mu_\Delta$) factors and energy dissipation ($E_d$) were computed for all tested specimens and are listed in Table 3.1.

The predictions using the EC2 design model (EN1992-1-1 2004) for the unstrengthened walls were in good agreement with the test results. The same cannot be said for the strengthened ones; simplifications made in the pre-test design phase e.g. neglecting load eccentricity, seem to have produced inaccurate predictions. Thus, a design model capable of capturing complex effects such as load eccentricity and large aspect ratios of elements' cross-sections was proposed; its features are presented in Chapter 4.

# Chapter 4

# Failure load prediction using a rigid-plastic approach

## 4.1 Background

Current design codes offer little guidance on strengthening walls with openings, and less still on the use of non-metallic reinforcements such as CFRP to ensure sufficient load-carrying capacity. A review of design models capable of predicting the axial capacity of walls with openings was presented in *Paper I*. Most such models are empirical and calibrated using data from a limited range of OW and TW action tests. Moreover, it was only possible to identify a single study in the literature on the strengthening of axially-loaded concrete walls with cut-out openings using CFRP (Mohammed et al. 2013). Unfortunately, this study only considered OW walls, and so the associated design model is only valid for such walls. Therefore, there is a clear need for a theory-based method that can describe TW effects on panels restrained on all sides and also account for the effects of openings and the contribution of CFRP strengthening materials.

Information obtained from the analysis of failure modes of unstrengthened walls, reported in *Paper II,* was used to identify a suitable strengthening configuration. It was believed that by confining the wall piers with CFRP, an enhanced concrete compressive strength would be obtained. The strengthening design was carried out using a well-known confinement model proposed by Lam and Teng (2003). It is worth remembering that simplifications made in the pre-test design phase e.g. walls considered as concentrically loaded, may influence the performance of the design model (Lam and Teng 2003). However, the lack of better models prevented the incorporation of appropriate parameters to simulate all test characteristics such as load eccentricity or a biaxial effect. Also, the increase in capacity relative to reference specimens was somewhat higher for specimens with small openings. This suggests that, in addition to dilatation of concrete in compression, the yield lines developed at failure may further increase the capacity. Thus, the larger the yield lines, the greater the increase in capacity. The yield lines developed at failure, as a result of a biaxial effect (Fig. 3.7), were similar to that of a member under transverse loading. This similarity suggested that the ultimate load of concrete walls with cut-out openings should be evaluated using a rigid-plastic approach. This chapter introduces some of the principles of the rigid-plastic approach and its subsequent development for structural elements with openings strengthened with CFRP.

The *rigid-plastic* method assumes that no elastic displacements occur, implying a rigid behaviour

until the plastic plateau is reached. After this point, large deformations are allowed, however, without any change in the stress level (Nielsen 1999). This working assumption would make the formulation of the yield conditions rather complicated for elastic materials without a yield plateau. An example is the use of CFRP, where the fibres exhibit a linear-elastic behaviour with no plasticity. However, two attempts are proposed to incorporate the contribution of CFRP into the rigid-plastic approach. These refers to two scenarios: one when the panel is flexure-dominant (transverse loading) and the other when the panel is compression-dominant (in-plane loading). These are described in detail in *Paper IV* (for flexure-dominant specimens) and *Paper V* (for compression-dominant specimens), and only briefly presented herein.

## 4.2 Assumptions and yield conditions

The rigid-plastic approach is a well-known design method for slabs, also known as the *yield line theory*. The method was first described by Ingerslev (1923) and further developed by Johansen (1962). The analysis is carried out by means of *virtual work* or using the *equilibrium method*. In this study, the virtual work method was employed, in which a possible plastic collapse mechanism occurs along predefined yield lines. For assessment purposes, multiple collapse mechanisms are tested and the yield line solution is defined as the solution with the lowest load at failure. This process, especially for plates with asymmetric openings, includes several unknowns which define the theoretical positions of the yield lines. Due to nonlinearity of the equations, the mathematical procedures become laborious. In addition, the simplifications made to handle a specimen's boundaries (neither a perfect hinge nor a full rotation restraint could be achieved in the laboratory environment, much less in practice) may yield unsatisfactory results. However, it is well known that openings tend to attract yield lines (Nielsen 1999) and, thus, the most likely collapse mechanism can be easily predicted. This engineering judgement should preferably be supported by experimental evidence, FE analysis, or both. The yield conditions for all constituent materials involved in the analysis i.e. concrete, steel reinforcement and CFRP are briefly described now.

### *4.2.1 Concrete*

The concrete material is considered as meeting the modified Coulomb criterion with tensile strength neglected and introduced as zero tension cut-off. The ultimate strength of concrete under uniaxial stress state has to be reduced to an equivalent plastic compressive strength using an effectiveness factor, $\nu_1 < 1$, because of material brittleness and the influence of transverse strains on concrete strength (*fib* Model Code 2010 2013). Figure 4.1a shows both the real stress-strain law and the idealised failure criterion for concrete.

### *4.2.2 Reinforcement*

The steel reinforcement was also assumed to behave in a rigid-plastic manner in both tension and compression as seen in Fig. 4.1b. The value attributed to the plastic plateau was chosen as the yielding point reached in uniaxial tensile tests on reinforcement coupons.

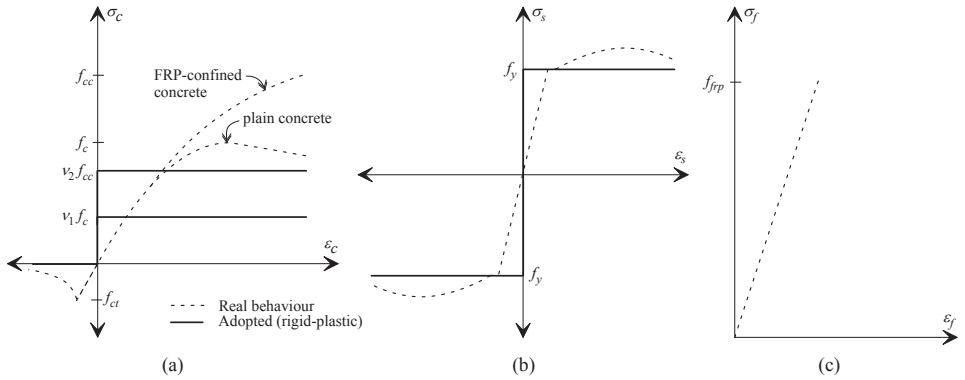


**Figure 4.1** Yield conditions for: (a) concrete; (b) steel reinforcement and (c) CFRP

### *4.2.3 Fibre-reinforced polymers*

In regards to non-metallic reinforcement i.e. CFRP, the real behaviour is linear elastic, retaining no plasticity or softening branch (Fig 4.1c). Two alternatives to account for CFRP contribution were selected, representing two different cases. In the first case, the yield point corresponds to the stress level associated with strain at debonding. This assumption is valid for flexure-dominant specimens where the interfaces between concrete and CFRP are prone to debond i.e. interlaminar crack debonding or end peeling. This scenario was investigated for *Paper IV*, where slabs with cut-out openings were strengthened with CFRP. The debonding value used was approximated using *fib* Bulletin 14 (2001). In the second case, valid for compression-dominant specimens (see *Paper V*), a proposal was made to update the concrete model using an enhanced confined compressive strength ($f_{cc}$) because of FRP confinement. The procedure uses the equations from Lam and Teng (2003), as discussed previously in Section 3.1.3, together with an updated effectiveness factor ($\nu_2$) which incorporates (in addition to material brittleness and the influence of transverse strains) eccentricity and slenderness effects.

## 4.3 Virtual work

This method assumes that the energy dissipated along the yield lines i.e. the internal work, is equal to the energy used by the applied loads i.e. the external work. This assumption yields a work equation of the following form:

$$\sum\left(\iint S_u \delta dxdy\right)_{\text{each region}} = \sum\left(\int m_b \theta ds\right)_{\text{each yield line}} \tag{4.1}$$

where the integrals on the left-hand and right-hand sides represent the external and internal work, respectively, with $S_u$ denoting the uniformly distributed load per unit area, $\delta$ the virtual displacement, $m_b$ the bending moment, and $\theta$ the rotation of the region about its axis of rotation. The bending moment along the yield line can be found by considering the equilibrium condition, as shown in Fig. 4.2:

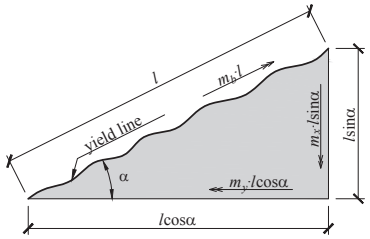


**Figure 4.2** Bending moment along a yield line

$$m_b l = \left(m_x \cdot l \sin\alpha\right)\sin\alpha + \left(m_y \cdot l \cos\alpha\right)\cos\alpha \tag{4.2}$$

$$m_b = m_x \sin^2\alpha + m_y \cos^2\alpha \tag{4.3}$$

where $m_x$, $m_y$ are the moment capacities per unit width in the $x$ and $y$ directions, respectively.

Equation (4.1) represents the classical solution, valid for plates loaded perpendicular to the mid-plane of the elements. A diagram used to develop a work equation applicable to situations where the transverse loads may be accompanied by in-plane loads is shown in Fig. 4.3.

The work equation now becomes:

$$\sum\left(\iint S_u \delta dxdy\right)_{\text{each region}} - \int\left(n_{ux,uy}\delta dx, y\right)_{\text{each boundary}} = \sum\left(\int m_b \theta ds\right)_{\text{each yield line}} \tag{4.4}$$

where $n_{ux}$, $n_{uy}$ are the uniform in-plane compressive force per unit length applied in the $x$ (horizontal) and $y$ (vertical) directions, respectively.

Depending on their magnitude, the compressive forces can either favourably contribute to the wall's capacity or govern its ultimate failure. For axially-loaded walls, these forces govern the failure which means that $n_{uy} >> S_u$. Therefore, the main contribution to the ultimate capacity comes from the concrete in compression (compressive membrane action) that depends solely on the concrete's plasticity. Considering the deflections of the wall reached before the plastic collapse, $\delta_{peak}$, the membrane moment [as proposed by Nielsen (1999)] can be expressed as:

$$m_c = \frac{1}{4} f_c \left(t - \delta_{peak}\right)^2 \tag{4.5}$$

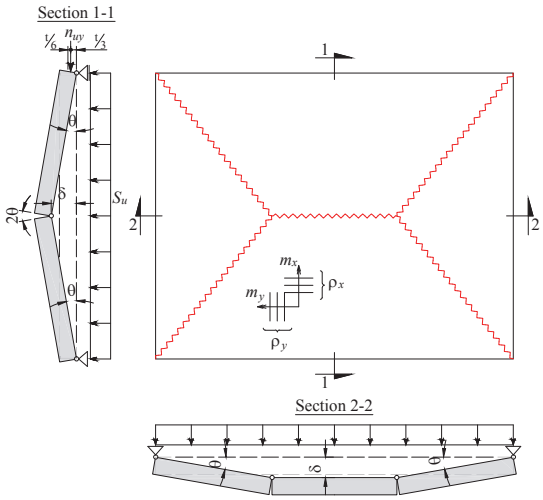


**Figure 4.3** Yield line pattern for a simply supported plate under in-plane and out-of-plane loads

The internal work is determined by replacing the bending moment $m_b$ with the membrane moment $m_c$ in the yield line solution. The compressive strength of concrete in Eq. (4.5) is modified by the effectiveness factors previously described. The derivation of internal and external work for axially-loaded walls was presented in *Paper V* and, for the sake of brevity, will not be reproduced here.

## 4.4 Comparison with experimental results

The average ratio of experimental to predicted loads was computed for both flexure-dominant (*Paper IV*) and compression-dominant (*Paper V*) failure modes. The strategy proposed showed that good predictions can be made when the yield line theory is employed. For specimens where the flexure governs the failure mode, average ratios between experimentally and theoretically determined capacity of 1.03 and a coefficient of variance of about 10% were obtained (Table 4.1). In the case of axially-loaded walls, this value was 1.06 with a coefficient of variance of about 13% (Table 4.2). In the latter case, the results for the FRP-strengthened walls were somewhat overestimated but were evaluated using a safety factor of 1; a carefully chosen safety factor must be used in practice.

**Table 4.1** Comparison of the measured ultimate flexural loads and yield line predictions

| Slab | Ultiamte axial load (kN) | | Accuracy |
|---|---|---|---|
| | Experimental ($S_{exp}$) | Predicted ($S_u$) | $S_{exp}/S_u$ |
| FS-01 | 118 | 122 | 0.97 |
| RSC-01 | 87 | 90 | 0.97 |
| RLC-01 | 75 | 62 | 1.20 |
| RLC-02 | 67 | 60 | 1.11 |
| FS-01-FRP | 186 | 180 | 1.03 |
| RSC-01-FRP | 86 | 82 | 1.05 |
| RLC-01-FRP | 75 | 86 | 0.87 |
| RLC-02-FRP | 147 | 137 | 1.07 |
| Average | | | 1.03 |
| CoV (%) | | | 9.97 |

Note: Presented data as taken from Floruţ et al. (2014)

**Table 4.2** Comparison of the measured ultimate axial loads and yield line predictions

| Wall | Ultimate axial load (kN) | | Accuracy |
|---|---|---|---|
| | Experimental ($N_{exp}$) | Predicted ($N_u$) | $N_{exp}/N_u$ |
| I-C | 2363 | 1872 | 1.26 |
| I-S | 1500 | 1328 | 1.13 |
| I-L | 1180 | 1046 | 1.13 |
| II-S | 2241 | 1942 | 1.15 |
| II-L | 1497 | 1569 | 0.95 |
| III-S1 | 2178 | 2034 | 1.07 |
| III-S2 | 2009 | 2520 | 0.80 |
| III-L1 | 1334 | 1230 | 1.08 |
| III-L2 | 1482 | 1504 | 0.99 |
| Average | | | 1.06 |
| CoV (%) | | | 12.7 |

Note: Presented data as taken from Popescu et al. (2016c)

It should be noted that the predictions made, presented in Table 4.1 and Table 4.2, are based on the failure mechanism observed in experimental tests. This is important since different mechanisms may arise for walls with different slenderness and/or aspect ratios. Furthermore, the presence of an opening may further complicate the issue, with its size and location likely to influence the type of failure mechanism. Thus, more tests are required, primarily regarding the effect of slenderness and aspect ratios, and also including walls with intermediate-sized openings. The model could further be improved by testing more walls with different eccentricities in order to calibrate the effectiveness factor to account for confinement non-uniformity.

# Chapter 5

# Conclusions and discussion

## 5.1 Research questions

In this section, the conclusions are formulated based on answers to the research questions. In addition, a general discussion will follow where future work is described. Four research questions were formulated in Chapter 1 of this thesis in order to comply with the aim of this research project. Based on the results obtained and described in *Papers I – V*, these questions are again addressed:

**I. Do existing models accurately predict the ultimate capacity of axially-loaded concrete walls with and without openings?**

From the literature review carried out for *Paper I,* existing design models were collected from major design codes and research literature. For solid walls, it was found that design models available from international standards provide conservative results, while those proposed in other studies (Robinson et al. 2013, Saheb and Desayi 1990a, 1989, Ganesan et al. 2012) showed a certain level of non-conservatism. Furthermore, only the European (EN1992-1-1 2004) and Australian (AS3600 2009) design codes account for the effects of restraining the lateral edges. This is in contrast to the American (CAN/CSA-A23.3 2004, ACI 318 2011) design code where only guidance for OW members is given. Failure to account for the effect of lateral restraints yields very conservative load predictions.

There are no straightforward methods in the design codes to evaluate the ultimate capacity of walls with openings. A simplified method which divides the wall with openings into isolated columns connected by beams is generally suggested. One can therefore find the capacity of individual members (i.e. piers) but not the strength of the entire system. A direct strategy was proposed in *Paper II* by idealising the entire ensemble as a hybrid system i.e. a combination of series and parallel subsystems. Here, the piers can be regarded as a parallel system with brittle elements connected in series with a spandrel above the openings. Using this procedure, design codes were in good agreement with test results.

Empirical design formulae can be found in the research literature that aim to predict the ultimate capacity of walls with openings. These were derived using limited test results, thus, giving in some cases, inaccurate predictions. The equations derived by Doh and Fragomeni (2005) and Doh and Fragomeni (2006), which address the axial strength of walls without and with openings,

respectively, provided good predictions when compared against test results. This conclusion is drawn on the basis of the statistical analysis of a database collected by the author and presented in *Paper I*. The findings provided in *Paper I*, together with the database, are useful because they highlight areas where the current literature is lacking, and where systematic studies could provide important insights into the behaviour of wall types that are poorly understood.

**II. What are the effects when cut-out openings are introduced into solid walls?**

Most previous studies of the effects of openings in RC walls have focused on design aspects of walls with appropriate reinforcement detailing around the edges of the openings. Moreover, the effects of door-type openings have not been investigated as intensively as window-type openings, and only one study (Mohammed et al. 2013) investigated the effects of window-type cut-out openings in OW walls. In addition, the existing knowledge was increased by the current study through the investigation of the failure progression using 3D-DIC and the addressing of serviceability aspects (crack widths) in assessments of walls with cut-out openings. Thus, this research question addresses a clear research gap.

To answer this question, three half-scaled specimens were loaded to failure and their structural behaviour monitored. These were a solid panel, a panel with a small opening and a panel with a large opening. The small and large openings represented 25% and 50% reductions, respectively, in the cross-sectional area of the solid wall. Thus, these tests enabled evaluation of the effects of creating new openings in a solid wall. The damage level was evaluated in terms of ultimate load, crack pattern, displacement profiles, strains in concrete and steel reinforcement, ductility, and energy release at failure (see *Paper II*). After validating the procedure proposed for evaluating the systems' capacity (see *research question I*), a parametric study was carried out to further understand the effects of opening sizes.

Test results indicated that the 25% and 50% reductions in cross-sectional area of the solid wall, caused by introducing the small and large opening, reduced the load-carrying capacity by nearly 36% and 50%, respectively. The parametric study carried out in *Paper II* revealed that the axial strength reduction is more sensitive to eccentricity when the opening size ratio ($A_0/A$, where $A$ and $A_0$ are the cross-sectional areas of the wall and opening, respectively) is minimal, and becomes less sensitive as this ratio increases. Furthermore, the axial strength declines nonlinearly as the opening size is increased.

The effect of a cut-out opening was also evaluated in terms of displacement-based ductility and energy dissipation, defined as the area under the load-displacement curves. Sharp reductions in computed factors were obtained when openings were created in solid walls. Thus, according to Park's classification (Park 1988), the walls with openings would be classified as elements with restricted ductility. The failure progression was monitored on a limited area using 3D-DIC measurements, which indicated a transition from a wall to a frame behaviour when the opening was enlarged from a small to a large one. However, in both scenarios, the failure was brittle due to crushing of concrete with spalling and reinforcement buckling.

**III. Does the failure mechanism of a concrete wall with an opening change after strengthening with CFRP?**

The most important outcome of the findings from the previous research question was the design of the strengthening configuration. It was decided that a strengthening configuration based on confinement is necessary, in order to recover the load-carrying capacity lost as a result of cutting new openings.

The CFRP strengthening increased the axial capacity of walls with small and large openings by 34 – 50% and 13 – 27%, respectively (see *Paper III*). This partially restored their load-carrying capacities to 85 – 95% and 57 – 63% of their precutting capacity (i.e. solid wall), respectively. After strengthening, however, reductions in energy dissipation and ductility factors were noted which reduce the system's effectiveness.

After strengthening with CFRP, the concrete crushing failure mode did not change. The failure mode was not as explosive as for the unstrengthened specimens and no reinforcement buckling was noted. The location where the crushing occurred was, however, changed. While crushing appeared along the diagonal line from wall corner to opening corner for unstrengthened walls, crushing at the bottom part of the piers occurred for strengthened ones. The opening was placed symmetrically and the piers were theoretically equal in capacity. When one of the piers failed, the entire wall triggered a failure of the other. Due to material randomness, uncertainty in boundary conditions and redistribution of stresses, it is therefore difficult to predict the exact location where the failure will occur.

**IV. Is it possible to adapt the rigid-plastic approach in order to devise a new model for RC walls strengthened using CFRPs?**

It was shown in *Paper I* that the empirical models available have certain shortcomings (for example, they rely on coefficients obtained by curve-fitting using limited data available at the time of development) and their application in practical contexts is likely to give rise to considerable variation in prediction accuracy, in terms of both understatement and overstatement. In addition, the experimental results showed [in contrast to what American (ACI 318 2011, CAN/CSA-A23.3 2004) design codes use] that the lateral restraints transform the problem into a plate mechanism rather than a one-dimensional problem. Therefore, there is a clear need for a theory-based method that can describe biaxial effects on panels restrained on all sides (see *Paper IV* and *V*). One such approach, adapted to predict the ultimate capacity of concrete walls strengthened by CFRP, is the rigid-plastic theory. It assumes a perfect plastic behaviour for all constituent materials, a limitation when linear-elastic materials (e.g. CFRP) are involved in the analysis. This drawback was avoided by indirectly taking into account the CFRP materials by updating the concrete model with an enhanced compressive strength (see *Paper V*). This enhanced capacity was achieved by confining the piers with CFRP sheets. In this way, reasonably good agreement with test results could be achieved, although some of the predictions were on the unsafe side. Further work will be required to vali-

date the model, including walls with different slenderness and aspect ratios, and load eccentricities, to make it practically useful in assessments. In conclusion, the author believes that the rigid-plastic approach is a valid way to evaluate the ultimate capacity of RC walls strengthened with FRP materials.

### 5.2 Future research and general discussion

Apart from the results obtained, expertise and experience, the author also gained an insight into the future work needed. Recommendations are given in the following, focusing on two topics: structural behaviour of RC walls with openings and strengthening strategies.

From the literature study, it was found that fewer tests exist for walls under TW action, walls with different size openings or higher eccentricities, so more tests are required in these experimental areas to facilitate the development of appropriate design models. Society calls for a better resource utilisation, and thus, the construction industry requires lighter and thinner (which implies greater slenderness) structural elements. This can usually be achieved by using materials such as ultra-high performance concrete. In order to extend the remit of the simplified design models (limited to a slenderness ratio – height/thickness – up to 30), more tests are required including walls with higher slenderness ratios. Experiments on walls are costly and time-consuming due to the more complex test set-up and mechanical behaviour. Therefore, nonlinear FE modelling could be a useful tool to supplement the tests and assess effects of the aforementioned parameters.

The experiments described were focused at a component level rather than on an entire building. In reality, structural changes – such as introducing new openings in solid walls – must be rigorously assessed prior to taking any decisions about the interventions required. At this stage, one can observe important additional capacities due to the membrane effect, redistribution of stresses and real boundary conditions (e.g. slabs, transversal walls, flanges/barbells). For example, many buildings have a ground floor that is higher than the upper floors, yet the door height remains the same. Thus, the part above the opening, that extends across the doorway, has a greater height-to-span ratio on the first floor. Thus, a deep beam behaviour would be expected, influencing the load distribution on the wall piers and, ultimately, the peak load. Again, nonlinear FE analyses may prove useful to evaluate the opening's effect accurately and to identify optimal strengthening procedures. For this, it would be relevant to carry out a parametric study on a real case study.

In order to make the CFRP strengthening method more effective, steel bolts were used as anchorages. As described previously, these were placed at certain distances and prestressed up to certain levels in order to provide an active confinement (Harajli and Hantouche 2015). Thus, the optimal distance (both horizontally and vertically) between steel anchorages should be further investigated. Moreover, it would be of interest to examine the influence of the prestressing force on the effectiveness of CFRP confinement.

The type of CFRP sheets used to strengthen the specimens was unidirectional. It is believed that bidirectional fibres may have been more effective in order to exploit the CFRP fibres better and further increase the axial strength. Similarly, to increase the effectiveness of the CFRP strengthening (in terms of ductility factors and energy dissipation), the use of a different system that uses mortar as

the bonding agent instead of epoxy (e.g. textile-reinforced mortars) could be an alternative. A study is currently underway at Luleå Univ. of Technology, where a number of walls with openings have been strengthened using textile-reinforced mortars.

The specimens were strengthened when they were unloaded. However, real walls are usually subjected to a relatively high sustained load. It is, therefore, necessary to take into account the effect of sustained loading when strengthening such elements or to unload the walls prior to applying the strengthening. The best situation would be to perform an in-situ application where the increasing availability of automated systems and sensor technology to monitor structure health can be exploited. In that way, a benchmark could be established and FE analyses extended to a variety of scenarios.

# References


ACI 224R-01 (2001). "Control of cracking in concrete structures." American Concrete Institute (ACI). ACI Committee 224, Farmington Hills, MI.

ACI 318 (2011). "Building code requirements for structural concrete and commentary ", American Concrete Institute (ACI), Farmington Hills, MI.

AS3600 (2009). "Concrete structures." Standards Australia, Sydney, Australia.

Ascent (2012). "Envelope tolerances for architectural precast." Precast/Prestressed Concrete Institute, Chicago, IL.

Bengtsson, B. A. (1946). "Om enkelarmering i centriskt belastade betongväggar." Chalmers Tekniska Högskola, Göteborg, Sweden.

Blanksvärd, T., Täljsten, B., and Carolin, A. (2009). "Shear strengthening of concrete structures with the use of mineral-based composites." *Journal of Composites for Construction*, 13(1), 25-34.

Blanksvärd, T. (2009). "Strengthening of concrete structures by the use of mineral-based composites." PhD Thesis, Luleå Univ. of Technology, Luleå, Sweden.

Box, G. E. P., Hunter, W. G., and Hunter, J. S. (1978). *Statistics for experimenters: An introduction to design, data analysis, and model building*, John Wiley & Sons, Inc, New York.

CAN/CSA-A23.3 (2004). "Design of concrete structures." Canadian Standards Association, Mississauga, Ontario.

Csoknyai, T., Hrabovszky-Horváth, S., Georgiev, Z., Jovanovic-Popovic, M., Stankovic, B., Villatoro, O., and Szendrő, G. (2016). "Building stock characteristics and energy performance of residential buildings in Eastern-European countries." *Energy and Buildings*, 132, 39-52.

De Luca, A., Nardone, F., Lignola, G.P., Prota, A., and Nanni, A. (2013). "Wall-like reinforced concrete columns externally confined by means of glass FRP laminates." *Advances in Structural Engineering*, 16(4), 593-604.

Delatte, N. (2009). *Failure, distress and repair of concrete structures*, Woodhead Publishing, Cambridge, UK.

Demeter, I. (2011). "Seismic retrofit of precast RC walls by externally bonded CFRP composites." PhD Thesis, Politehnica Univ. of Timisoara, Timisoara, Romania.

Doh, J., and Fragomeni, S. (2005). "Evaluation of experimental work on concrete walls in one-way and two-way action." *Australian Journal of Structural Engineering*, 6(1), 37–52.

Doh, J. H. (2002). "Experimental and theoretical studies of normal and high strength concrete wall panels." PhD Thesis, Griffith Univ., Gold Coast, Australia.

Doh, J. H., and Fragomeni, S. (2006). "Ultimate load formula for reinforced concrete wall panels with openings." *Advances in Structuctural Engineering*, 9(1), 103-115.

Dol, K., and Haffner, M. (2010). *Housing statistics in the European Union 2010*, OTB Research Institute for the Built Environment, Delft Univ. of Technology, Delft, Netherlands.

Econometrica Inc. (2007). *Measuring overcrowding in housing,* U.S. Department of Housing and Urban Development. Office of Policy Development and Research. Bethesda, Maryland.

EN1990 (2004). "Basis of structural design." European Committee for Standardization (CEN), Brussels, Belgium.

EN1992-1-1 (2004). "Design of concrete structures – Part 1–1: General rules and rules for buildings." European Committee for Standardization (CEN), Brussels, Belgium.

Engel, P. (n.d.). "General rehabilitation techniques using steel." <http://www.constructalia.com/english/renovation_with_steel/ii_general_rehabilitation_techniques_using_steel#.VMPsNP6G9Wg>. (2016.05.05).

Enochsson, O., Lundqvist, J., Täljsten, B., Rusinowski, P., and Olofsson, T. (2007). "CFRP strengthened openings in two-way concrete slabs – An experimental and numerical study." *Construction and Building Materials*, 21(4), 810-826.

Eriksson, A. (1978). "Structural behaviour of vertical joints in large panel buildings." PhD Thesis, Chalmers Tekniska Högskola, Göteborg, Sweden.

*fib* Bulletin 14 (2001). "Externally bonded FRP reinforcement for RC structures ", International Federation for Structural Concrete (FIB), Lausanne, Switzerland.

*fib* Model Code 2010 (2013). "*fib* Model Code 2010 for Concrete Structures." International Federation for Structural Concrete (FIB), Lausanne, Switzerland.

FIEC (2014). "Construction activity in Europe." European Construction Industry Federation (FIEC), Brussels, Belgium.

Floruţ, S.-C., Sas, G., Popescu, C., and Stoian, V. (2014). "Tests on reinforced concrete slabs with cut-out openings strengthened with fibre-reinforced polymers." *Composites Part B: Engineering*, 66C, 484–493.

Fragomeni, S. (1995). "Design of normal and high strength reinforced concrete walls." PhD Thesis, Univ. of Melbourne, Melbourne, Australia.

Fragomeni, S., Mendis, P. A., and Grayson, W. R. (1994). "Review of reinforced concrete wall design formulas." *ACI Structural Journal*, 91(5), 521-529.

Frangopol, D. M., and Liu, M. (2007). "Maintenance and management of civil infrastructure based on condition, safety, optimization, and life-cycle cost." *Structure and Infrastructure Engineering*, 3(1), 29-41.

Ganesan, N., Indira, P.V., and Rajendra Prasad, S. (2012). "Strength and behavior of SFRSCC and SFRC wall panels under one-way in-plane action." *High Performance Fiber Reinforced Cement Composites* (*HPFRCC 6*), Springer, Dordrecht, Netherlands, 279-286.

Ganesan, N., Indira, P.V., and Santhakumar, A. (2013). "Prediction of ultimate strength of reinforced geopolymer concrete wall panels in one-way action." *Construction and Building Materials*, 48, 91-97.

Glarbo, O. (1951). "Uarmerede betonvaegges baereevne."Ingenioren, Årg. 60, Nr. 25, 482-485, Copenhagen.

GOM mbH "ARAMIS - Optical 3D Deformation Analysis." <http://www.gom.com/metrology-systems/system-overview/aramis.html>. (2016-05-05).

Hanjari, K. Z., Utgenannt, P., and Lundgren, K. (2011). "Experimental study of the material and bond properties of frost-damaged concrete." *Cement and Concrete Research*, 41(3), 244-254.

Hansen, C. S., and Stang, H. (2012). "Modeling and characterization of strengthened concrete tension members." *Engineering Fracture Mechanics*, 82, 85-99.

Harajli, M. H., and Hantouche, E. G. (2015). "Effect of active versus passive confinement on seismic response of wide RC columns with lap splices." *Journal of Structural Engineering*, 141(9), 04014221.

Huang, Y., Hamed, E., Chang, Z.-T., and Foster, S. J. (2015). "Theoretical and experimental investigation of failure behavior of one-way high-strength concrete wall panels." *Journal of Structural Engineering*, 141(5), 04014143.

Ingerslev, A. (1923). "The strength of rectangular slabs." *Journal of Institution of Structural Engineers*, 1(1), 3–14.

Johansen, K. W. (1962). *Yield line theory*, Cement and Concrete Association, London.

Johnson, A. I. (1957). "Slanka oarmerade betongväggars hållfasthet."Nordisk Betong, Årg. 1, Nr. 2,, 75-83, Stockholm.

Karbhari, V. M., and Seible, F. (1998). "Design considerations for the use of fiber reinforced polymeric composites in the rehabilitation of concrete structures." *Proceedings of NIST Workshop on Standards Development for the Use of Fiber Reinbforced Polymers for the Rehabilitation of Concrete and Masonry Structures*, National Institute of Standards and Technology (NIST), Springfield, VA.

Lam, L., and Teng, J. G. (2003). "Design-oriented stress-strain model for FRP-confined concrete in rectangular columns." *Journal of Reinforced Plastics and Composites*, 22(13), 1149-1186.

Larsson, L.-E. (1959). "Bearing capacity of plain and reinforced concrete walls." PhD Thesis, Chalmers Tekniska Högskola, Göteborg, Sweden.

Lee, D.-J. (2008). "Experimental and theoretical study of normal and high strength concrete wall panels with openings." PhD Thesis, Griffith Univ., Gold Coast, Australia.

Li, B., Kai Qian, and Tran, C. T. N. (2013). "Retrofitting earthquake-damaged RC structural walls with openings by externally bonded FRP strips and sheets." *Journal of Composites for Construction*, 17(2), 259-270.

Liu, H.-X., Liu, G.-J., Wang, X.-Z., and Kong, X.-Q. (2015). "Effect of cross-sectional aspect ratio and basalt fiber-reinforced polymer-confined number on axial compression behavior of short columns." *Journal of Reinforced Plastics and Composites*, 34(10), 782-794.

Matthys, S., Toutanji, H., and Taerwe, L. (2006). "Stress–strain behavior of large-scale circular columns confined with FRP composites." *Journal of Structural Engineering*, 132(1), 123-133.

Mirmiran, A., Shahawy, M., Samaan, M., Echary, H., Mastrapa, J., Pico, O. (1998). "Effect of column parameters on FRP-confined concrete." *Journal of Composites for Construction*, 2(4), 175-185.

Mohammed, B., Ean, L. W., and Malek, M. A. (2013). "One way RC wall panels with openings strengthened with CFRP." *Construction and Building Materials*, 40, 575-583.

Mosallam, A. S., and Nasr, A. (2016). "Structural performance of RC shear walls with post-construction openings strengthened with FRP composite laminates." *Composites Part B: Engineering* (*in press*).

Nielsen, M. P. (1999). *Limit analysis and concrete plasticity, Second Edition*, CRC Press, Boca Raton, FL.

Oberlender, G. D., and Everard, N. J. (1977). "Investigation of reinforced concrete walls." *ACI Structural Journal*, 74(6), 256-263.

Park, R. (1988). "State of the art report: Ductility evaluation from laboratory and analytical testing." *Proceedings of 9th World Conference on Earthquake Engineering,* Vol.VIII, International Association for Earthquake Engineering (IAEE), Tokyo, 605-616.

Pessiki, S., Harries, K.A., Kestner, J.T., Sause, R., Ricles, J.M. (2001). "Axial behavior of reinforced concrete columns confined with FRP jackets." *Journal of Composites for Construction*, 5(4), 237-245.

Pillai, S. U., and Parthasarathy, C.V. (1977). "Ultimate strength and design of concrete walls." *Build ing and Environment*, 12(1), 25-29.

Plos, M., Shu, J., Zandi, K., and Lundgren, K. (2017). "A multi-level structural assessment strategy for reinforced concrete bridge deck slabs." *Structure and Infrastructure Engineering*, 13(2), 223-241.

Popescu, C., Sas, G., Blanksvärd, T., and Täljsten, B. (2015). "Concrete walls weakened by openings as compression members: A review." *Engineering Structures*, 89, 172-190.

Popescu, C., Sas, G., Sabău, C., and Blanksvärd, T. (2016a). "Effect of cut-out openings on the axial strength of concrete walls." *Journal of Structural Engineering*, 142(11), 04016100.

Popescu, C. (2015). "FRP strengthening of concrete walls with openings." Licentiate Thesis, Luleå Univ. of Technology, Luleå, Sweden.

Popescu, C., Sas, G., Blanksvärd, T., and Täljsten, B. (2016b). "Concrete walls with cut-out openings strengthened by FRP-confinement." *Journal of Composites for Construction*, (*in press*).

Popescu, C., and Sas, G. (2014). "The development of an experimental program through design of experiments and FEM analysis: A preliminary study." *Nordic Concrete Research*, 51, 29-42.

Popescu, C., Schmidt, J. W., Goltermann, P., and Sas, G. (2016c). "Assessment of RC walls with cut-out openings strengthened by FRP using a rigid-plastic approach." Submitted to *Engineering Structures*.

Prota, A., Manfredi, G., and Cosenza, E. (2006). "Ultimate behavior of axially loaded RC wall-like columns confined with GFRP." *Composites Part B: Engineering*, 37(7–8), 670-678.

Puurula, A. M., Enochsson, O., Sas, G., Blanksvärd, T., Ohlsson, U., Bernspång, L., Täljsten, B., Carolin, A., Paulsson, B., and Elfgren, L. (2015). "Assessment of the strengthening of an RC railway bridge with CFRP utilizing a full-scale failure test and finite-element analysis." *Journal of Structural Engineering*, 141(1), D4014008.

Reu, P. (2012). "Hidden Components of DIC: Calibration and Shape Function – Part 1." *Experimental Techniques*, 36(2), 3-5.

Richart, F. E., and Newmark, N. M. (1935). "The strength of monolithic concrete walls." Univ. of Illinois, Engineering Experiment Station, Bulletin No. 277, Urbana, IL.

RILEM TC 50-FMC (1985). "Determination of the fracture energy of mortar and concrete by means of three-point bend tests on notched beams." *Materials and Structures*, 18(4), 287-290.

Robinson, G., Palmeri, A., and Austin, S. (2013). "Design methodologies for one way spanning eccentrically loaded minimally or centrally reinforced pre-cast RC panels." *Engineering Structures*, 56, 1945-1956.

Rocca, S., Galati, N., and Nanni, A. (2008). "Review of design guidelines for FRP confinement of reinforced concrete columns of noncircular cross sections." *Journal of Composites for Construction*, 12(1), 80-92.

Safi, M., Sundquist, H., and Karoumi, R. (2015). "Cost-efficient procurement of bridge infrastructures by incorporating life-cycle cost analysis with bridge management systems." *Journal of Bridge Engineering*, 20(6), 04014083.

Saheb, M., and Desayi, P. (1989). "Ultimate strength of RC wall panels in one-way in-plane action." *Journal of Structural Engineering*, 115(10), 2617-2630.

Saheb, S.M., and Desayi, P. (1990a). "Ultimate strength of RC wall panels in two-way in-plane action." *Journal of Structural Engineering*, 116(5), 1384-1402.

Saheb, M., and Desayi, P. (1990b). "Ultimate strength of RC wall panels with openings." *Journal of Structural Engineering*, 116(6), 1565-1578.

Schlune, H., Plos, M., and Gylltoft, K. (2012). "Safety formats for non-linear analysis of concrete structures." *Magazine of Concrete Research*, 64(7), 563-574.

Seddon, A. E. (1956a). "The strength of concrete walls under axial and eccentric loads." *Symposium on the Strength of Concrete Structures,* Cement and Concrete Association, London, 445-486.

Seddon, A. E. (1956b). "Concrete walls in compression under short-term axial and eccentric loads." International Association for Bridge and Structural Engineering (IABSE), Zürich, Switzerland

Silfwerbrand, J. L. "Improving preventive bridge maintenance." American Concrete Institute (ACI) *Special Publication*, 277, 67-78.

SS-EN 12390-3:2009 (2009). "Testing hardened concrete – Part 3: Compressive strength of test specimens." Swedish Standards Institute (SIS), Stockholm, Sweden.

SS-EN ISO 898-1 (2013). "Mechanical properties of fasteners made of carbon steel and alloy steel - Part 1: Bolts, screws and studs with specified property classes - Coarse thread and fine pitch thread." Swedish Standards Institute (SIS), Stockholm, Sweden.

SS-EN ISO 6892-1:2009 (2009). "Metallic materials – Tensile testing – Part 1: Method of test at room temperature." Swedish Standards Institute (SIS), Stockholm, Sweden.

Swartz, S. E., Rosebraugh, V. H., and Rogacki, S. A. (1974). "A method for determining the buckling strength of concrete panels." *Experimental Mechanics*, 14(4), 138-144.

Svenska Cementföreningen (1935). "Provning av enkelarmerade och dubbelarmerade betongväggar." Chalmers Materialprovningsanstalt.

Tan, K. H. (2002). "Strength enhancement of rectangular reinforced concrete columns using fiber-reinforced polymer." *Journal of Composites for Construction*, 6(3), 175-183.

Tanwongsval, S., Maalej, M., and Paramasivam, P. (2003). "Strengthening of RC wall-like columns with FRP under sustained loading." *Materials and Structures*, 36(5), 282-290.

Timoshenko, S. P., and Gere, J. M. (1961). *Theory of Elastic Stability*, McGRAW-HILL International Book Co., New York.

Todut, C., Dan, D., and Stoian, V. (2015). "Numerical and experimental investigation on seismically damaged reinforced concrete wall panels retrofitted with FRP composites." *Composite Structures*, 119, 648-665.

Triantafillou, T. C., Choutopoulou, E., Fotaki, E., Skorda, M., Stathopoulou, M., and Karlos, K. (2016). "FRP confinement of wall-like reinforced concrete columns." *Materials and Structures*, 49(1), 651-664.

Täljsten, B., Blanksvärd, T., and Sas, G. (2012). *Handbok för dimensionering och utförande i samband med förstärkning av betongkonstruktioner med pålimmade fiberkompositer*, Luleå Univ. of Technology, Luleå, Sweden.

Täljsten, B., Carolin, A., and Nordin, H. (2003). "Concrete structures strengthened with near surface mounted reinforcement of CFRP." *Advances in Structural Engineering*, 6(3), 201-213.

Vu, K. A. T., and Stewart, M. G. (2000). "Structural reliability of concrete bridges including improved chloride-induced corrosion models." *Structural Safety*, 22(4), 313-333.

Wu, Y.-F., and Wei, Y.-Y. (2010). "Effect of cross-sectional aspect ratio on the strength of CFRP-confined rectangular concrete columns." *Engineering Structures*, 32(1), 32-45.

Zielinski, Z. A., Troitsky, M. S., and Christodoulou, H. (1982). "Full-scale bearing strength Investigation of thin wall-ribbed reinforced concrete panels." *ACI Structural Journal*, 79(4), 313-321.

# Doctoral and licentiate theses

**Division of Structural and Fire Engineering**
**Luleå University of Technology**

**Doctoral theses**

1980 Ulf Arne Girhammar: *Dynamic fail-safe behaviour of steel structures*. Doctoral Thesis 1980:060D. 309 pp.

1983 Kent Gylltoft: *Fracture mechanics models for fatigue in concrete structures*. Doctoral Thesis 1983:25D. 210 pp.

1985 Thomas Olofsson: *Mathematical modelling of jointed rock masses*. Doctoral Thesis 1985:42D. 143 pp. (In collaboration with the Division of Rock Mechanics).

1988 Lennart Fransson: *Thermal ice pressure on structures in ice covers*. Doctoral Thesis 1988:67D. 161 pp.

1989 Mats Emborg: *Thermal stresses in concrete structures at early ages*. Doctoral Thesis 1989:73D. 285 pp.

1993 Lars Stehn: *Tensile fracture of ice. Test methods and fracture mechanics analysis*. Doctoral Thesis 1993:129D, September 1993. 136 pp.

1994 Björn Täljsten: *Plate bonding. Strengthening of existing concrete structures with epoxy bonded plates of steel or fibre reinforced plastics*. Doctoral Thesis 1994:152D, August 1994. 283 pp.

1994 Jan-Erik Jonasson: *Modelling of temperature, moisture and stresses in young concrete*. Doctoral Thesis 1994:153D, August 1994. 227 pp.

1995 Ulf Ohlsson: *Fracture mechanics analysis of concrete structures*. Doctoral Thesis 1995:179D, December 1995. 98 pp.

1998 Keivan Noghabai: *Effect of tension softening on the performance of concrete structures*. Doctoral Thesis 1998:21, August 1998. 150 pp.

1999 Gustaf Westman: *Concrete creep and thermal stresses. New creep models and their effects on stress development*. Doctoral Thesis 1999:10, May 1999. 301 pp.

1999 Henrik Gabrielsson: *Ductility in high performance concrete structures. An experimental investigation and a theoretical study of prestressed hollow core slabs and prestressed cylindrical pole elements*. Doctoral Thesis 1999:15, May 1999. 283 pp.

2000 Patrik Groth: Fibre r*einforced concrete – Fracture mechanics methods applied on self-compacting concrete and energetically modified binders*. Doctoral Thesis 2000:04, January 2000. 214 pp. ISBN 978-91-85685-00-4.

2000 Hans Hedlund: *Hardening concrete. Measurements and evaluation of non-elastic deformation and associated restraint stresses*. Doctoral Thesis 2000:25, December 2000. 394 pp. ISBN 91-89580-00-1.

2003 Anders Carolin: *Carbon fibre reinforced polymers for strengthening of structural members*. Doctoral Thesis 2003:18, June 2003. 190 pp. ISBN 91-89580-04-4.

2003 Martin Nilsson: *Restraint factors and partial coefficients for crack risk analyses of early age concrete structures*. Doctoral Thesis 2003:19, June 2003. 170 pp. ISBN: 91-89580-05-2.

2003 Mårten Larson: *Thermal crack estimation in early age concrete – Models and methods for practical application*. Doctoral Thesis 2003:20, June 2003. 190 pp. ISBN 91-86580-06-0.

2005 Erik Nordström: *Durability of sprayed concrete. Steel fibre corrosion in cracks*. Doctoral Thesis 2005:02, January 2005. 151 pp. ISBN 978-91-85685-01-1.

2006 Rogier Jongeling: *A process model for work-flow management in construction. Combined use of location-based scheduling and 4D CAD*. Doctoral Thesis 2006:47, October 2006. 191 pp. ISBN 978-91-85685-02-8.

2006 Jonas Carlswärd: *Shrinkage cracking of steel fibre reinforced self compacting concrete overlays – Test methods and theoretical modelling*. Doctoral Thesis 2006:55, December 2006. 250 pp. ISBN 978-91-85685-04-2.

2006 Håkan Thun: *Assessment of fatigue resistance and strength in existing concrete structures*. Doctoral Thesis 2006:65, December 2006. 169 pp. ISBN 978-91-85685-03-5.

2007 Lundqvist Joakim: *Numerical analysis of concrete elements strengthened with carbon fiber reinforced polymers*. Doctoral Thesis 2007:07, March 2007. 50 pp. ISBN 978-91-85685-06-6.

2007 Arvid Hejll: *Civil structural health monitoring – Strategies, methods and applications*. Doctoral Thesis 2007:10, March 2007. 189 pp. ISBN 978-91-85685-08-0.

2007 Stefan Woksepp: *Virtual reality in construction: Tools, methods and processes*. Doctoral Thesis 2007:49, November 2007. 191 pp. ISBN 978-91-85685-09-7.

2007 Romuald Rwamamara: *Planning the healthy construction workplace through risk assessment and design methods*. Doctoral Thesis 2007:74, November 2007. 179 pp. ISBN 978-91-85685-11-0.

2008 Björnar Sand: *Nonlinear finite element simulations of ice forces on offshore structures*. Doctoral Thesis 2008:39, September 2008. 241 pp.

2008 Bengt Toolanen: *Lean contracting: relational contracting influenced by lean thinking*. Doctoral Thesis 2008:41, October 2008. 190 pp.

2008 Sofia Utsi: *Performance based concrete mix-design: Aggregate and micro mortar optimization applied on self-compacting concrete containing fly ash*. Doctoral Thesis 2008:49, November 2008. 190 pp.

2009 Markus Bergström: *Assessment of existing concrete bridges: Bending stiffness as a performance indicator*. Doctoral Thesis, March 2009. 241 pp. ISBN 978-91-86233-11-2.

2009 Tobias Larsson: *Fatigue assessment of riveted bridges*. Doctoral Thesis, March 2009. 165 pp. ISBN 978-91-86233-13-6.

2009 Thomas Blanksvärd: *Strengthening of concrete structures by the use of mineral based composites: System and design models for flexure and shear*. Doctoral Thesis, April 2009. 156 pp. ISBN 978-91-86233-23-5.

2011 Anders Bennitz: *Externally unbonded post-tensioned CFRP tendons – A system solution*. Doctoral Thesis, February 2011. 68 pp. ISBN 978-91-7439-206-7.

2011 Gabriel Sas: *FRP shear strengthening of reinforced concrete beams*. Doctoral Thesis, April 2011. 97 pp. ISBN 978-91-7439-239-5.

2011 Peter Simonsson: *Buildability of concrete structures: processes, methods and material*. Doctoral Thesis, April 2011. 64 pp. ISBN 978-91-7439-243-2.

2011 Stig Bernander: *Progressive landslides in long natural slopes. Formation, potential extension and configuration of finished slides in strain-softening soils*. Doctoral Thesis, May 2011, rev. August 2011 and April 2012. 250 pp. ISBN 978-91-7439-238-8. (In collaboration with the Division of Soil Mechanics and Foundation Engineering).

2012 Arto Puurula: *Load carrying capacity of a strengthened reinforced concrete bridge: non-linear finite element modeling of a test to failure. Assessment of train load capacity of a two span railway trough bridge in* Örnsköldsvik *strengthened with bars of carbon fibre reinforced polymers (CFRP)*. Doctoral Thesis, May 2012. 100 pp. ISBN 978-91-7439-433-7.

2015 Mohammed Salih Mohammed Mahal: *Fatigue behaviour of RC beams strengthened with CFRP, Analytical and experimental investigations*. Doctoral Thesis, March 2015. 138 pp. ISBN 978-91-7583-234-0.

2015 Jonny Nilimaa: C*oncrete bridges: Improved load capacity*. Doctoral Thesis, June 2015. 180 pp. ISBN 978-91-7583-344-6.

2015 Tarek Edrees Saaed: *Structural control and identification of civil engineering structures*. Doctoral Thesis, June 2015. 314 pp. ISBN 978-91-7583-241-8.

2015 Majid Al-Gburi: *Restraint effect in early age concrete structures*. Doctoral Thesis, September 2015. 190 pp. ISBN 978-91-7583-374-3.

**Licentiate theses**

1984 Lennart Fransson: *Bärförmåga hos ett flytande istäcke. Beräkningsmodeller och experimentella studier av naturlig is och av is förstärkt med armering*. Licentiate Thesis 1984:012L. 137 pp. (In Swedish).

1985 Mats Emborg: *Temperature stresses in massive concrete structures. Viscoelastic models and laboratory tests*. Licentiate Thesis 1985:011L, May 1985. rev. November 1985. 163 pp.

1987 Christer Hjalmarsson: *Effektbehov i bostadshus. Experimentell bestämning av effektbehov i små- och flerbostadshus*. Licentiate Thesis 1987:009L, October 1987. 72 pp. (In Swedish).

1990 Björn Täljsten: *Förstärkning av betongkonstruktioner genom pålimning av stålplåtar*. Licentiate Thesis 1990:06L, May 1990. 205 pp. (In Swedish).

1990 Ulf Ohlsson: *Fracture mechanics studies of concrete structures*. Licentiate Thesis 1990:07L, May 1990. 66 pp.

1990 Lars Stehn: *Fracture toughness of sea ice. Development of a test system based on chevron notched specimens*. Licentiate Thesis 1990:11L, September 1990. 88 pp.

1992 Per Anders Daerga: *Some experimental fracture mechanics studies in mode I of concrete and wood*. Licentiate Thesis 1992:12L, April 1992, rev. June 1992. 81 pp.

1993 Henrik Gabrielsson: *Shear capacity of beams of reinforced high performance concrete*. Licentiate Thesis 1993:21L, May 1993. 109 pp.

1995 Keivan Noghabai: *Splitting of concrete in the anchoring zone of deformed bars. A fracture mechanics approach to bond*. Licentiate Thesis 1995:26L, May 1995. 123 pp.

1995 Gustaf Westman: *Thermal cracking in high performance concrete. Viscoelastic models and laboratory tests*. Licentiate Thesis 1995:27L, May 1995. 125 pp.

1995 Katarina Ekerfors: *Mognadsutveckling i ung betong. Temperaturkänslighet, hållfasthet och värmeutveckling*. Licentiate Thesis 1995:34L, October 1995. 137 pp. (In Swedish).

1996 Patrik Groth: *Cracking in concrete. Crack prevention with air-cooling and crack distribution with steel fibre reinforcement*. Licentiate Thesis 1996:37L, October 1996. 128 pp.

1996 Hans Hedlund: *Stresses in high performance concrete due to temperature and moisture variations at early ages*. Licentiate Thesis 1996:38L, October 1996. 240 pp.

2000 Mårten Larson: *Estimation of crack risk in early age concrete. Simplified methods for practical use*. Licentiate Thesis 2000:10, April 2000. 170 pp.

2000 Stig Bernander: *Progressive landslides in long natural slopes. Formation, potential extension and configuration of finished slides in strain-softening soils*. Licentiate Thesis 2000:16, May 2000. 137 pp. (In collaboration with the Division of Soil Mechanics and Foundation Engineering).

2000 Martin Nilsson: *Thermal cracking of young concrete. Partial coefficients, restraint effects and influences of casting joints*. Licentiate Thesis 2000:27, October 2000. 267 pp.

2000 Erik Nordström: *Steel fibre corrosion in cracks. Durability of sprayed concrete*. Licentiate Thesis 2000:49, December 2000. 103 pp.

2001 Anders Carolin: *Strengthening of concrete structures with CFRP – Shear strengthening and full-scale applications*. Licentiate thesis 2001:01, June 2001. 120 pp. ISBN 91-89580-01-X.

2001 Håkan Thun: *Evaluation of concrete structures. Strength development and fatigue capacity*. Licentiate Thesis 2001:25, June 2001. 164 pp. ISBN 91-89580-08-2.

2002 Patrice Godonue: *Preliminary design and analysis of pedestrian FRP bridge deck*. Licentiate Thesis 2002:18. 203 pp.

2002 Jonas Carlswärd: *Steel fibre reinforced concrete toppings exposed to shrinkage and temperature deformations*. Licentiate Thesis 2002:33, August 2002. 112 pp.

2003 Sofia Utsi: *Self-compacting concrete – Properties of fresh and hardening concrete for civil engineering applications*. Licentiate Thesis 2003:19, June 2003. 185 pp.

2003 Anders Rönneblad: *Product models for concrete structures – Standards, applications and implementations*. Licentiate Thesis 2003:22, June 2003. 104 pp.

2003 Håkan Nordin: *Strengthening of concrete structures with pre-stressed CFRP*. Licentiate Thesis 2003:25, June 2003. 125 pp.

2004 Arto Puurula: *Assessment of prestressed concrete bridges loaded in combined shear, torsion and bending*. Licentiate Thesis 2004:43, November 2004. 212 pp.

2004 Arvid Hejll: *Structural health monitoring of bridges. Monitor, assess and retrofit*. Licentiate Thesis 2004:46, November 2004. 128 pp.

2005 Ola Enochsson: *CFRP strengthening of concrete slabs, with and without openings. Experiment, analysis, design and field application*. Licentiate Thesis 2005:87, November 2005. 154 pp.

2006 Markus Bergström: *Life cycle behaviour of concrete structures – Laboratory test and probabilistic evaluation*. Licentiate Thesis 2006:59, December 2006. 173 pp. ISBN 978-91-85685-05-9.

2007 Thomas Blanksvärd: *Strengthening of concrete structures by mineral based composites*. Licentiate Thesis 2007:15, March 2007. 300 pp. ISBN 978-91-85685-07-3.

2008 Peter Simonsson: *Industrial bridge construction with cast in place concrete: New production methods and lean construction philosophies*. Licentiate Thesis 2008:17, May 2008. 164 pp. ISBN 978-91-85685-12-7.

2008 Anders Stenlund: *Load carrying capacity of bridges: Three case studies of bridges in northern Sweden where probabilistic methods have been used to study effects of monitoring and strengthening*. Licentiate Thesis 2008:18, May 2008. 306 pp. ISBN 978-91-85685-13-4.

2008 Anders Bennitz: *Mechanical anchorage of prestressed CFRP tendons – Theory and tests*. Licentiate Thesis 2008:32, November 2008. 319 pp.

2008 Gabriel Sas: *FRP shear strengthening of RC beams and walls*. Licentiate Thesis 2008:39, December 2008. 107 pp.

2010 Tomas Sandström: *Durability of concrete hydropower structures when repaired with concrete overlays*. Licentiate Thesis, February 2010. 179 pp. ISBN 978-91-7439-074-2.

2013 Johan Larsson: *Mapping the concept of industrialized bridge construction: Potentials and obstacles*. Licentiate Thesis, January 2013. 66 pp. ISBN 978-91-7439-543-3.

2013 Jonny Nilimaa: *Upgrading concrete bridges: Post-tensioning for higher loads*. Licentiate Thesis, January 2013. 300 pp. ISBN 978-91-7439-546-4.

2013 Katalin Orosz: *Tensile behaviour of mineral-based composites*. Licentiate Thesis, May 2013. 92 pp. ISBN 978-91-7439-663-8.

2013 Peter Fjellström: *Measurement and modelling of young concrete properties*. Licentiate Thesis, May 2013. 121 pp. ISBN 978-91-7439-644-7.

2014 Majid Al-Gburi: *Restraint in structures with young concrete: Tools and estimations for practical use*. Licentiate Thesis, September 2014. 106 pp. ISBN 978-91-7439-977-6.

2014 Niklas Bagge: *Assessment of concrete bridges models and tests for refined capacity estimates*. Licentiate Thesis, November 2014. 132 pp. ISBN 978-91-7583-163-3.

2014 Tarek Edrees Saaed: *Structural identification of civil engineering structures*. Licentiate Thesis, November 2014. 135 pp. ISBN 978-91-7583-053-7.

2015 Cosmin Popescu: *FRP strengthening of concrete walls with openings*. Licentiate Thesis, December 2015. 134 pp. ISBN 978-91-7583-453-5.

2016 Faez Sayahi: *Plastic shrinkage cracking in concrete.* Licentiate Thesis, November 2016. 134 pp. ISBN: 978-91-7583-678-2.

2016 Jens Häggström: *Evaluation of the load carrying capacity of a steel truss railway bridge: testing, theory and evaluation*. Licentiate Thesis, December 2016. 139 pp. ISBN: 978-91-7583-739-0.

# Paper I

## Concrete walls weakened by openings as compression members: A review

Cosmin Popescu; Gabriel Sas; Thomas Blanksvärd; and Björn Täljsten

Published in:
*Engineering Structures*
Vol. 89, 2015
pp. 172–190

Engineering Structures 89 (2015) 172–190

Contents lists available at ScienceDirect

Engineering Structures

journal homepage: www.elsevier.com/locate/engstruct

Review article

# Concrete walls weakened by openings as compression members: A review

Cosmin Popescu [a,*], Gabriel Sas [b], Thomas Blanksvärd [a], Björn Täljsten [a]

[a] Luleå University of Technology, SE-97187, Sweden
[b] NORUT, Rombaksveien E-6 47, N-8517 Narvik, Norway

ARTICLE INFO

*Article history:*
Received 17 October 2014
Revised 4 February 2015
Accepted 5 February 2015
Available online 25 February 2015

*Keywords:*
Concrete walls
Openings
Axial load
Eccentricity
Out-of-plane behaviour
FRP
Strengthening

ABSTRACT

The purpose of this paper is to review the advances that have been made in the design of monolithic and precast reinforced concrete walls, both with and without openings, subject to eccentrically applied axial loads. Using the results of previous experimental studies, a database was assembled to enable statistical assessment of the reliability of existing design models. Several design aspects are highlighted, including the size and position of openings, and the roles of boundary conditions and geometric characteristics. In addition, the performance of fiber-reinforced polymers in strengthening wall openings is discussed. Overall it is found that design codes provide more conservative results than alternative design models that have been proposed in recent studies. Research into the strengthening of walls with openings is still in its early stages, and further studies in this area are needed. The paper therefore concludes by highlighting some areas where new investigations could provide important insights into the structural behaviour of strengthened elements.


**Contents**



* Corresponding author. Tel.: +46 702375433.
*E-mail addresses:* cosmin.popescu@ltu.se (C. Popescu), gabriel.sas@norut.no (G. Sas), thomas.blanksvard@ltu.se (T. Blanksvärd), bjorn.taljsten@ltu.se (B. Täljsten).

http://dx.doi.org/10.1016/j.engstruct.2015.02.006
0141-0296/

## 1. Introduction

Sustainable social development requires a safe, functional and durable built environment. Many structures around the world are made of reinforced concrete (RC), most of which were built before 1970 [1]. Functional modifications of these structures are common because existing structures must often be adapted to comply with current living standards. Such modifications may include the addition of new windows or doors and paths for ventilation and heating systems, all of which require openings to be cut into structural walls.

These openings can be divided into three types, namely already existing openings, existing openings that have been enlarged and newly created openings. Creating or modifying openings in walls may change the stress distribution within the wall, adversely influencing its behaviour. It is generally believed that the effects of small openings can often be neglected, while the presence of a large opening usually significantly alters the structural system [2]. However, in the existing literature there is currently no clear delimitation between small and large openings.

Experimental investigations have shown that cutting an opening into an RC wall decreases its ultimate load capacity, requiring the wall to be upgraded [3,4]. Traditionally, two methods have been used to strengthen RC walls with openings, these being either to create a frame around the opening using RC/steel members [5] or to increase the cross-sectional thickness [6]. Both methods increase the weight of the strengthened elements and may cause significant inconvenience by limiting the use of the structure during repairs. A superior alternative that has been used successfully in diverse contexts [7–10] is to use fiber-reinforced polymers (FRP) as the externally bonded material. This technique requires that thin laminates or bars be bonded to the surface of the structure using an adhesive to form a composite material.

The following sections provide a review of contemporary wall design methods that have been included in various design codes [11–14]. Two different design methods can be identified in these documents: (1) a simplified design method and (2) a method based on column theory; the latter is arguably the more rational approach. Although the simplified method is straightforward to implement, its applicability becomes limited when lateral loads need to be considered because in such cases the resultant of all loads on the wall must be located within the middle third of its overall thickness. As a result, the total load eccentricity must not exceed one sixth of the wall's thickness. In this way the walls may be considered as reasonably concentrically loaded [15]. The column method represents a viable alternative that provides more accurate results.

The purpose of this paper is to review the considerable advances that have been made in the design of concrete walls, both with and without openings that are subjected to eccentric axial loads. Additionally, the performance of FRP-strengthened walls is discussed on the basis of earlier studies. Design codes and research studies from across the world were taken into consideration in the analysis. Several aspects are highlighted, including the size and position of the openings, and the roles of boundary conditions and the wall's geometric characteristics (i.e. slenderness $\lambda = H/t$, aspect ratio $\delta = H/L$ and thickness ratio $\eta = L/t$, where $H$, $L$ and $t$ represent the wall's height, length and thickness, respectively).

A statistical analysis of available models was performed on a database collected by the authors, and is presented in this paper. The outcome of this study provides an overview of the performance of current design models and identifies research gaps. Overall, design codes were found to provide more conservative results than recent design models proposed in other studies. Research into the strengthening of RC walls with openings is still at an early stage, and further studies are undoubtedly required in this area. The findings presented herein will be used to define a new experimental programme that aims to characterize the behaviour of axially loaded RC walls strengthened with FRP; the results of these investigations will be presented in a future publication.

## 2. Previous experimental work

The results of 253 experimental tests on RC walls reported in the literature were compiled in a database, which is presented in Appendices A1–A3.

In line with the aim of this study, the database contains information on walls that were loaded gravitationally with uniformly distributed forces applied eccentrically at a maximum of 1/6 of their thickness. Tests on walls loaded gravitationally with eccentricities greater than 1/6 of their thickness have also been reported in the literature [16,17]. However, these results are omitted from the database because the design of such walls is not compatible with current industry standards. Data for walls that failed before reaching their ultimate capacity due to incorrect laboratory manipulation were also omitted.

### 2.1. Database description

The database is organized into six different sections:

(a) Name of authors and citation.
(b) Original description of the test as presented in the cited reference.
(c) Geometrical characteristics of the tested wall: height ($H$), length ($L$), thickness ($t$), number of steel reinforcement layers ($n$).

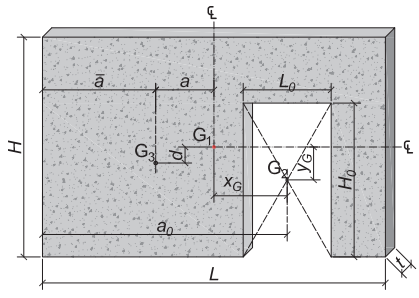


**Fig. 1.** Geometry of a wall with openings (G3 = centre of gravity of wall with opening, G1 = centre of gravity of solid wall, G2 = centre of gravity of opening) (adapted from [18]).

(d) Derived geometrical parameters of the tested wall: slenderness ($\lambda$), aspect ratio ($\delta$) and thickness ratio ($\eta$).
(e) The location(s) of opening(s) in the wall, given in Cartesian coordinates relative to the point at which the wall's centre of gravity would have been located if were completely solid with no openings.
(f) Material properties of the tested wall: compressive strength of concrete ($f_c$), yield strength of steel reinforcement ($f_y$) and steel reinforcement ratio ($\rho_h$ – horizontal, $\rho_v$ – vertical).
(g) Ultimate axial capacity of the tested wall ($N_u$) as reported in the original reference.

It should be noted that some of these parameters are referred to by different names in the original references. However, as shown in Fig. 1, a unified naming system was adopted in this work for the sake of clarity.

Because both the experimental boundary conditions and the presence of openings influence the failure modes of stressed walls, the walls listed in the database were initially divided into four main categories: (1) one-way (OW) solid walls (41.1%); (2) two-way (TW) solid walls (26.1%); (3) OW walls with openings (19.1%) and (4) TW walls with openings (13.1%). Fig. 2 summarizes the ranges (frequency distributions between different types of walls) covered by some of the most important parameters

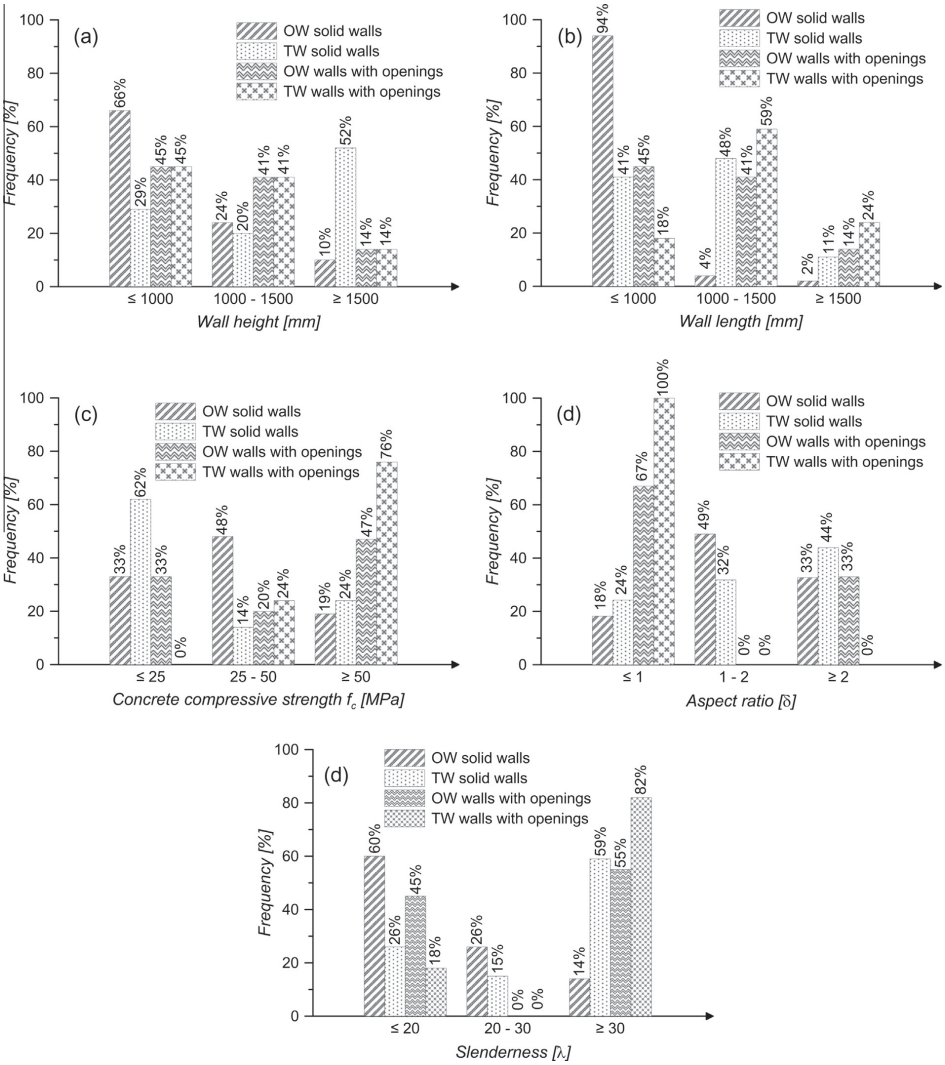


**Fig. 2.** Distribution of the main parameters included in the current database: (a) height; (b) length; (c) concrete strength; (d) aspect ratio; (e) slenderness ratio.

recorded in the database. For example, Fig. 2e shows that 60% of OW solid walls included in the database had slenderness values of less than 20, 26% had a slenderness between 20 and 30, and only 14% had a slenderness higher than 30.

### 2.2. Parameters that influence the wall's ultimate strength

#### 2.2.1. Boundary conditions

Walls restrained along top and bottom edges are referred to as OW action panels. Walls that are restrained in this fashion tend to develop a single out-of-plane curvature in parallel to the load direction, and are usually encountered in tilt-up concrete structures. Panels restrained along three or four sides are referred to as TW action panels. Walls restrained in this way generally deform along both the horizontal and vertical directions and are usually encountered in monolithic concrete structures. In all experimental tests found in the literature, restraining elements that were applied along the top and bottom edges were designed as hinged connections that prevented translation while allowing free rotation. The restraining elements applied along the lateral sides were also fixed to prevent translation without restricting rotation.

Restraints can reduce the wall's deformation and increase its ultimate strength. The use of lateral restraints increased ultimate strength by up to 29% for walls with $\delta \leqslant 1$; increases of up to 68% were achieved for walls of $\delta > 1$ [19]. The data gathered in [20] suggest that even greater increases of up to 300% are possible when $\delta = 1$.

Boundary conditions have a dominant influence on cracking patterns and failure modes. Tests on OW walls usually reveal the development of a horizontal main crack along the middle of the wall. According to Swartz et al. [21], TW walls behave similarly to transversely loaded slabs with simple supports. Typical crack patterns for walls both with and without openings are shown in Fig. 3.

#### 2.2.2. Slenderness and aspect ratio

In general, slender walls will have a lower ultimate strength [17,19,20,22–24]. Saheb and Desayi [22] and Saheb and Desayi [19] proved that increasing the slenderness ratio from 9 to 27 reduces strength by 35% for OW walls and 37% for TW walls. A separate study showed that the reduction in strength with increasing slenderness was more pronounced in walls made out of high-strength concrete than in those made of normal strength concrete [20]. El-Metwally et al. [25] subsequently showed that the failure mode is sensitive to both slenderness and end eccentricity.

In general, walls with a low slenderness may fail by crushing on the compressed face and bending on the tension face, while those with high slenderness may additionally fail through buckling. In either case, brittle types of failure have been observed in all experimental studies performed to date [15,16,19,20,22,24,26–29].

For OW walls the ultimate strength tends to decrease with an increase in aspect ratio, while for TW walls the opposite trend is found. For an increase in aspect ratio from 0.67 to 2, Saheb and Desayi reported a 16.6% decrease in the ultimate strength of OW walls, [22], and a 26% increase for TW walls [19].

#### 2.2.3. Reinforcement ratio

When RC walls are subject to axial loads, reinforcement is mainly required to offset creep and shrinkage effects in the

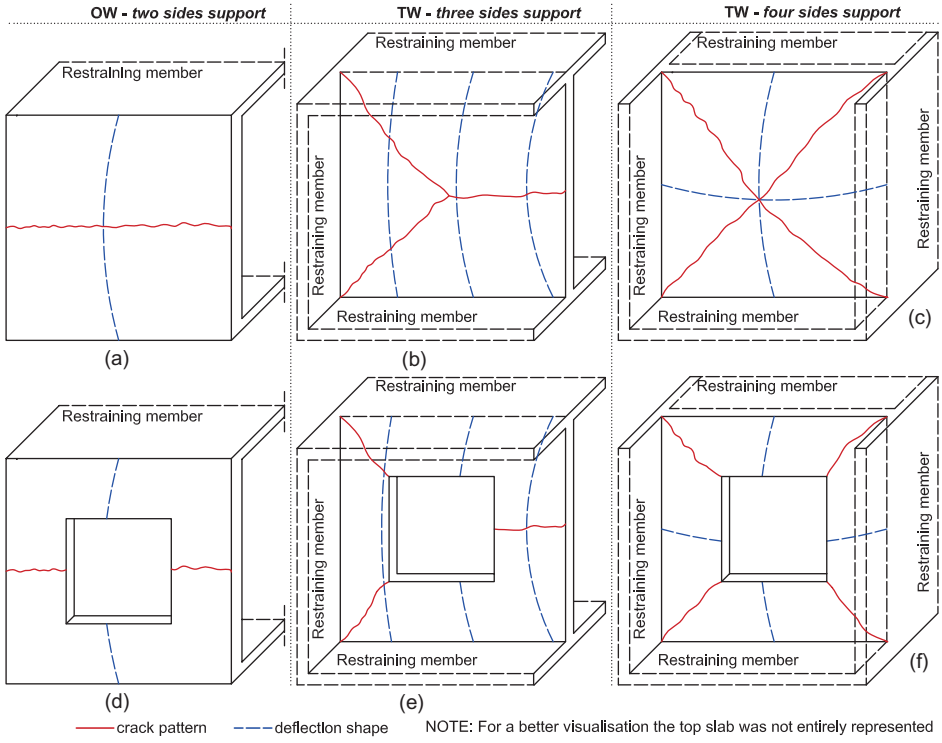


**Fig. 3.** Typical crack pattern and deflection shape of axially loaded RC walls.

concrete, and additionally due to accidental eccentricities in the applied loads [11–14]. When walls act as compression members it is generally believed that the contribution of the steel reinforcement should be neglected. Indeed, one of the first experimental studies conducted in Sweden [30] found that RC walls with the minimum level of steel reinforcement exhibited lower than expected ultimate strengths due to difficulties in compacting the concrete. However, no such effect was observed in subsequent studies on this phenomenon [2,15].

Pillai and Parthasarathy [15] found that varying the steel reinforcement ratio had a negligible influence on the ultimate strength when the reinforcement is placed centrally within one layer. When the reinforcement is placed in two layers, however, a significant increase in ultimate strength can be achieved [2,31]. With the reinforcement being placed in two layers it was found that an increase in vertical reinforcement ratio from 0.175% to 0.85% caused an increase in ultimate strength of 54–55% for panels with a slenderness of 12, and about 43–45% for slenderness equal to 24 [19,22]. Increasing the horizontal steel amount, on the other hand, has no influence on the ultimate strength of the walls [19,22]. These observations are valid for both OW and TW walls.

*2.2.4. Openings*

The presence of openings in a wall considerably reduces its ultimate load capacity relative to the equivalent solid wall. Saheb and Desayi [18] showed that although at 75% of the ultimate load cracking loads are higher for TW than OW walls, at ultimate load the presence of the openings negates the advantage of having restraints on all sides. On the other hand, Doh and Fragomeni [27] and Fragomeni et al. [28] observed that taking the side restraints into consideration could achieve significant gains in the ultimate capacity. It is believed that the differences between the above studies, even though they are studying the same parameter (the effects of restraints on walls with openings), can be explained in terms of the different layouts and opening sizes that the studies investigated. Furthermore, it is not clear whether the lateral restraints were able to function correctly in providing the desired restraining effect.

The magnitude of the ultimate load is governed by the premature failure of the column or beam strips that enclose the opening, however, how large the opening must be for the side restraints to play an important role in the ultimate capacity is currently unknown.

## 3. Design for ultimate strength

To the authors' knowledge, the design of axially loaded RC walls is generally based on column theory. This approach involves an analytical derivation that considers stress–strain compatibilities and the equilibrium of forces over the wall's cross section, as shown in Fig. 4. Two conditions are required for this method to be applicable: (1) the steel reinforcement ratio has to be higher than 1% and (2) the total amount of reinforcement has to be placed in two layers [17]. If treated as columns, walls can be regarded as compression members that carry mainly vertical loads. However, pure axial loads rarely occur in practice; a small eccentricity usually exists. In such cases the walls can still be regarded as compression members because compression forces control their failure. Fig. 4 shows a cross-section of an axially loaded wall with an eccentricity, $e$, from its centreline. The distribution of the strains along its thickness is also shown, together with the corresponding rectangular stress distribution proposed by Mattock et al. [32]. The width of the stress block is taken to be $0.85f_c$ acting on the uncracked depth, $x$.

The equilibrium between internal and external forces is described by Eq. (1), together with Eq. (2), which describes the equilibrium between internal and external moments. These expressions can be used to compute the interaction between the ultimate axial load, $N_u$, which is given by Eq. (3), and the capable moment, $M_u$, which is given by Eq. (4), at any eccentricity $e$.

$$\sum F = 0 \Rightarrow F_c + F_{sc} - F_{st} - N_u = 0 \tag{1}$$

$$\sum M = 0 \Rightarrow F_c\left(\frac{t}{2} - \frac{x}{2}\right) + F_{sc}\left(\frac{t}{2} - d_1\right) + F_{st}\left(\frac{t}{2} - d_2\right) - M_u = 0 \tag{2}$$

thus,

$$N_u = 0.85 f_c (xL - A_{st}) + f_y A_{st} \tag{3}$$

and,

$$M_u = F_c\left(\frac{t}{2} - \frac{x}{2}\right) + F_{sc}\left(\frac{t}{2} - d_1\right) + F_{st}\left(\frac{t}{2} - d_2\right) \tag{4}$$

Eq. (3) is valid for walls whose slenderness does not significantly affect their ultimate capacity. These walls are generally described in the literature as stocky or short walls with a slenderness of less than 15. Macgregor et al. [33] indicated that 98% of the columns in braced frames have a slenderness of less than 12.5, while 98% of the columns in unbraced frames have a slenderness of less than 18. With the increased use of high-strength materials and advanced methods for dimensioning, however, slender elements are becoming more common in current building practices [28].

For slender elements, the predicted ultimate capacity has to be reduced through a second-order analysis that takes into consideration the material nonlinearity, cracking stages and member curvature. A second-order analysis that takes into account variable wall stiffness, as well as the effects of member curvature and lateral drift, is proposed in all international design codes [11–14]. As an alternative to the refined second-order analysis, design may be based on axial forces and moments obtained from the moment magnifier approach. Through this method, the total design moment according to EN 1992-1-1 [14] may be expressed as,

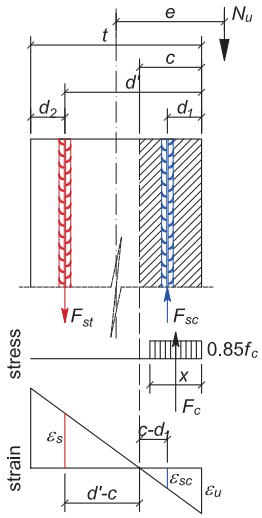


**Fig. 4.** Forces acting on the cross-section of a wall at equilibrium.

$$M_{Ed} = M_{0Ed}\left[1 + \frac{\beta}{(N_B/N_{Ed}) - 1}\right] \quad (5)$$

where $M_{0Ed}$ is the first order moment, $N_{Ed}$ is the design value of the axial load, $N_B$ is the critical buckling load based on nominal stiffness and $\beta = \pi^2/c_0$ is a factor accounting for the curvature distribution along the member, assuming that the second order moments have a sinusoidal distribution. The $c_0$ factor depends on the distribution of the first order moments and, according to EN 1992-1-1 [14], can be approximated as $c_0 = 8$ for a constant distribution, $c_0 = 9.6$ for a parabolic distribution, $c_0 = 12$ for a symmetric triangular distribution.

Parme [34] has suggested simplifying Eqs. (5) and (6), this form of expressing the second order effects being currently adopted in the European norm EN 1992-1-1 [14].

$$M_{Ed} = \frac{M_{0Ed}}{1 - N_{Ed}/N_B} \quad (6)$$

Robinson et al. [17] concluded that the equivalent column procedure should not be used to design RC walls with steel reinforcement ratios lower than 1%, or those with central reinforcements regardless of the reinforcement ratio (as observed in [15]). This is because in these cases the axial capacity depends mainly on the un-cracked wall section stiffness and the tensile strength of the concrete in flexure [17].

While the above method explicitly accounts for parameters such as eccentricity, slenderness and creep, it tends to not be used in practice because of its generalized form and complexity. Instead, numerous models have been derived empirically that are simpler but less accurate. Some of these models have been implemented in design codes, and the details of these models are presented in the following section.

### 3.1. Design models in codes

Currently the practical design of RC walls, described in standards such as ACI318 [11], AS3600 [12] or CAN/CSA-A23.3 [13] is based on empirical models whereas EN 1992-1-1 [14] is based on calibration against the results of non-linear analysis. The design equation of ACI318 [11] was developed over the time with contributions from several studies [15,35–38]. Its current form was first proposed by Kripanarayanan [35], and adopted by ACI Committee 318 [39]. Despite the subsequent completion of numerous studies, no modifications to this formula have been implemented. The design equation found in CAN/CSA-A23.3 [13] is similar to that of [11], the only differences being in the design factors. Doh [40] suggested that the simplified design method found in AS3600 [12] is based on the complementary moment method recommended in the British Concrete standard [41].

According to Hegger et al. [42] the EN 1992-1-1 [14] approach was adapted from the work of Haller [43], a method that was originally developed for masonry elements.

The empirical method is based on the following assumptions: (1) the steel reinforcement will not bring any contribution to the load capacity; (2) the tensile strength of concrete is disregarded; (3) the wall is loaded with an eccentricity applied only at the top. The most important differences between the design models discussed above will now be highlighted.

Differences exist between design codes regarding how they deal with the following parameters: variation of the compressive forces within the stress block, eccentricities, slenderness and creep. The first important difference in development occurs in the assumptions made on the distribution of stresses within the compressed concrete block. ACI318 [11], AS3600 [12], CAN/CSA-A23.3 [13] define a linear stress distribution, as shown in Fig. 5a, whereas EN 1992-1-1 [14] assume a rectangular stress distribution (Fig. 5b). The ultimate capacity is then defined as the resultant force of the stress distribution, where $\sigma_c$ is the allowable compressive stress and $x$ is the un-cracked depth of the concrete section.

Furthermore, the initial eccentricity caused by the applied loads, $e_i$, is further increased by an additional one, $e_a$, due to the lateral deflection of the wall. This factor accounts for the effect of slenderness, known also as second order effects (or $P$–$\Delta$ effects). The procedure described in [11–13] to find the maximum deflection at the critical wall section uses a sinusoidal curvature (Fig. 5a), using deflections obtained from the bending-moment theory [44]. Conversely a triangular curvature is assumed in [14], a consequence of a concentrated horizontal force at the critical point of the wall (Fig. 5b). This approach results in a linear, rather than parabolic, deformation, which acts to reduce the predicted ultimate capacity of slender walls [45]. For the sake of brevity the derivations of these models are not presented in this paper, and can be found in [40].

Most of the experimental studies involved short-term tests and so their results are not very relevant to real walls, which are always subject to a relatively high sustained load. Macgregor et al. [46] showed that sustained loads tend to weaken the performance of slender columns by increasing their deflections. The creep due to sustained loads may also decrease the column's ultimate capacity. Consequently, the effects of creep should always be considered for safety reasons. As shown by Doh [40], the AS3600 [12] standard accounts for the effects of creep by increasing the first-order eccentricity by 20%. Similarly, the EN 1992-1-1 [14] standard states that the normal effects of creep are included in its underlying model. However, Westerberg [47] has demonstrated that the effects of creep are not properly described in the EC model because it produces results that are inconsistent with those obtained using a general method that explicitly accounts for creep effects.

In order to facilitate their comparison, the wall design formulas presented in the design codes [9–12] have been rearranged into similar forms. For codes [9–11] the original equations are derived using an eccentricity of $t/6$, this assumption being used to further rearrange the equations given below. It is unclear how the European norm accounts for a maximum limit of the eccentricity.

ACI318-11 [11]

$$N_u = 0.55\phi\left[1 - \left(\frac{k\lambda}{32}\right)^2\right] f_c L t \quad (7)$$

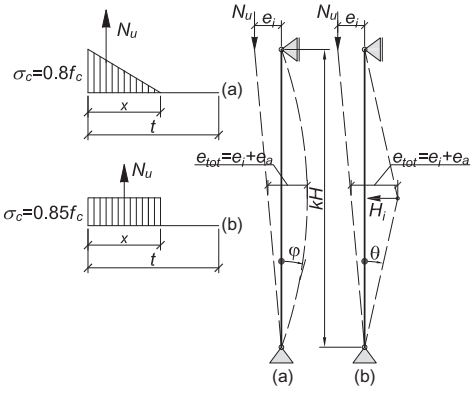


**Fig. 5.** Slender elements subjected to axial load and their corresponding stress distribution: (a) EN 1992-1-1 [14]; (b) ACI318 [11], AS3600 [12], CAN/CSA-A23.3 [13].

AS3600-09 [12]

$$N_u = 0.48\phi\left(1-\left(\frac{k\lambda}{31.6}\right)^2\right)f_cLt \tag{8}$$

CSA-04 [13]

$$N_u = 0.45\phi\left[1-\left(\frac{k\lambda}{32}\right)^2\right]f_cLt \tag{9}$$

EN 1992-1-1 [14]

$$N_u = \Phi\frac{1}{\gamma_c}f_cLt \text{ where } \Phi = 0.76 - 0.0257k\lambda \leqslant 0.67 - \frac{k\lambda}{200} \tag{10}$$

The term $\varphi$ in Eqs. 7–9 represents the strength reduction factor corresponding to compression-controlled sections. Its value ranges from 0.6 for AS3600 [12] to 0.65 for both ACI318 [11] and CAN/CSA-A23.3 [13], while for EN 1992-1-1 [14] an equivalent value would be $1/\gamma_c$, equal to 0.67.

Values for the effective height factor $k$ are given for the most commonly encountered restraints. The American and Canadian codes [11,13] only take into consideration restraints applied at the top and bottom of the wall, i.e. OW walls.

For OW walls, restrained against rotation provided at both ends, $k$, takes different values for different codes, i.e. $k = 0.75$ [12], $k = 0.8$ [11,13], $k = 0.85$ [14]. Unless no restraint against rotation is provided at one or both ends, the slenderness factor $k$ equals 1.

Both Australian [12] and European [14] design codes include the effect of the side restraints, applied to TW walls, through the effective height factor $k$ (Eqs. (11) and (12)). This factor is dependent on the aspect ratio of the wall and is given by Eq. (11) for walls restrained on three sides and Eq. (12) for walls restrained on all four sides.

$$k = 1/(1+\delta^2/9) \tag{11}$$

$$\begin{cases} k = 1/(1+\delta^2) & \text{if } \delta \leqslant 1 \\ k = 1/2\delta & \text{if } \delta > 1 \end{cases} \tag{12}$$

### 3.2. Other models proposed by researchers

Numerous studies have attempted to further improve the design models. Their proposed models incorporate the effects of the slenderness, aspect and thickness ratios, boundary conditions and steel reinforcement. The early studies that modelled RC walls as compression members were performed by [2,15,21,35,37,38], and subsequently reviewed by [48]. In this section only the most recently developed models are presented, although the results obtained from the earlier studies are included in the database and used for the performance assessment of the current models.

In the next section, the models proposed by recent studies will be given in chronological order. All models are abbreviated as OWM – one-way model for solid walls, TWM – two-way model for solid walls and OM – model for walls with openings.

#### 3.2.1. Design equations for solid walls

*3.2.1.1. Saheb and Desayi model (OWM1) [22].* To the best of the author's knowledge the first systematic study of solid concrete walls tested under both OW and TW actions was reported by Saheb and Desayi [22]. The influence of the aspect, thickness and slenderness ratios, as well as the vertical and horizontal steel reinforcement ratios, on the ultimate load was studied. Based on their own experimental results and those reported in [15,37,38], an empirical equation was proposed (Eq. (13)), valid for OW walls. In the assessment chapter (Section 4) this model is abbreviated as OWM1.

$$N_u = 0.55\phi[f_cLt + (f_y - f_c)A_{sv}]\left[1-\left(\frac{\lambda}{32}\right)^2\right]\left(1.20-\frac{\delta}{10}\right) \tag{13}$$

where $A_{sv}$ is the area of vertical steel reinforcement.

When compared to Eq. (7) this model additionally takes into account both the effect of the steel reinforcement and that of the aspect ratio. However, for walls with an aspect ratio higher than 2, the effect of the aspect ratio is not accounted for (i.e. the term $(1.20 - \delta/10) = 1$). This model has been validated for axially loaded walls with an eccentricity of $t/6$ and a slenderness of up to 27. Another important assumption was that the minimum amount of steel reinforcement placed in two layers yields at ultimate load. Therefore, this model may not be suitable for walls that are centrally reinforced, or when the eccentricity is less than $t/6$.

*3.2.1.2. Saheb and Desayi model (TWM1 & TWM1*) [19].* In the same way as the authors did for OW panels, the influence of the aspect, thickness and slenderness ratios, as well as the vertical and horizontal steel reinforcement ratios, on the ultimate load was studied for TW action panels. It was found that the ultimate load increased as the percentage of vertical steel increased, this was due to the reinforcement being placed in two layers. From their results it can also be concluded that the steel ratio has a more pronounced effect on the ultimate capacity when the panels have a high slenderness.

Before the Saheb and Desayi study there were no equations for predicting the ultimate strength of TW wall panels, because of this the authors proposed both an empirical and a semi-empirical model. The first one (*TWM1*) is an empirical formulation that was validated using their own experimental data and that published by Swartz et al. [21]. Shown in Eq. (14), it is limited to those panels whose aspect ratio is between 0.5 and 2, and the maximum limit of the thickness ratio is 60.

$$N_u = 0.67\phi\left[1-\left(\frac{\eta}{120}\right)^2\right](1+0.12\delta)f_cLt \tag{14}$$

The second proposal (*TWM1**) is a semi-empirical method (Eq. (15)), developed from a modification of the buckling strength theory of thin rectangular metal sheets, proposed by Timoshenko and Gere [49]. The original formulation of Timoshenko and Gere [49] was modified by substituting the yield strength of the metal plate with the compressive strength of the concrete wall.

$$N_u = \phi cR \tag{15}$$

with, $R = \frac{f_cLt + A_{sv}f_{yv}\left(1+\frac{A_{sh}f_{yh}}{A_{sv}f_{yv}}\right)}{\eta}$ and $c = 0.8352\eta - 0.0052\eta^2$, where $A_{sv}$, $A_{sh}$ are the areas of vertical and horizontal steel reinforcement, respectively.

Unlike the model for OW panels, the effect of the steel reinforcement could not be directly accounted for because of limited available data; however, it was included indirectly through the term $R$.

*3.2.1.3. Aghayere and MacGregor model [50].* A procedure for obtaining the maximum eccentricity, $e_y$, for a given set of loads, $N_x$ and $N_y$, was proposed by Aghayere and MacGregor [50]. By obtaining the $M$–$N$–$\varphi$ relationship for sections of unit length at the centre of the plate, one can determine the internal resisting moments per unit length $M_{xi}$ and $M_{yi}$, corresponding to the maximum curvatures $\varphi_{xo}$ and $\varphi_{yo}$, respectively. Different eccentricities can be obtained for various load levels, and through interpolation the maximum in-plane load for a given eccentricity can be obtained [50].

$$N_y e_y = \delta^2 \left( M_{xi} - \frac{N_x L^2 \phi_{xo}}{\pi^2} - N_x e_x \right) + \left( M_{yi} - \frac{N_y H^2 \phi_{yo}}{\pi^2} \right) + \delta \sqrt{M_{xi} M_{yi}} \tag{16}$$

where $e_x$ and $e_y$ give the eccentricity of the in-plane load in the $x$ and $y$ directions, respectively, $N_x$ and $N_y$ are compressive forces per unit length in the $x$ and $y$ directions, respectively, $M_{xi}$ and $M_{yi}$ are the internal resisting moments per unit length in the $x$ and $y$ directions, respectively, and $\varphi_{xo}$ and $\varphi_{yo}$ give the maximum curvature in the $x$ and $y$ directions, respectively.

The model proposed by Aghayere and MacGregor [50] takes into account material nonlinearities including tension-stiffening effects. Owing to its complexity and the limited information reported in previous experimental tests, however, this model was not included in the assessment.

*3.2.1.4. Fragomeni and Mendis model (OWM2) [51].* The experimental programme undertaken by Fragomeni [52] focused on investigating the axial load capacity of normal and high-strength concrete OW walls. It was found that the ultimate load capacity is not influenced by the minimum amount of steel reinforcement when this reinforcement is placed centrally in one layer. It was also found that the ultimate load capacity did increase for aspect ratios higher than 2, in contradiction to the results reported in [22]. Significant differences exist, however, between these two studies, for instance the concrete compressive strength and steel ratio are both higher for the specimens tested in [52].

The proposed model [51], that suggests modifications to the Australian code, accounts for the high strength concrete contribution through Eqs. (17a) and (17b).

$$N_u = 0.6 \left[ t_w - 1.2e - 2\left( \frac{k^2 \lambda H}{2500} \right) \right] f_c L \quad \text{for } f_c < 50 \text{ MPa} \tag{17a}$$

$$N_u = \left[ t_w - 1.2e - 2\left( \frac{k^2 \lambda H}{2500} \right) \right] 30 \left[ 1 + \frac{(f_c - 50)}{80} \right] L \quad \text{for } f_c > 50 \text{ MPa} \tag{17b}$$

*3.2.1.5. Doh and Fragomeni model (OWM3) [20].* Following the suggestions of Fragomeni [52], who took high concrete strength values into account to increase the wall strength, Doh [40] attempted to refine the existing equation through an extensive experimental study on OW concrete walls. The design equation that this research produced, shown in Eq. (18), applies to walls with larger slenderness ratios and a variety of concrete strengths.

$$N_u = \phi \left[ t - 1.2e - 2\left( \frac{k^2 \lambda H}{2500} \right) \right] 2.0 f_c^{0.7} L \tag{18}$$

where the effective length factor $k$ *is* $k = 1$ for $\lambda < 27$ and $k = 18/\lambda^{0.88}$ for $\lambda \geqslant 27$.

This model omits the centrally placed reinforcement and the aspect ratio effects.

*3.2.1.6. Doh and Fragomeni model (TWM2) [20].* In addition to the above tests performed on OW wall panels, Doh [40] tested walls in TW action in order to extend the applicability of their design equation. In this way they were able to extend Eq. (18) to include the effects of side restraints, through the effective length factor $k$.

$$k = \begin{cases} \alpha/(1+\delta^2) & \text{for } \delta \leqslant 1 \\ \alpha/2\delta & \text{for } \delta > 1 \end{cases} \tag{19}$$

where $\alpha$ is an eccentricity parameter equal to,

$$\alpha = \begin{cases} 1/(1-e/t) & \text{for } \lambda < 27 \\ 18/[(1-e/t)\cdot\lambda^{0.88}] & \text{for } \lambda \geqslant 27 \end{cases} \tag{20}$$

*3.2.1.7. Hegger et al. model (OWM4) [42].* Hegger et al. [42] have proposed a new model valid for OW walls, based on the methodology presented in [43]. Their model is similar to [14] and, by taking into account the concrete tensile strength and material nonlinearity, predicts an increase in ultimate capacity. This increase is more pronounced when considering specimens of high slenderness and eccentricity. Chen and Atsuta [53] suggested that the tensile strength of normal concrete has a significant effect on the wall strength, and should therefore be taken into account when computing ultimate strengths.

In the study Hegger et al. [42] proposed two functions for the purposes described above, one to describe the nonlinear behaviour of concrete material, Eq. (21), and the other to describe the linear-elastic behaviour, Eq. (22). Eq. (21) is in accordance with the paper of Kirtschig and Anstötz [54], and is valid only for normal strength concrete. Eq. (22) was first proposed by Glock [55], who showed that the formulation is valid only for high slenderness and eccentricity values, i.e. $e \geqslant 0.2t$.

$$\Phi_{non\,lin} = (1 - 2e/t) \exp\left\{ -\left[ \frac{k\lambda\sqrt{\varepsilon_{c2}}}{A(1-2e/t)} \right]^B \Big/ 2 \right\} \tag{21}$$

with $\varepsilon_{c2} = 2f_{cd}/E_{c0d}$, $A = 1.25$ and $B = 1.70$. Here $\varepsilon_{c2}$ is the strain in the concrete at the peak stress $f_{cd}$ and $E_{c0d}$ is the design value of the modulus of elasticity of concrete.

$$\Phi_{lin-el} = -\frac{1}{2}\frac{f_{ctd}}{f_{cd}} + \frac{\pi^2 E_{c0d}}{24(k\lambda)^2 f_{cd}} \times \left[ 1 - 6e/t + \sqrt{\left( \frac{1-6e}{h - 12((k\lambda)^2/\pi^2 E_{c0d}) f_{ctd}} \right)^2 + 48\frac{(k\lambda)^2}{\pi^2 E_{c0d}} f_{ctd}} \right] \tag{22}$$

The maximum value between $\Phi_{non\,lin}$ and $\Phi_{lin\text{-}el}$ has to be used in connection with Eq. (23) with a minimum eccentricity of $e = 0.2t$, suggesting that the formula would be suitable for higher eccentricities as well.

$$N_u = \Phi f_{cd} L t \tag{23}$$

This model requires specific material characteristics, namely the tensile strength and modulus of elasticity of concrete, and as such information is limited in the experimental test reports it is difficult to test the model precisely. Instead the required characteristics where estimated using the equations proposed in fib Model Code 2010 [56].

*3.2.1.8. Ganesan et al. model (OWM5) [23].* In two recent studies, Ganesan et al. [23,24] tested wall panels under OW action to study the axial strength of steel fiber reinforced concrete and geopolymer concrete. The authors reported that if the slenderness is kept constant, the ultimate strength of the concrete panels decreases as the aspect ratio increases. Their proposed model is similar to the one developed by Saheb and Desayi [22], including both the effect of the steel reinforcement and that of the aspect ratio. The specimens used to derive the model, however, had aspect ratios lower than 2, meaning that for higher values the model may not be valid.

$$N_u = 0.56\phi [f_c L t + (f_y - f_c) A_{sv}] \left[ 1 + \left( \frac{\lambda}{29} \right) - \left( \frac{\lambda}{26} \right)^2 \right] \left[ 1 - \left( \frac{\delta}{11} \right) \right] \tag{24}$$

Furthermore, due to the differences between the material characteristics of the concrete, the authors suggested new modifications to Eq. (24). Eq. (25) is suitable for reinforced geopolymer concrete walls under OW action.

$$N_u = 0.585\phi[f_c Lt + (f_y - f_c)A_{sv}]\left[1 + \left(\frac{\lambda}{40}\right) - \left(\frac{\lambda}{30}\right)^2\right]\left[1 - \left(\frac{\delta}{18}\right)\right] \quad (25)$$

*3.2.1.9. Robinson et al. model (OWM6) [17].* From experimental results obtained in a series of tests performed on slender OW wall panels Robinson et al. [17] found that current design methodologies are considerably conservative. The authors devised a new model using the semi-empirical semi-probabilistic DAT (Design Assisted by Testing) methodology [57], based on the "lumped plasticity" concept. This concept allows the entire inelasticity of the element to be concentrated at the critical section, using a "non-linear" fibre hinge [17].

The model (Eq. (26)) has been validated using their experimental data, and was calibrated using statistical techniques.

$$N_u = \frac{1}{2}\left(\frac{10}{e} - \frac{\lambda}{100e} - 4 \cdot 10^{-4} \cdot \lambda^2\right) \cdot f_c Lt \quad (26)$$

*3.2.2. Design equations for walls with openings*

The design codes that have been reviewed above [11–14] do not provide design equations to evaluate the axial strength of a concrete wall that contains openings. There is very little information in the research literature, therefore, probably due to the complex failure mechanisms of such elements. Some guidelines are provided, such as in AS3600 [12] and EN 1992-1-1 [14]. These state that if the walls are restrained on all sides, and enclose an opening with an area less than 1/10 of the total, the effects of this opening on the axial strength can be neglected. The height of the opening should also be less than 1/3 of the wall height. If these conditions are not accomplished, the portion between restraining member and opening has to be treated as being supported on three sides, and the area between the openings (if more than one) has to be treated as being supported on two sides. This approach is only valid if the openings are included at the early stages of the design, as special reinforcement bars have to be placed around openings to avoid premature failure. No recommendations are given, therefore, if the openings are created in an existing wall.

*3.2.2.1. Saheb and Desayi model (OM1) [18].* The effect of one or two openings, placed either symmetrically or asymmetrically, and combinations of door or window openings, have been studied by Saheb and Desayi [18]. To extend the usefulness of their empirical method to account for the presence, size and location of an opening, the authors proposed a new equation that is given below.

$$N_{uo} = (k_1 - k_2\alpha_x)N_u \quad (27)$$

where $N_u$ is the ultimate load of an identical panel without openings under OW (Eq. (13)) or TW action (Eq. (14)). The constants $k_1$ and $k_2$ were obtained using curve-fitting techniques. Under OW action this procedure yields $k_1 = 1.25$ and $k_2 = 1.22$, while under TW action $k_1 = 1.02$ and $k_2 = 1.00$. The effect of the size and location of the opening in the wall is taken into account through a dimensionless parameter, $\alpha_x$, defined as,

$$\alpha_x = \frac{A_{0x}}{A_x} + \frac{a}{L} \quad (28)$$

where $A_{0x}$ and $A_x$ represent the horizontal wall cross-sectional area of the opening (i.e. $A_{0x} = L_0 t$) and of the solid wall (i.e. $A_x = Lt$), respectively. All parameters involved in Eq. (28) can be easily determined from Fig. 1, however, for simplicity the term $\bar{a}$ is calculated according to Eq. (29).

$$\bar{a} = \frac{L^2 t/2 - L_0 t a_0}{Lt - L_0 t} \quad (29)$$

*3.2.2.2. Doh and Fragomeni model (OM2) [27].* Based on a new series of tests on walls with openings under both OW and TW actions, Doh and Fragomeni [27] proposed a new set of constants for Eq. (27). The only differences between this model and the Saheb and Desayi model (OM1) are:

- Provide different values for the constants, based on a new set of experimental tests.
- The ultimate load of the solid wall is calculated according to Eq. (18).

Again, the constants $k_1$ and $k_2$ were obtained using curve-fitting techniques, this time through a larger number of tests. For OW panels this yielded $k_1 = 1.175$ and $k_2 = 1.188$, while for TW panels $k_1 = 1.004$ and $k_2 = 0.933$.

While the differences between these constants are not large, the main contributor to the ultimate load comes from the load capacity of the solid wall, which is calculated in a different way. Both models take into account the size and position of an opening through the parameter $\alpha_x$, allowing a reduction in the ultimate capacity.

Fragomeni et al. [28] found that this model gives results in good agreement with the test results from another experimental study [58].

*3.2.2.3. Guan et al. model (OM3) [59].* Guan et al. [59] found that increasing both the length and the height of an opening has the most significant effect on the capacity, and proposed a new model to account for this effect. Having established a benchmark model, the authors performed a parametric study by varying the parameters that the capacity was most sensitive to. Their analysis proceeded through a nonlinear finite element method. In the model a three-dimensional stress state was used with elastic brittle fracture behaviour for concrete in tension, and a strain hardening plasticity approach was assumed for concrete in compression. Their model is nearly identical to that proposed by Doh and Fragomeni (OM2), the only difference being that $\alpha_x$ was changed to $\alpha_{xy}$ to account for the opening height.

$$\alpha_{xy} = \frac{\alpha_x + \gamma\alpha_y}{1 + \gamma} \quad (30)$$

where

$$\alpha_y = \frac{A_{0y}}{A_y} + \frac{d}{H} \quad (31)$$

in which $A_{0y}$ represents the vertical cross-sectional area of the opening (i.e. $A_{0y} = H_0 t$), $A_y$ represents the vertical cross-sectional area of the solid wall (i.e. $A_y = Ht$) and $d$ represents the distance between centres of gravity ($G_1$ and $G_3$) of the wall with and without the opening, in the vertical direction (Fig. 1). In Eq. (30), $\gamma$ represents "the weighting ratio indicating the percentage of $\alpha_y$ in relation to $\alpha_x$". Using regression analysis, a new set of constants was determined; $\gamma = 0.21$, $k_1 = 1.361$ and $k_2 = 1.952$ for OW walls and $\gamma = 0.40$, $k_1 = 1.358$ and $k_2 = 1.795$ for TW walls. It should be noted that this model was derived from walls with a fixed slenderness ratio (i.e. $\lambda = 30$) and an aspect ratio of unity.

*3.2.2.4. Mohammed et al. model [4].* In a more recent study, Mohammed et al. [4] tested OW walls with cut-out openings. The size of the openings was varied from 5% to 30% of the solid wall. It was found that the presence of a cut-out opening in a solid OW wall led to the formation of disturbance zones. Discontinuities in these disturbance zones cause high stresses in the concrete, and cracks will form at the corners of the opening if improperly reinforced.

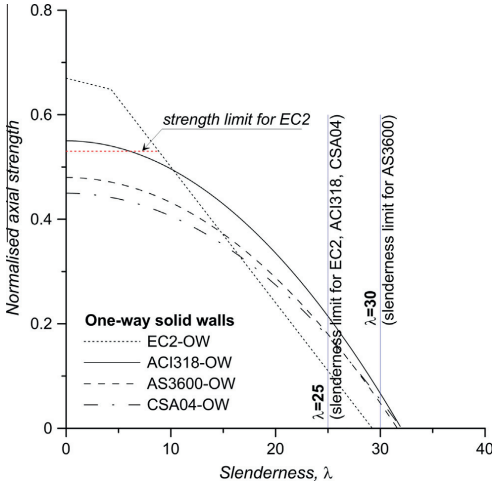


**Fig. 6.** Comparison of different design models in the investigated codes [11–14] for OW solid walls.

For this case, Mohammed et al. [4] suggested a new set of constants to be used in Eq. (27). The authors tested one-way panels only, obtaining $k_1 = 1.281$ and $k_2 = 0.737$. It should be noted that Eq. (27), proposed by Saheb and Desayi [19], considers steel reinforcement placed in two layers that yields at ultimate, whereas the experimental programme presented in [4] consisted only of centrally reinforced panels.

Since the model was calibrated on walls with cut-out openings (i.e. no diagonal bars around corners) it cannot be assessed through the current database. However, the results of the experiments by Mohammed et al. [4] were incorporated into the current database and used in the assessment of other models (i.e. OM1, OM2, and OM3).

## 4. Assessment of existing design models

The empirical design models reviewed above were derived using a limited number of either experimental tests or numerical simulations. Some models were developed solely from tests performed by the researchers themselves, while others additionally used tests from other sources, therefore the predictions of the latter may give more reasonable outcomes by covering a broader spectrum of designs. The studies focussed on either the variation of geometric characteristics (i.e. slenderness, aspect ratio, size and position of the opening) or the variation of material properties (i.e. concrete strength, influence of steel reinforcement). If one has to design a compression member under conditions that were not specifically covered by any of the available design models, then it remains unclear how accurate the models will be. In order to quantify this a statistical analysis was performed on each model in turn, using all of the experimental results available (these are included in Appendices A1–A3), unless the model explicitly specifies its limiting parameters.

**Table 1**
Statistical summary for OW models of the solid walls.

| Model | One-way solid walls | | | |
|---|---|---|---|---|
| | Avg | St Dev | CoV (%) | $R^2$ |
| ACI318 [11] | 0.69 | 0.25 | 36 | 0.91 |
| AS3600 [12] | 0.59 | 0.22 | 38 | 0.90 |
| CSA-04 [13] | 0.57 | 0.20 | 36 | 0.91 |
| EC2 [14] | 0.62 | 0.24 | 39 | 0.87 |
| OWM1 [22] | 0.77 | 0.28 | 37 | 0.90 |
| OWM2 [51] | 0.59 | 0.25 | 37 | 0.90 |
| OWM3 [20] | 0.74 | 0.20 | 27 | 0.94 |
| OWM4 [42] | 0.89 | 0.17 | 19 | 0.98 |
| OWM5 [23] | 1.10 | 0.35 | 32 | 0.92 |
| OWM6 [17] | 1.24 | 0.68 | 55 | 0.68 |
| OWM6* [17] | 1.10 | 0.41 | 37 | 0.82 |

The accuracy of the models was evaluated using the following statistical indicators; the average (Avg), the standard deviation (St Dev) which measures the amount of variation from the average, the coefficient of variation (CoV) which shows the extent of variation and the coefficient of determination ($R^2$) that indicates how well the data fit a model within a 95% confidence interval.

The analysis was conducted separately for solid OW action, solid TW action and for walls with openings. For all models, the material strength reduction factor, $\varphi$, was set to 1.0.

### 4.1. Assessment of predicted values for OW solid walls

Fig. 6 shows the normalized strength versus slenderness, as predicted by the investigated design codes for a typical wall that is assumed to be loaded axially with an eccentricity of $t/6$ and has a strength reduction factor $\varphi = 1$. ACI318 [11] model provides higher loads for slenderness values above 10 when compared to EN 1992-1-1 [14].

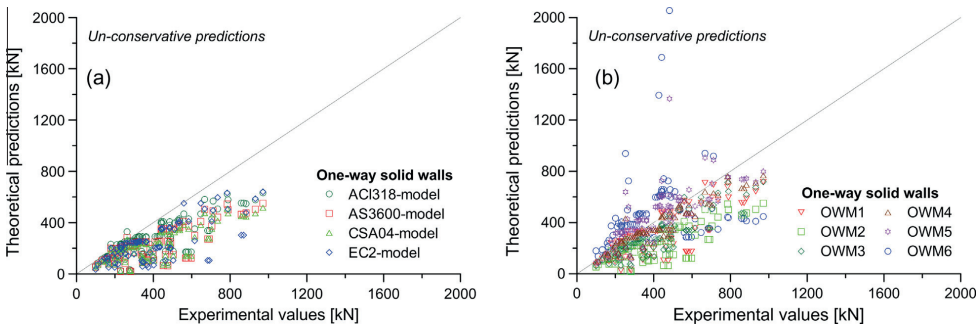


**Fig. 7.** Assessment of the current design models of one-way solid walls: (a) design codes; (b) design equation from different studies.

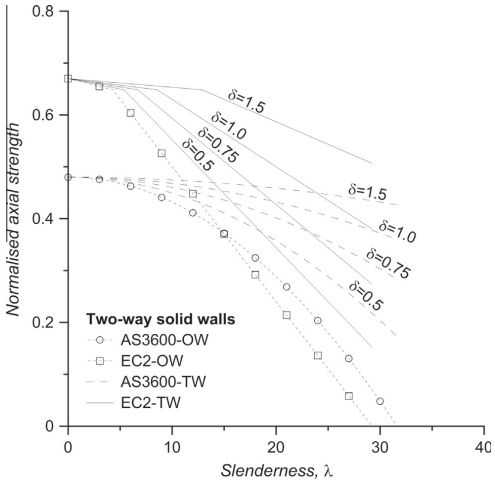


**Fig. 8.** Comparison of different design models in the investigated codes [12,14] for TW solid walls.

The AS3600 [12] and CAN/CSA-A23.3 [13] models predict the lowest load values for slenderness values lower than 15, above this value the load value predictions increase above those of EN 1992-1-1 [14], while remaining lower than ACI318 [11].

The limits of the slenderness values given in the codes are also plotted in Fig. 6. Beyond these limits, presumably imposed by the data available at the time of development, the models are not accurately calibrated and can yield negative values for the normalized strength. Recent studies have shown that the slenderness limit can be increased with confidence [15,17,23,40], however, suggesting that there is a need to update the current design codes.

How these models perform when assessed using experimental tests from the database is shown in Fig. 7a and b. While code models [11–14] present a natural degree of conservationism, due to statistical calibration, the trend is opposite for the models presented in the literature [17,20,22,23,51] (see Fig. 7b). A statistical summary for these models is presented in Table 1. Overall, the most conservative model is that proposed by CAN/CSA-A23.3 [13], with an average ratio between theoretically and experimentally determined capacity of 0.57 and a standard deviation of 0.20. The least conservative model is OWM6 [17], with an average ratio between theoretically and experimentally determined capacities of 1.24 and a standard deviation of 0.68. However, most of the extreme non-conservative results for the later model come from walls made of high-strength concrete. Since this aspect was not discussed in [17], the authors assumed that using the OWM6 model for normal strength concrete would provide better results. The new results obtained excluding high-strength concrete values are abbreviated as OWM6* and are listed in Table 1. The model proposed by Hegger et al. [42] (OWM4) is the most statistically accurate, with an average ratio between the theoretically and experimentally determined capacities of 0.89 and a standard deviation of 0.17.

### 4.2. Assessment of predicted values for TW solid walls

In the case of TW walls, EC2 and AS3600 are the only major codes that provide a methodology to account for a higher capacity due to restraints on all sides. It remains unclear whether the limitations placed on the slenderness values in these models ($\lambda = 25$ [14] and $\lambda = 30$ [12]) apply only to OW walls or to both OW and TW walls. By plotting both models with aspect ratios usually encountered in practice, one can observe that such limitations would be highly restrictive. The way that these codes account for lateral restraints is by using a subunitary coefficient ($k$), based on the end-restraint of the wall and its aspect ratio (Eqs. (11) and (12)). Significant increases in strength can be achieved by restraining the walls on all their sides, as can be observed in Fig. 8.

Fewer testes were carried out on walls restrained on all sides; correspondingly less models are also available. The performances of these models are shown in Fig. 9a for design codes and Fig. 9b for models found in the literature.

The outliers in Fig. 9a (EC2 and AS3600) and Fig. 9b (TWM1 and TWM1*), enclosed by the ellipsoids, originated from walls made of high-strength concrete. In addition, the tests were performed in a horizontal position with the eccentricity acting in favour of the strength, due to effect of gravity, and are consequently extremely non-conservative. A statistical summary for these models is presented in Table 2. The most conservative model is that proposed by AS3600 [12], with an average ratio between the theoretically and experimentally determined capacities of 0.71 and a standard deviation of 0.40. The least conservative model is TWM1* [19], with an average ratio between the theoretically and experimentally determined capacities of 1.44 and a standard deviation of 0.87. The most accurate model in terms of average ratio is TWM2 [20], however, a relatively high standard deviation of 0.30 weakens its precision.

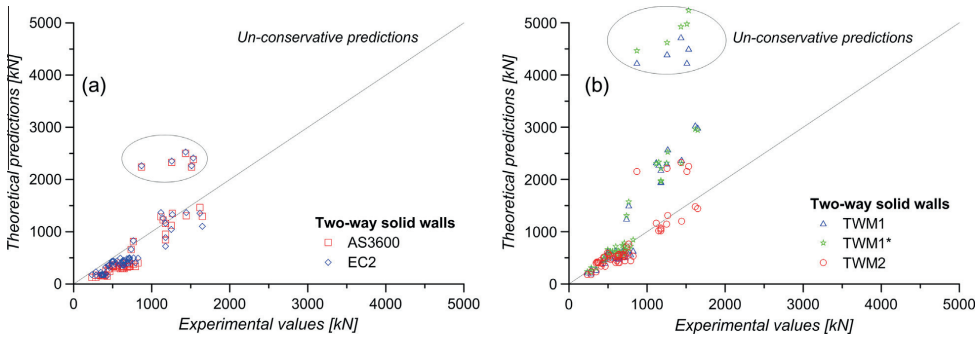


**Fig. 9.** Assessment of the current design models of two-way solid walls: (a) design codes; (b) design equation from different studies.

**Table 2**
Statistical summary for TW models of the solid walls.

| Model | Two-way solid walls | | | |
|---|---|---|---|---|
| | Avg | St Dev | CoV (%) | $R^2$ |
| AS3600 [12] | 0.71 | 0.40 | 56 | 0.81 |
| EC2 [14] | 0.80 | 0.38 | 47 | 0.83 |
| TWM1 [19] | 1.35 | 0.84 | 62 | 0.80 |
| TWM1* [19] | 1.44 | 0.87 | 61 | 0.79 |
| TWM2 [20] | 0.95 | 0.30 | 32 | 0.89 |

### 4.3. Assessment of predicted values for walls with openings

The first model to include the effect of the openings, OM1 [18], was derived using six OW and six TW specimens, while model OM2 [27] was derived using ten OW and ten TW specimens. The model OM3 [59] was calibrated on thirty-six OW and thirty-seven TW specimens. The number of tests used to calibrate these models, therefore, is rather limited. This means that their predictive value may not extend to the design of openings in walls with different material and geometric characteristics.

#### 4.3.1. OW walls with openings

The OM1 model provides the most conservative results, with the smallest value of the average ratio between the theoretically and experimentally determined capacities of 0.77 and a standard deviation of 0.16, while the best model in terms of average is OM2, i.e. 0.95 with a standard deviation of 0.19. The performances of these models are shown in Fig. 10 and the statistical summary is presented in Table 3.

#### 4.3.2. TW walls with openings

Owing to its limited number of tests, OM1 model shows a large scatter from the bisector for those walls restrained on all their sides. A significantly more accurate model is OM2, with an average of 0.90 and a standard deviation of 0.13, proposed by Doh and Fragomeni [27].

## 5. FRP – based strengthening

The successful application of FRP to strengthen solid concrete walls has been achieved in several studies [60–62]. All of them performed a rehabilitation of structural walls using externally bonded FRPs to increase the flexural and/or shear strength, stiffness and energy dissipation. The creation of large openings in walls removes a significant quantity of concrete and steel reinforcement, necessarily reducing the load capacity of the wall. FRPs are able to strengthen such walls by redistributing the stresses, allowing the wall to recover almost its full capacity before the opening was created, if not more [3,4,63,64].

As the size of the opening increases, the global behaviour of the wall will change to that of a frame, and consequently new failure modes may arise. This has an influence on the optimal strengthening configuration. The research conducted so far on strengthening structural members with openings, such as slabs, walls or beams, using FRPs is promising [3,4,63,65–67]. The alignment of the fibres was based on observations of the failure modes of the un-strengthened elements. Usually the FRP material is placed around openings in a vertical, horizontal or inclined alignment, or a combination of these. In some cases the side strips were fully or partially wrapped to provide confinement. In general, the amount of FRPs were chosen intuitively, or by converting the amount of steel reinforcement

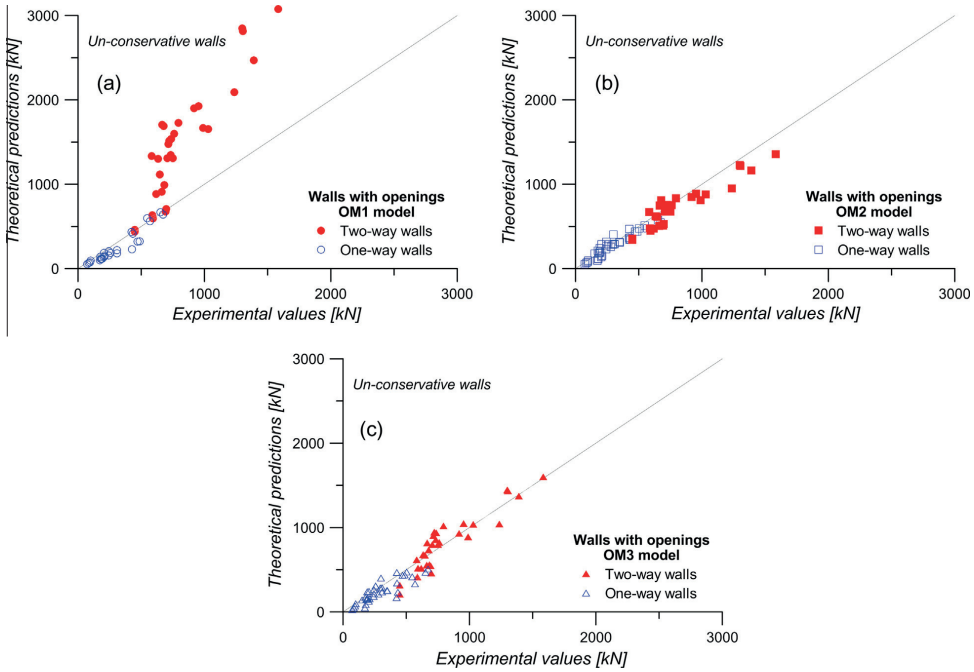


**Fig. 10.** Assessment of design equations for one-way and two-way walls with openings. (a) OM1 model; (b) OM2 model; (c) OM3 model.

**Table 3**
Statistical summary for OW & TW walls with openings.

| Model | One-way action | | | |
|---|---|---|---|---|
| | Avg | St Dev | CoV (%) | $R^2$ |
| OM1 [18] | 0.77 | 0.16 | 21 | 0.96 |
| OM2 [27] | 0.95 | 0.19 | 20 | 0.98 |
| OM3 [59] | 0.83 | 0.24 | 29 | 0.98 |
| | Two-way action | | | |
| | Avg | St Dev | CoV (%) | $R^2$ |
| OM1 [18] | 1.76 | 0.42 | 26 | 0.96 |
| OM2 [27] | 0.90 | 0.13 | 14 | 0.98 |
| OM3 [59] | 0.99 | 0.20 | 20 | 0.98 |

removed into FRP material. Li and Qian [63] have demonstrated that the optimization of the direction, width, and number of layers of the FRP strips by using a strut-and-tie model can provide rigorous results.

Mohammed et al. [4] tested 1/3-scale one-way RC walls with cut out openings, these openings having areas varying from 5% to 30% of the total wall area. The specimens were tested with a uniformly distributed axial load applied with an eccentricity of $t/6$. The introduction of small openings (5% area) reduced the axial capacity by 9%, while large openings (30% area) reduced the capacity by nearly 33%. While keeping the same geometric characteristics and applying two different CFRP patterns (see Fig. 11), the capacity was increased as the principal stresses on the opening corners were reduced. When applied to small openings the first pattern, in which the CFRP was applied around the corners, increased the axial strength by 49.9%. The second pattern, with CFRP placed at the corners, performed better on small openings, causing an increase in axial strength of 75.4%. When applied to large openings, however, the efficiency of these reinforcements was significantly reduced, with 11.3% and 15.1% increases for the first and second patterns, respectively. This confirms the aforementioned claim that different sized openings lead to different failure modes, and consequently require different strengthening patterns. A configuration that may yield better results for large openings would be to fully wrap the side chords, as their thickness ratio was slightly above 2. EN 1992-1-1 [14] emphasizes that elements with a thickness ratio below 4 should be considered as columns rather than walls.

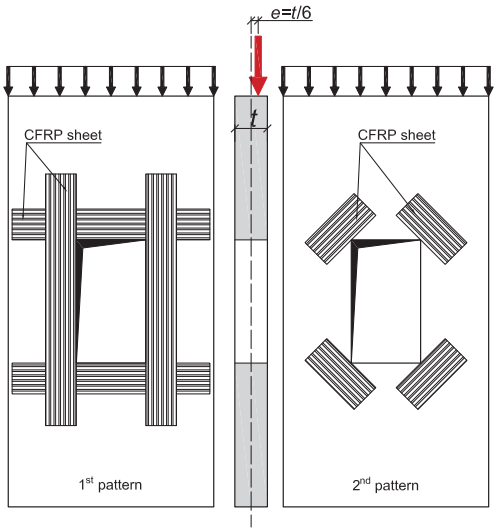


**Fig. 11.** CFRP patterns used to strengthen axially loaded RC walls with openings (adapted from [4]).

The research conducted so far on the rehabilitation of walls using FRPs was promising, however, the repaired walls were loaded principally in the horizontal direction to simulate the effects of earthquakes. The proposed strengthening schemes, therefore, may not be suitable for the repair of gravitationally loaded walls, and more research is required with the loads applied vertically.

Just one study was found in the literature that focused on using FRPs to strengthen axially loaded RC walls with cut-out openings [4]. In order to better understand the structural behaviour of such a configuration, therefore, more studies are required. To this end a research programme at the Luleå University of Technology is currently underway. This study will test a number of concrete walls with different parameters, such as size opening and strengthening configurations, under TW action. The results are expected to be published upon completion of the study.

## 6. Conclusions and future directions

Through the statistical analysis of existing experimental studies this study indicated areas where further testing is required in order to enhance the reliability of current design models. It was found that most experimental studies have focussed on testing RC walls under OW action, with a fixed eccentricity of $t/6$. Fewer tests exist on walls under TW action, walls with openings or different eccentricities, and more tests are required in these experimental regimes to facilitate the development of appropriate design models. The current database is useful because it highlights areas where the current literature is lacking, and where systematic studies could provide important insights into the behaviour of wall types that are poorly understood (e.g. walls with eccentricities above $t/6$ or OW solid walls with high slenderness ratios) or the effects of parameters that are not well covered by existing design provisions (e.g. the presence of an opening or the influence of steel reinforcement).

The design of the experimental programme has a significant role in determining the accuracy of the regression-based models derived. Although the design is carried out assuming a perfect hinge, laboratory evidence shows that neither a perfect hinge nor a full rotation restraint could be achieved in the laboratory environment, much less in practice. All design models empirically derived from such tests, therefore, will necessarily contain a certain level of inaccuracy.

Since the simplified methods assume that the walls are unreinforced elements, the contribution of any steel reinforcement is disregarded. This occurs regardless of the location of the steel mesh layer, or if the reinforcement is placed in one or two layers. For centrally reinforced walls this seems to be valid, although in some cases it may bring some ductility at higher loads. For double-reinforced walls, however, the enhanced capacity should be accounted for, even when the steel ratio is at a minimum level.

The design models found in established design codes provide the most conservative results, while those proposed in other studies showed a certain level of non-conservatism. However, all design models were plotted using $\varphi = 1$, while a carefully chosen safety factor should be used in practice.

FRPs have been recognised as a viable alternative for the strengthening of concrete structures. The potential applications of FRPs in strengthening walls that have been weakened by new openings need to be further studied. There are only a few research

studies in the literature on the FRP strengthening of walls with openings, and almost all the experimental tests involved wall openings that were initially planned. The case of RC walls with cut-out openings is still largely unexplored, with just one research study focussing on this problem [4]. Currently there are no design philosophies or reliable theoretical guidelines for calculating the capacity of strengthened walls in the literature. Safe and clear design procedures for strengthening walls with openings are needed. In the bullet points listed below the main gaps in the research literature, that require further study, are presented.

1. Openings can be of different sizes and may have different positions with respect to a reference point of the RC wall. Therefore, it is natural to ask: How do these parameters influence the FRP contribution to the overall capacity of the wall?
2. What are the efficiencies of different FRP strengthening configurations and systems (sheets, plates or bars) when strengthening RC walls with openings?
3. How does the failure mechanism of an RC wall with an opening change after strengthening with FRP?
4. When designing RC walls with openings, engineers tend to adopt a simplified method by dividing the wall openings into isolated columns connected by beams. While this method provides acceptable results it is overly conservative, and it would be beneficial to know how to delineate small and large openings in walls, and where the transition from RC walls to RC frames should occur in the design of structural elements.

## Acknowledgements

The authors would like to acknowledge The Research Council of Norway (RFF) and Development Fund of the Swedish Construction Industry (SBUF) for financing their work within this project. The authors also like to thank Dr. Bo Westerberg for his contribution in reviewing the paper.

## Appendix A

See Tables A1–A3.

**Table A1**

| Refs. | Designation | Geometrical dimensions | | | | | | | | Material properties | | | | | Capacity |
|---|---|---|---|---|---|---|---|---|---|---|---|---|---|---|---|
| | | $H$ (mm) | $t$ (mm) | $L$ (mm) | $\delta$ | $\lambda$ | $\eta$ | $e$ | $n$ | $\rho_v$ (%) | $f_{yv}$ (MPa) | $\rho_h$ (%) | $f_{yh}$ (MPa) | $f_c$ (MPa) | $N_u$ (kN) |
| Pillai and Parthasarathy [15] | A1 | 1200 | 40 | 400 | 3 | 30 | 10 | $t/6$ | 1 | 0.156 | 273 | 0.250 | 273 | 25.0 | 229 |
| | A2 | 1200 | 48 | 500 | 2.4 | 25 | 10.4 | $t/6$ | 1 | 0.150 | 233 | 0.241 | 233 | 25.0 | 367 |
| | A3 | 1200 | 60 | 550 | 2.2 | 20 | 9.2 | $t/6$ | 1 | 0.153 | 233 | 0.244 | 233 | 20.8 | 382 |
| | A5 | 800 | 80 | 700 | 1.1 | 10 | 8.8 | $t/6$ | 1 | 0.150 | 347 | 0.241 | 347 | 20.8 | 932 |
| | A6 | 400 | 80 | 700 | 0.6 | 5 | 8.8 | $t/6$ | 1 | 0.150 | 347 | 0.250 | 347 | 15.6 | 647 |
| | B1 | 1200 | 40 | 400 | 3 | 30 | 10 | $t/6$ | 1 | 0.300 | 233 | 0.500 | 233 | 24.3 | 282 |
| | B2 | 1200 | 48 | 500 | 2.4 | 25 | 10.4 | $t/6$ | 1 | 0.300 | 233 | 0.500 | 233 | 24.3 | 402 |
| | B3 | 1200 | 60 | 560 | 2.1 | 20 | 9.3 | $t/6$ | 1 | 0.301 | 233 | 0.500 | 233 | 31.1 | 616 |
| | B4 | 1200 | 80 | 700 | 1.7 | 15 | 8.8 | $t/6$ | 1 | 0.300 | 347 | 0.500 | 347 | 22.8 | 883 |
| | B5 | 800 | 80 | 700 | 1.1 | 10 | 8.8 | $t/6$ | 1 | 0.300 | 347 | 0.500 | 347 | 22.8 | 971 |
| | B6 | 400 | 80 | 700 | 0.6 | 5 | 8.8 | $t/6$ | 1 | 0.300 | 347 | 0.500 | 347 | 15.6 | 559 |
| | C1 | 1200 | 40 | 400 | 3 | 30 | 10 | $t/6$ | 1 | 0 | 0 | 0 | 0 | 31.0 | 277 |
| | C2 | 1200 | 48 | 500 | 2.4 | 25 | 10.4 | $t/6$ | 1 | 0 | 0 | 0 | 0 | 20.6 | 343 |
| | C3 | 1200 | 60 | 560 | 2.1 | 20 | 9.3 | $t/6$ | 1 | 0 | 0 | 0 | 0 | 24.0 | 490 |
| | C4 | 1200 | 80 | 700 | 1.7 | 15 | 8.8 | $t/6$ | 1 | 0 | 0 | 0 | 0 | 24.0 | 789 |
| | C5 | 800 | 80 | 700 | 1.1 | 10 | 8.8 | $t/6$ | 1 | 0 | 0 | 0 | 0 | 22.5 | 785 |
| | C6 | 400 | 80 | 700 | 0.6 | 5 | 8.8 | $t/6$ | 1 | 0 | 0 | 0 | 0 | 16.9 | 735 |
| Saheb and Desayi [22] | WAR-1 | 600 | 50 | 900 | 0.7 | 12 | 18 | $t/6$ | 2 | 0.2 | 297 | 0.199 | 286 | 17.9 | 484 |
| | WAR-2 | 600 | 50 | 600 | 1 | 12 | 12 | $t/6$ | 2 | 0.173 | 297 | 0.199 | 286 | 17.9 | 315 |
| | WAR-3 | 600 | 50 | 400 | 1.5 | 12 | 8 | $t/6$ | 2 | 0.173 | 297 | 0.199 | 286 | 17.9 | 198 |
| | WAR-4 | 600 | 50 | 300 | 2 | 12 | 6 | $t/6$ | 2 | 0.173 | 297 | 0.199 | 286 | 17.9 | 147 |
| | WSR-1 | 450 | 50 | 300 | 1.5 | 9 | 6 | $t/6$ | 2 | 0.165 | 297 | 0.199 | 286 | 17.3 | 214 |
| | WSR-2 | 600 | 50 | 400 | 1.5 | 12 | 8 | $t/6$ | 2 | 0.165 | 297 | 0.199 | 286 | 17.3 | 254 |
| | WSR-3 | 900 | 50 | 600 | 1.5 | 18 | 8 | $t/6$ | 2 | 0.165 | 297 | 0.199 | 286 | 17.3 | 299 |
| | WSR-4 | 1350 | 50 | 900 | 1.5 | 27 | 18 | $t/6$ | 2 | 0.165 | 297 | 0.199 | 286 | 17.3 | 374 |
| | WSTV-2 | 600 | 50 | 900 | 0.7 | 12 | 18 | $t/6$ | 2 | 0.331 | 286 | 0.199 | 286 | 20.1 | 535 |
| | WSTV-3 | 600 | 50 | 900 | 0.7 | 12 | 18 | $t/6$ | 2 | 0.528 | 581 | 0.199 | 286 | 20.1 | 584 |
| | WSTV-4 | 600 | 50 | 900 | 0.7 | 12 | 18 | $t/6$ | 2 | 0.845 | 570 | 0.199 | 286 | 20.1 | 704 |
| | WSTV-5 | 1200 | 50 | 800 | 1.5 | 24 | 16 | $t/6$ | 2 | 0.177 | 297 | 0.199 | 286 | 18.3 | 339 |
| | WSTV-6 | 1200 | 50 | 800 | 1.5 | 24 | 16 | $t/6$ | 2 | 0.335 | 286 | 0.199 | 286 | 18.3 | 399 |
| | WSTV-7 | 1200 | 50 | 800 | 1.5 | 24 | 16 | $t/6$ | 2 | 0.528 | 581 | 0.199 | 286 | 18.3 | 463 |
| | WSTV-8 | 1200 | 50 | 800 | 1.5 | 24 | 16 | $t/6$ | 2 | 0.856 | 570 | 0.199 | 286 | 18.3 | 503 |
| | WSTH-2 | 600 | 50 | 900 | 0.7 | 12 | 18 | $t/6$ | 2 | 0.173 | 297 | 0.352 | 581 | 19.6 | 538 |
| | WSTH-3 | 600 | 50 | 900 | 0.7 | 12 | 18 | $t/6$ | 2 | 0.173 | 297 | 0.440 | 581 | 19.6 | 528 |
| | WSTH-4 | 600 | 50 | 900 | 0.7 | 12 | 18 | $t/6$ | 2 | 0.173 | 297 | 0.507 | 570 | 19.6 | 528 |
| | WSTH-6 | 1200 | 50 | 800 | 1.5 | 24 | 16 | $t/6$ | 2 | 0.176 | 297 | 0.352 | 581 | 16.1 | 349 |
| | WSTH-7 | 1200 | 50 | 800 | 1.5 | 24 | 16 | $t/6$ | 2 | 0.176 | 297 | 0.440 | 581 | 16.1 | 344 |
| | WSTH-8 | 1200 | 50 | 800 | 1.5 | 24 | 16 | $t/6$ | 2 | 0.176 | 297 | 0.507 | 570 | 16.1 | 349 |
| Fragomeni [52] | 1a | 1000 | 50 | 200 | 5 | 20 | 4 | $t/6$ | 1 | 0.250 | 450 | 0.250 | 450 | 40.7 | 162 |
| | 1b | 1000 | 50 | 200 | 5 | 20 | 4 | $t/6$ | 1 | 0.250 | 450 | 0.250 | 450 | 58.9 | 187 |
| | 2a | 1000 | 50 | 300 | 3.3 | 20 | 6 | $t/6$ | 1 | 0.250 | 450 | 0.250 | 450 | 42.4 | 232 |
| | 2b | 1000 | 50 | 300 | 3.3 | 20 | 6 | $t/6$ | 1 | 0.250 | 450 | 0.250 | 450 | 65.4 | 264 |
| | 3a | 1000 | 40 | 200 | 5 | 25 | 5 | $t/6$ | 1 | 0.310 | 450 | 0.280 | 450 | 37.1 | 100 |
| | 3b | 1000 | 40 | 200 | 5 | 25 | 5 | $t/6$ | 1 | 0.310 | 450 | 0.280 | 450 | 54.0 | 168 |

(*continued on next page*)

**Table A1** (*continued*)

| Refs. | Designation | Geometrical dimensions | | | | | | | | Material properties | | | | | Capacity |
|---|---|---|---|---|---|---|---|---|---|---|---|---|---|---|---|
| | | $H$ (mm) | $t$ (mm) | $L$ (mm) | $\delta$ | $\lambda$ | $\eta$ | $e$ | $n$ | $\rho_v$ (%) | $f_{yv}$ (MPa) | $\rho_h$ (%) | $f_{yh}$ (MPa) | $f_c$ (MPa) | $N_u$ (kN) |
| | 4a | 1000 | 40 | 300 | 3.3 | 25 | 7.5 | $t/6$ | 1 | 0.210 | 450 | 0.280 | 450 | 35.7 | 199 |
| | 4b | 1000 | 40 | 300 | 3.3 | 25 | 7.5 | $t/6$ | 1 | 0.210 | 450 | 0.280 | 450 | 54.0 | 217 |
| | 5a | 1000 | 40 | 500 | 2 | 25 | 12.5 | $t/6$ | 1 | 0.250 | 450 | 0.280 | 450 | 35.7 | 201 |
| | 5b | 1000 | 40 | 500 | 2 | 25 | 12.5 | $t/6$ | 1 | 0.250 | 450 | 0.280 | 450 | 59.7 | 269 |
| | 6a | 600 | 40 | 200 | 3 | 15 | 5 | $t/6$ | 1 | 0.310 | 450 | 0.260 | 450 | 38.3 | 163 |
| | 6b | 600 | 40 | 200 | 3 | 15 | 5 | $t/6$ | 1 | 0.310 | 450 | 0.260 | 450 | 67.4 | 178 |
| | 7a | 600 | 40 | 150 | 4 | 15 | 3.8 | $t/6$ | 1 | 0.260 | 450 | 0.260 | 450 | 32.9 | 111 |
| | 7b | 600 | 40 | 150 | 4 | 15 | 3.8 | $t/6$ | 1 | 0.260 | 450 | 0.260 | 450 | 45.1 | 132 |
| | 8a | 420 | 35 | 210 | 2 | 12 | 6 | $t/6$ | 1 | 0.320 | 450 | 0.260 | 450 | 39.6 | 158 |
| | 8b | 420 | 35 | 210 | 2 | 12 | 6 | $t/6$ | 1 | 0.320 | 450 | 0.260 | 450 | 67.4 | 233 |
| Doh [40] | OWNS2 | 1200 | 40 | 1200 | 1 | 30 | 30 | $t/6$ | 1 | 0.310 | 500 | 0.310 | 500 | 35.7 | 253 |
| | OWNS3 | 1400 | 40 | 1400 | 1 | 35 | 35 | $t/6$ | 1 | 0.310 | 500 | 0.310 | 500 | 52.0 | 427 |
| | OWNS4 | 1600 | 40 | 1600 | 1 | 40 | 40 | $t/6$ | 1 | 0.310 | 500 | 0.310 | 500 | 51.0 | 442 |
| | OWHS2 | 1200 | 40 | 1200 | 1 | 30 | 30 | $t/6$ | 1 | 0.310 | 500 | 0.310 | 500 | 78.2 | 483 |
| | OWHS3 | 1400 | 40 | 1400 | 1 | 35 | 35 | $t/6$ | 1 | 0.310 | 500 | 0.310 | 500 | 63.0 | 442 |
| | OWHS4 | 1600 | 40 | 1600 | 1 | 40 | 40 | $t/6$ | 1 | 0.310 | 500 | 0.310 | 500 | 75.9 | 456 |
| Ganesan et al. [23] | OWSFN-1 | 480 | 40 | 320 | 1.5 | 12 | 8 | $t/6$ | 1 | 0.880 | 445 | 0.740 | 445 | 42.3 | 299 |
| | OWSFN-2 | 600 | 40 | 400 | 1.5 | 15 | 10 | $t/6$ | 1 | 0.880 | 445 | 0.740 | 445 | 42.3 | 323 |
| | OWSFN-3 | 840 | 40 | 560 | 1.5 | 21 | 14 | $t/6$ | 1 | 0.880 | 445 | 0.740 | 445 | 42.3 | 476 |
| | OWSFN-4 | 1200 | 40 | 800 | 1.5 | 30 | 20 | $t/6$ | 1 | 0.880 | 445 | 0.740 | 445 | 42.3 | 451 |
| | OWAFN-1 | 600 | 40 | 320 | 1.9 | 15 | 8 | $t/6$ | 1 | 0.880 | 445 | 0.740 | 445 | 42.3 | 235 |
| | OWAFN-2 | 600 | 40 | 400 | 1.5 | 15 | 10 | $t/6$ | 1 | 0.880 | 445 | 0.740 | 445 | 42.3 | 343 |
| | OWAFN-3 | 600 | 40 | 560 | 1.1 | 15 | 14 | $t/6$ | 1 | 0.880 | 445 | 0.740 | 445 | 42.3 | 486 |
| | OWAFN-4 | 600 | 40 | 800 | 0.8 | 15 | 20 | $t/6$ | 1 | 0.880 | 445 | 0.740 | 445 | 42.3 | 667 |
| | OWSFS-1 | 480 | 40 | 320 | 1.5 | 12 | 8 | $t/6$ | 1 | 0.880 | 445 | 0.740 | 445 | 42.3 | 309 |
| | OWSFS-2 | 600 | 40 | 400 | 1.5 | 15 | 10 | $t/6$ | 1 | 0.880 | 445 | 0.740 | 445 | 42.3 | 363 |
| | OWSFS-3 | 840 | 40 | 560 | 1.5 | 21 | 14 | $t/6$ | 1 | 0.880 | 445 | 0.740 | 445 | 41.3 | 491 |
| | OWSFS-4 | 1200 | 40 | 800 | 1.5 | 30 | 20 | $t/6$ | 1 | 0.880 | 445 | 0.740 | 445 | 41.3 | 476 |
| | OWAFS-1 | 600 | 40 | 320 | 1.9 | 15 | 8 | $t/6$ | 1 | 0.880 | 445 | 0.740 | 445 | 41.3 | 250 |
| | OWAFS-2 | 600 | 40 | 400 | 1.5 | 15 | 10 | $t/6$ | 1 | 0.880 | 445 | 0.740 | 445 | 41.3 | 363 |
| | OWAFS-3 | 600 | 40 | 560 | 1.1 | 15 | 14 | $t/6$ | 1 | 0.880 | 445 | 0.740 | 445 | 41.3 | 510 |
| | OWAFS-4 | 600 | 40 | 800 | 0.8 | 15 | 20 | $t/6$ | 1 | 0.880 | 445 | 0.740 | 445 | 41.3 | 711 |
| Ganesan et al. [24] | OPCSR-1 | 480 | 40 | 320 | 1.5 | 12 | 8 | $t/6$ | 1 | 0.880 | 445 | 0.740 | 445 | 42.3 | 279 |
| | OPCSR-1 | 480 | 40 | 320 | 1.5 | 12 | 8 | $t/6$ | 1 | 0.880 | 445 | 0.740 | 445 | 42.3 | 290 |
| | OPCSR-2 | 600 | 40 | 400 | 1.5 | 15 | 10 | $t/6$ | 1 | 0.880 | 445 | 0.740 | 445 | 42.3 | 330 |
| | OPCSR-2 | 600 | 40 | 400 | 1.5 | 15 | 10 | $t/6$ | 1 | 0.880 | 445 | 0.740 | 445 | 42.3 | 328 |
| | OPCSR-3 | 840 | 40 | 560 | 1.5 | 21 | 14 | $t/6$ | 1 | 0.880 | 445 | 0.740 | 445 | 42.3 | 435 |
| | OPCSR-3 | 840 | 40 | 560 | 1.5 | 21 | 14 | $t/6$ | 1 | 0.880 | 445 | 0.740 | 445 | 42.3 | 429 |
| | OPCAR-1 | 600 | 40 | 320 | 1.9 | 15 | 8 | $t/6$ | 1 | 0.880 | 445 | 0.740 | 445 | 42.3 | 228 |
| | OPCAR-1 | 600 | 40 | 320 | 1.9 | 15 | 8 | $t/6$ | 1 | 0.880 | 445 | 0.740 | 445 | 42.3 | 233 |
| | OPCAR-2 | 600 | 40 | 560 | 1.1 | 15 | 14 | $t/6$ | 1 | 0.880 | 445 | 0.740 | 445 | 42.3 | 441 |
| | OPCAR-2 | 600 | 40 | 560 | 1.1 | 15 | 14 | $t/6$ | 1 | 0.880 | 445 | 0.740 | 445 | 42.3 | 451 |
| | GPCSR-1 | 480 | 40 | 320 | 1.5 | 12 | 8 | $t/6$ | 1 | 0.880 | 445 | 0.740 | 445 | 41.3 | 261 |
| | GPCSR-1 | 480 | 40 | 320 | 1.5 | 12 | 8 | $t/6$ | 1 | 0.880 | 445 | 0.740 | 445 | 41.3 | 251 |
| | GPCSR-2 | 600 | 40 | 400 | 1.5 | 15 | 10 | $t/6$ | 1 | 0.880 | 445 | 0.740 | 445 | 41.3 | 310 |
| | GPCSR-2 | 600 | 40 | 400 | 1.5 | 15 | 10 | $t/6$ | 1 | 0.880 | 445 | 0.740 | 445 | 41.3 | 319 |
| | GPCSR-3 | 840 | 40 | 560 | 1.5 | 21 | 14 | $t/6$ | 1 | 0.880 | 445 | 0.740 | 445 | 41.3 | 420 |
| | GPCSR-3 | 840 | 40 | 560 | 1.5 | 21 | 14 | $t/6$ | 1 | 0.880 | 445 | 0.740 | 445 | 41.3 | 409 |
| | GPCAR-1 | 600 | 40 | 320 | 1.9 | 15 | 8 | $t/6$ | 1 | 0.880 | 445 | 0.740 | 445 | 41.3 | 232 |
| | GPCAR-1 | 600 | 40 | 320 | 1.9 | 15 | 8 | $t/6$ | 1 | 0.880 | 445 | 0.740 | 445 | 41.3 | 210 |
| | GPCAR-2 | 600 | 40 | 560 | 1.1 | 15 | 14 | $t/6$ | 1 | 0.880 | 445 | 0.740 | 445 | 41.3 | 445 |
| | GPCAR-2 | 600 | 40 | 560 | 1.1 | 15 | 14 | $t/6$ | 1 | 0.880 | 445 | 0.740 | 445 | 41.3 | 440 |
| Robinson et al. [17] | 7 | 2500 | 100 | 500 | 5 | 25 | 5 | $t/6$ | 1 | – | – | – | – | 51.5 | 871 |
| | 8 | 2500 | 100 | 500 | 5 | 25 | 5 | $t/6$ | 1 | – | – | – | – | 51.5 | 858 |
| | 9 | 2800 | 100 | 500 | 5.6 | 28 | 5 | $t/6$ | 1 | – | – | – | – | 52.4 | 692 |
| | 10 | 2800 | 100 | 500 | 5.6 | 28 | 5 | $t/6$ | 1 | – | – | – | – | 52.4 | 683 |
| | 11 | 3000 | 100 | 500 | 6 | 30 | 5 | $t/6$ | 1 | – | – | – | – | 51.6 | 582 |
| | 12 | 3000 | 100 | 500 | 6 | 30 | 5 | $t/6$ | 1 | – | – | – | – | 51.6 | 597 |
| | 13 | 3000 | 100 | 500 | 6 | 30 | 5 | $t/6$ | 1 | – | – | – | – | 51.6 | 572 |
| | 14 | 3000 | 100 | 500 | 6 | 30 | 5 | $t/6$ | 1 | – | – | – | – | 51.6 | 568 |

**Table A2**

| Refs. | Designation | Geometrical dimensions | | | | | | | | Material properties | | | | | Capacity |
|---|---|---|---|---|---|---|---|---|---|---|---|---|---|---|---|
| | | $H$ (mm) | $t$ (mm) | $L$ (mm) | $\delta$ | $\lambda$ | $\eta$ | $e$ | $n$ | $\rho_v$ (%) | $f_{yv}$ (MPa) | $\rho_h$ (%) | $f_{yh}$ (MPa) | $f_c$ (MPa) | $N_u$ (kN) |
| Sanjayan and Maheswaran [16] | 2 | 2000 | 50 | 1500 | 1.3 | 40 | 30 | $t$/6 | 1 | 0.850 | 513 | 0.850 | 513 | 80.5 | 1256.0 |
| | 3 | 2000 | 50 | 1500 | 1.3 | 40 | 30 | $t$/6 | 1 | 0.850 | 513 | 0.850 | 513 | 86.5 | 1435.0 |
| | 5 | 2000 | 50 | 1500 | 1.3 | 40 | 30 | $t$/6 | 1 | 0.850 | 513 | 0.850 | 513 | 77.5 | 871.0 |
| | 6 | 2000 | 50 | 1500 | 1.3 | 40 | 30 | $t$/6 | 1 | 1.690 | 513 | 1.690 | 513 | 77.5 | 1510.0 |
| | 8 | 2000 | 50 | 1500 | 1.3 | 40 | 30 | $t$/6 | 1 | 1.690 | 513 | 1.690 | 513 | 82.5 | 1533.0 |
| Swartz et al. [21] | 1 | 2438 | 25.4 | 1219 | 2 | 96 | 48 | 0 | 1 | 0.200 | 530 | 0.200 | 530 | 26.9 | 490.2 |
| | 2 | 2438 | 25.4 | 1219 | 2 | 96 | 48 | 0 | 1 | 0.200 | 530 | 0.200 | 530 | 26.2 | 506.7 |
| | 3 | 2438 | 25.4 | 1219 | 2 | 96 | 48 | 0 | 2 | 0.500 | 530 | 0.200 | 530 | 21.8 | 444.4 |
| | 4 | 2438 | 25.4 | 1219 | 2 | 96 | 48 | 0 | 2 | 0.500 | 530 | 0.200 | 530 | 23.7 | 534.2 |
| | 5 | 2438 | 25.4 | 1219 | 2 | 96 | 48 | 0 | 2 | 0.750 | 530 | 0.200 | 530 | 22.7 | 623.6 |
| | 6 | 2438 | 25.4 | 1219 | 2 | 96 | 48 | 0 | 2 | 0.750 | 530 | 0.200 | 530 | 24.5 | 691.7 |
| | 7 | 2438 | 25.4 | 1219 | 2 | 96 | 48 | 0 | 2 | 1.000 | 530 | 0.200 | 530 | 25.4 | 640.1 |
| | 8 | 2438 | 25.4 | 1219 | 2 | 96 | 48 | 0 | 2 | 1.000 | 530 | 0.200 | 530 | 22.1 | 455.1 |
| | 9 | 2438 | 31.8 | 1219 | 2 | 77 | 38 | 0 | 1 | 0.200 | 530 | 0.200 | 530 | 17.7 | 625.9 |
| | 10 | 2438 | 31.8 | 1219 | 2 | 77 | 38 | 0 | 1 | 0.200 | 530 | 0.200 | 530 | 18.3 | 696.2 |
| | 11 | 2438 | 31.8 | 1219 | 2 | 77 | 38 | 0 | 2 | 0.500 | 530 | 0.200 | 530 | 16.6 | 636.5 |
| | 12 | 2438 | 31.8 | 1219 | 2 | 77 | 38 | 0 | 2 | 0.500 | 530 | 0.200 | 530 | 17.9 | 639.7 |
| | 13 | 2438 | 31.8 | 1219 | 2 | 77 | 38 | 0 | 2 | 0.750 | 530 | 0.200 | 530 | 17.6 | 512.0 |
| | 14 | 2438 | 31.8 | 1219 | 2 | 77 | 38 | 0 | 2 | 0.750 | 530 | 0.200 | 530 | 19.8 | 716.2 |
| | 15 | 2438 | 31.8 | 1219 | 2 | 77 | 38 | 0 | 2 | 1.000 | 530 | 0.200 | 530 | 19.9 | 766.4 |
| | 16 | 2438 | 31.8 | 1219 | 2 | 77 | 38 | 0 | 2 | 1.000 | 530 | 0.200 | 530 | 17.9 | 722.0 |
| | 17 | 2438 | 19 | 1219 | 2 | 128 | 64 | 0 | 1 | 0.200 | 530 | 0.200 | 530 | 22.6 | 429.3 |
| | 18 | 2438 | 19 | 1219 | 2 | 128 | 64 | 0 | 1 | 0.200 | 530 | 0.200 | 530 | 23.3 | 396.3 |
| | 19 | 2438 | 19 | 1219 | 2 | 128 | 64 | 0 | 1 | 0.500 | 530 | 0.200 | 530 | 23.8 | 377.7 |
| | 20 | 2438 | 19 | 1219 | 2 | 128 | 64 | 0 | 1 | 0.500 | 530 | 0.200 | 530 | 24.5 | 372.8 |
| | 21 | 2438 | 19 | 1219 | 2 | 128 | 64 | 0 | 1 | 0.750 | 530 | 0.200 | 530 | 25.0 | 368.3 |
| | 22 | 2438 | 19 | 1219 | 2 | 128 | 64 | 0 | 1 | 0.750 | 530 | 0.200 | 530 | 24.8 | 355.9 |
| | 23 | 2438 | 19 | 1219 | 2 | 128 | 64 | 0 | 1 | 1.000 | 530 | 0.200 | 530 | 23.4 | 347.0 |
| | 24 | 2438 | 19 | 1219 | 2 | 128 | 64 | 0 | 1 | 1.000 | 530 | 0.200 | 530 | 27.0 | 400.3 |
| Saheb and Desayi [19] | WAR-1(P) | 600 | 50 | 900 | 0.7 | 12 | 18 | $t$/6 | 2 | 0.173 | 297 | 0.199 | 286 | 17.9 | 556.0 |
| | WAR-2(P) | 600 | 50 | 600 | 1 | 12 | 12 | $t$/6 | 2 | 0.173 | 297 | 0.199 | 286 | 17.9 | 413.5 |
| | WAR-3(P) | 600 | 50 | 400 | 1.5 | 12 | 8 | $t$/6 | 2 | 0.173 | 297 | 0.199 | 286 | 17.9 | 284.9 |
| | WAR-4(P) | 600 | 50 | 300 | 2 | 12 | 6 | $t$/6 | 2 | 0.173 | 297 | 0.199 | 286 | 17.9 | 235.2 |
| | WSR-1(P) | 450 | 50 | 300 | 1.5 | 9 | 6 | $t$/6 | 2 | 0.165 | 297 | 0.199 | 286 | 17.3 | 283.9 |
| | WSR-2(P) | 600 | 50 | 400 | 1.5 | 12 | 8 | $t$/6 | 2 | 0.165 | 297 | 0.199 | 286 | 17.3 | 346.7 |
| | WSR-3(P) | 900 | 50 | 600 | 1.5 | 18 | 12 | $t$/6 | 2 | 0.165 | 297 | 0.199 | 286 | 17.3 | 463.3 |
| | WSR-4(P) | 1350 | 50 | 900 | 1.5 | 27 | 18 | $t$/6 | 2 | 0.165 | 297 | 0.199 | 286 | 17.3 | 534.0 |
| | WSTV-2(P) | 600 | 50 | 900 | 0.7 | 12 | 18 | $t$/6 | 2 | 0.331 | 297 | 0.199 | 286 | 20.1 | 597.8 |
| | WSTV-3(P) | 600 | 50 | 900 | 0.7 | 12 | 18 | $t$/6 | 2 | 0.528 | 581 | 0.199 | 286 | 20.1 | 709.4 |
| | WSTV-4(P) | 600 | 50 | 900 | 0.7 | 12 | 18 | $t$/6 | 2 | 0.845 | 570 | 0.199 | 286 | 20.1 | 823.0 |
| | WSTV-5(P) | 1200 | 50 | 900 | 1.3 | 24 | 18 | $t$/6 | 2 | 0.177 | 297 | 0.199 | 286 | 18.3 | 498.2 |
| | WSTV-6(P) | 1200 | 50 | 800 | 1.5 | 24 | 16 | $t$/6 | 2 | 0.335 | 286 | 0.199 | 286 | 18.3 | 612.7 |
| | WSTV-7(P) | 1200 | 50 | 800 | 1.5 | 24 | 16 | $t$/6 | 2 | 0.528 | 581 | 0.199 | 286 | 18.3 | 717.4 |
| | WSTV-8(P) | 1200 | 50 | 800 | 1.5 | 24 | 16 | $t$/6 | 2 | 0.856 | 570 | 0.199 | 286 | 18.3 | 790.1 |
| | WSTH-2(P) | 600 | 50 | 900 | 0.7 | 12 | 18 | $t$/6 | 2 | 0.173 | 297 | 0.352 | 581 | 19.6 | 712.4 |
| | WSTH-3(P) | 600 | 50 | 900 | 0.7 | 12 | 18 | $t$/6 | 2 | 0.173 | 297 | 0.440 | 581 | 19.6 | 712.4 |
| | WSTH-4(P) | 600 | 50 | 900 | 0.7 | 12 | 18 | $t$/6 | 2 | 0.173 | 297 | 0.507 | 570 | 19.6 | 682.6 |
| | WSTH-6(P) | 1200 | 50 | 800 | 1.5 | 24 | 16 | $t$/6 | 2 | 0.176 | 297 | 0.352 | 581 | 16.1 | 597.8 |
| | WSTH-7(P) | 1200 | 50 | 800 | 1.5 | 24 | 16 | $t$/6 | 2 | 0.176 | 297 | 0.440 | 581 | 16.1 | 647.7 |
| | WSTH-8(P) | 1200 | 50 | 800 | 1.5 | 24 | 16 | $t$/6 | 2 | 0.176 | 297 | 0.507 | 570 | 16.1 | 632.7 |
| Doh [40] | TWNS1 | 1000 | 40 | 1200 | 0.8 | 25 | 30 | $t$/6 | 1 | 0.310 | 500 | 0.310 | 500 | 45.4 | 765.8 |
| | TWNS2 | 1200 | 40 | 1200 | 1 | 30 | 30 | $t$/6 | 1 | 0.310 | 500 | 0.310 | 500 | 37.0 | 735.8 |
| | TWNS3 | 1400 | 40 | 1400 | 1 | 35 | 35 | $t$/6 | 1 | 0.310 | 500 | 0.310 | 500 | 51.0 | 1177.2 |
| | TWNS4 | 1600 | 40 | 1600 | 1 | 40 | 40 | $t$/6 | 1 | 0.310 | 500 | 0.310 | 500 | 45.8 | 1177.2 |
| | TWHS1 | 1000 | 40 | 1200 | 0.8 | 25 | 30 | $t$/6 | 1 | 0.310 | 500 | 0.310 | 500 | 68.7 | 1147.8 |
| | TWHS2 | 1200 | 40 | 1200 | 1 | 30 | 30 | $t$/6 | 1 | 0.310 | 500 | 0.310 | 500 | 64.8 | 1177.2 |
| | TWHS3 | 1400 | 40 | 1400 | 1 | 35 | 35 | $t$/6 | 1 | 0.310 | 500 | 0.310 | 500 | 60.1 | 1250.8 |
| | TWHS4 | 1600 | 40 | 1600 | 1 | 40 | 40 | $t$/6 | 1 | 0.310 | 500 | 0.310 | 500 | 70.2 | 1648.1 |
| | TAHS1 | 1600 | 40 | 1400 | 1.1 | 40 | 35 | $t$/6 | 1 | 0.310 | 500 | 0.310 | 500 | 77.8 | 1618.7 |
| | TAHS2 | 1400 | 40 | 1000 | 1.4 | 35 | 25 | $t$/6 | 1 | 0.310 | 500 | 0.310 | 500 | 77.8 | 1118.3 |
| | TAHS3 | 1600 | 40 | 1200 | 1.3 | 40 | 30 | $t$/6 | 1 | 0.310 | 500 | 0.310 | 500 | 73.8 | 1265.5 |
| | TAHS4 | 1600 | 40 | 1000 | 1.6 | 40 | 25 | $t$/6 | 1 | 0.310 | 500 | 0.310 | 500 | 77.8 | 1442.1 |

**Table A3**

| Refs. | | Designation | Geometrical dimensions | | | | | | | | | | | | | | | | Material properties | | | | | Capacity |
|---|---|---|---|---|---|---|---|---|---|---|---|---|---|---|---|---|---|---|---|---|---|---|---|---|
| | | | $H$ | $t$ | $L$ | $\delta$ | $\lambda$ | $\eta$ | 1st Opening | | | | 2nd Opening | | | | $e$ | $n$ | $\rho_v$ | $f_{yv}$ | $\rho_h$ | $f_{yh}$ | $f_c$ | $N_u$ |
| | | | | | | | | | $H_0$ | $L_0$ | $X_{G1}$ | $y_{G1}$ | $H_0$ | $L_0$ | $x_{G2}$ | $y_{G2}$ | | | | | | | | |
| | | | (mm) | (mm) | (mm) | | | | (mm) | (mm) | (mm) | (mm) | (mm) | (mm) | (mm) | (mm) | | | (%) | (MPa) | (%) | (MPa) | (MPa) | (kN) |
| Saheb and Desayi [18] | OW | WWO-1 | 600 | 50 | 900 | 0.7 | 12 | 18 | 240 | 240 | 0 | 0 | 0 | 0 | 0 | 0 | $t/6$ | 2 | 0.173 | 297 | 0.236 | 297 | 28.2 | 672.6 |
| | | WWO-2 | 600 | 50 | 900 | 0.7 | 12 | 18 | 240 | 240 | −230 | 0 | 0 | 0 | 0 | 0 | $t/6$ | 2 | 0.173 | 297 | 0.236 | 297 | 28.2 | 568.9 |
| | | WWO-3 | 600 | 50 | 900 | 0.7 | 12 | 18 | 240 | 240 | −230 | 0 | 240 | 240 | 230 | 0 | $t/6$ | 2 | 0.173 | 297 | 0.236 | 297 | 28.2 | 433.5 |
| | | WWO-4 | 600 | 50 | 900 | 0.7 | 12 | 18 | 420 | 210 | 0 | −90 | 0 | 0 | 0 | 0 | $t/6$ | 2 | 0.173 | 297 | 0.236 | 297 | 28.2 | 652.7 |
| | | WWO-5 | 600 | 50 | 900 | 0.7 | 12 | 18 | 420 | 210 | −245 | −90 | 0 | 0 | 0 | 0 | $t/6$ | 2 | 0.173 | 297 | 0.236 | 297 | 28.2 | 548.0 |
| | | WWO-6 | 600 | 50 | 900 | 0.7 | 12 | 18 | 420 | 210 | −245 | −90 | 240 | 240 | 230 | 0 | $t/6$ | 2 | 0.173 | 297 | 0.236 | 297 | 28.2 | 423.5 |
| | TW | WWO-1(P) | 600 | 50 | 900 | 0.7 | 12 | 18 | 240 | 240 | 0 | 0 | 0 | 0 | 0 | 0 | $t/6$ | 2 | 0.173 | 297 | 0.236 | 297 | 28.2 | 692.5 |
| | | WWO-2(P) | 600 | 50 | 900 | 0.7 | 12 | 18 | 240 | 240 | −230 | 0 | 0 | 0 | 0 | 0 | $t/6$ | 2 | 0.173 | 297 | 0.236 | 297 | 28.2 | 592.8 |
| | | WWO-3(P) | 600 | 50 | 900 | 0.7 | 12 | 18 | 240 | 240 | −230 | 0 | 240 | 240 | 230 | 0 | $t/6$ | 2 | 0.173 | 297 | 0.236 | 297 | 28.2 | 448.4 |
| | | WWO-4(P) | 600 | 50 | 900 | 0.7 | 12 | 18 | 420 | 210 | 0 | −90 | 0 | 0 | 0 | 0 | $t/6$ | 2 | 0.173 | 297 | 0.236 | 297 | 28.2 | 697.5 |
| | | WWO-5(P) | 600 | 50 | 900 | 0.7 | 12 | 18 | 420 | 210 | −245 | −90 | 0 | 0 | 0 | 0 | $t/6$ | 2 | 0.173 | 297 | 0.236 | 297 | 28.2 | 587.8 |
| | | WWO-6(P) | 600 | 50 | 900 | 0.7 | 12 | 18 | 420 | 210 | −245 | −90 | 240 | 240 | 230 | 0 | $t/6$ | 2 | 0.173 | 297 | 0.236 | 297 | 28.2 | 448.4 |
| Doh and Fragomeni [27] | OW | OW11 | 1200 | 40 | 1200 | 1 | 30 | 30 | 300 | 300 | 0 | 0 | 0 | 0 | 0 | 0 | $t/6$ | 1 | 0.310 | 500 | 0.310 | 500 | 53 | 309.0 |
| | | OW12 | 1600 | 40 | 1600 | 1 | 40 | 40 | 400 | 400 | 0 | 0 | 0 | 0 | 0 | 0 | $t/6$ | 1 | 0.310 | 500 | 0.310 | 500 | 47 | 294.3 |
| | | OW21 | 1200 | 40 | 1200 | 1 | 30 | 30 | 300 | 300 | −250 | 0 | 300 | 300 | 250 | 0 | $t/6$ | 1 | 0.310 | 500 | 0.310 | 500 | 50 | 185.4 |
| | | OW22 | 1600 | 40 | 1600 | 1 | 40 | 40 | 400 | 400 | −333 | 0 | 400 | 400 | 333 | 0 | $t/6$ | 1 | 0.310 | 500 | 0.310 | 500 | 51.1 | 195.7 |
| | TW | TW11 | 1200 | 40 | 1200 | 1 | 30 | 30 | 300 | 300 | 0 | 0 | 0 | 0 | 0 | 0 | $t/6$ | 1 | 0.310 | 500 | 0.310 | 500 | 50.3 | 750.5 |
| | | TW12 | 1600 | 40 | 1600 | 1 | 40 | 40 | 400 | 400 | 0 | 0 | 0 | 0 | 0 | 0 | $t/6$ | 1 | 0.310 | 500 | 0.310 | 500 | 50.3 | 1030.1 |
| | | TW21 | 1200 | 40 | 1200 | 1 | 30 | 30 | 300 | 300 | −250 | 0 | 300 | 300 | 250 | 0 | $t/6$ | 1 | 0.310 | 500 | 0.310 | 500 | 50.3 | 618.0 |
| | | TW22 | 1600 | 40 | 1600 | 1 | 40 | 40 | 400 | 400 | −333 | 0 | 400 | 400 | 333 | 0 | $t/6$ | 1 | 0.310 | 500 | 0.310 | 500 | 50.3 | 647.5 |
| Lee [58] | OW | O50W1C1.2 | 1200 | 40 | 1200 | 1 | 30 | 30 | 300 | 300 | 0 | 0 | 0 | 0 | 0 | 0 | $t/6$ | 1 | 0.310 | 500 | 0.310 | 500 | 53 | 309 |
| | | O70W1C1.2 | 1200 | 40 | 1200 | 1 | 30 | 30 | 300 | 300 | 0 | 0 | 0 | 0 | 0 | 0 | $t/6$ | 1 | 0.310 | 500 | 0.310 | 500 | 67.7 | 426.7 |
| | | O90W1C1.2 | 1200 | 40 | 1200 | 1 | 30 | 30 | 300 | 300 | 0 | 0 | 0 | 0 | 0 | 0 | $t/6$ | 1 | 0.310 | 500 | 0.310 | 500 | 95.1 | 470.9 |
| | | O95W1C1.2 | 1200 | 40 | 1200 | 1 | 30 | 30 | 300 | 300 | 0 | 0 | 0 | 0 | 0 | 0 | $t/6$ | 1 | 0.310 | 500 | 0.310 | 500 | 96.2 | 488.5 |
| | | O45W1C1.4 | 1400 | 40 | 1400 | 1 | 35 | 35 | 350 | 350 | 0 | 0 | 0 | 0 | 0 | 0 | $t/6$ | 1 | 0.310 | 500 | 0.310 | 500 | 38 | 191.3 |
| | | O90W1C1.4 | 1400 | 40 | 1400 | 1 | 35 | 35 | 350 | 350 | 0 | 0 | 0 | 0 | 0 | 0 | $t/6$ | 1 | 0.310 | 500 | 0.310 | 500 | 80 | 300.2 |
| | | O95W1C1.4 | 1400 | 40 | 1400 | 1 | 35 | 35 | 350 | 350 | 0 | 0 | 0 | 0 | 0 | 0 | $t/6$ | 1 | 0.310 | 500 | 0.310 | 500 | 99.3 | 426.1 |
| | | O50W1C1.6 | 1600 | 40 | 1600 | 1 | 40 | 40 | 400 | 400 | 0 | 0 | 0 | 0 | 0 | 0 | $t/6$ | 1 | 0.310 | 500 | 0.310 | 500 | 47 | 294.3 |
| | | O90W1C1.6 | 1600 | 40 | 1600 | 1 | 40 | 40 | 400 | 400 | 0 | 0 | 0 | 0 | 0 | 0 | $t/6$ | 1 | 0.310 | 500 | 0.310 | 500 | 97.1 | 503.3 |
| | | O50W2C1.2 | 1200 | 40 | 1200 | 1 | 30 | 30 | 300 | 300 | −250 | 0 | 300 | 300 | 250 | 0 | $t/6$ | 1 | 0.310 | 500 | 0.310 | 500 | 50.3 | 191.3 |
| | | O70W2C1.2 | 1200 | 40 | 1200 | 1 | 30 | 30 | 300 | 300 | −250 | 0 | 300 | 300 | 250 | 0 | $t/6$ | 1 | 0.310 | 500 | 0.310 | 500 | 67.7 | 242.8 |
| | | O95W2C1.2 | 1200 | 40 | 1200 | 1 | 30 | 30 | 300 | 300 | −250 | 0 | 300 | 300 | 250 | 0 | $t/6$ | 1 | 0.310 | 500 | 0.310 | 500 | 96.2 | 308.1 |
| | | O45W2C1.4 | 1400 | 40 | 1400 | 1 | 35 | 35 | 350 | 350 | −292 | 0 | 350 | 350 | 292 | 0 | $t/6$ | 1 | 0.310 | 500 | 0.310 | 500 | 44.5 | 150.7 |
| | | O90W2C1.4 | 1400 | 40 | 1400 | 1 | 35 | 35 | 350 | 350 | −292 | 0 | 350 | 350 | 292 | 0 | $t/6$ | 1 | 0.310 | 500 | 0.310 | 500 | 80 | 244.3 |
| | | O95W2C1.4 | 1400 | 40 | 1400 | 1 | 35 | 35 | 350 | 350 | −292 | 0 | 350 | 350 | 292 | 0 | $t/6$ | 1 | 0.310 | 500 | 0.310 | 500 | 99.3 | 350.8 |
| | | O50W2C1.6 | 1600 | 40 | 1600 | 1 | 40 | 40 | 400 | 400 | −333 | 0 | 400 | 400 | 333 | 0 | $t/6$ | 1 | 0.310 | 500 | 0.310 | 500 | 51.1 | 195.7 |
| | | O70W2C1.6 | 1600 | 40 | 1600 | 1 | 40 | 40 | 400 | 400 | −333 | 0 | 400 | 400 | 333 | 0 | $t/6$ | 1 | 0.310 | 500 | 0.310 | 500 | 74.1 | 279 |
| | | O90W2C1.6 | 1600 | 40 | 1600 | 1 | 40 | 40 | 400 | 400 | −333 | 0 | 400 | 400 | 333 | 0 | $t/6$ | 1 | 0.310 | 500 | 0.310 | 500 | 97.1 | 347.3 |
| | | O65W1W1.2 | 1200 | 40 | 1200 | 1 | 30 | 30 | 300 | 600 | 0 | 0 | 0 | 0 | 0 | 0 | $t/6$ | 1 | 0.310 | 500 | 0.310 | 500 | 60.3 | 176 |
| | | O65W1L1.2 | 1200 | 40 | 1200 | 1 | 30 | 30 | 300 | 300 | −250 | 0 | 0 | 0 | 0 | 0 | $t/6$ | 1 | 0.310 | 500 | 0.310 | 500 | 60.3 | 258.4 |
| | | O65W1U1.2 | 1200 | 40 | 1200 | 1 | 30 | 30 | 300 | 300 | −250 | 150 | 0 | 0 | 0 | 0 | $t/6$ | 1 | 0.310 | 500 | 0.310 | 500 | 60.3 | 257.8 |
| | | O65D1C1.2 | 1200 | 40 | 1200 | 1 | 30 | 30 | 750 | 300 | 0 | −225 | 0 | 0 | 0 | 0 | $t/6$ | 1 | 0.310 | 500 | 0.310 | 500 | 60.3 | 243.7 |
| | | O65D1L1.2 | 1200 | 40 | 1200 | 1 | 30 | 30 | 750 | 300 | −250 | −225 | 0 | 0 | 0 | 0 | $t/6$ | 1 | 0.310 | 500 | 0.310 | 500 | 60.3 | 206 |
| | TW | T50W1C1.2 | 1200 | 40 | 1200 | 1 | 30 | 30 | 300 | 300 | 0 | 0 | 0 | 0 | 0 | 0 | $t/6$ | 1 | 0.310 | 500 | 0.310 | 500 | 50.3 | 706.3 |
| | | T70W1C1.2 | 1200 | 40 | 1200 | 1 | 30 | 30 | 300 | 300 | 0 | 0 | 0 | 0 | 0 | 0 | $t/6$ | 1 | 0.310 | 500 | 0.310 | 500 | 74.1 | 953.5 |
| | | T45W1C1.4 | 1400 | 40 | 1400 | 1 | 35 | 35 | 350 | 350 | 0 | 0 | 0 | 0 | 0 | 0 | $t/6$ | 1 | 0.310 | 500 | 0.310 | 500 | 45.5 | 732.8 |
| | | T90W1C1.4 | 1400 | 40 | 1400 | 1 | 35 | 35 | 350 | 350 | 0 | 0 | 0 | 0 | 0 | 0 | $t/6$ | 1 | 0.310 | 500 | 0.310 | 500 | 95.1 | 1303.7 |
| | | T95W1C1.4 | 1400 | 40 | 1400 | 1 | 35 | 35 | 350 | 350 | 0 | 0 | 0 | 0 | 0 | 0 | $t/6$ | 1 | 0.310 | 500 | 0.310 | 500 | 96.2 | 1298.4 |
| | | T50W1C1.6 | 1600 | 40 | 1600 | 1 | 40 | 40 | 400 | 400 | 0 | 0 | 0 | 0 | 0 | 0 | $t/6$ | 1 | 0.310 | 500 | 0.310 | 500 | 50.3 | 1030.1 |
| | | T70W1C1.6 | 1600 | 40 | 1600 | 1 | 40 | 40 | 400 | 400 | 0 | 0 | 0 | 0 | 0 | 0 | $t/6$ | 1 | 0.310 | 500 | 0.310 | 500 | 75.1 | 1390.6 |

| | | | | | | | | | | | | | | | | | | | | | | | |
|---|---|---|---|---|---|---|---|---|---|---|---|---|---|---|---|---|---|---|---|---|---|---|---|
| | | T90W1C1.6 | 1600 | 40 | 1600 | 1 | 40 | 40 | 400 | 400 | 0 | 0 | 0 | 0 | 0 | 0 | $t/6$ | 1 | 0.310 | 500 | 0.310 | 500 | 93.6 | 1583.3 |
| | | T50W2C1.2 | 1200 | 40 | 1200 | 1 | 30 | 30 | 300 | 300 | −250 | 0 | 300 | 300 | 250 | 0 | $t/6$ | 1 | 0.310 | 500 | 0.310 | 500 | 50.3 | 618 |
| | | T70W2C1.2 | 1200 | 40 | 1200 | 1 | 30 | 30 | 300 | 300 | −250 | 0 | 300 | 300 | 250 | 0 | $t/6$ | 1 | 0.310 | 500 | 0.310 | 500 | 74.1 | 633.4 |
| | | T90W2C1.2 | 1200 | 40 | 1200 | 1 | 30 | 30 | 300 | 300 | −250 | 0 | 300 | 300 | 250 | 0 | $t/6$ | 1 | 0.310 | 500 | 0.310 | 500 | 97.1 | 665.1 |
| | | T45W2C1.4 | 1400 | 40 | 1400 | 1 | 35 | 35 | 350 | 350 | −292 | 0 | 350 | 350 | 292 | 0 | $t/6$ | 1 | 0.310 | 500 | 0.310 | 500 | 45.5 | 662.2 |
| | | T90W2C1.4 | 1400 | 40 | 1400 | 1 | 35 | 35 | 350 | 350 | −292 | 0 | 350 | 350 | 292 | 0 | $t/6$ | 1 | 0.310 | 500 | 0.310 | 500 | 95.1 | 918.2 |
| | | T95W2C1.4 | 1400 | 40 | 1400 | 1 | 35 | 35 | 350 | 350 | −292 | 0 | 350 | 350 | 292 | 0 | $t/6$ | 1 | 0.310 | 500 | 0.310 | 500 | 80 | 759.9 |
| | | T50W2C1.6 | 1600 | 40 | 1600 | 1 | 40 | 40 | 400 | 400 | −333 | 0 | 400 | 400 | 333 | 0 | $t/6$ | 1 | 0.310 | 500 | 0.310 | 500 | 50.3 | 647.5 |
| | | T70W2C1.6 | 1600 | 40 | 1600 | 1 | 40 | 40 | 400 | 400 | −333 | 0 | 400 | 400 | 333 | 0 | $t/6$ | 1 | 0.310 | 500 | 0.310 | 500 | 75.1 | 988.8 |
| | | T90W2C1.6 | 1600 | 40 | 1600 | 1 | 40 | 40 | 400 | 400 | −333 | 0 | 400 | 400 | 333 | 0 | $t/6$ | 1 | 0.310 | 500 | 0.310 | 500 | 94.2 | 1236.1 |
| | | T65W1W1.2 | 1200 | 40 | 1200 | 1 | 30 | 30 | 300 | 600 | 0 | 0 | 0 | 0 | 0 | 0 | $t/6$ | 1 | 0.310 | 500 | 0.310 | 500 | 56.4 | 682.2 |
| | | T65W1L1.2 | 1200 | 40 | 1200 | 1 | 30 | 30 | 300 | 300 | −250 | 0 | 0 | 0 | 0 | 0 | $t/6$ | 1 | 0.310 | 500 | 0.310 | 500 | 65 | 737.5 |
| | | T65W1U1.2 | 1200 | 40 | 1200 | 1 | 30 | 30 | 300 | 300 | −250 | 150 | 0 | 0 | 0 | 0 | $t/6$ | 1 | 0.310 | 500 | 0.310 | 500 | 62.4 | 715.7 |
| | | T65D1C1.2 | 1200 | 40 | 1200 | 1 | 30 | 30 | 750 | 300 | 0 | −225 | 0 | 0 | 0 | 0 | $t/6$ | 1 | 0.310 | 500 | 0.310 | 500 | 65 | 676.9 |
| | | T65D1L1.2 | 1200 | 40 | 1200 | 1 | 30 | 30 | 750 | 300 | −250 | −225 | 0 | 0 | 0 | 0 | $t/6$ | 1 | 0.310 | 500 | 0.310 | 500 | 56.4 | 582.7 |
| | | T65W1SB1.2 | 1200 | 40 | 1200 | 1 | 30 | 30 | 240 | 240 | 0 | −120 | 0 | 0 | 0 | 0 | $t/6$ | 1 | 0.310 | 500 | 0.310 | 500 | 62.4 | 794.6 |
| | | T65W1SL1.2 | 1200 | 40 | 1200 | 1 | 30 | 30 | 240 | 240 | 120 | 0 | 0 | 0 | 0 | 0 | $t/6$ | 1 | 0.310 | 500 | 0.310 | 500 | 56.4 | 721 |
| Mohammed et al. [4] | OW | WO1 | 800 | 50 | 400 | 2 | 16 | 8 | 170 | 95 | 0 | 0 | 0 | 0 | 0 | 0 | $t/6$ | 1 | 0.400 | 478 | 0.700 | 478 | 16.9 | 210 |
| | | WO2 | 800 | 50 | 400 | 2 | 16 | 8 | 240 | 135 | 0 | 0 | 0 | 0 | 0 | 0 | $t/6$ | 1 | 0.400 | 478 | 0.700 | 478 | 17.7 | 203.8 |
| | | WO3 | 800 | 50 | 400 | 2 | 16 | 8 | 340 | 185 | 0 | 0 | 0 | 0 | 0 | 0 | $t/6$ | 1 | 0.400 | 478 | 0.700 | 478 | 18.4 | 179.8 |
| | | WO4 | 800 | 50 | 400 | 2 | 16 | 8 | 420 | 230 | 0 | 0 | 0 | 0 | 0 | 0 | $t/6$ | 1 | 0.400 | 478 | 0.700 | 478 | 19.8 | 172.8 |
| | | WO1a | 800 | 40 | 400 | 2 | 20 | 10 | 170 | 95 | 0 | 0 | 0 | 0 | 0 | 0 | $t/6$ | 1 | 0.500 | 478 | 0.900 | 478 | 16 | 100 |
| | | WO2a | 800 | 40 | 400 | 2 | 20 | 10 | 240 | 135 | 0 | 0 | 0 | 0 | 0 | 0 | $t/6$ | 1 | 0.500 | 478 | 0.900 | 478 | 13.9 | 95.3 |
| | | WO3a | 800 | 40 | 400 | 2 | 20 | 10 | 340 | 185 | 0 | 0 | 0 | 0 | 0 | 0 | $t/6$ | 1 | 0.500 | 478 | 0.900 | 478 | 15.6 | 85 |
| | | WO4a | 800 | 40 | 400 | 2 | 20 | 10 | 420 | 230 | 0 | 0 | 0 | 0 | 0 | 0 | $t/6$ | 1 | 0.500 | 478 | 0.900 | 478 | 15.8 | 73.7 |

## References


[1] Dol K, Haffner M. Housing Statistics in the European Union 2010. Delft University of Technology, Netherlands: OTB Research Institute for the Built Environment; 2010.

[2] Seddon AE. The strength of concrete walls under axial and eccentric loads. In: Andrew RP, editor. Symposium on the strength of concrete structures. London, UK: Cement and Concrete Association; 1956. p. 445–86.

[3] Demeter I. Seismic retrofit of precast RC walls by externally bonded CFRP composites. Romania: PhD Thesis, Politehnica University of Timisoara; 2011.

[4] Mohammed B, Ean LW, Malek MA. One way RC wall panels with openings strengthened with CFRP. Constr Build Mater 2013;40:575–83.

[5] Engel P. General rehabilitation techniques using steel. <http://www.constructalia.com/english/renovation_with_steel/ii_general_rehabilitation_techniques_using_steel#.VMPsNP6G9Wg> [accessed 01.23.15]

[6] Delatte N. Failure, distress and repair of concrete structures. Woodhead Publishing; 2009.

[7] Bakis CE, Bank LC, Brown VL, Cosenza E, Davalos JF, Lesko JJ, et al. Fiber-reinforced polymer composites for construction – state-of-the-art review. J Compos Constr 2002;6:73–87.

[8] Van Den Einde L, Zhao L, Seible F. Use of FRP composites in civil structural applications. Constr Build Mater 2003;17:389–403.

[9] Hollaway LC, Hollaway LC. A review of the present and future utilisation of FRP composites in the civil infrastructure with reference to their important in-service properties. Constr Build Mater 2010;24:2419–45.

[10] Täljsten B, Blanksvärd Thomas, Sas G. FRP strengthening of existing concrete structures. Design guideline (in Swedish). Luleå, Sweden: Luleå University of Technology, Division of Structural Engineering; 2012.

[11] ACI318. Building code requirements for structural concrete and commentary (ACI 318–11). Farmington Hills: AMERICAN CONCRETE INSTITUTE; 2011. p. 503.

[12] AS3600. Concrete structures. Sydney, Australia: Standards Australia; 2009.

[13] CAN/CSA-A23.3. Design of concrete structures. Mississauga, Ontario: CANADIAN STANDARDS ASSOCIATION; 2004.

[14] EN 1992-1-1. Eurocode 2: design of concrete structures – Part 1–1: General rules and rules for buildings. Brussels: COMITÉ EUROPÉEN DE NORMALISATION; 2004.

[15] Pillai SU, Parthasarathy CV. Ultimate strength and design of concrete walls. Build Environ 1977;12:25–9.

[16] Sanjayan JG, Maheswaran T. Load capacity of slender high-strength concrete walls with side supports. ACI Struct J 1999;96:571–6.

[17] Robinson G, Palmeri A, Austin S. Design methodologies for one way spanning eccentrically loaded minimally or centrally reinforced pre-cast RC panels. Eng Struct 2013;56:1945–56.

[18] Saheb SM, Desayi P. Ultimate strength of RC wall panels with openings. J Struct Eng-Asce 1990;116:1565–78.

[19] Saheb SM, Desayi P. Ultimate strength of R.C. wall panels in two-way in-plane action. J Struct Eng-Asce 1990;116:1384–402.

[20] Doh JH, Fragomeni S. Evaluation of experimental work on concrete walls in one-way and two-way action. Aust J Struct Eng 2005;6:37–52.

[21] Swartz SE, Rosebraugh VH, Rogacki SA. A method for determining the buckling strength of concrete panels. Exp Mech 1974;14:138–44.

[22] Saheb SM, Desayi P. Ultimate strength of RC wall panels in one-way in-plane action. J Struct Eng-Asce 1989;115:2617–30.

[23] Ganesan N, Indira PV, Rajendra Prasad S. Strength and behavior of SFRSCC and SFRC wall panels under one-way in-plane action. In: Parra-Montesinos G, Reinhardt H, Naaman AE, editors. High performance fiber reinforced cement composites 6. Netherlands: Springer; 2012. p. 279–86.

[24] Ganesan N, Indira PV, Santhakumar A. Prediction of ultimate strength of reinforced geopolymer concrete wall panels in one-way action. Constr Build Mater 2013;48:91–7.

[25] El-Metwally S, Ashour F, Chen W. Instability analysis of eccentrically loaded concrete walls. J Struct Eng-Asce 1990;116:2862–80.

[26] Doh JH, Loo YC, Fragomeni S. Concrete walls with and without openings supported on three sides. In: Sam Fragomeni SV, Lam Nelson TK, Setunge Sujeeva, editor. Incorporating sustainable practice in mechanics and structures of materials. Taylor & Francis Group; 2010. p. 209–14.

[27] Doh JH, Fragomeni S. Ultimate load formula for reinforced concrete wall panels with openings. Adv Struct Eng 2006;9:103–15.

[28] Fragomeni S, Doh JH, Lee DJ. Behavior of axially loaded concrete wall panels with openings: an experimental study. Adv Struct Eng 2012;15:1345–58.

[29] Fragomeni S, Mendis PA, Grayson WR. Axial load tests on normal and high strength concrete wall panels. Transact Institut Eng, Austr/CE 1994;36:257–63.

[30] Larsson L-E. Bearing capacity of plain and reinforced concrete walls [PhD Thesis]. Göteborg: Chalmers Tekniska Högskola; 1959.

[31] Fragomeni S, Mendis P. Instability analysis of normal- and high-strength reinforced-concrete walls. J Struct Eng 1997;123:680–4.

[32] Mattock AH, Kriz LB, Hognestad E. Rectangular concrete stress distribution in ultimate strength design. ACI Struct J 1961;57:875–928.

[33] Macgregor JG, Breen JE, Pfrang EO. Design of slender concrete columns. ACI Struct J 1970;67:6–28.

[34] Parme AL. Capacity of restrained eccentrically loaded long columns. Symposium of reinforced concrete columns SP-13, American Concrete Institute; 1966. p. 325–67.

[35] Kripanarayanan KM. Interesting aspect of the empirical wall design equation. ACI Struct J 1977;74:204–7.

[36] Leabu VF. Problems and performances of precast concrete wall panels. ACI Struct J 1959;56:287–98.

[37] Oberlender GD, Everard NJ. Investigation of reinforced concrete walls. ACI Struct J 1977;74:256–63.

[38] Zielinski ZA, Troitsky MS, Christodoulou H. Full-scale bearing strength investigation of thin wall-ribbed reinforced concrete panels. ACI Struct J 1982;79:313–21.

[39] ACI Committee 318. Building code requirements for reinforced concrete (ACI 318–77). Detroit: American Concrete Institute; 1977.

[40] Doh JH. Experimental and theoretical studies of normal and high strength concrete wall panels. Australia: PhD Thesis, Griffith University; 2002.

[41] BS8110-1997. Structural use of concrete, Part 1 – Code of practice for Design and Construction. London: British Standards Institution; 1997.

[42] Hegger J, Dressen T, Will N. Load-bearing capacity of plain concrete walls. Mag Concr Res 2009;61:173.

[43] Haller P. Load capacity of brick masonry. Designing. Engineering and constructing with masonry products ed. Houstion, TX, USA: Gulf Publishing; 1969.

[44] Gere JM, Timoshenko SP. Mechanics of materials. 3rd ed. Massachusetts, USA: PWS-KENT; 1990.

[45] Robinson G, Palmeri A, Austin S. Implications of EC2 on the design of simply supported precast RC panels under eccentric axial load. In: Proceedings of fib symposium on concrete engineering for excelence and efficiency; 2011.

[46] Macgregor JG, Simmonds SH, Warwaruk J. Seminar on building code requirements, ACI318-71. University of Alberta, Department of Civil Engineering, Structural engineering report no. 36; 1971.

[47] Westerberg B. Load bearing capacity of unreinforced walls. Second International Workshop in DESIGN OF CONCRETE STRUCTURES AND BRIDGES USING EUROCODES. Bratislava, Slovakia: Slovak University of Technology in Bratislava, Faculty of Civil Engineering; 2011.

[48] Fragomeni S. Review of reinforced concrete wall design formulas. ACI Struct J 1994;91:521–9.

[49] Timoshenko SP, Gere JM. Theory of elastic stability. New York: McGRAW-HILL International Book Co.; 1961.

[50] Aghayere AO, MacGregor JG. Analysis of concrete plates under combined in-plane and transverse loads. ACI Struct J 1990;87:539–47.

[51] Fragomeni S, Mendis P. Improved axial load formulae for normal and high strength reinforced concrete walls. Aust Civ Eng 1996;38:71–81.

[52] Fragomeni S. Design of normal and high strength reinforced concrete walls. Australia: PhD Thesis, University of Melbourne; 1995.

[53] Chen WF, Atsuta T. Strength of eccentrically loaded walls. Int J Solids Struct 1973;9:1283–300.

[54] Kirtschig K, Anstötz W. Knickuntersuchungen an Mauerwerksprosben. In: Proceedings of the 9th international brick/block masonry conference. Berlin: Deutsche Gesellschaft für Mauerwerksbau e.V., Bonn, Germany; 1991. p. 202–9.

[55] Glock C. Traglast unbewehrter Beton- und Mauerwerkswände. TU Darmstadt: Institute for Concrete and Masonry Structures; 2004.

[56] fib Model Code 2010. fib Model Code 2010 for Concrete Structures. Lausanne, Switzerland: Fédération Internationale du Béton; 2013.

[57] EN 1990. Eurocode 0: Basis of structural design. Brussels: COMITÉ EUROPÉEN DE NORMALISATION; 2004.

[58] Lee D-J. Experimental and theoretical study of normal and high strength concrete wall panels with openings. Australia: PhD Thesis, Griffith University; 2008.

[59] Guan H, Cooper C, Lee D-J. Ultimate strength analysis of normal and high strength concrete wall panels with varying opening configurations. Eng Struct 2010;32:1341–55.

[60] Antoniades K, Salonikios T, Kappos A. Tests on seismically damaged reinforced concrete walls repaired and strengthened using fiber-reinforced polymers. J Compos Constr 2005;9:236–46.

[61] Dan D. Experimental tests on seismically damaged composite steel concrete walls retrofitted with CFRP composites. Eng Struct 2012;45:338–48.

[62] Li B, Lim C. Tests on seismically damaged reinforced concrete structural walls repaired using fiber-reinforced polymers. J Compos Constr 2010;14:597–608.

[63] Li B, Qian K. Retrofitting earthquake-damaged RC structural walls with openings by externally bonded FRP strips and sheets. J Compos Constr 2013;17:259–70.

[64] Todut C, Dan D, Stoian V. Numerical and experimental investigation on seismically damaged reinforced concrete wall panels retrofitted with FRP composites. Compos Struct 2015;119:648–65.

[65] El Maaddawy T, Sherif S, El Maaddawy T, Sherif S. FRP composites for shear strengthening of reinforced concrete deep beams with openings. Compos Struct 2009;89:60–9.

[66] Enochsson O, Lundqvist J, Taljsten B, Rusinowski P, Olofsson T. CFRP strengthened openings in two-way concrete slabs – an experimental and numerical study. Constr Build Mater 2007;21:810–26.

[67] Floruț S-C, Sas G, Popescu C, Stoian V. Tests on reinforced concrete slabs with cut-out openings strengthened with fibre-reinforced polymers. Compos Part B – Eng 2014;66:484–93.

# Paper II

## Effect of cut-out openings on the axial strength of concrete walls

Cosmin Popescu; Gabriel Sas; Cristian Sabău; and Thomas Blanksvärd

Published in:
*Journal of Structural Engineering*
Vol. 142, No. 11, 2016
Article ID 04016100

# Effect of Cut-Out Openings on the Axial Strength of Concrete Walls

Cosmin Popescu, S.M.ASCE[1]; Gabriel Sas[2]; Cristian Sabău[3]; and Thomas Blanksvärd[4]

**Abstract:** Old structures are frequently modified to comply with current living standards and/or legislation. Such modifications may include the addition of new windows or doors and paths for ventilation and heating systems, all of which require openings to be cut into structural walls. However, effects of the required openings are not sufficiently understood. Thus, the objective of the work reported here was to analyze openings' effects on the axial strength of large concrete wall panels. Three half-scaled walls with two opening configurations, corresponding to small and large door openings, were subjected to a uniformly distributed axial load with a small eccentricity. The results indicate that the 25 and 50% reductions in cross-sectional area of the solid wall caused by introducing the small and large openings reduced the load-carrying capacity by nearly 36 and 50%, respectively. The failure progression was captured using digital image correlation technique and the results indicated involvement of a plate mechanism rather than uniaxial behavior as adopted in current design codes. Using a simplified procedure, the load-carrying capacity was predicted using existing design models found in the research literature and design codes. **DOI: 10.1061/(ASCE)ST.1943-541X.0001558.** 

**Author keywords:** Concrete walls; Openings; Axial load; Out-of-plane behavior; Digital image correlation; Concrete and masonry structures.

## Introduction

Refurbishment of concrete structures has greatly increased in recent decades due to aging, changes in role (e.g., conversions of apartment buildings to office spaces), design errors, construction faults, and exceptional events such as natural disasters or explosions. Sometimes this involves cutting out new openings, which causes changes in structural parameters that should be rigorously assessed. This paper deals with methods for assessing the effects of creating openings in existing concrete walls.

Openings are usually avoided in RC structural elements, whenever possible, in order to minimize unfavorable effects of discontinuous regions. However, in recent years there has been increasing interest in enlarging spaces by connecting adjacent rooms through creating openings in existing solid walls. These openings are a source of weakness and can size-dependently reduce the structures' stiffness and load-bearing capacity. It is generally believed that effects of small openings can often be neglected, while a large opening usually significantly alters the structural system (Seddon 1956b), but there is no clear definition of the size threshold in the literature.

Numerous experimental studies have examined the behavior of solid RC walls, but the performance of RC walls with openings has been studied much less intensively, although new openings may be required for various reasons, e.g., to install new doors, windows, or paths for ventilation or heating systems. Exceptions include contributions by Ali and Wight (1991), Taylor et al. (1998), Wang et al. (2012), Mosoarca (2014), and Todut et al. (2014). However, the cited studies focused on structural walls subjected to seismic forces; effects of openings in walls that are only designed to withstand axial compression loads have received much less attention. Literature on the behavior of axially loaded walls has been reviewed by Fragomeni et al. (1994) and Popescu et al. (2015). Both of these reviews concluded that the performance of walls with openings has not been thoroughly addressed, and some results are conflicting, thus more experimental tests are needed. For example, it is generally believed that reinforcement does not significantly affect the ultimate load (Pillai and Parthasarathy 1977). However, Ganesan et al. (2013) found that all equations in the literature are conservative, and thus proposed a model that takes into consideration the amount of reinforcement and "was found to compare satisfactorily with the experimental results." Furthermore, most relevant research has focused on one-way (OW) action walls (panels restrained only along their top and bottom edges). Walls restrained in this fashion tend to develop a single out-of-plane curvature parallel to the load direction, and are usually encountered in tilt-up concrete structures. Walls or panels restrained along three or four sides are referred to as two-way (TW) action panels. They generally deform in both the horizontal and vertical directions, are usually found in monolithic concrete structures, and their behavior has also received relatively little attention. However, some aspects of the behavior of OW and TW walls have been addressed, and relevant previous studies include the following. The first systematic study of axially loaded OW and TW concrete walls with openings was reported by Saheb and Desayi (1990b), who examined effects of aspect, thickness, slenderness, and steel reinforcement ratios (vertical and horizontal) on their ultimate load. Doh and Fragomeni (2006) and Fragomeni et al. (2012) subsequently reported two experimental

[1]Ph.D. Candidate, Northern Research Institute–NORUT, Rombaksveien E6-47, N-8517 Narvik, Norway (corresponding author). E-mail: cosmin.popescu@norut.no

[2]Associate Senior Lecturer, Dept. of Civil, Environmental and Natural Resources Engineering, Luleå Univ. of Technology, SE-97187 Luleå, Sweden.

[3]Ph.D. Candidate, Dept. of Civil, Environmental and Natural Resources Engineering, Luleå Univ. of Technology, SE-97187 Luleå, Sweden.

[4]Associate Senior Lecturer, Dept. of Civil, Environmental and Natural Resources Engineering, Luleå Univ. of Technology, SE-97187 Luleå, Sweden.

Note. This manuscript was submitted on July 23, 2015; approved on March 1, 2016; published online on June 6, 2016. Discussion period open until November 6, 2016; separate discussions must be submitted for individual papers. This paper is part of the ***Journal of Structural Engineering***, © ASCE, ISSN 0733-9445.

programs on walls with different opening configurations and slenderness ratios, which provided foundations for calibrating simplified design equations for predicting ultimate load capacities (Doh and Fragomeni 2006; Guan 2010).

Design codes such as AS 3600 (Standards Australia 2009) and EN 1992-1-1 (CEN 2004) provide some guidance. According to these codes, effects of an opening can be neglected if the wall is restrained on all sides, and the opening's area and height are less than 1/10 and 1/3 of the wall's total area and height, respectively. If these conditions are not met, the portion between a restraining member and opening has to be treated as a separate member, supported on three sides, and areas between openings (if there are more than one) must be treated as being supported on two sides. However, the effect of walls being restrained along all their sides is not recognized by two major codes [ACI 318 (2011) and CAN/CSA-A23.3 (Canadian Standards Association 2004)], and all current design codes ignore the contribution of the steel reinforcement to the axial strength. The validity of ignoring this contribution is supported by some empirical data (Pillai and Parthasarathy 1977) for reinforcement placed within one layer, but not when two reinforcing layers are used (Fragomeni and Mendis 1997).

A recent state-of-the-art review (Popescu et al. 2015) highlighted gaps in this research field, and aspects that warrant systematic analysis to improve both understanding of the behavior of walls with openings and design provisions. These aspects include boundary conditions, eccentricity, layout and ratio of the reinforcement, slenderness, aspect ratio, and the focal aspect of this work: effects of openings' sizes. Three half-scale walls were tested in TW action and subjected to axial loading with small eccentricity. The results were then used to assess the accuracy of current design models. The reported work is part of a larger research program on the effectiveness of fiber-reinforced polymers (FRPs) for strengthening large concrete panels when new openings are made. Use of FRPs has already proved to be a viable solution when cut-out openings are required in structural elements (Li et al. 2013; Todut et al. 2015; Floruţ et al. 2014), but the ongoing program is expected to significantly extend the findings and their practical utility.

## Research Significance

Most previous studies on the effects of openings in RC walls have focused on design aspects of walls with appropriate reinforcement detailing around the edges of the openings. In contrast, the experimental study reported here addresses assessment of the axial strength of walls with openings introduced in structures that have already been built. This is a problem that frequently arises in refurbished structures in which there is very limited scope for proper detailing around openings. Moreover, effects of door-type openings have not been investigated as intensively as window-type openings, and only one study (Mohammed et al. 2013) has investigated effects of window-type cut-out openings in OW walls. Thus, this study addresses a clear research gap. Furthermore, previous studies have only captured crack patterns (which are influenced by openings' sizes, among other factors) at failure, while in this study three-dimensional digital image correlation (3D-DIC) was used to investigate behavior at both service and ultimate limit states. This has provided better overviews of the failure mechanism by recording the crack pattern development and deformation of the walls throughout the loading history. In addition, the proposed procedure for evaluating the capacity of walls with openings by treating them as hybrid systems, i.e., a combination of series and parallel subsystems, provided good agreement with the test results.

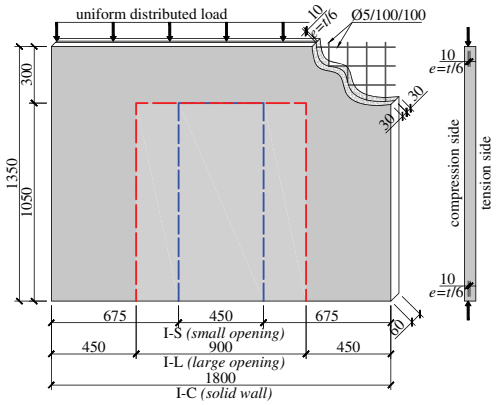


**Fig. 1.** (Color) Configuration and details of the tested walls

## Specimen Design and Construction

Three specimens designed to represent typical wall panels in residential buildings at half-scale (1,800 mm long, 1,350 mm tall, and 60 mm thick) were constructed for testing to failure. One was a solid panel, one had a symmetric half-scaled single door-type opening (450 × 1,050 mm, hereafter small opening), and the other had a symmetric half-scaled double door-type opening (900 × 1,050 mm, hereafter large opening). For convenience, these specimens were designated I-C, I-S, and I-L (solid, small opening, and large opening, respectively). Small and large are used here as convenient designations rather than as clearly delimited terms with specific thresholds and implications. The specimens' dimensions are illustrated in Fig. 1.

The specimens were all cast as solid panels, i.e., with constant thickness, no voids, and no insulating layers. They are considered as load-bearing concrete walls designed to carry vertical loads with no transverse loads between supports or lateral in-plane forces. The specimens represent interior walls of a structure with regular floor plans that carry only axial loads. However, pure axial loads rarely occur in practice, eccentricity is usually present. Thus, a predefined eccentricity of one-sixth of the wall thickness was applied in the loading to represent permitted imperfections in several design codes [ACI 318 (2011), AS 3600 (Standards Australia 2009), and EN 1992-1-1 (CEN 2004)] due to thickness variations and misalignment of the panels in the construction process. These deficiencies would cause offsets of the front or rear faces of the panels, thus affecting the eccentricity. Recommended tolerance limits for the accumulated misalignment and thickness variation in published guidelines (Ascent 2012) are a 12th of the wall's thickness (smaller than the eccentricity chosen here). In this manner the walls can still be considered as concentrically loaded (Pillai and Parthasarathy 1977), allowing specimens to be treated as compression members. Consequently, the resultant of all loads passes through the middle third of the wall's overall thickness, enabling evaluation of the empirical methods in design codes [ACI 318 (2011) and AS 3600 (Standards Australia 2009)] and research literature (Doh and Fragomeni 2006). Results obtained from the empirically developed design models may deviate from real values in cases where there is greater eccentricity due to the presence of, for example, wind loads.

The design codes all specify minimum wall reinforcement, primarily to control cracking due to shrinkage and temperature

stresses. For example, ACI 318 (2011) states that the minimum vertical wall reinforcement does not increase the axial strength of a wall above that of a plain concrete wall; however, the vertical and horizontal reinforcement to cross-section area ratios should be at least 0.12 and 0.20%, respectively. Consequently, welded wire fabric reinforcement was used to reinforce the walls, consisting of deformed 5-mm-diameter bars with 100-mm spacing in both orthogonal directions and centrally placed in a single layer. The vertical and horizontal steel reinforcement ratios resulting from this configuration are 0.327 and 0.315%, respectively. The specimens with openings were detailed to replicate solid walls with sawn cutouts, i.e., no additional reinforcement was placed around the edges or corners of the openings. When scaling the specimens it would be difficult to scale reinforcement for practical reasons (bars with less than commercially available diameters would be needed). Hence, the reinforcement ratio was higher than the minimum required. Nevertheless, the detailing (a single layer of reinforcement centrally placed) allowed the elements to be treated as unreinforced elements, with no contribution to their capacity from reinforcement.

In order to avoid misalignment of the reinforcement in the molds, the dimensions of the reinforcement mesh were measured from edge to edge of the concrete wall (i.e., bars were cut off with no additional anchorage provided at the specimen's edges such as bends or hooks). Before casting, electrical resistance strain gauges (5 mm long, 120 Ω nominal resistance) were bonded to the reinforcement. To avoid malfunction due to agents in the surrounding environment (i.e., water or mechanical damage), the strain gauges were protected by sealing using aluminum foil coated with a 3-mm layer of kneading compound. The walls were cast in a long-line form in lying position resting on a steel platform. The reinforcement layer was centrally placed with the horizontal bars resting on 25-mm-high plastic chairs. To avoid risks of premature cracking due to handling (which could have arisen because no additional reinforcing was used) a cast-in-steel plate was attached at the bottom of each pier. Then a steel tie was welded to the plate, temporarily connecting the piers and effectively stiffening the wall. The tie was removed prior to testing. The walls were manufactured at a local precast concrete plant in an indoor area with controlled curing conditions. On reception, the specimens were visually inspected for casting defects. No air voids or stains were observed on the exposed surfaces. Regions around openings were also inspected for cracks due to handling. None were found. No tolerances were specified in the technical drawings; the contractor was instructed to follow standard practices for this kind of element.

## Material Properties

The concrete used to cast the specimens was a self-consolidating mix that could be poured without vibrating it, including Dynamon NRG-700 (MAPEI AB, Sweden), a superplasticizer added to provide high workability and early strength. The target design strength for the concrete (class C32/40) was chosen to reflect standard Swedish construction practices. However, because the specimens were allowed to harden in the formwork for only 48 h, ensuring high early strength was very important. Hence, the actual compressive strength was higher than expected, but this does not compromise the study's objectives. Information on the mix proportion is provided in Table 1. To determine mechanical characteristics of the concrete (average compressive strength, $f_{cm}$, and fracture energy, $G_F$), five cubes and beams with standardized sizes were cast and cured in identical conditions to the specimens. The ultimate compressive strain in the concrete, $\varepsilon_{cu}$, was computed as a function of the cube strength [Eq. (1)] according to EN 1992-1-1 (CEN 2004).

**Table 1.** Mix Proportion of the Concrete

| Property | Value |
|---|---|
| Concrete class | C32/40 |
| Water-to-cement ratio | 0.55 |
| Cement (kg) | 380 |
| Aggregate size (kg) | |
| 1–4 mm | 1,030 |
| 8–16 mm | 630 |
| Additives: (%) of cement weight | 2.6 |

**Table 2.** Mechanical Properties of the Concrete and Steel Reinforcement

| Property | Value |
|---|---|
| Concrete | |
| $f_{cm}$ (MPa) | 62.8 (3.2%) |
| $G_F$ (N/m) | 168 (11.9%) |
| $\varepsilon_{cu}$ (‰) | 3.2 |
| Reinforcement | |
| $f_y$ (MPa) | 632 (0.35%) |
| $\varepsilon_y$ (‰) | 2.83 (8.45%) |
| $f_u$ (MPa) | 693 (0.40%) |
| $\varepsilon_u$ (‰) | 48.7 (4.82%) |

Note: $f_c$ = concrete cylinder compressive strength, which is assumed to be equal to $0.83 f_{cm}$; COVs are given in parentheses.

Welded wire fabric (grade NPS500) was used to reinforce the walls, with characteristic and design strengths of 500 and 435 MPa, respectively. In addition, five coupons were taken from the reinforcing steel meshes and tested to determine their actual stress-strain properties. The results [means and corresponding coefficients of variation (COVs)] are given in Table 2

$$\varepsilon_{cu} = 2.8 + 27[(98 - f_{cm})/100]^4 \quad (1)$$

## Test Setup and Loading Strategy

The following considerations were applied when designing the test rig:

1. The side edges were restrained to simulate TW effects for real transverse walls under as-built conditions that permitted rotation but prevented translation (Section 1-1 in Fig. 2).
2. It had to simulate hinged connections at the top and bottom boundaries of the specimen. To apply eccentric loading, a steel rod was welded to each loading beam, designed to fit into a guide system attached to the top and bottom of the specimen (Section 2-2 in Fig. 2). This detail provided a hinge connection that allowed full free rotation. At each contact surface between the specimen and the steel loading beams, a 2-mm strap of deformable plywood was introduced to limit local damage due to surface irregularities.
3. The walls would be loaded gravitationally with a small eccentricity at both ends (one-sixth of the wall thickness) to simulate effects of imperfections that occur in normal construction practices and are accounted for in standards.

Four hydraulic jacks, each with a maximum capacity of 1.4 MN, were networked together to enable a single operator to apply a uniformly distributed load, with controlled total force, along the wall length (through the loading beam with a slope of 1:1, i.e., under 45° as shown in Fig. 2). The hydraulic fluid was supplied from a power steering pump with user-adjustable relief valves, allowing the operator to easily set working pressures. Hydraulic load cells were used to measure the induced force as the load was incrementally

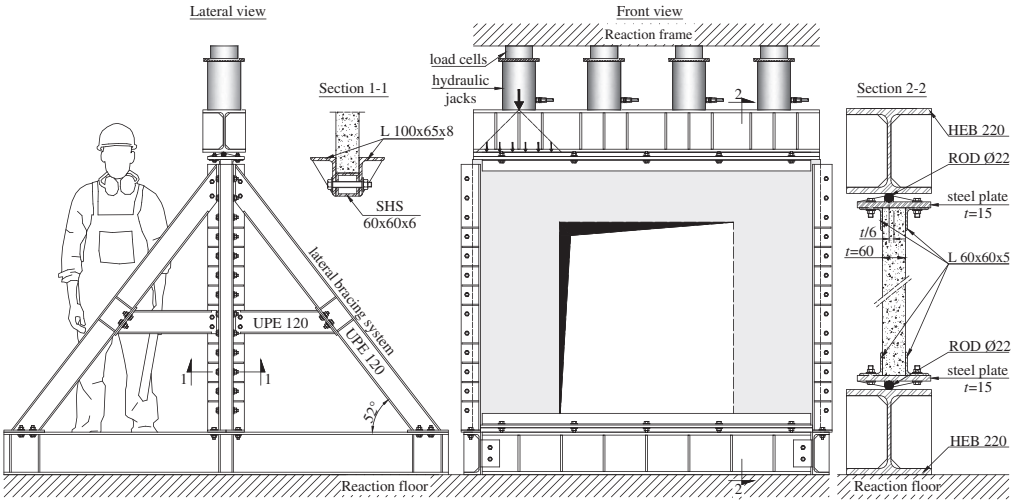


**Fig. 2.** Test setup and boundary conditions (all dimensions in millimeters); Sections 1-1 and 2-2 are scaled up to show details

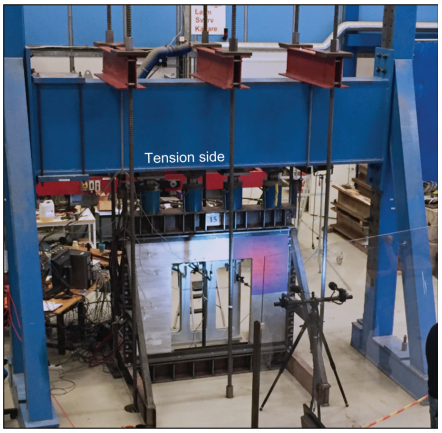


**Fig. 3.** (Color) General overview of the test setup (image by Cosmin Popescu)

increased at 30 kN/min with breaks every 250 kN to allow stress distribution and to monitor the cracks in the specimens. All reactions were transmitted to a reaction frame fixed in a strong floor by three additional pairs of high-strength steel rods (prestressed because the existing anchorage of the reaction frame did not provide sufficient capacity). A general view of the test setup is shown in Fig. 3.

## Instrumentation

Out-of-plane and in-plane displacements were monitored using linear displacement sensors, a fully active 350-Ω strain-gauge bridge giving the measurements infinite resolution. They were attached on the back side of the wall (hereafter compression side) at locations shown in Fig. 4. Strain gauges intercepting potential yield lines (derived from nonlinear finite-element analysis) were installed on the steel reinforcement and compression side of the concrete surface. In addition to yield lines, other relevant information such as crack patterns and ultimate loads was obtained.

To measure the mean strain of the concrete, 60-mm gauges (three times longer than the maximum diameter of the aggregate to even out local strain variations) were selected. To measure tensile stresses of the reinforcement, general purpose strain gauges were used. In addition to classical approaches for measuring strains and displacements, optical 3D measurements were also acquired by the DIC technique. For this the authors used a 5M system configuration (GOM mbH, Brunswick, Germany) (GOM mbH 2015) with a strain measuring accuracy of 0.005% to monitor the strain and displacement fields. Ideally, a stochastic point pattern should be used, but due to the large area monitored a regular pattern applied using a stencil and spray was utilized here. First a white base layer was applied, then a black-dot pattern was sprayed. The area monitored was the right-upper corner on the tension side of the specimen (780 × 660 mm, highlighted in Fig. 3), an area of particular interest for monitoring strain and crack development in discontinuous regions. These measurements were supplemented with several video and still camera recordings. To avoid interfering with the optical measurement system, the reinforcement was only instrumented with strain gauges on half of each specimen (the left pier, on the tension side), as permitted by the symmetry of the test setup.

## Experimental Results

### *General Observations*

No anomalies were observed during the specimen loading. The walls behaved as expected, deflecting in both vertical and horizontal directions. The displacements were generally symmetric,

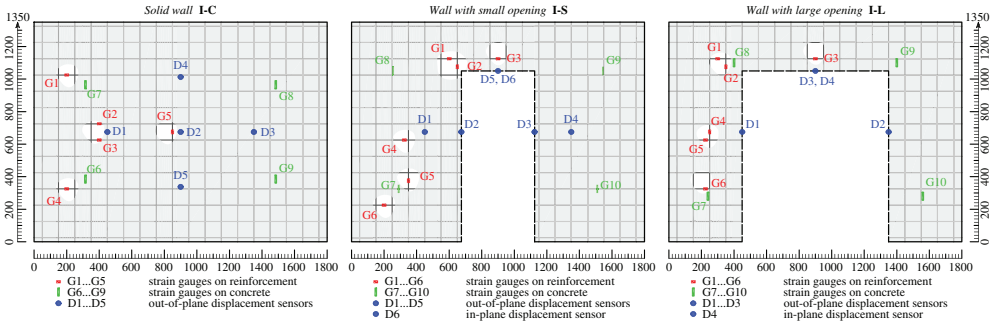


**Fig. 4.** (Color) Instrumentation scheme

with some deviations due to the test rig and random variations in material properties. The lateral bracing of the test rig was designed to be connected to the foundation support through oval holes to account for variations in the thickness of the wall panels, thus allowing small sliding of the entire system. The crack pattern was also symmetrical, except that the crack patterns in panels with openings only retained symmetry until the onset of failure. When one of the piers failed, the entire wall triggered failure of the other. The ultimate loads given do not include the weight of the loading beam. The failure of the specimens can be seen in Video S1.

## *Solid Wall I-C*

### Axial Load-Displacement Relationship

Between 0 and approximately 500 kN small negative displacements (−0.26 mm) were recorded due to settlement of the test setup. As the loads were increased to failure, the stiffness degradation increased, reflecting opening of the cracks and utilization of the steel reinforcement. The maximum load capacity was reached at 2,363 kN when the out-of-plane displacement registered by displacement sensor D2 was approximately 18.95 mm [Fig. 5(a)]. An instant jump to 26 mm was recorded immediately after failure when the entire specimen was divided into distinct disks along the yield lines.

### Steel Reinforcement and Concrete Strain Responses

Four strain gauges (G1–G4) were glued on the horizontal reinforcement and one (G5) on the vertical reinforcement. The G5 strain readings increased linearly up to the failure load, when the out-of-plane displacements of the specimens increased rapidly. The compressive strain reached a maximum of 0.68‰. When crushing of the concrete began, the neutral axis of the cross section shifted rapidly and the vertical reinforcement was subjected to tensile forces. All horizontal bars were subjected to tensile strain linearly up to 60–75% of the peak load [Fig. 5(b)]. After this the strains were more pronounced with yielding at failure. Four strain gauges (G6–G9) were glued on the compression side of the specimen to monitor the compressive strains [Fig. 5(c)]. The measurements provided good indications of imminent failure of the specimen, with collapse occurring at about 3.2‰ compressive strain. The readings showed consistent patterns, indicating that the loads were transferred uniformly toward the supports.

### Failure Mode and Crack Pattern

At up to 85% of its ultimate capacity, the solid panel showed no cracks. As the load increased, several major tensile cracks (0.2 mm wide) opened, starting from the corners of the wall at 55° inclination. The wall had a brittle failure due to crushing of concrete with little forewarning (visible out-of-plane deflection) prior to failure. The crack pattern at failure, shown in Fig. 6(a) for both tension and compression sides, was similar to a pattern previously reported in panels with all sides restrained (Swartz et al. 1974). Several secondary tensile cracks were distributed parallel to each other around the major tensile cracks, indicating that the reinforcement mesh played an active role in redistributing tensile stresses in the concrete.

## *Wall with Small Opening I-S*

### Axial Load-Displacement Relationship

The maximum load capacity of the specimen with a small opening was reached at 1,500 kN when the out-of-plane displacements registered by D2 and D3 were approximately 26.6 and 18.4 mm, respectively. The failure occurred on the left pier [corresponding to D3, Fig. 7(a)] where the displacements developed more slowly than on the right pier. The differences in displacement symmetry were more pronounced after the first crack appeared in the right pier. Load-displacement diagrams are shown in Fig. 7(a).

### Steel Reinforcement and Concrete Strain Responses

Four strain gauges (G1, G3, G4, and G6) were glued on the horizontal reinforcement and two (G2 and G5) on the vertical reinforcement. All horizontal bars were subjected to tensile strains, but recorded strains were low up to 90% of the peak load [Fig. 7(b)]. At G4 and G6, yielding occurred at failure, while ultimate strains recorded by G1 and G3 were below 1.5‰. Strains recorded by G3 (the gauge glued on the first bar above the opening) increased more progressively. As observed in loading of the solid specimen (I-C), the vertical bars were compressed and G2 (adjacent to the opening) recorded higher strains than G5. However, the maximum compressive strain, reached at failure, did not exceed 1.5‰.

### Failure Mode and Crack Pattern

When the specimen was under approximately 50% of its peak load, a 0.05-mm-wide crack opened in the middle of the spandrel, followed by two diagonal cracks from the bottom right corner of the wall with 55° inclination at 65% of its ultimate capacity. These

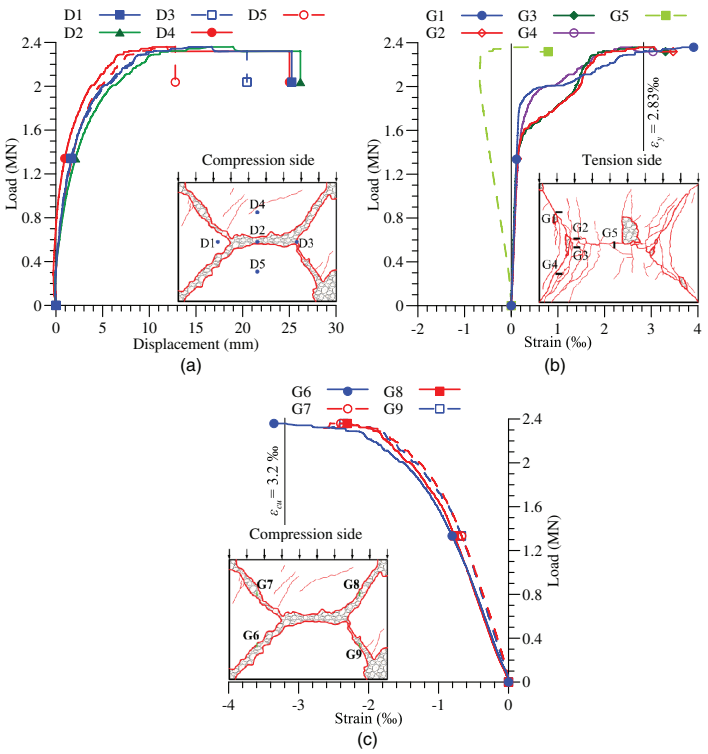


**Fig. 5.** (Color) Responses of the solid wall I-C: (a) load displacement; (b) strain in steel reinforcement; (c) strain in concrete; D1–D5 and G1–G9 refer to displacement sensors and strain gauges, respectively, at indicated positions (Fig. 4 for details)

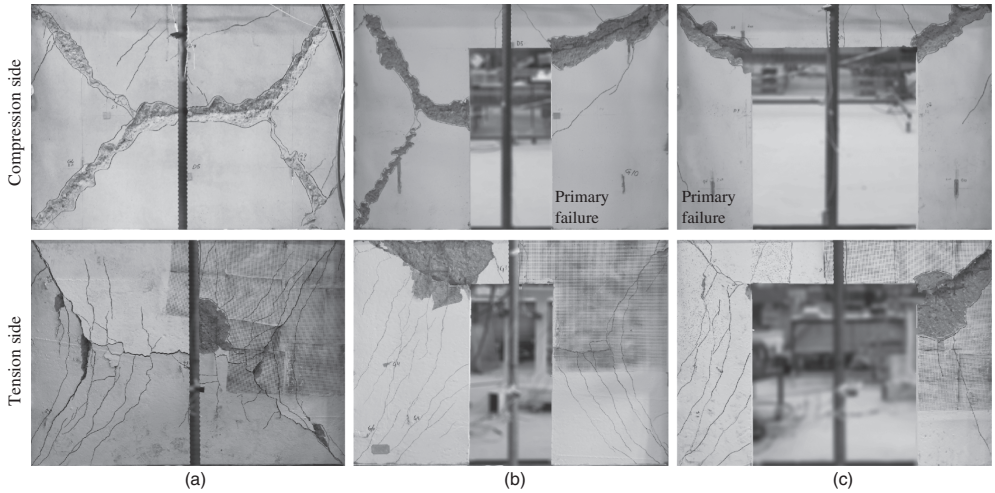


**Fig. 6.** Crack pattern and failure mode of the tested specimens (images by Cosmin Popescu): (a) Specimen I-C; (b) Specimen I-S; (c) Specimen I-L

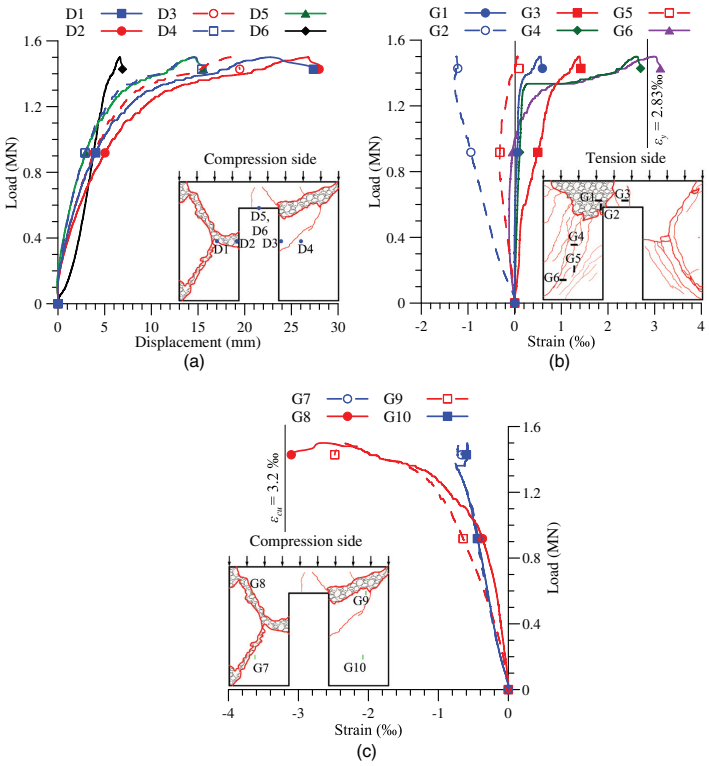


**Fig. 7.** (Color) Responses of the wall with a small opening I-S: (a) load displacement; (b) strain in steel reinforcement; (c) strain in concrete; D1–D6 and G1–G10 refer to displacement sensors and strain gauges, respectively, at indicated positions (Fig. 4 for details)

cracks continued to widen up to 85% of the failure load when several other cracks around the same location began to emerge. For safety reasons, no information regarding the crack opening beyond this load was collected. The wall had a brittle failure due to crushing of concrete with spalling and reinforcement buckling along the line between the corner of the wall and opening corner of one pier [Fig. 8(a)]. The other pier failed immediately thereafter, with a typical crack pattern for panels restrained on three sides. The crack patterns after collapse in both the tension and compression sides are shown in Fig. 6(b).

### *Wall with Large Opening I-L*

#### Axial Load-Displacement Relationship

The maximum load capacity of the specimen with a large opening was reached at 1,180 kN, when the out-of-plane displacements registered by D1 and D2 were approximately 8.5 and 11.2 mm, respectively. The failure occurred on the left pier (where the displacements were smaller), following a very similar pattern to the one observed in the test of the wall with a small opening.

#### Steel Reinforcement and Concrete Strain Responses

Four strain gauges (G1, G3, G5, and G6) were glued on the horizontal reinforcement and two (G2 and G4) on the vertical reinforcement. The trends and strain values were very similar to those observed in the reinforcement of the specimen with a small opening. The reinforcement bar above the opening was tensioned more than in the panel with a small opening, thus accelerating the redistribution of the forces to piers. Load-strain diagrams for the reinforcement and concrete are shown in Figs. 9(b and c), respectively.

#### Failure Mode and Crack Pattern

The first crack (0.3 mm wide) was identified in the middle of the spandrel early in the load history (at approximately 20% of its peak load). Another two diagonal cracks (0.05 mm wide) from the bottom corner of the wall with 53° inclination were observed at approximately 85% of its peak load. The wall had a brittle failure due to crushing of concrete with spalling and reinforcement buckling along the line between the wall corner and opening corner of one pier [Fig. 8(b)]. As in the wall with a small opening, this local failure caused failure of the entire wall with no typical crack pattern in the other pier. The crack patterns in both the tension and compression sides after collapse are shown in Fig. 6(c).

## Monitoring Failure Progression by 3D-DIC

Several studies have shown that DIC methodology (based on imaging specimens' surfaces in initial undeformed and later deformed

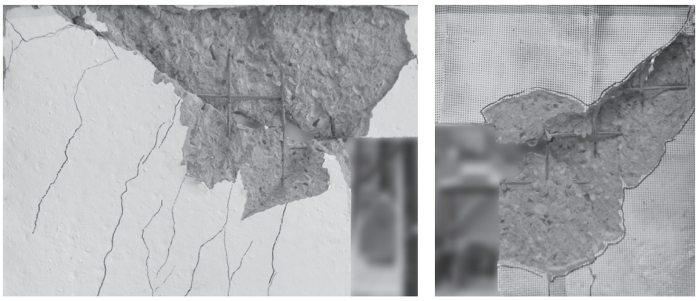


**Fig. 8.** Failure at the corner opening with concrete spalling and reinforcement buckling (images by Cosmin Popescu): (a) Specimen I-S; (b) Specimen I-L

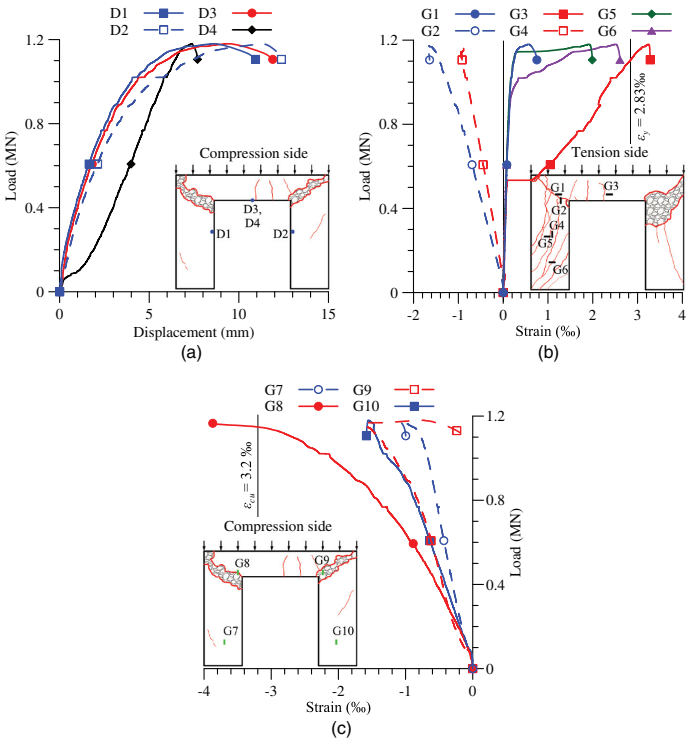


**Fig. 9.** (Color) Responses of the wall with a large opening I-L: (a) load displacement; (b) strain in steel reinforcement; (c) strain in concrete; D1–D4 and G1–G10 refer to displacement sensors and strain gauges, respectively, at indicated positions (Fig. 4 for details)

stages to obtain displacement data) can provide stable and reliable strain and displacement measurements in both laboratory environments (Smith et al. 2011; Mahal et al. 2015) and field tests (Sas et al. 2012). The 3D-DIC system applied here captured well the strain development and distribution around the openings during loading of the specimens. Figs. 10 and 11 illustrate major strains in the wall with a small opening (I-S) and large opening (I-L) at 30%, 75%, peak load, and onset of collapse. The major strains were

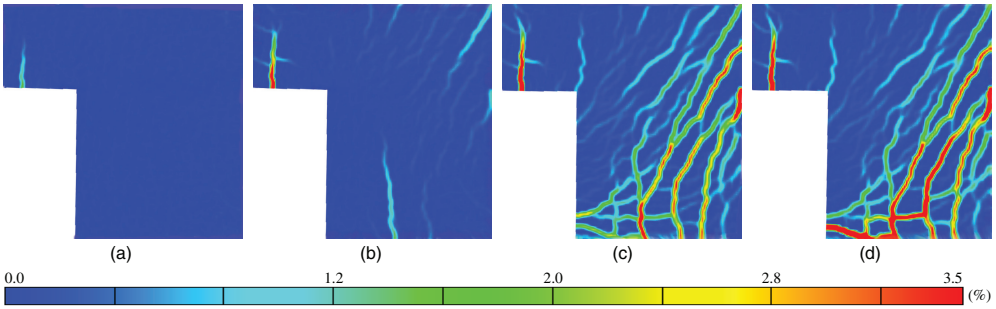


**Fig. 10.** (Color) Principal plane strain development on the tension side of Specimen I-S at (a) 30% of the peak load; (b) 75% of the peak load; (c) peak load; (d) onset of failure

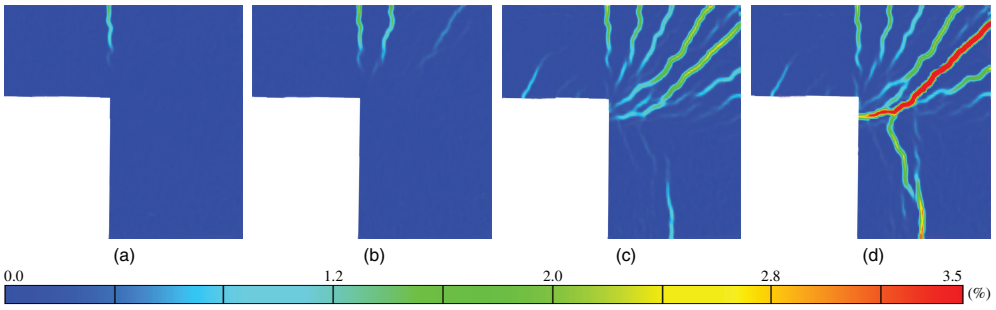


**Fig. 11.** (Color) Principal plane strain development on the tension side of Specimen I-L at (a) 30% of the peak load; (b) 75% of the peak load; (c) peak load; (d) onset of failure

analyzed to study the crack formation throughout the loading history. In both the I-S and I-L specimens the first cracks appeared in the spandrel and were concentrated in the piers at later loading stages. Because the monitored area included less than half of the spandrel's length, its behavior is not further discussed at this point, although it might be relevant for the overall behavior of the wall. The recorded crack pattern in the pier of Specimen I-S clearly shows a three-way action behavior with no major cracks around the corner of the opening. In contrast, cracks were more concentrated around the opening corner of Specimen I-L. Crack widths were estimated as follows. Positions and lengths of cracks were determined from the known crack patterns at onset of failure, then displacements across them were recorded by virtual gauges placed at 50-mm intervals along each crack. Fig. 12 presents load-width diagrams for three representative cracks in the I-S and I-L specimens—the first crack to open during loading ($w_{c,1}$), the widest crack at peak load ($w_{c,2}$), and the crack that opened most rapidly in final loading stages ($w_{c,3}$). In both cases, the three cracks showed similar behavior. The first crack that formed on the piers (Crack 1) appeared relatively early in the loading history, but did not open more than 0.25 mm. The second crack (Crack 2), which became the widest, subsequently formed and developed more slowly initially, while the third crack (Crack 3), which opened most rapidly close to failure, is considered to be the one responsible for the specimens' ultimate failure. For Specimen I-S, the first crack that formed on the piers was found to be the same as the one responsible for the specimens' ultimate failure.

The DIC measurements were also used to compute out-of-plane displacement profiles along a section line (called the zero line section) representative for both specimens with openings (i.e., in the same locations relative to the specimen edge). The resulting profiles for the specimens with large and small openings are shown in Fig. 13, above and below the zero line section, respectively (again at 30, 75, and 100% of the peak load, and onset of collapse). The data clearly showed that most displacement occurred after 75% of peak load for specimens with both types of openings. Maximum out-of-plane displacements recorded by the DIC systems were higher for Specimen I-S than for Specimen I-L. This observation agrees with the measurements taken by displacement sensors, which recorded higher deformations for Specimen I-S on the side where 3D-DIC was recorded. The DIC technique did not record results up to the specimen edges due to the edge restraints (Fig. 2), which limited the view of the cameras (60 mm from the upper part and 40 mm from the side edge).

## Failure Mechanism and Design for Ultimate Strength

This section briefly overviews analytical formulations recommended in current design codes and literature for predicting

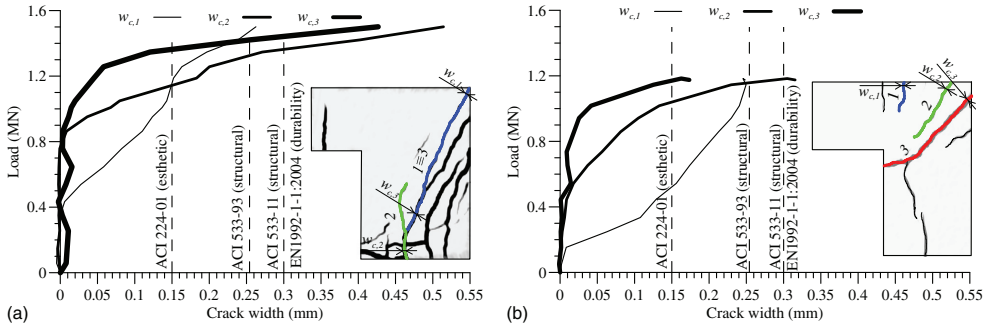


**Fig. 12.** (Color) Crack width development, as monitored by 3D-DIC, in Specimens (a) I-S; (b) I-L

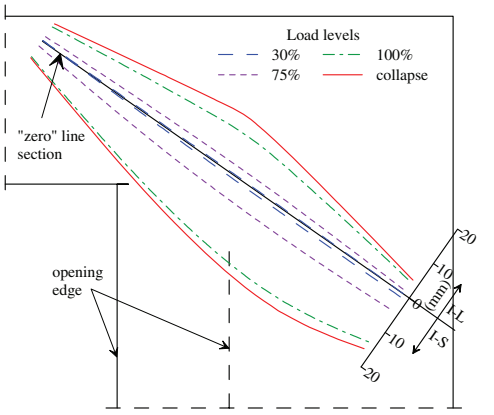


**Fig. 13.** (Color) Displacement profiles along a predefined line for the specimens with large and small openings, above and below the zero line section

ultimate capacities of walls with or without openings. The experimentally measured ultimate loads for the tested walls are then compared to their axial strengths as computed using these formulas. Currently, the practical design of RC walls, prescribed in standards such as ACI 318 (ACI 2011) and AS 3600 (Standards Australia 2009), is based on empirical models, whereas EN 1992-1-1 (CEN 2004) is based on calibration against the results of nonlinear analysis. Despite numerous relevant subsequent studies, no modifications to the formula presented in ACI 318 (ACI 2011) have been implemented to incorporate the effect of restraints on all sides, thus it will not be considered in the following analysis. EN 1992-1-1 (CEN 2004) and AS 3600 (Standards Australia 2009) are the only major codes that provide methodology to account for the increase in capacity this gives. Numerous studies have attempted to further improve the design models. A comprehensive recent review and assessment of existing design models (Popescu et al. 2015) concluded that the best models in terms of average deviations between theoretically and experimentally determined capacities were those proposed by Doh and Fragomeni (2006, 2005) for walls with and without openings, respectively.

### *Column Theory*

The most widely used method to calculate capacities of axially loaded RC walls (to the authors' knowledge) is based on column theory, considering stress-strain compatibilities and the equilibrium of forces over their cross sections. In current design codes, walls regarded as compression members that carry mainly vertical loads (accepting some eccentricity as long as the resultant passes through the middle third of the wall's cross section) are treated as columns. For such cases, a simplified procedure is employed in which all design codes investigated here agree that the steel reinforcement and tensile strength of concrete will not contribute to the load capacity. However, there are differences between design codes, mostly regarding distributions of compressive forces and slenderness. AS 3600 (Standards Australia 2009) and Doh and Fragomeni (2005) define the stress block as a linear stress distribution, as shown in Fig. 14(a), whereas EN 1992-1-1 (CEN 2004) assumes a rectangular stress block [Fig. 14(b)]. Furthermore, the initial eccentricity caused by the applied loads, $e_i$, is increased by eccentricity, $e_a$, due to the lateral deflection of the wall. This factor accounts for slenderness effects, also known as second-order or $P-\Delta$ effects. The procedure described in AS 3600 (Standards Australia 2009) and Doh and Fragomeni (2005) to find the maximum deflection at the critical wall section applies sinusoidal curvature [Fig. 14(a)], using deflections obtained from bending-moment theory (Gere and Timoshenko 1990). In contrast, triangular curvature is assumed in EN 1992-1-1 (CEN 2004) due to a concentrated horizontal force at the critical point of the wall [Fig. 14(b)]. According to Robinson et al. (2011) this approach results in a linear, rather than parabolic, deformation, which reduces the predicted ultimate capacity of slender walls. For brevity, derivations of these models are not presented here but can be found in Doh (2002). Based on the aforementioned theoretical assumptions, design models have been proposed in both design codes and research literature. These are reviewed subsequently and assessed in terms of consistency with the presented data.

#### Solid Wall

Following the existing design models, the ultimate load capacity of the solid specimen was computed using Eqs. (2)–(4) and the resulting values are designated $N_{EC2}$ [EN 1992-1-1 (CEN 2004)],

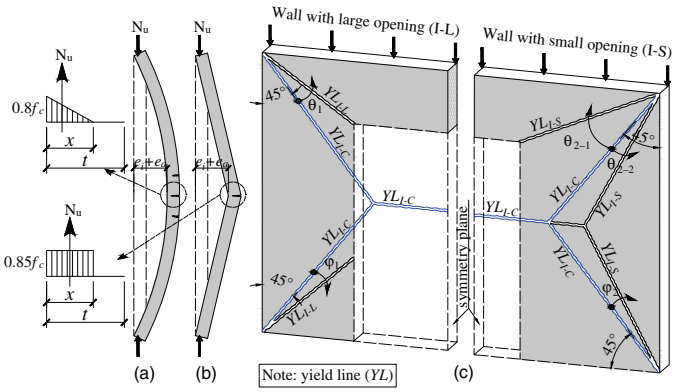


**Fig. 14.** (Color) Schematic representation of the failure mechanism: one-dimensional behavior according to (a) AS 3600 (Standards Australia 2009) and Doh and Fragomeni (2005); (b) EN 1992-1-1 (CEN 2004); (c) three-dimensional behavior in line with plate theory

$N_{AS3600}$ [AS 3600 (Standards Australia 2009)], and $N_{D-F}$ (Doh and Fragomeni 2005), respectively

$$N_{\mathrm{EC2}} = f_c \cdot L \cdot t \cdot \Phi \tag{2}$$

where

$$\Phi = 1.14\left(1 - 2\frac{e+e_a}{t}\right) - 0.02 \cdot \frac{H_{\mathrm{eff}}}{t} \le \left(1 - 2\frac{e+e_a}{t}\right)$$

$$N_{\mathrm{AS3600}} = 0.6 f_c (t - 1.2e - 2e_a)L \tag{3}$$

$$N_{D-F} = 2f_c^{0.7}(t - 1.2e - 2e_a)L \tag{4}$$

where $t$ = wall thickness; $L$ = wall length; $f_c$ = mean concrete cylinder compressive strength; $e$ = initial eccentricity, $e = t/6$; and $e_a$ = additional eccentricity due to lateral deflection of the wall.

The additional eccentricity, $e_a$, accounts for the effect of slenderness, also known as second-order (or $P-\Delta$) effects. Several approaches may be used to compute the additional eccentricities, which are a function of the curvature applied to find the maximum deflection at the critical wall section

$$e_a = \begin{cases} \frac{H_{\mathrm{eff}}}{400} & \mathrm{EN1992\text{-}1\text{-}1(2004)} \\ \frac{(H_{\mathrm{eff}})^2}{2{,}500t} & \mathrm{AS\ 3600(2009)\ and\ Doh\ and\ Fragomeni\ (2005)} \end{cases}$$

with $H_{\mathrm{eff}} = \beta H$ being the effective height. Values for the effective height factor $\beta$ are given for the most commonly encountered restraints. ACI 318 (ACI 2011) only considers walls with restraints at the top and bottom (OW walls). For walls restrained against rotation at both ends, $k = 0.8$. Unless no restraint against rotation is provided at one or both ends, the effective height factor $k = 1$. According to Fragomeni et al. (1994), these effective height factors that consider the lateral restraints provided by transverse walls were first introduced by the German code [DIN 1045 (Design and Construction 1988)] and later adopted by EN 1992-1-1 (CEN 2004) and AS 3600 (Standards Australia 2009) [Eq. (5)]

$$\beta = \begin{cases} \frac{1}{1+(\frac{H}{2L})^2} & \text{three sides} \\ \frac{1}{1+(\frac{H}{L})^2} & \text{four sides with } L \ge H \\ \frac{L}{2H} & \text{four sides with } L < H \end{cases} \tag{5}$$

Doh and Fragomeni (2005) slightly modified the effective height factor to account for loading eccentricities by incorporating an additional eccentricity parameter, $\alpha$

$$\alpha = \begin{cases} 1/(1+e/t) & \text{when } H/t < 27 \\ 18/[(1-e/t)(H/t)^{0.88}] & \text{when } H/t \ge 27 \end{cases} \tag{6}$$

### Walls with Openings

To the authors' knowledge, there are no straightforward methods to evaluate the ultimate capacity of a wall with openings. However, some guidelines are available, such as those in AS 3600 (Standards Australia 2009) and EN 1992-1-1 (CEN 2004), which state that effects of an opening on a wall's axial strength can be neglected if the wall is restrained on all sides, while the opening's area and height are less than 1/10 and 1/3 of the wall's total surface area and height, respectively. If these conditions are not fulfilled, areas between openings (if more than one) must be treated as being supported on two sides. Portions between restraining members and openings must be treated as being supported on three sides according to AS 3600 (Standards Australia 2009), while EN 1992-1-1 (CEN 2004) does not clearly prescribe their treatment. In the preceding sections the ultimate capacity of individual elements has been considered, independently of others. However, it is important to evaluate the reliability of entire systems (in this context walls with openings), but design codes do not provide such information or clear methodology for calculating their reliability. Consequently, the following procedure was applied.

The entire ensemble may be idealized as a hybrid system, i.e., a combination of series and parallel subsystems. In a serial system, if one of the components fails, the entire system will fail, whereas failure of all components is required for a parallel system to fail (Novak and Collins 2012). In a wall with one or more openings, the piers behave as a parallel system connected in series with the spandrel above the openings, and failure will occur when the axial strength of all piers or the shear-flexural strength of the spandrel is

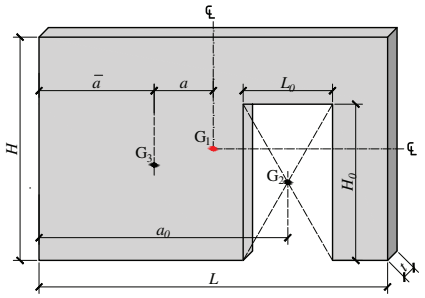


**Fig. 15.** (Color) Geometry of a wall with openings (G3 = center of gravity of the wall with opening, G1 = center of gravity of corresponding solid wall, G2 = center of gravity of opening) (adapted from Saheb and Desayi 1990b, © ASCE)

exceeded. Thus, the system's strength is the sum of all the piers' axial strength, assuming that the spandrel continues to distribute the forces until one of the piers fails completely.

The experimental results indicate that the spandrel was the first element to fail because the first crack occurred in it. In reality, failure involves not only the ultimate failure but also excessive deflections and cracks. The loads applied on the spandrel are redistributed directly to the piers until one of the piers fails completely and the whole system collapses. Thus it can be regarded as a parallel system with brittle elements, which will fail if one of the brittle components fails (and the system's strength can be obtained by multiplying the axial strength of the weakest pier by the number of piers).

In order to extend the scope of their design equation, Doh and Fragomeni (2006) proposed a new formula [Eq. (7)] for calculating the ultimate capacity of walls with openings

$$N_{uo} = (k_1 - k_2\chi)N_{D-F} \tag{7}$$

where $N_{D-F}$ = ultimate load of an identical panel without openings under TW action [Eq. (4)].

Here, the constants $k_1$ and $k_2$ were obtained by curve fitting, with $k_1 = 1.004$ and $k_2 = 0.933$. Effects of the size and location of openings are taken into account through a dimensionless parameter, $\chi$, defined as

$$\chi_x = (A_0/A + a/L) \tag{8}$$

where $A_0$ and $A$ = horizontal cross-sectional areas of the opening (i.e., $A_0 = L_0 t$) and the solid wall (i.e., $A = Lt$), respectively. All parameters involved in Eq. (8) can be easily determined from Fig. 15.

As already shown, all design models presented here [Eqs. (2)–(4)] consider the positive effect of having walls restrained along all their sides. However, when introducing an opening with an area larger than 1/10 of the wall's total area, regardless of its height, the edge toward the opening is assumed to be free (unrestrained for both translational and rotational movements). This is important because the ground floor of many structures is taller than the upper floors, but the door height remains constant. Thus, the portion above the opening, which spans the doorways, has a greater height-to-span ratio. Hence, a deep beam behavior is expected, which may influence the load distribution toward the wall piers and ultimately the peak load. Guan (2010) found that increasing

**Table 3.** Comparison of Axial Loads Predicted Using Formulas from Design Codes [Eqs. (2)–(4) and (7)] with Experimental Values

| Specimen | $N_{test}$ (kN) | $N_{EC2}/N_{test}$ | $N_{AS3600}/N_{test}$ | $N_{D-F}/N_{test}$ |
|---|---|---|---|---|
| I-C | 2,363 | 0.93 | 0.91 | 0.82 |
| I-S | 1,500 | 1.01 | 1.02 | 0.99 |
| I-L | 1,180 | 1.12 | 1.00 | 0.88 |
| Average | — | 1.02 | 0.98 | 0.90 |
| COV (%) | — | 9.6 | 6.3 | 9.8 |

both the length and height of an opening has the most significant effect on capacity, and proposed a new model to account for this effect. The methodology involved nonlinear finite-element analysis, and thus further tests are needed to validate Guan's findings. Consequently, the restraining factors should be calibrated to account for these scenarios too.

The test results are summarized in Table 3, together with the failure loads predicted by the presented design models. Design models overestimated the ultimate capacity of the tested specimens. However, the model proposed by Doh and Fragomeni (2006) provides more conservative results. A safety factor, $\phi$, of 1 was applied in all design equations, while a carefully chosen safety factor should be used in practice. Any possible size effects should also be considered, however Seddon (1956a) found that scale effects were negligible.

### Plate Theory

Results presented so far have been assessed in relation to cited design models in terms of ultimate load, but the failure mechanism also warrants attention. The experimental observations indicated biaxial curvature of the walls and an essentially plate failure mode. Basically, the lateral restraints transform the problem from a one-dimensional to a three-dimensional problem, and the failure mechanism to that schematically shown in Fig. 14(c). For a solid wall the energy is dissipated through yield lines that develop at roughly 45° ($YL_{I-C}$) according to plate theory (Kennedy and Goodchild 2004). However, openings tend to attract yield lines (Kennedy and Goodchild 2004). Thus, in specimens with openings, the yield lines of a solid wall are interrupted by openings and the remaining ones change positions ($YL_{I-L}$ and $YL_{I-S}$). In Specimens I-L and I-S, the yield lines starting at the bottom part of the wall rotate clockwise and anticlockwise through angles of $\varphi_1$ and $\varphi_2$, respectively. The yield line starting at the upper part of the wall rotates anticlockwise through an angle of $\theta_1$ until it connects with the corner of the opening in Specimen I-L, while in Specimen I-S this initial yield line divides into two, rotating through angles of $\theta_{2-1}$ and $\theta_{2-2}$ clockwise and anticlockwise, respectively. Final failure occurs along yield lines connecting the upper corner of the wall with the corner of the openings in both Specimens I-S and I-L (Fig. 8). The limited number of tests reported here provide useful indications of general patterns, but more are needed to obtain general values of $\varphi_1$, $\varphi_2$, $\theta_1$, $\theta_{2-1}$, and $\theta_{2-2}$ and obtain a better overview.

Furthermore, the experimental observations indicate that the global failure mode could be related to plate buckling. Thus, the failure mode is also reviewed in the context of plates under uniform compression. Although the design provisions limit the slenderness ratio ($H/t$) to avoid elastic buckling failure, inelastic buckling may sometimes occur, depending on the edge boundary conditions, imperfections, or geometrical nonlinearities. Inelastic buckling occurs when material yields prior to elastic critical buckling stress (Ziemian 2010). Many studies have addressed the stability of steel plates based on generalization of Euler's equation. There have been

fewer corresponding studies of RC plates, but Swartz et al. (1974) proposed an empirical plate equation for predicting the critical stress in concrete at the onset of buckling [Eq. (9)]

$$\sigma_{cr} = 0.425 f_c B(-B + \sqrt{4 + B^2}) \tag{9}$$

where

$$B = \frac{\pi^2}{6\varepsilon_{cu}}\left(\frac{1}{l} + l\right)^2\left(\frac{t}{L}\right)^2 \quad \text{and,} \quad l = H/L \le 1$$

Eq. (9) is valid only for simply supported rectangular plates under uniaxial compression. It does not cover other edge conditions, i.e., clamped or free. Thus, it was only possible to compute the critical stress in the solid wall ($\sigma_{cr}/f_c \approx 0.74$) from the current test results. The value was then transformed into critical strain and used to find the load at which inelastic buckling occurs.

The critical strain at the onset of buckling was found from Eq. (10), describing the stress-strain relation for concrete in compression based on experimental observations of van Mier (1986)

$$\sigma_c = f_{c0} + (f_c - f_{c0})\sqrt{1 - \left(\frac{\varepsilon_c - \varepsilon_{c1}}{\varepsilon_c}\right)^2} \tag{10}$$

where $\sigma_c$ = compressive stress in concrete; $f_{c0}$ = onset of nonlinear behavior defined as $2f_t$, with $f_t$ the tensile strength of concrete; $\varepsilon_c$ = compressive strain in concrete; and $\varepsilon_{c1} = 0.7f_c^{0.31}$ is the plastic strain at compressive strength.

With $\sigma_c = \sigma_{cr}$ known and assuming $\varepsilon_c = \varepsilon_{cr}$, the critical strain at the onset of buckling was determined, then compared with strains measured by gauges intercepting the crushing regions [Fig. 5(c)] and the corresponding critical load was extracted. The results showed a ratio between the critical and peak loads of about 0.82, demonstrating that the solid wall experienced inelastic buckling.

## Analysis of the Test Results and Discussion

### *Effects of Opening Size*

Displacements of all three specimens (recorded at the same position, D1 and symmetric to D1 on the other pier) were plotted on the same graph (Fig. 16) to assess effects of the size of openings. The results indicate that the 25 and 50% reductions in cross-sectional area of the solid wall caused by introducing the small opening and large opening reduced its load-carrying capacity by nearly 36 and 50%, respectively. As shown in Fig. 17, these variables are clearly correlated (as expected), but not linearly. The axial strength ratio ($N_{\text{test}}/A_c f_c$, where $A_c$ represents the cross-section area of the wall) responses markedly differed, being very similar for the solid wall and wall with a large opening, but much lower for the wall with a small opening. This may be due to the boundaries becoming more active as the aspect ratio (height/length) of the piers increases, thereby utilizing the material's strength more effectively in compression. The lateral boundary conditions are among parameters that influence the axial strength of a panel through the effective height factor. As the aspect ratio of the wall increases, the effective height factor decreases, and thus decreases the slenderness effect. This positive effect of lateral restraints is only accounted for in European [EN 1992-1-1 (CEN 2004)] and Australian [AS 3600 (Standards Australia 2009)] design codes. This behavior also confirms results of a previous analysis of published data by Saheb and Desayi (1990a).

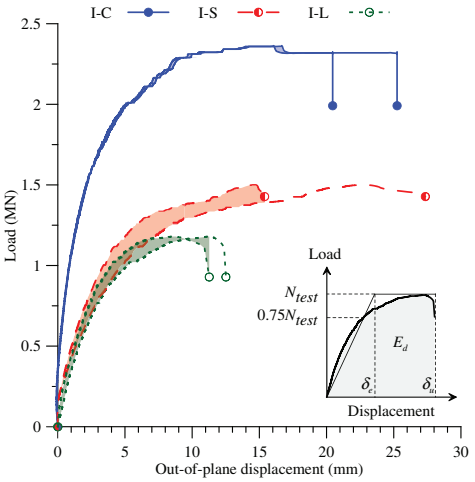


**Fig. 16.** (Color) Load-displacement responses of the three specimens showing effects of opening size

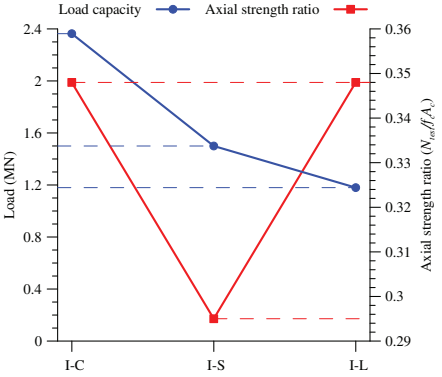


**Fig. 17.** (Color) Ultimate loads and axial strength ratios of the solid wall (I-C) and walls with small (I-S) and large (I-L) openings

Numerous simplified procedures have been proposed in the literature for calculating two other highly relevant variables: ductility and energy release at failure. Ductility is commonly expressed in terms of displacements, curvature, or rotations (Park 1988). In this study, displacement-based ductility factors (defined as the ratios between elastic and ultimate displacements, $\mu_\Delta = \delta_u/\delta_e$) were computed. Because a distinct elastic displacement cannot be easily found, a simplified procedure proposed by Park (1988) was adopted. This is based on the assumption that the most realistic approach for RC structures is to compute the elastic displacement for an equivalent elastoplastic system with reduced stiffness. The reduced stiffness is found as the secant stiffness related to 75% of the peak load and the horizontal plateau corresponding to the peak load ($N_{\text{test}}$) of the real system (Fig. 16). The maximum

**Table 4.** Ductility Factors and Energy Release Values at Failure Evaluated according to Park (1988)

| | | Pier 1 (measurements at D1) | | | | Pier 2 (symmetric to D1) | | | |
|---|---|---|---|---|---|---|---|---|---|
| Specimen | $N_{test}$ (kN) | $\delta_\varepsilon$ (mm) | $\delta_v$ (mm) | $\mu_\Delta = \delta_v/\delta_\varepsilon$ | $E_d$ (kNm) | $\delta_\varepsilon$ (mm) | $\delta_u$ (mm) | $\mu_\Delta = \delta_v/\delta_e$ | $E_d$ (kNm) |
| I-C | 2,363 | 4.55 | 18.43 | 4.05 | 39.37 | 4.77 | 18.02 | 3.78 | 38.08 |
| I-S | 1,500 | 8.53 | 27.35 | 3.21 (−21%) | 34.21 (−13%) | 5.95 | 15.40 | 2.59 (−32%) | 18.55 (−51%) |
| I-L | 1,180 | 4.05 | 11.27 | 2.78 (−31%) | 10.88 (−72%) | 5.15 | 12.51 | 2.43 (−36%) | 11.55 (−70%) |

displacement corresponds to the post-peak deformation when the load has decreased by 20% or the reinforcement buckles, whichever occurs first. In addition to ductility factors, energy dissipation ($E_d$) was also evaluated as the area under the load-displacement curves.

The introduction of the small and large openings resulted in similar, sharp reductions in computed ductility factors (Table 4). However, the differences in size between the openings strongly affected the energy dissipation; on average, the wall with no opening could be classified as a ductile element according to Park (1988), having a ductility factor between 3 and 6, while the walls with small and large opening would be both classified as elements with restricted ductility (ductility factors <3).

### Effect of Reinforcement

The stress levels were monitored in the steel reinforcement to assess the assumption that reinforcement does not contribute to the overall performance of the wall in terms of crack occurrence, ductility, and axial strength. The strength parameter is only discussed in terms of observed strains: whether or not it really made a contribution cannot be determined because no control specimens made of plain concrete were included in the tests. However, no strains in reinforcement of this type of element have been previously reported, so the information could be useful for further studies to calibrate nonlinear finite-element models. The DIC results showed that the reinforcement enabled good stress redistribution in the walls. After crack initiation in the piers, multiple cracks opened with further loading. The width of these cracks remained acceptably small, suggesting that the reinforcement was well anchored and distributed. Although the minimum amount of reinforcement prescribed by design codes was exceeded, the tensile or compressive strains that developed in the reinforcement were significant at higher loads, with yielding of some bars occurring at failure. While the vertical bars were more gradually stressed during the specimen loading, none of them yielded at failure. The horizontal reinforcement yielded or was close to yielding and buckled at failure, but no rupture was observed in any of the tests. In contrast, Huang et al. (2015) tested high-strength OW walls axially loaded with a $t/6$ eccentricity and enclosing reinforcement ratio of 0.233%. In their tests the reinforcement ruptured at failure load regardless of its arrangement (one or two layers), reportedly due to "the brittleness" (Huang et al. 2015). No significant effect was observed on the ultimate load, but failure was more ductile when the quantity of reinforcement was doubled and placed in two layers.

The failure of the specimens with openings occurred in the pier with lower deformations, presumably at least partly because as geometric nonlinearities increase the reinforcement starts to be more active. El-Metwally et al. (1990) also showed that the failure mode is sensitive to the initial eccentricity, and here too the reinforcement has a significant effect for large eccentricities. These findings suggest that reinforcement may significantly affect ultimate load as the eccentricity increases. However, the threshold eccentricity at which reinforcement may increase ultimate load is currently unknown and more tests are required. Nevertheless, no current design codes recognize the contribution of the steel reinforcement for eccentricities up to one-sixth of the wall's thickness.

Although cracks occurred at late loading stages in the reported tests, the possibility of sustained loads causing cracks should not be neglected, especially around corners of openings if there is no diagonal reinforcement. This is because real structures are subjected to relatively high sustained loads, which tend to impair the performance of slender elements by increasing their long-term deflections (Macgregor et al. 1971). The study presented here involved only short-term tests, thus creep effects were not considered.

### Parametric Study

Tests on just three specimens are insufficient to draw quantitative conclusions about effects of cutting openings in solid walls. Moreover, eccentricity significantly affects walls' axial strength, but in all tests an eccentricity of a sixth of the specimens' thickness was applied. Thus, more tests with different eccentricities (but less than $t/6$ to retain compression failure of the walls) are required. The Eurocode 2 approach was initially validated with the experimental results, and subsequently applied to generalize the decrease in ultimate strength while varying both opening size ratio ($A_0/A$) and initial eccentricity ratio ($e/t$). All other material and geometric parameters were kept constant at values used in the experimental program. The eccentricity was varied from 0 mm (pure axial load) to 10 mm ($t/6$) in 2.5-mm ($t/24$) increments. The opening size was varied from 0% of the total cross-section area of the wall to the point where the cross-sectional aspect ratio of the part remaining after introducing the opening was less than 4:1 (in 5% increments). The lower limit represents an infinitesimal opening, i.e., a plane cut, which could represent a contraction joint or two adjacent panels. Furthermore, EN 1992-1-1 (CEN 2004) emphasizes that elements with a cross-sectional aspect ratio below 4:1 should be considered as columns rather than walls, thus setting the upper limit of the current parametric study.

The results are plotted in Fig. 18 in terms of axial load reduction relative to a reference element, i.e., a solid wall under pure axial loading (with no eccentricity). A sudden approximately 12% drop in axial capacity occurs when a plane cut ($A_0/A = 0\%$) is introduced, regardless of the eccentricity. Although mathematically correct, such results are not physically meaningful in terms of openings, but show that plane cuts have negative effects even when the cross-section area remains the same because they break the horizontal strips and thus change effects of lateral restraints. Furthermore, axial capacity linearly (defined by the hatched area in Fig. 18) declines with increases in opening size ratios and nonlinearly with further increases in this ratio at every eccentricity considered. The limit between linear and nonlinear trend was defined at the point where the trend line of all data points reached an $R$-squared value equal to 1. The effect of eccentricity is highest with a minimal opening size, for which axial capacity declines linearly in approximately 12% increments per step of load eccentricity. However, eccentricity effects are much weaker with large openings (approximately 2.7% drops per step of load eccentricity). For intermediate opening size ratios, a much steeper decline is observed for low eccentricities ($e = 0$) than for high eccentricities ($e = t/6$).

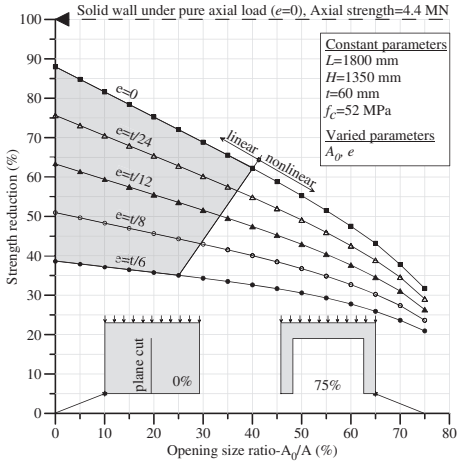


**Fig. 18.** Results of parametric study based on the Eurocode 2 model: effects of load eccentricity and opening size ratio on axial strength

### *Serviceability Considerations*

For RC elements subjected to tension and flexure, ACI 224R-01 (ACI 2001) presents general design guidelines for acceptable crack widths on tensile faces (ranging from 0.1 mm for water-retaining structures to 0.41 mm for dry structures). It also suggests that cracks wider than 0.15 mm could be considered aesthetically unacceptable because they can be seen by a casual observer. ACI 533R-11 (ACI 2012) states that under normal service conditions cracks up to 0.3 mm wide are structurally acceptable in precast wall panels. This is a more relaxed limit than the one (0.254 mm) in the previous version [ACI 533R-93 (ACI 1993)]. EN 1992-1-1 (CEN 2004) indicates that cracks in structural members should be limited sufficiently to avoid unacceptable impairment of an element's functionality, durability, or appearance. The admissible indicated value is 0.3 mm. Crack width limits provided in the guides discussed previously are presented in Fig. 12, and determined loads associated with these limits are presented in Table 5.

Another serviceability condition for a wall panel is its out-of-plane deflection. ACI 533R-11 (ACI 2012) sets limits of $H/360$ and $\leq 20$ mm immediate maximum deflection under service load, where $H$ is the free height of the panel. According to EN 1992-1-1 (CEN 2004), the deflection of members should not exceed $H/250$ under quasi-permanent loads. Loads associated with the maximum allowable deflections for each specimen were determined from Figs. 7(a) and 9(a) and are presented in Table 5. Only the deformation of the elements under short-term loads are considered here. Combinations of short- and long-term loads (e.g., permanent or self-weight) might lead to larger displacements. That explains why EN1992-1-1 (CEN 2004) allows considerably higher deflection than ACI 533R-11 (2012), which only takes into account immediate deflections. Further discussion is based solely on ACI codes.

For Specimen I-S, cracks wider than 0.15 mm, the aesthetic limit according to ACI 224R-01 (ACI 2001) appeared at 48% of peak load, very similar to the load corresponding to the deflection limit (52% of peak load). Cracks wider than 0.254 and 0.3 mm—structural limits according to ACI 533R-93 (ACI 1993) and ACI 533R-11 (ACI 2012), respectively—appeared at more than 90% of peak load. Similarly, for Specimen I-L the first cracks wider than the 0.15-mm aesthetic limit and the structural limit appeared at 44% and more than 90% of peak load, respectively. However, the 3.75-mm deflection limit was only reached at 75% of peak load (23% higher than for the I-S specimen). These values are single point measurements (for displacements) or pertain to a limited area of the wall (for cracks) and are not necessarily the highest in the specimens.

The results in Table 5 show that serviceability limits given by the elements' out-of-plane deflection are close to the loads at which cracks become visible to the casual observer. The structural limits are only reached very close to peak load, therefore serviceability will be dictated by the deflection criterion if there are no other stringent limits due to aesthetic or durability concerns. However, a small out-of-plane displacement of 3.75 mm cannot be noticed as easily as cracks on an element's surface. As seen in members subjected to eccentric compression, cracks wider than 0.25 mm could herald an elements' imminent failure. Thus, using design provisions in current guidelines to evaluate service states of walls with cut-out openings could lead to overlaps with ultimate state criteria. More research is needed to adapt current cracking criteria for assessment of the service state of walls with cut-out openings.

## Conclusion and Future Work

The effects of steel reinforcement and the presence of cut-out openings on axially loaded concrete walls were examined in the presented experimental program. The main conclusions were as follows:

- Recorded strains in the steel reinforcement indicate that it may make no significant contribution at serviceability limit states, but yielding may occur close to failure when second-order effects start to be more active, thus contributing to the overall ductility. More tests are needed to determine reinforcement's contribution to the overall load-bearing capacity of walls with openings. However, crack patterns recorded with DIC show that it can ensure good redistribution of stresses.
- Reducing the cross-sectional area by 25 and 50% by cutting out openings led to 36 and 50% reductions in peak loads, respectively. Overall, the specimen with a small opening was stiffer than the specimen with a large opening (and hence had higher ductility and energy release at failure). The parametric study

**Table 5.** Recommended Serviceability Limits for Precast Walls and Associated Load Levels

| | | Crack width limits | | | Deflection limits |
|---|---|---|---|---|---|
| | | Aesthetic | Structural | | — |
| Specimen | $N_{test}$ (kN) | ACI 224R-01 (0.15 mm) (kN) | ACI 533-93 (0.254 mm) (kN) | ACI 533-11 (0.3 mm) (kN) | ACI 533-11 (3.75 mm) (kN) |
| I-S | 1,500 | 720 (48) | 1,390 (93) | 1,420 (95) | 790 (52) |
| I-L | 1,180 | 520 (44) | 1,080 (92) | 1,150 (97) | 880 (75) |

Note: Numbers in parentheses are associated load levels as percentages of peak load ($N_{test}$).

revealed that the axial strength reduction is more sensitive to eccentricity when the opening size ratio is minimal, and becomes minor as this ratio increases. In addition, the axial strength declines nonlinearly as the opening size is increased.
- The critical buckling strength analysis showed that material failure (inelastic buckling) rather than a stability failure occurred first. Because of limitations of buckling theory for concrete plates, these conclusions are only based on the test with the solid specimen.
- The 3D DIC system proved to be a reliable noncontact tool for monitoring strain and displacement fields in regions of interest. The observed crack patterns indicate that the specimen with a large opening behaved more like a RC frame than a RC wall, with all major strains oriented toward the opening corner. In order to set suitable thresholds for small and large openings in walls (with negligible and nonnegligible effects, respectively) and the optimal transition point between RC walls and RC frames in design codes for structural elements, more tests are required including walls with intermediate size openings. The method is particularly useful because hairline cracks are difficult to observe with the naked eye, especially during specimen loading. Structurally acceptable crack widths based on design codes appear to be uncomfortably close to those associated with ultimate loads. Because crack width is usually used as an indicator of structures' degradation, more restrictive limits for walls with cut-out openings may be needed to increase gaps between service and ultimate limit states, potentially avoiding failure.
- The procedure proposed for evaluating the systems' capacity, based on generic equations from design codes, provided good agreements with the test results and the closed-form solution given by Doh and Fragomeni, which addresses the axial strength of walls with and without openings. The results have been reviewed in terms of both ultimate capacity and failure mechanisms. They show (inter alia) that the lateral restraints transform the problem into a three-dimensional (plate mechanism) rather than one-dimensional problem.

The findings open new avenues for studying the behavior of concrete walls with openings and may provide foundations for future research. Nonlinear analysis could be applied with a larger test matrix to assess effects of other important parameters (e.g., higher eccentricities, asymmetric openings, and/or different boundary conditions). However, despite the clear need to extend the analyses, the presented results may be useful for improving existing design models, assessing requirements for strengthening concrete structure, and identifying optimal strengthening procedures.

## Acknowledgments

The authors would like to acknowledge The Research Council of Norway (RFF), Development Fund of the Swedish Construction Industry (SBUF), and Skanska for financing the presented work and associated, ongoing project.

## Supplemental Data

Video S1 is available online in the ASCE Library (http://www.ascelibrary.org).

## References

ACI (American Concrete Institute). (1993). "Guide for precast concrete wall panels." *ACI 533R-93*, Farmington Hills, MI.

ACI (American Concrete Institute). (2001). "Control of cracking in concrete structures." *ACI 224R-01*, Farmington Hills, MI.

ACI (American Concrete Institute). (2011). "Building code requirements for structural concrete and commentary." *ACI 318*, Farmington Hills, MI.

ACI (American Concrete Institute). (2012). "Guide for precast concrete wall panels." *ACI 533R-11*, Farmington Hills, MI.

Ali, A., and Wight, J. (1991). "RC structural walls with staggered door openings." *J. Struct. Eng.*, 10.1061/(ASCE)0733-9445(1991)117:5(1514), 1514–1531.

Ascent. (2012). "Envelope tolerances for architectural precast." Precast/Prestressed Concrete Institute, Chicago.

Canadian Standards Association. (2004). "Design of concrete structures." *CAN/CSA-A23.3*, Mississauga, ON, Canada.

CEN (European Committee for Standardization). (2004). "Design of concrete structures—Part 1-1: General rules and rules for buildings." *EN1992-1-1*, Eurocode 2, Brussels, Belgium.

DIN (Deutsches Institut für Normung). (1988). "Reinforced concrete structures: Design and construction." *DIN 1045*, Berlin.

Doh, J., and Fragomeni, S. (2005). "Evaluation of experimental work on concrete walls in one-way and two-way action." *Aust. J. Struct. Eng.*, 6(1), 37–52.

Doh, J. H. (2002). "Experimental and theoretical studies of normal and high strength concrete wall panels." Ph.D. thesis, Griffith Univ., Gold Coast, Australia.

Doh, J. H., and Fragomeni, S. (2006). "Ultimate load formula for reinforced concrete wall panels with openings." *Adv. Struct. Eng.*, 9(1), 103–115.

El-Metwally, S. E., Ashour, A. F., and Chen, W. F. (1990). "Instability analysis of eccentrically loaded concrete walls." *J. Struct. Eng.*, 10.1061/(ASCE)0733-9445(1990)116:10(2862), 2862–2880.

Floruţ, S.-C., Sas, G., Popescu, C., and Stoian, V. (2014). "Tests on reinforced concrete slabs with cut-out openings strengthened with fibre-reinforced polymers." *Compos. Part B: Eng.*, 66, 484–493.

Fragomeni, S., Doh, J. H., and Lee, D. J. (2012). "Behavior of axially loaded concrete wall panels with openings: An experimental study." *Adv. Struct. Eng.*, 15(8), 1345–1358.

Fragomeni, S., and Mendis, P. (1997). "Instability analysis of normal- and high-strength reinforced-concrete walls." *J. Struct. Eng.*, 10.1061/(ASCE)0733-9445(1997)123:5(680), 680–684.

Fragomeni, S., Mendis, P. A., and Grayson, W. R. (1994). "Review of reinforced concrete wall design formulas." *ACI Mater. J.*, 91(5), 521–529.

Ganesan, N., Indira, P. V., and Santhakumar, A. (2013). "Prediction of ultimate strength of reinforced geopolymer concrete wall panels in one-way action." *Constr. Build. Mater.*, 48(16), 91–97.

Gere, J. M., and Timoshenko, S. P. (1990). *Mechanics of materials*, 3rd Ed., PWS-KENT, Boston.

GOM mbH. (2015). "ARAMIS—Optical 3D deformation analysis." ⟨http://www.gom.com/metrology-systems/system-overview/aramis.html⟩ (May 20, 2015).

Guan, H. (2010). "Ultimate strength analysis of normal and high strength concrete wall panels with varying opening configurations." *Eng. Struct.*, 32(5), 1341–1355.

Huang, Y., Hamed, E., Chang, Z.-T., and Foster, S. J. (2015). "Theoretical and experimental investigation of failure behavior of one-way high-strength concrete wall panels." *J. Struct. Eng.*, 10.1061/(ASCE)ST.1943-541X.0001072, 04014143.

Kennedy, G., and Goodchild, C. H. (2004). "Practical yield line design." Concrete Centre, Camberley, Surrey, U.K.

Li, B., Kai, Q., and Tran, C. T. N. (2013). "Retrofitting earthquake-damaged RC structural walls with openings by externally bonded FRP strips and sheets." *J. Compos. Constr.*, 10.1061/(ASCE)CC.1943-5614.0000336, 259–270.

Macgregor, J. G., Simmonds, S. H., and Warwaruk, J. (1971). "Seminar on building code requirements, ACI 318-71." *Structural Engineering Rep. No. 36*, Univ. of Alberta, Dept. of Civil Engineering, Edmonton, AB, Canada.

Mahal, M., Blanksvärd, T., Täljsten, B., and Sas, G. (2015). "Using digital image correlation to evaluate fatigue behavior of strengthened reinforced concrete beams." *Eng. Struct.*, 105(16), 277–288.

Mohammed, B., Ean, L. W., and Malek, M. A. (2013). "One way RC wall panels with openings strengthened with CFRP." *Constr. Build. Mater.*, 40(16), 575–583.

Mosoarca, M. (2014). "Failure analysis of RC shear walls with staggered openings under seismic loads." *Eng. Failure Anal.*, 41(0), 48–64.

Novak, A. S., and Collins, K. R. (2012). *Reliability of structures*, 2nd Ed., CRC Press/Taylor & Francis Group, Boca Raton, FL.

Park, R. (1988). "State of the art report: Ductility evaluation from laboratory and analytical testing." *Proc., 9th World Conf. on Earthquake Engineering*, Vol. VIII, International Association for Earthquake Engineering (IAEE), Tokyo, 605–616.

Pillai, S. U., and Parthasarathy, C. V. (1977). "Ultimate strength and design of concrete walls." *Build. Environ.*, 12(1), 25–29.

Popescu, C., Sas, G., Blanksvärd, T., and Täljsten, B. (2015). "Concrete walls weakened by openings as compression members: A review." *Eng. Struct.*, 89(16), 172–190.

Robinson, G. P., Palmeri, A., and Austin, S. A. (2011). "Implications of EC2 on the design of simply supported precast RC panels under eccentric axial load." *Proc., fib Symp. on Concrete Engineering for Excellence and Efficiency*, Czech Concrete Society (CBS), Prague.

Saheb, M., and Desayi, P. (1990a). "Ultimate strength of R.C. wall panels in two-way in-plane action." *J. Struct. Eng.*, 10.1061/(ASCE)0733-9445(1990)116:5(1384), 1384–1402.

Saheb, M., and Desayi, P. (1990b). "Ultimate strength of RC wall panels with openings." *J. Struct. Eng.*, 10.1061/(ASCE)0733-9445(1990)116:6(1565), 1565–1577.

Sas, G., Blanksvärd, T., Enochsson, O., Täljsten, B., and Elfgren, L. (2012). "Photographic strain monitoring during full-scale failure testing of Örnsköldsvik bridge." *Struct. Health Monitor.*, 11(4), 489–498.

Seddon, A. E. (1956a). "Concrete walls in compression under short-term axial and eccentric loads." IABSE (International Association for Bridge and Structural Engineering), Zürich, Switzerland.

Seddon, A. E. (1956b). "The strength of concrete walls under axial and eccentric loads." *Symp. on the Strength of Concrete Structures*, Cement and Concrete Association, London, 445–486.

Smith, B., Kurama, Y., and McGinnis, M. (2011). "Design and measured behavior of a hybrid precast concrete wall specimen for seismic regions." *J. Struct. Eng.*, 10.1061/(ASCE)ST.1943-541X.0000327, 1052–1062.

Standards Australia. (2009). "Concrete structures." *AS 3600*, Sydney, Australia.

Swartz, S. E., Rosebraugh, V. H., and Rogacki, S. A. (1974). "A method for determining the buckling strength of concrete panels." *Exp. Mech.*, 14(4), 138–144.

Taylor, C. P., Cote, P. A., and John, W. W. (1998). "Design of slender reinforced concrete walls with openings." *ACI Struct. J.*, 95(4), 420–433.

Todut, C., Dan, D., and Stoian, V. (2014). "Theoretical and experimental study on precast reinforced concrete wall panels subjected to shear force." *Eng. Struct.*, 80(16), 323–338.

Todut, C., Dan, D., and Stoian, V. (2015). "Numerical and experimental investigation on seismically damaged reinforced concrete wall panels retrofitted with FRP composites." *Compos. Struct.*, 119(16), 648–665.

van Mier, J. M. (1986). "Multiaxial strain-softening of concrete." *Mater. Struct.*, 19(3), 179–190.

Wang, J., Sakashita, M., Kono, S., and Tanaka, H. (2012). "Shear behaviour of reinforced concrete structural walls with eccentric openings under cyclic loading: Experimental study." *Struct. Des. Tall Special Build.*, 21(9), 669–681.

Ziemian, R. D. (2010). *Guide to stability design criteria for metal structures*, 6th Ed., Wiley, Hoboken, NJ.

# Paper III

## Concrete walls with cut-out openings strengthened by FRP confinement

Cosmin Popescu; Gabriel Sas; Thomas Blanksvärd; and Björn Taljsten

Published in:
*Journal of Composites for Construction*
Published online: October 2016
Article ID 04016106

# Concrete Walls with Cutout Openings Strengthened by FRP Confinement

Cosmin Popescu, S.M.ASCE[1]; Gabriel Sas[2]; Thomas Blanksvärd[3]; and Björn Täljsten[4]

**Abstract:** Redesigning buildings to improve their space efficiency and allow changes in use is often essential during their service lives to comply with shifts in living standards and functional demands. This may require the introduction of new openings in elements such as beams, walls, and slabs, which inevitably reduces their structural performance and hence requires repair or strengthening. However, there are uncertainties regarding both the effects of openings and the best remedial options for them. Here, the authors report on an experimental investigation of the effectiveness of fiber-reinforced polymer (FRP)–based strengthening for restoring the axial capacity of a solid RC wall after cutting openings. Nine half-scale specimens, designed to represent typical wall panels in residential buildings with and without door-type openings, were tested to failure. It was found that FRP-confinement and mechanical anchorages increased the axial capacity of walls with small and large openings (which had 25 and 50% reductions in cross-sectional area, respectively) by 34–50% and 13–27%, to 85–94.8% and 56.5–63.4% of their precutting capacity, respectively. **DOI: 10.1061/(ASCE)CC.1943-5614.0000759.** 

**Author keywords:** Strengthening; Fiber-reinforced polymers (FRPs); Concrete walls; Openings; Axial strength; Eccentricity; Mechanical anchorages; Confinement; Disturbed regions.

## Introduction

Openings in RC structural elements such as beams, slabs, or walls are often needed for technical or functionality reasons; i.e., to improve their space efficiency, meet shifts in functional requirements, or both. However, openings have clear negative effects, as addressed in numerous studies (e.g., Mohammed et al. 2013; Floruţ et al. 2014; Todut et al. 2014; Popescu et al. 2016), through the introduction of disturbed regions that significantly decrease the elements' ultimate load capacity, stiffness, and energy dissipation. Thus, the effects of any opening must be carefully considered in the design stage and addressed by specifying appropriate reinforcement detailing around the edges. However, when openings must be introduced in structures that have already been built, the scope for such detailing is very limited. Instead, repair is often required (*repair* being defined here as actions that fully or partially restore the structure's load-carrying capacity). New repair options are being developed and applied, but both further development of innovative approaches and more knowledge of their effects are needed.

European [EN1992-1-1 (CEN 2004)] and Australian (AS 2009) design codes provide some guidance regarding the design of walls with openings subjected to vertical loads. Both assume that the effects of a *small* opening (i.e., with area and height less than 1/10 and 1/3 of the wall's total area and height, respectively) on the structural integrity of the element can be neglected if the wall is restrained on all sides. For a *large* opening exceeding these proportions, each remaining portion should be considered separately. The portion between a restraining member and an opening should be treated as a separate member, supported on three sides, while areas between openings (if there are more than one) must be treated as being supported on two sides. Several other empirical models have also been proposed (e.g., Saheb and Desayi 1990; Doh and Fragomeni 2006; Guan 2010) that are calibrated using data from limited numbers of one-way (OW) and two-way (TW) action tests, with loading eccentricity up to one-sixth of the wall thickness (Popescu et al. 2015). The terms *OW action* and *TW action* refer here to cases where, due to eccentricity, flexure occurs in one and two directions, respectively, as in panels restrained along the top and bottom edges (which develop out-of-plane curvature parallel to the load direction), and panels restrained along three or four sides (which generally deform in both the horizontal and vertical directions).

The aim of the study presented here was to contribute to efforts to develop a convenient new repair system that can substantially restore the axial strength of concrete walls after openings have been cut. Traditionally, RC walls with openings have been strengthened by either installing a frame around the openings using RC/steel members (Engel 2016) or increasing the elements' cross-sectional thickness (Delatte 2009). Nowadays, intervention in existing buildings must be minimal in order to minimize inconvenience due to limitations in use of the structure during repairs. An option is to use externally bonded fiber-reinforced polymers (FRPs). This has been tested successfully by several authors in seismic retrofitting contexts (Demeter 2011; Li et al. 2013; Todut et al. 2015; Mosallam and Nasr 2016). Thus, the strengthening schemes proposed in the cited studies may not be suitable for repairing gravitationally loaded walls, and more research regarding their effects on elements' responses to vertically applied loads is required (Popescu et al. 2015).

The performance of nonseismically designed walls with openings strengthened with FRP has only been examined by Mohammed et al. (2013), who strengthened OW, 1/3-scale RC walls with openings varying in size from 5 to 30% of the total wall area by placing carbon FRP (CFRP) sheets around the edges of the

[1]Ph.D. Candidate, Northern Research Institute—NORUT, Rombaksveien E6-47, N-8517 Narvik, Norway (corresponding author). ORCID: http://orcid.org/0000-0001-9423-7436. E-mail: cosmin.popescu@norut.no

[2]Associate Senior Lecturer, Dept. of Civil, Environmental, and Natural Resources Engineering, Luleå Univ. of Technology, 971 87 Luleå, Sweden.

[3]Senior Lecturer, Dept. of Civil, Environmental, and Natural Resources Engineering, Luleå Univ. of Technology, 971 87 Luleå, Sweden.

[4]Professor, Dept. of Civil, Environmental, and Natural Resources Engineering, Luleå Univ. of Technology, 971 87 Luleå, Sweden.

Note. This manuscript was submitted on June 6, 2016; approved on August 11, 2016; published online on October 20, 2016. Discussion period open until March 20, 2017; separate discussions must be submitted for individual papers. This paper is part of the ***Journal of Composites for Construction***, © ASCE, ISSN 1090-0268.

openings. As expected, the walls' load-carrying capacity increased as the principal stresses on the opening corners decreased. A limitation of the study by Mohammed et al. (2013) was that it only involved OW walls with no strengthening procedures for walls in TW action. Furthermore, the failure mode (concrete crushing) of unstrengthened TW walls with openings observed in experimental tests (Popescu et al. 2016) indicates that the strengthening configuration proposed by Mohammed et al. (2013) would not be suitable for them, and a better strengthening solution may be confinement.

Confinement with FRP has proved to be an efficient strategy for enhancing the strength and ductility of axially loaded members, although its effects are the most effective only for elements with circular cross sections. For elements with rectangular cross sections, only parts of the cross section are effectively confined (Mirmiran et al. 1998; Pessiki et al. 2001; Wu and Wei 2010; Liu et al. 2015). Design/analysis-oriented models developed by various researchers, as reviewed by (Lam and Teng 2003; Rocca et al. 2008), have shown that as the aspect ratio of the cross section increases, the enhancement of compressive strength provided by FRP-confinement decreases. Members with aspect ratios higher than 3:1 are usually regarded as walllike columns. Creating a new opening in a concrete wall inevitably increases the aspect ratio of the remaining portions, hereafter piers (or walllike columns), and reduces the effectiveness of FRP-confinement. Few studies have addressed this problem. However, it has been shown that the axial strength and ductility of short (1.5-m) columns with an aspect ratio of 3.65 to 1 can be increased by confinement using longitudinal and transversal FRP sheets in combination with placing fiber anchor spikes along the wider faces of the column (Tan 2002) or adding semicylindrical attachments (high-strength mortar) to increase the cross-sectional area (Tanwongsval et al. 2003). In addition, quadridirectional CFRP can improve seismic performance, but not other strength parameters, according to Prota et al. (2006). Adding heavy anchor spikes or cross-sectional enlargement with high-strength mortar can also double the confining effect of circumferential FRP, but excessively light fiber anchor spikes fail prematurely and thus have little effect on strength, relative to controls with no anchors (Triantafillou et al. 2015). In contrast to these findings, De Luca et al. (2013) found that confining walllike columns with an aspect ratio of 2.92 to 1 with FRP (but no longitudinal or anchor fibers) could enhance axial ductility, but not axial capacity. Hence, it is necessary to use a hybrid method (FRP-confinement and longitudinal FRP fibers, anchors, or increases in cross section) when it is necessary to increase both the axial strength and ductility of walllike columns.

Before such an approach can be used with confidence, more information about the response of the overall system is required. Hence, in this paper, the effectiveness of FRP-confinement with mechanical anchorages for increasing the axial strength of concrete walls weakened by cutout openings was investigated. Increases in axial strength, ductility, steel reinforcement, and FRP strain utilization were measured to improve understanding of such elements' structural behavior. The results provide information that it is believed will assist efforts to develop a new design model capable of capturing complicating effects such as load eccentricity and large aspect ratios of elements' cross sections.

## Experimental Testing

### *Specimen Design and Test Matrix*

Half-scale walls designed to represent typical wall panels in residential buildings with and without cutout openings (with dimensions 1,800 mm long, 1,350 mm wide, and 60 mm thick), were constructed for testing to failure. The specimens are designed to carry vertical loads with no transverse loads between supports or lateral in-plane forces. The walls were tested in TW action and subjected to axial loading with small eccentricity (1/6 of the wall thickness), as typically found in practice and applied in previous studies. Moreover, the simplified design formulas found in the literature were calibrated for eccentricity at up to one-sixth of a wall's thickness to ensure that the resultant axial force passes through the middle third of the wall's overall thickness. Thus, the selected eccentricity facilitates comparison of results with those of previous tests and further development of published equations.

Minimum wall reinforcement was provided according to American and Australian design codes (i.e., ACI 2011; AS 2009). In the European code [EN1992-1-1 (CEN 2004)], such specimens are treated as lightly reinforced or unreinforced elements, as the sections contain reinforcement placed within a single layer and do not contribute to the overall capacity. Consequently, welded wire fabric reinforcement was used to reinforce the walls, consisting of deformed 5-mm-diameter bars with 100-mm spacing in both orthogonal directions and centrally placed in a single layer. The vertical and horizontal steel reinforcement ratios resulting from this configuration are 0.327 and 0.339%, respectively. The specimens with openings were detailed to replicate solid walls with sawn cutouts; i.e., no additional reinforcement was placed around the edges or corners of the openings. More details about the fabrication process are given in Popescu et al. (2016). The test matrix can be divided into three stages, designated I-III, in which reference (unstrengthened) specimens, precracked specimens strengthened by FRP, and uncracked specimens strengthened by FRP (duplicated to increase the reliability of the data) were tested, respectively.

Three specimens were loaded to failure in stage I: a solid panel; a panel with a *small* symmetric, half-scaled single-door-type opening (450 × 1,050 mm); and a panel with a *large* symmetric, half-scaled double-door-type opening (900 × 1,050 mm). The specimens' dimensions and reinforcement details are presented in Fig. 1. The small and large openings represent 25 and 50% reductions, respectively, in the cross-sectional area of the solid wall. Thus, these tests enabled evaluation of the effects of putting new openings in a solid wall. The damage level was evaluated in terms of ultimate load, crack pattern, displacement profiles, strains in concrete and steel reinforcement, ductility, and energy release at failure.

In stage II, two specimens (one with a small opening and one with a large opening) were first loaded to the point required to create a significant crack based on nonlinear finite element analyses and observations of the reference specimens in stage I. Of course, the significance of a crack depends on many factors, including the building's functions and environmental exposure. However, according to ACI 224R-01 (ACI 2001) a crack wider than 0.15 mm may require repair. To create cracks of this width, the specimens were loaded at up to 75% of their unstrengthened axial capacity. They were subsequently completely unloaded, and then strengthened by FRP and tested to failure. This procedure mimics scenarios in which the creation of openings and subsequent presence of a sustained load results in the degradation of a wall. In stage III, duplicated specimens with openings of each size were strengthened with the FRP system in an uncracked state and then loaded to failure.

For convenience, the specimens are designated according to the stage when they were tested (I, II, or III), their type (C, S, or L, for solid wall and walls with small and large openings, respectively) and (for specimens used in stage III) by a serial number. It should be noted that the words *small* and *large* are used here as convenient designations rather than as clearly delimited terms with specific thresholds and implications.

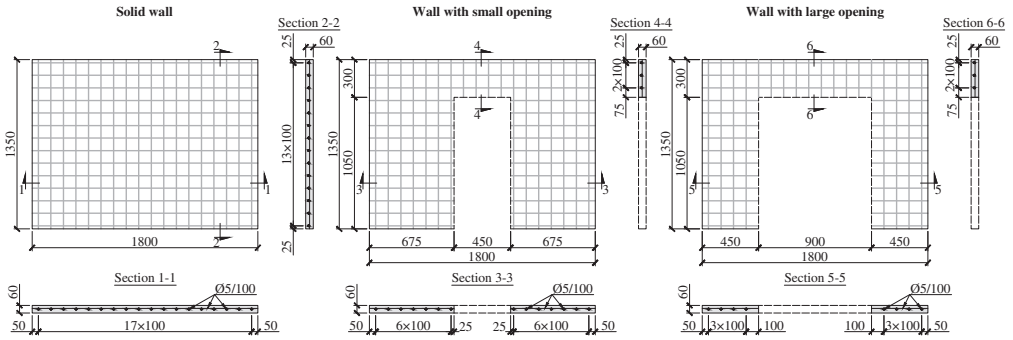


**Fig. 1.** Specimen dimensions and reinforcement details (dimensions in millimeters)

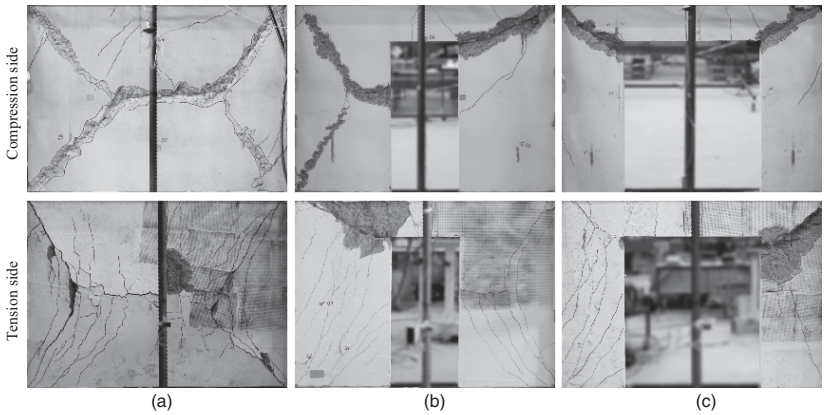


**Fig. 2.** Crack pattern and failure mode of the unstrengthened specimens (reprinted from Popescu et al. 2016): (a) Specimen I-C; (b) Specimen I-S; (c) Specimen I-L

### *CFRP Strengthening*

#### Design Method

Information obtained from the analysis of failure modes of unstrengthened walls reported by Popescu et al. (2016) was used to identify a suitable FRP configuration. In all cases, the walls had a brittle failure due to crushing of concrete, with spalling and reinforcement buckling (Fig. 2). In order to increase the axial strength of walls with openings, confinement strengthening was designed as follows. First, the decrease in capacity caused by introducing new openings was found by testing the unstrengthened elements. The results indicate that the 25 and 50% reductions in cross-sectional area of the solid wall caused by introducing the small and large openings reduced the load-carrying capacity by nearly 36 and 50%, respectively. In order to regain the loss of capacity, two choices were available: increasing the specimen's thickness or the concrete compressive strength through confinement. Increasing the concrete compressive strength through FRP-confinement was the focal aspect of the work presented here.

Next, the EC2 [EN1992-1-1 (CEN 2004)] design model for TW walls [Eq. (1)] was used to find the confined compressive strength ($f_{cc}$) needed to restore the capacity of the solid wall:

$$N_{I-C} = 2 f_{cc} L_{\text{pier}} t \Phi \tag{1}$$

where

$$\Phi = 1.14\left(1 - 2\frac{e + e_a}{t}\right) - 0.02 \cdot \frac{H_{\text{eff}}}{t} \leq \left(1 - 2\frac{e + e_a}{t}\right) \tag{2}$$

where $N_{I-C}$ = experimentally obtained axial capacity of a solid wall; $t$ = wall thickness; $L_{\text{pier}}$ = length of a pier; $f_{cc}$ = theoretical compressive strength of the confined concrete; $e$ = initial eccentricity, $e = t/6$; and $e_a$ = additional eccentricity due to lateral deflection of the wall. The additional eccentricity, $e_a$, accounts for the effect of slenderness, also known as *second-order* (or $P - \Delta$) effects, and can be computed using the EC2 approach: $e_a = H_{\text{eff}}/400$.

In this instance, $H_{\text{eff}} = \beta H$ is the effective height. Values for the effective height factor $\beta$ are given for the most commonly encountered restraints:

$$\beta = \begin{cases} \dfrac{1}{1+\left(\frac{H}{3L}\right)^2} & \text{three-sides} \\ \dfrac{1}{1+\left(\frac{H}{L}\right)^2} & \text{four-sides with } L \geq H \\ \dfrac{L}{2H} & \text{four-sides with } L < H \end{cases} \tag{3}$$

Solving Eq. (1) yields a ratio between the confined and unconfined compressive strengths, $f_{cc}/f_c$, of about 1.26 and 1.44 for walls with small and large openings, respectively. The resulting value was then used in conjunction with the model presented by Lam and Teng (2003) to estimate the required thickness of the FRP jacket.

For FRP-wrapped rectangular concrete columns, Lam and Teng (2003) proposed an analytical relationship, Eq. (4), which considers the effect of nonuniformity of confinement through a shape factor ($k_{s1}$):

$$\frac{f_{cc}}{f_c} = 1 + k_1 k_{s1} \frac{f_l}{f_c} \tag{4}$$

where $f_c$ = compressive strength of the unconfined concrete; $f_{cc}$ = compressive strength of the confined concrete; $k_1$ = confinement effectiveness coefficient (3.3); and $f_l$ = confining pressure.

The shape factor, $k_{s1}$, is defined as

$$k_{s1} = \left(\frac{b}{h}\right)^2 \frac{A_e}{A_c} \tag{5}$$

The effective confinement area ratio $A_e/A_c$ is calculated as

$$\frac{A_e}{A_c} = \frac{1 - [(b/h)(h-2R)^2 + (h/b)(b-2R)^2]/3A_g - \rho_{sc}}{1-\rho_{sc}} \tag{6}$$

where $b$ and $h$ = width and height of the cross section, respectively; $A_e$ = effective confinement area; $A_c$ = total area of the cross section; $R$ = corner radius; $\rho_{sc}$ = cross-sectional area proportion of longitudinal steel; and $A_g$ = gross area of the column section with rounded corners.

The confining pressure, $f_l$, is given by

$$f_l = \frac{2 \cdot f_{\text{frp}} \cdot t_{\text{frp}}}{D'} = \frac{2 \cdot f_{\text{frp}} \cdot t_{\text{frp}}}{\sqrt{h^2+b^2}} \tag{7}$$

where $f_{\text{frp}}$ and $t_{\text{frp}}$ = tensile strength and thickness of the FRP jacket, respectively.

As the model is not valid for members with high cross-section aspect ratios, the following procedure was employed. The transverse fiber sheets were fixed using steel bolts in a configuration that created virtual cross sections with an aspect ratio limited to 2:1 (60 × 120 mm starting from the edge of the opening, as shown in Fig. 3). Following the assumption by Tan (2002) that such internal transverse links provide additional anchor points for FRP jackets, the effectively confined area for pure compression is shown in Fig. 3. One virtual column strip was extracted so that Eq. (6) would be applicable; the results were then extrapolated to the rest of the wall-pier. Based on the required thicknesses of FRP layers under these conditions back-calculated from Eq. (7), two and three 0.17-mm-thick FRP layers were used to strengthen the specimens with small and large openings, respectively. The authors are aware that loading eccentricity (included in the tests to mimic imperfections in routine construction practices) may reduce the effectiveness of the confinement, but the lack of better models prevented the incorporation of appropriate parameters to simulate its effects. Thus, as noted by Mukherjee et al. (2004), more tests are required to extend current confinement models to account for loading imperfections.

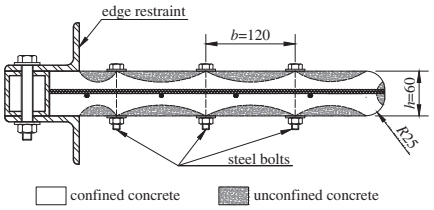


**Fig. 3.** Effectively confined area of a wall-pier (dimensions in millimeters)

Analyzing the failure mechanism of the unstrengthened specimens, the authors saw no decisive failure of the beam above the opening except for some small cracks. The same number of FRP layers as of wall-piers were conservatively used to strengthen the beam above the opening in order to redirect the load toward the wall-piers. The FRP material was placed along both lateral faces from edge to edge of the wall and bent under the bottom part of the beam.

### Specimen Preparation and Material Properties

The walls were cast in a long-line form, in a lying position, and resting on a steel platform that can accommodate up to five specimens, in two batches: the specimens used in stages I and II in the first batch, and those used in stage III in the second batch. The concrete used to cast the specimens was a self-consolidating mix that could be poured without vibrating them, including dynamon NRG-700, a superplasticizer added to provide high workability and early strength. To determine mechanical characteristics of the concrete (compressive strength and fracture energy), five cubes and beams from each batch with standardized sizes were cast and cured in identical conditions to the specimens. The average cubic compressive strength of the concrete was determined in accordance with SS-EN 12390-3:2009 (SIS 2009b), while the fracture energy was determined following the recommendations in RILEM TC 50-FMC (1985). In addition, five coupons were taken from the reinforcing steel meshes and tested according to SS-EN ISO 6892-1:2009 (SIS 2009a) to determine their stress-strain properties. The results—i.e., the means and corresponding coefficient of variation (COV)—are given in Table 1.

Temporary timber supports were created for all six specimens to replicate the vertical positions of the elements in a structure and provide access around the specimens. The concrete surfaces were prepared by grinding and cleaning with compressed air [Figs. 3(a and b)]. The corners adjacent to the opening edge were rounded with a corner radius of 25 mm to avoid premature failure of the FRP and to increase the effect of confinement. The strength enhancement relies on the continuity (fully wrapped) of the fiber sheets in the transverse direction. The as-built boundary conditions limited access to lateral edges of the cross section. Therefore, the authors applied U-shaped CFRP sheets fixed with mechanical anchorages, installed in 8-mm holes drilled through the wall at positions premarked on the concrete surface.

The sheets were applied using the wet layup procedure illustrated in Figs. 4(c and d). A two-component epoxy primer (StoPox 452 EP) was applied to the prepared surfaces of the specimens,

**Table 1.** Mechanical Properties of the Concrete and Steel Reinforcement

| | Concrete | | | | Steel reinforcement | | | | | | | |
|---|---|---|---|---|---|---|---|---|---|---|---|---|
| | | | | | Yield | | | | Tensile | | | |
| | Compressive strength | | Fracture energy | | Strength | | Strain | | Strength | | Strain | |
| Batch | $f_c$ (MPa) | COV (%) | $G_F$ (N/m) | COV (%) | $f_y$ (MPa) | COV (%) | $\varepsilon_y$ (‰) | COV (%) | $f_u$ (MPa) | COV (%) | $\varepsilon_u$ (‰) | COV (%) |
| Batch 1 | 62.8 | 3.2 | 168 | 11.9 | 632 | 0.35 | 2.8 | 8.45 | 693 | 0.40 | 4.87 | 4.82 |
| Batch 2 | 64.4 | 2.8 | 228 | 12.5 | | | | | | | | |

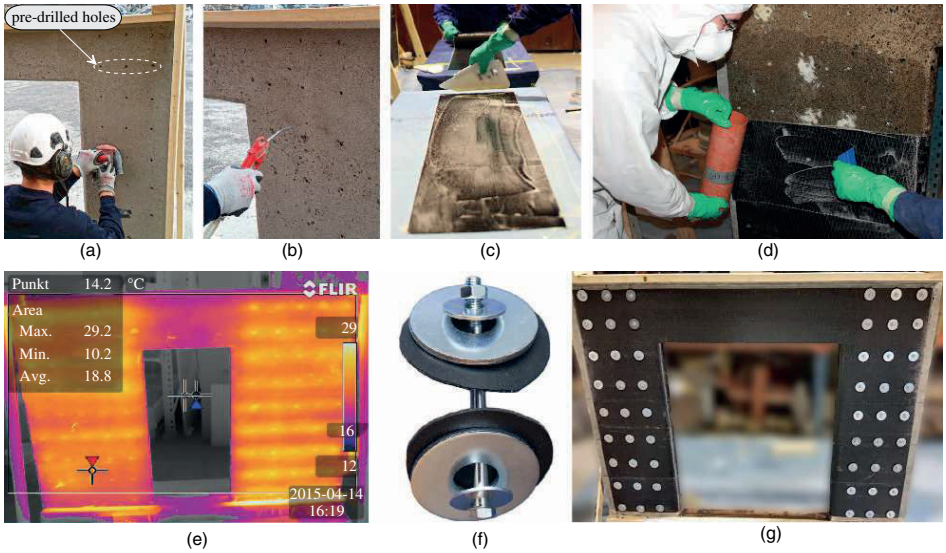


**Fig. 4.** (Color) Strengthening process: (a) grinding the concrete surface; (b) cleaning with compressed air; (c) impregnating the fibers; (d) applying the fibers to the specimen; (e) thermal image indicating positions of the holes; (f) mechanical anchorage; (g) specimen prepared for testing

while CFRP (StoFRP IMS300 C300) sheets were impregnated with StoPox LH two-component epoxy resin (elastic modulus 2 GPa) then applied approximately 6 h later. According to the supplier, these sheets have unidirectional fibers with an areal weight of about 300 g/m$^2$, high tensile strength (5,500 MPa), and intermediate elastic modulus (290 GPa). The ultimate tensile elongation of the fibers was about 19‰.

The specimens were stored indoors at around 18°C for about seven days to allow the epoxy resin to cure. The surface of each specimen surface was then locally heated with a heat gun, and a thermal imaging camera (FLIR T620bx, FLIR Systems, Wilsonville, Oregon) was used to look for areas with poor adhesion or air voids (none were detected) and find the predrilled holes [Fig. 4(e)]. Steel anchorage bolts, M6S 8.8–SS-EN ISO 4014 (SIS 2011), were then inserted into predrilled holes and prestressed with a torque estimated from the clamp load as 75% of the proof load, as specified in SS-EN ISO 898-1 (SIS 2013). It was believed that prestressing the steel bolts would increase their strengthening performance by providing an active confinement, as suggested by Harajli and Hantouche (2015). Neoprene padding was placed between the 50-mm steel washers providing the anchorage and the CFRP to avoid shearing of the fibers. The whole strengthening process is illustrated in Fig. 4. The strengthening entirely covers the concrete surface, so humidity and moisture issues may arise. However, the panels used in this study were intended to mimic indoor elements, classified as environmental Class 0 (i.e., structures located in a dry environment with low humidity) according to Täljsten (1999). The strengthening was applied without any sustained load due to permanent and partly due to imposed load.

## Test Setup and Instrumentation

All specimens were tested gravitationally in a test rig designed to represent the as-built boundary conditions (Fig. 5). The test rig had to simulate hinged connections at the top and bottom edges of the specimen. The side edges were restrained to simulate TW effects for real transverse walls under as-built conditions that permitted rotation but prevented translation (see Section 1-1 in Fig. 5). The axial load was applied eccentrically (at 1/6 of the wall thickness) in increments of 30 kN/min, with inspection stops every 250 kN to monitor cracks in the specimens. The eccentricity was induced by a 22-mm-diameter steel rod welded to each loading beam (HEB220). Four hydraulic jacks, each with a maximum

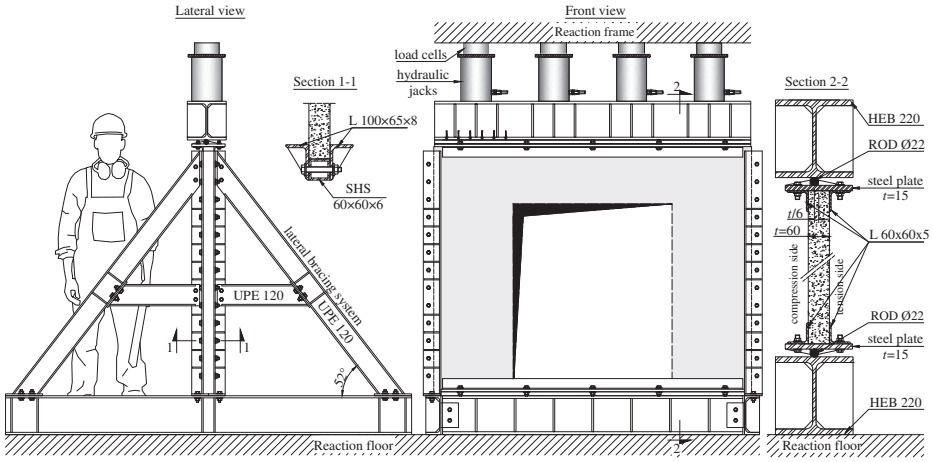


**Fig. 5.** Test setup and boundary conditions (dimensions in millimeters) (reprinted from Popescu et al. 2016); Sections 1-1 and 2-2 scaled up to show details

**Fig. 6.** (Color) General view of the test setup

capacity of 1.4 MN (1 MN = $10^6$ N), were networked together to apply a uniformly distributed load along the wall length. A general view of the test setup is shown in Fig. 6.

Out-of-plane and in-plane displacements were monitored using linear displacement sensors, and strain gauges intercepting potential yield lines (obtained from nonlinear finite element analysis) were installed on the steel reinforcement and CFRP. Data obtained from the strain gauges and linear displacement sensors were then supplemented by measuring full-field strain distributions using the digital image correlation (DIC) technique. Several studies have shown that DIC methodology can provide stable and reliable strain and displacement measurements in both laboratory environments (Smith et al. 2011; Mahal et al. 2015) and field tests (Sas et al. 2012).

A system (GOM mbH 2016) capable of capturing three-dimensional (3D) displacements was then used to facilitate the DIC measurements. The area of each specimen monitored by the optical DIC system was the right-upper corner on the tension side (780 × 660 mm, Fig. 7), an area of particular interest for monitoring strain and crack development in discontinuous regions. Patterning of the monitored surfaces (required for this equipment) was applied for the unstrengthened specimens using a stencil and spray, and it was applied manually for the strengthened elements since access to the surface was obstructed by the anchorages. A regular pattern was obtained when the stencil was used, while a random pattern was manually applied. To avoid interference with the optical measurement system, the reinforcement and outer FRP layer were instrumented only with strain gauges on half of each specimen (the left pier, on the tension side), as permitted by the symmetry of the test setup. The instrumentation scheme for walls with openings is shown in Fig. 7. The arrangement of the monitoring system for the solid wall differed, but the position of D1 was identical to enable comparison of all specimens.

## Test Results and Discussion

### *Tests on Reference Specimens—Stage I*

This section briefly summarizes results from stage I; i.e., tests with reference specimens, which behaved typically for elements restrained on all sides, deflecting in both the horizontal and vertical directions. The displacements were generally symmetric, but there were some asymmetries due to variations in material properties. All specimens failed by concrete crushing, with spalling and reinforcement buckling. Cracks opened late in the loading of the solid wall (at 85% of the peak load), and earlier in the loading of specimens with both small and large openings (at 50 and 20% of the peak load, respectively). The peak loads are presented in Table 2, and the effects of opening size on the load-displacement curves for the three specimens (recorded at the same position, D1, and symmetric to D1 on the other pier) are shown in Fig. 8. Crack pattern at failure is shown in Fig. 2 for both the tension and compression sides of the specimens. Strain responses in steel reinforcement and concrete were also recorded and are given elsewhere (Popescu et al. 2016),

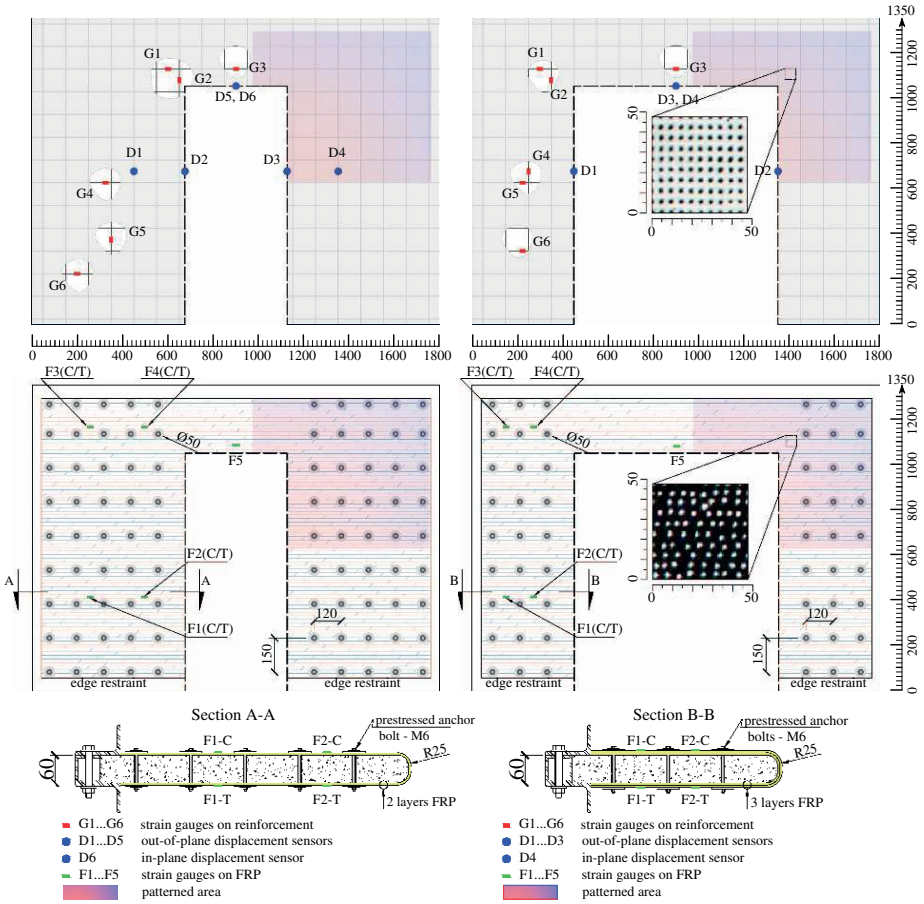


**Fig. 7.** (Color) Specimen configurations, FRP strengthening details, and instrumentation (dimensions in millimeters)

**Table 2.** Summary of Test Results

| | | $\varepsilon_{u,\mathrm{frp}}$ (‰) | | | | | | | | | | | | |
|---|---|---|---|---|---|---|---|---|---|---|---|---|---|---|
| | | F1 | | F2 | | F3 | | F4 | | F5 | | | | |
| Specimen | $N_{\mathrm{test}}$ (kN) | T | C | T | C | T | C | T | C | T | $\delta_e$ (mm) | $\delta_u$ (mm) | $\mu_\Delta$ | $E_d$ (kN · m) |
| I-C | 2,363 | | | | | — | | | | | 4.6 | 18.4 | 4.05 | 39.37 |
| I-S | 1,500 | | | | | | | | | | 8.5 | 27.4 | 3.21 | 34.21 |
| I-L | 1,180 | | | | | | | | | | 4.1 | 11.3 | 2.78 | 10.88 |
| II-S | 2,241 | 0.88 | 0.23 | 0.87 | 0.10 | 0.70 | 0.08 | 1.38 | −0.18 | 1.51 | 9.1 | 18.0 | 1.97 | 31.23 |
| II-L | 1,497 | 0.46 | 0.21 | 0.21 | 0.13 | 0.27 | 0.21 | 0.39 | 0.08 | 1.24 | 4.1 | 5.0 | 1.23 | 4.66 |
| III-S1 | 2,178 | 0.80 | 0.20 | 0.96 | 0.20 | 0.73 | −0.25 | 0.95 | 0.20 | 1.89 | 8.2 | 15.9 | 1.94 | 26.61 |
| III-S2 | 2,009 | 0.94 | −0.02 | 0.81 | 0.22 | 0.99 | 0.37 | 1.64 | −0.11 | 1.57 | 4.6 | 15.5 | 3.38 | 29.89 |
| III-L1 | 1,334 | 0.24 | 0.05 | 0.22 | 0.18 | 0.47 | 0.25 | 0.88 | −0.14 | 1.63 | 8.0 | 8.4 | 1.05 | 6.60 |
| III-L2 | 1,482 | N/A | 0.11 | N/A | 0.10 | N/A | 0.53 | 0.54 | 0.44 | 1.48 | 3.4 | 7.4 | 2.18 | 9.66 |

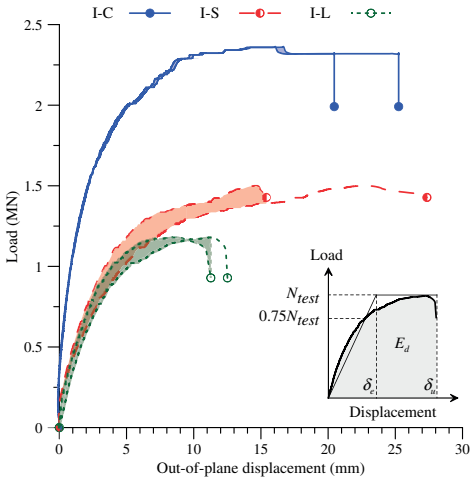


**Fig. 8.** (Color) Load-displacement responses of the three reference specimens showing effects of opening size (reprinted from Popescu et al. 2016)

but strains in the reinforcement at selected load levels are given in comparison with those from strengthened specimens to evaluate the strain utilization.

### *Tests on Strengthened Specimens—Stages II and III*

#### Precracking

The specimens used in stage II were loaded at up to 75% of the reference walls' axial capacity. At this point, the strains recorded in the steel reinforcement were lower than yielding. The maximum values were −0.63‰ (compressed bar) and 0.43‰ (tensioned bar) for the specimen with a small opening and −0.91 and 2.25‰ for the specimen with a large opening. A few cracks were observed, mainly in the spandrel above the opening, followed by other diagonal cracks from the bottom corner of the wall with an approximately 50° inclination, similar to those reported for the reference specimens. When the target damage (precracking) level was reached, the specimens were completely unloaded and removed from the test setup to apply the strengthening. Thus, the precracks were nearly closed during this manipulation.

#### Failure Modes

No cracks could be seen in the following loading cycles because the specimens were fully covered by FRP sheets. Thus, in contrast to the reference specimens, for which increases in deformations and cracking provided clear visual warnings of imminent failure, sounds provided more warning of imminent failure in the strengthened specimens. Crushing of the concrete, accompanied by debonding of the FRP sheets, occurred at failure. In all but one of the tests (III-S2, discussed next), the primary failure occurred at the bottom of one of the piers and was followed immediately by bulging of the FRP on the diagonally opposite side (i.e., the region around the opening's corner). The debonding of the FRP started in regions between the steel anchorage rows (Fig. 9), highlighting the need for vertical strips (or even bidirectional fibers) to improve the utilization of the CFRP fibers and further increase the element's axial strength.

After each test, the FRP sheets were removed to observe crack patterns. None were detected, apart from those located around the failure region. However, as already mentioned, specimen III-S2 had a different failure mode, with crushing of concrete and debonding of the FRP along the line between the wall corner and opening corner of one pier [Fig. 9(c)]. After stripping the FRP jacket [Fig. 9(c)], another diagonal crack was revealed on the spandrel starting from the reentrant corner. The failure modes of all specimens, both precracked and uncracked, were similar.

#### Axial Load versus Displacement Response

Fig. 10 shows load-displacement data recorded at the D1 location (identical for all specimens) of both strengthened and reference elements. As shown in Table 2, the strengthening increased maximum loads at failure of precracked specimens with small and large openings by 49 and 27%, respectively. Slightly lower increases were observed for uncracked specimens: 45 and 34% for specimens III-S1 and III-S2 with small openings, respectively, and 13 and 26% for specimens III-L1 and III-L2 with large openings, respectively. Thus, FRP strengthening seems to be most effective for precracked elements. It also changed the initial stiffness of the elements, but less so for precracked specimens than for uncracked specimens. Similar behavior was reported by Wu et al. (2014) for FRP-confined concrete cylinders with varying damage levels.

The increase in axial strength and initial stiffness of specimen III-L1 were relatively low due to an error during the test. The lateral bracing of the test rig was designed to be connected to the foundation support through slotted holes to account for variations in the thickness of the wall panels, allowing a little sliding of the entire system. The bolts were then prestressed to obtain high friction between the foundation support and lateral bracing elements. However, the bolts were accidentally loosened for specimen III-L1, and so friction was lost, permitting greater deformation of the specimen's lateral edges. This was detected by analyzing the measurements on the lateral bracing system, which for the sake of brevity are not plotted here.

The strengthening did not increase the load-carrying capacity of any of the specimens with openings to that of a solid wall. The axial strength of specimens with a small opening were between 85 and 94.8% of that of a solid wall (target I-C, Fig. 10), while the axial strength of specimens with a large opening were 56.5–63.4% of that of a solid wall (target I-C) and 88.9–99.8% of that of a wall with a small opening (target I-S, Fig. 10). The higher increase in capacity of specimens with a small opening can be attributed to the larger aspect ratios of the piers. Thus, both dilatation of concrete in compression and yield lines of the concrete in tension contribute to the increase in capacity.

#### Steel Reinforcement and FRP Strain Responses

It was believed that the strengthening method would affect local performance measures, such as demands on the steel reinforcement. Thus, before casting electrical resistance strain gauges with preattached lead wires were bonded to the reinforcement to monitor such demands. Selected strain values at certain loadings (50, 75, and 100% of the peak load) are compared with those obtained for the reference specimens in Figs. 11 and 12. Unfortunately, the connections between some of these wires and the strain gauges were damaged during the strengthening process (e.g., grinding of the concrete surface). These gauges are indicated with asterisks in the figures.

The comparison is plotted as bar charts in Fig. 11 for precracked, strengthened specimens and Fig. 12 for uncracked, strengthened specimens. Overall, FRP strengthening reduced strain on the steel reinforcement during the tests. It should be noted that Figs. 11 and 12 compare strains recorded at the same proportions of the

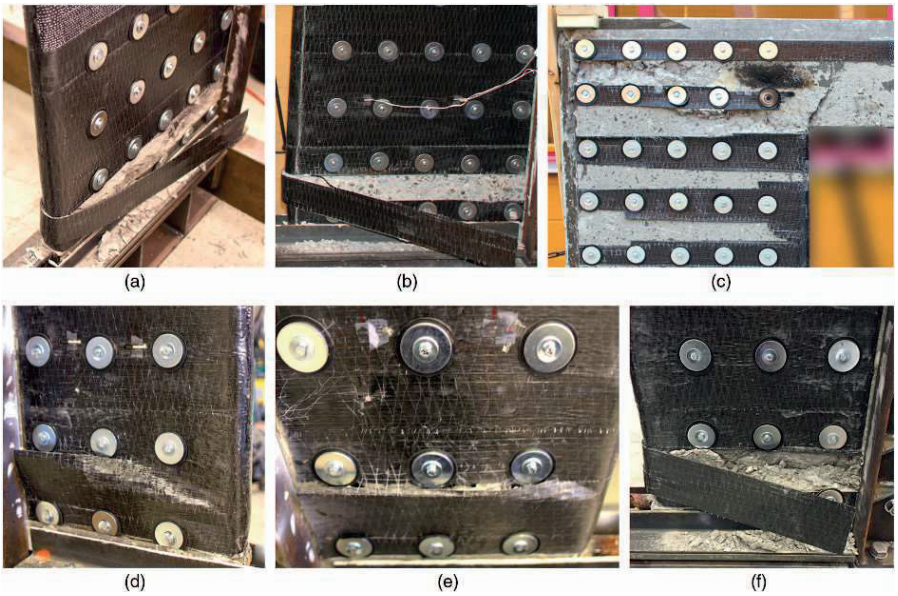


**Fig. 9.** (Color) Failure of the strengthened specimens: (a) II-S; (b) III-S1; (c) III-S2; (d) II-L; (e) III-L1; (f) III-L2

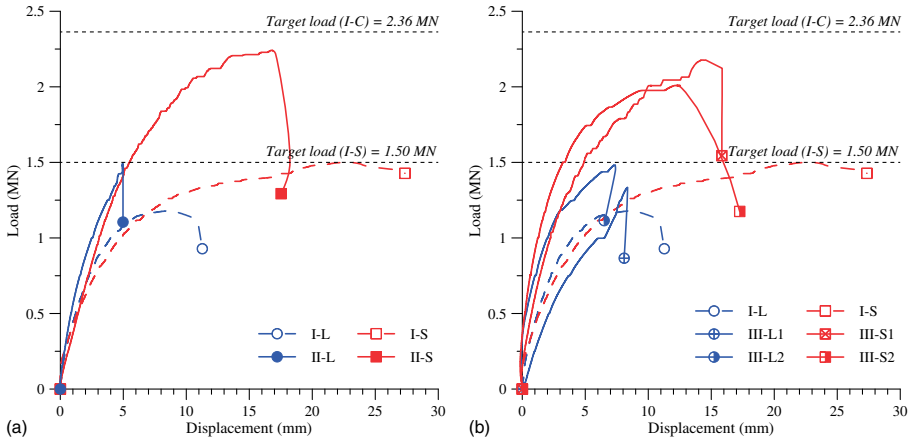


**Fig. 10.** (Color) Load-displacement curves for reference (stage I) specimens: (a) precracked strengthened (stage II) specimens; (b) uncracked strengthened specimens (stage III)

specimens' peak loads. Thus, as peak loads were higher for the strengthened specimens, the effectiveness of the strengthening in this respect was even greater than the figures visually indicate. Some of the strains recorded for reference specimens reached the yielding point at failure, with buckling of the reinforcement, specifically of horizontal bars G4 and G6, located in the pier of the wall with a small opening, and G3, located in the midspan—bottom bar of the spandrel for the wall with large opening. Above the 75% load level, the strains increased rapidly for all horizontal bars regardless of the opening size, while a more gradual increase was observed for the vertical bars. For strengthened elements, the demands on the steel reinforcement were somewhat lower during the specimen loading, and more evident as failure approached. The strains in these cases gradually increased, with no sudden jumps or either yielding or

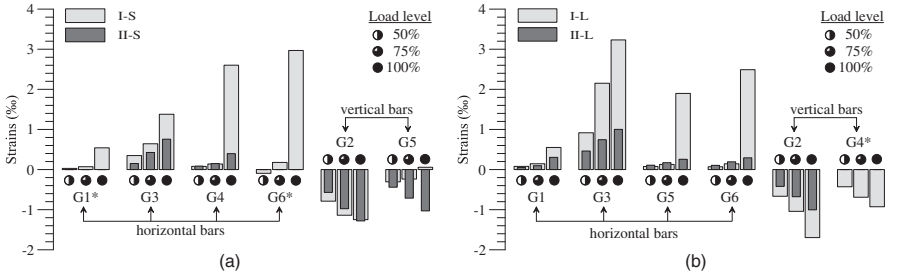


**Fig. 11.** Strain utilization of the steel reinforcement for reference specimens (stage I) and precracked strengthened specimens (stage II): (a) with a small opening (I/II-S); (b) with a large opening (I/II-L); *strains not recorded for strengthened specimens due to malfunction of the strain gauge

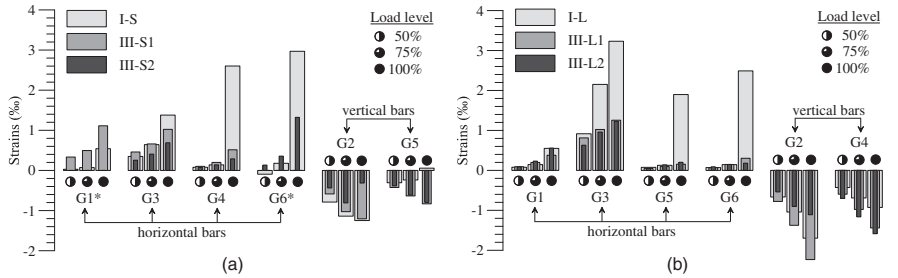


**Fig. 12.** Strain utilization of the steel reinforcement for reference specimens (stage I) and uncracked strengthened specimens (stage III): (a) with a small opening (I/III-S); (b) with a large opening (I/II-L); *strains not recorded for strengthened specimens due to malfunction of the strain gauge

buckling of the reinforcement. The amelioration provided by the FRP fibers is less evident for vertical bars because the fibers had been aligned only horizontally, thus providing relatively little vertical contribution. Strains were reduced (relative to those in corresponding unstrengthened specimens) particularly strongly in the horizontal bar above the opening, and most strongly in the specimens with large openings since the stresses on the reinforcement (and hence utilization of the composite material) increase with increases in the spandrel's span. No noticeable differences in these observations were detected between the precracked and uncracked specimens.

Strains in the FRP of strengthened specimens at peak load were also recorded, as listed in Table 2, where (for instance) F1-T and F1-C indicate strains recorded at position F1 in the wall's plane at the tension and compression sides of the element, respectively (Fig. 7). The *tension side* is defined as the specimens' surface where tensile cracks occur due to load eccentricity. In a hypothetical, eccentrically loaded, one-dimensional (1D) element, strain gauges located on the compression side would register different strains from those located on the tension side. In the design process, this effect of nonuniformity in strain efficiency was not considered, which may explain why lower-than-predicted ultimate loads were registered for the strengthened elements. On average, strains on the tension side were more than two times higher than the readings on the compression side for specimens with large openings, and more than six times higher for specimens with small openings. The strain gauge located at the midspan of the spandrel (F5) recorded the highest strains, peaking at about 1.89‰.

It should be noted that these values are measured strains, and not necessarily the highest in the specimens, since the strain paths may have differed from those expected. Moreover, single-point information is less valuable than full-field information. Therefore, the authors also examined full-field surface displacements and transformed them into surface strain fields. To reduce the computation time, areas around the anchorages (slightly larger than in reality to prevent their contours from complicating the analysis) were masked and ignored. Major strains in other areas of each specimen at the peak load were plotted [Figs. 13(a–h)] to gain insight into the full-strain field around the corner openings. Cracks were denser and more distinct in unstrengthened specimens [Figs. 13(a and e)], than in strengthened specimens, where they were more scattered. Furthermore, in all strengthened specimens, the major strains tended to form a diagonal path through the spandrel, indicating that the arching effect canceled by introducing the opening is reactivated through the addition of strengthening material. This effect is clearest for walls with large openings. For unstrengthened specimens, 3D-DIC also offers more detailed, and valuable, information on crack patterns than the one captured at failure shown in Fig. 2. This is partly because some cracks closed after failure, and partly because hairline cracks are difficult to observe with the naked eye, especially during specimen loading.

### Ductility Factors and Energy Dissipation at Failure

Displacement-based ductility factors (defined as the ratios between elastic and ultimate displacements recorded at D1, $\mu_\Delta = \delta_e/\delta_u$)

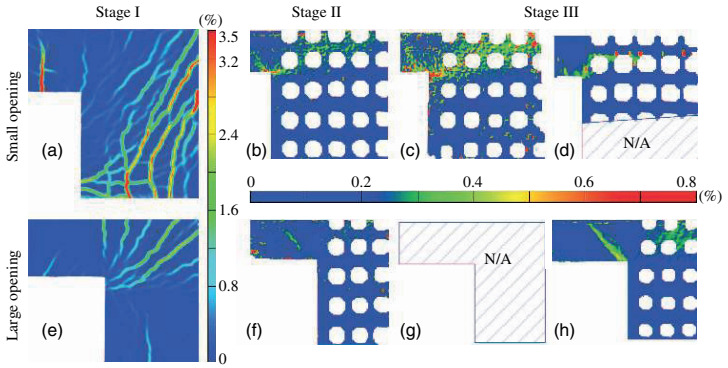


**Fig. 13.** (Color) Major strains detected by 3D-DIC analysis at peak loads of specimens: (a) I-S; (b) II-S; (c) III-S1; (d) III-S2; (e) I-L; (f) II-L (90% of peak load); (g) III-L1; (h) III-L2

were computed and are listed in Table 2. A simplified procedure proposed by Park (1988) was adopted to identify a distinct elastic displacement. The method assumes that the elastic displacement should be computed for an equivalent elastoplastic system with reduced stiffness (arguably the most realistic approach for RC structures). The reduced stiffness is found as the secant stiffness related to 75% of the peak load and the horizontal plateau corresponding to the peak load of the real system (Fig. 8). The maximum displacement corresponds to either the postpeak deformation when the load has decreased by 20% or the buckling of the reinforcement, whichever occurs first. In addition to ductility factors, energy dissipation ($E_d$) was evaluated as the area under the load-displacement curves.

Neither energy dissipation nor ductility factors were improved by the strengthening with FRP. In fact, in most cases, reductions were noted for the strengthened specimens in relation to the corresponding unstrengthened specimens. The introduction of the small and large openings in a solid wall resulted in similar, sharp reductions in the computed ductility factors and energy dissipation. Perhaps an alternative to avoid this drawback is to use textile-reinforced mortars (TRMs). Tetta et al. (2016) reported that TRM jackets were more effective than FRP jackets, considering the specimen's deformation capacity.

## Conclusion and Future Work

The main conclusions drawn from the reported tests on the effectiveness of FRP-confinement of walls with cutout openings can be briefly summarized as follows:

- Creating new openings in solid walls dramatically reduces their axial strength. The small and large openings in these tests resulted in 36 and 50% reductions, respectively. More tests are required, including walls with intermediate-size openings, to identify the optimal size thresholds and transition points between RC walls and RC frames in design codes for structural elements.
- The strengthening method increased the axial strength of specimens with small and large openings by 34–50% and 13–27% relative to that of the corresponding unstrengthened specimens. However, the FRP strengthening method did not fully restore the axial strength of a solid wall in any of the tests. The type of FRP sheet used to strengthen the specimens was unidirectional, but bidirectional fibers or vertical strips may have been more effective. Also, anchoring the FRP sheets to the wall foundation and adjacent elements (i.e., transverse walls or floors) may delay debonding, thereby increasing the axial strength. The optimal distances between steel anchorages, as well as the potential effects of the prestressing force of the bolts, should be investigated further.
- The strengthening did not avoid brittle failure (i.e., concrete crushing). However, it could avoid the buckling of the reinforcement and the explosive failure mode observed in unstrengthened specimens.
- Reductions in energy dissipation and ductility factors of strengthened specimens, relative to corresponding unstrengthened specimens, reduce the system's effectiveness.

The lateral restraints transformed the problem into a 3D rather than a 1D problem. It is, therefore, necessary to develop a design model that can better describe current stress states. In this study, the design of the FRP strengthening was based on a 1D element with no load eccentricity assumptions. However, it may be possible to develop disk theory (Nielsen 1999) to derive a theoretical model that provides better estimates of the capacities of FRP-strengthened walls with openings.

## Acknowledgments

The authors would like to acknowledge the Research Council of Norway (RFF), Development Fund of the Swedish Construction Industry (SBUF), and Skanska for financing the work in this project. Special thanks are due to the technicians of CompLab, the structural engineering laboratory at Luleå University of Technology (LTU). The authors would also like to express gratitude to others who provided help during this research program, including Dr. Dan Diaconu from Politehnica University Timisoara, for helping with the strengthening work; and Ph.D. students Cristian Sabau and Niklas Bagge (both from LTU), for providing help with optical measurements and fruitful discussions, respectively.

## Notation

*The following symbols are used in this paper:*

$A_c$ = cross-sectional area of concrete;

$A_e$ = effective confinement area;

$A_g$ = gross area of column section with rounded corners;
$b$ = width of a cross section;
$E_d$ = energy dissipation;
$e$ = test eccentricity;
$e_a$ = additional eccentricity;
$f_c$ = compressive strength of unconfined concrete;
$f_{cc}$ = compressive strength of confined concrete;
$f_{\text{frp}}$ = tensile strength of a FRP jacket;
$f_l$ = confining pressure;
$f_u$ = mean value of tensile strength of reinforcement;
$f_y$ = mean value of yield strength of reinforcement;
$G_F$ = fracture energy;
$H$ = height of the wall;
$H_{\text{eff}}$ = effective height of the wall;
$h$ = height of cross section;
$k_1$ = confinement effectiveness coefficient;
$k_{s1}$ = shape factor for strength enhancement;
$L$ = length of the wall;
$L_{\text{pier}}$ = length of the wall-pier;
$N_{\text{test}}$ = peak load;
$N_{I-C}$ = failure load of the solid wall;
$R$ = corner radius;
$t_{\text{frp}}$ = thickness of a FRP jacket;
$\beta$ = effective height factor which depends on the support conditions;
$\delta_e$ = elastic displacement;
$\delta_u$ = ultimate displacement;
$\varepsilon_u$ = mean value of tensile strain of reinforcement;
$\varepsilon_{u,\text{frp}}$ = strain in a FRP jacket;
$\varepsilon_y$ = mean value of yield strain of reinforcement;
$\mu_\Delta$ = ductility index;
$\rho_{sc}$ = cross-sectional area ratio of longitudinal steel; and
$\Phi$ = factor taking into account eccentricity, including second order effects and normal effects of creep.

## References


ACI (American Concrete Institute). (2001). "Control of cracking in concrete structures." *ACI 224 R*, Farmington Hills, MI.

ACI (American Concrete Institute). (2011). "Building code requirements for structural concrete and commentary." *ACI 318*, Farmington Hills, MI.

AS (Standards Australia). (2009). "Concrete structures." *AS 3600*, Sydney, Australia.

CEN (European Committee for Standardization). (2004). "Design of concrete structures. Part 1–1: General rules and rules for buildings." *EN1992-1-1*, Brussels, Belgium.

Delatte, N. (2009). *Failure, distress, and repair of concrete structures*, Woodhead Publishing, Cambridge, U.K.

De Luca, A., Nardone, F., Lignola, G., Prota, A., and Nanni, A. (2013). "Wall-like reinforced concrete columns externally confined by means of glass FRP laminates." *Adv. Struct. Eng.*, 16(4), 593–604.

Demeter, I. (2011). "Seismic retrofit of precast RC walls by externally bonded CFRP composites." Ph.D. thesis, Politehnica Univ. of Timisoara, Timisoara, Romania.

Doh, J. H., and Fragomeni, S. (2006). "Ultimate load formula for reinforced concrete wall panels with openings." *Adv. Struct. Eng.*, 9(1), 103–115.

Engel, P. (2016). "General rehabilitation techniques using steel." ⟨http://www.constructalia.com/english/renovation_with_steel/ii_general_rehabilitation_techniques_using_steel#.VMPsNP6G9Wg⟩ (May 5, 2016).

Floruţ, S.-C., Sas, G., Popescu, C., and Stoian, V. (2014). "Tests on reinforced concrete slabs with cut-out openings strengthened with fibre-reinforced polymers." *Compos. Part B: Eng.*, 66, 484–493.

GOM mbH. (2016). "ARAMIS—Optical 3D deformation analysis." ⟨http://www.gom.com/metrology-systems/system-overview/aramis.html⟩ (May 5, 2016).

Guan, H., Cooper, C., and Lee, D.-J. (2010). "Ultimate strength analysis of normal and high-strength concrete wall panels with varying opening configurations." *Eng. Struct.*, 32(5), 1341–1355.

Harajli, M. H., and Hantouche, E. G. (2015). "Effect of active versus passive confinement on seismic response of wide RC columns with lap splices." *J. Struct. Eng.*, 10.1061/(ASCE)ST.1943-541X.0001196, 04014221.

Lam, L., and Teng, J. G. (2003). "Design-oriented stress-strain model for FRP-confined concrete in rectangular columns." *J. Reinf. Plast. Compos.*, 22(13), 1149–1186.

Li, B., Kai, Q., and Tran, C. T. N. (2013). "Retrofitting earthquake-damaged RC structural walls with openings by externally bonded FRP strips and sheets." *J. Compos. Constr.*, 10.1061/(ASCE)CC.1943-5614.0000336, 259–270.

Liu, H.-X., Liu, G.-J., Wang, X.-Z., and Kong, X.-Q. (2015). "Effect of cross-sectional aspect ratio and basalt fiber-reinforced polymer-confined number on axial compression behavior of short columns." *J. Reinf. Plast. Compos.*, 34(10), 782–794.

Mahal, M., Blanksvärd, T., Täljsten, B., and Sas, G. (2015). "Using digital image correlation to evaluate fatigue behavior of strengthened reinforced concrete beams." *Eng. Struct.*, 105, 277–288.

Mirmiran, A., Shahawy, M., Samaan, M., Echary, H., Mastrapa, J., and Pico, O. (1998). "Effect of column parameters on FRP-confined concrete." *J. Compos. Constr.*, 10.1061/(ASCE)1090-0268(1998)2:4(175), 175–185.

Mohammed, B., Ean, L. W., and Malek, M. A. (2013). "One-way RC wall panels with openings strengthened with CFRP." *Constr. Build. Mater.*, 40, 575–583.

Mosallam, A. S., and Nasr, A. (2016). "Structural performance of RC shear walls with post-construction openings strengthened with FRP composite laminates." *Compos. Part B: Eng.*, in press.

Mukherjee, A., Boothby, T., Bakis, C., Joshi, M., and Maitra, S. (2004). "Mechanical behavior of fiber-reinforced polymer-wrapped concrete columns—Complicating effects." *J. Compos. Constr.*, 10.1061/(ASCE)1090-0268(2004)8:2(97), 97–103.

Nielsen, M. P. (1999). *Limit analysis and concrete plasticity*, 2nd Ed., CRC Press, Boca Raton, FL.

Park, R. (1988). "State of the art report: Ductility evaluation from laboratory and analytical testing." *Proc., 9th World Conf. on Earthquake Engineering*, Vol. 8, International Association for Earthquake Engineering, Tokyo, 605–616.

Pessiki, S., Harries, K., Kestner, J., Sause, R., and Ricles, J. (2001). "Axial behavior of reinforced concrete columns confined with FRP jackets." *J. Compos. Constr.*, 10.1061/(ASCE)1090-0268(2001)5:4(237), 237–245.

Popescu, C., Sas, G., Blanksvärd, T., and Täljsten, B. (2015). "Concrete walls weakened by openings as compression members: A review." *Eng. Struct.*, 89, 172–190.

Popescu, C., Sas, G., Sabău, C., and Blanksvärd, T. (2016). "Effect of cut-out openings on the axial strength of concrete walls." *J. Struct. Eng.*, 10.1061/(ASCE)ST.1943-541X.0001558, 04016100.

Prota, A., Manfredi, G., and Cosenza, E. (2006). "Ultimate behavior of axially loaded RC wall-like columns confined with GFRP." *Compos. Part B Eng.*, 37(7–8), 670–678.

RILEM TC 50-FMC. (1985). "Determination of the fracture energy of mortar and concrete by means of three-point bend tests on notched beams." *Mater. Struct.*, 18(4), 287–290.

Rocca, S., Galati, N., and Nanni, A. (2008). "Review of design guidelines for FRP confinement of reinforced concrete columns of noncircular cross sections." *J. Compos. Constr.*, 10.1061/(ASCE)1090-0268(2008)12:1(80), 80–92.

Saheb, M., and Desayi, P. (1990). "Ultimate strength of RC wall panels with openings." *J. Struct. Eng.*, 10.1061/(ASCE)0733-9445(1990)116:6(1565), 1565–1577.

Sas, G., Blanksvärd, T., Enochsson, O., Täljsten, B., and Elfgren, L. (2012). "Photographic strain monitoring during full-scale failure testing of Örnsköldsvik bridge." *Struct. Health Monit.*, 11(4), 489–498.

SIS (Swedish Standards Institute). (2005). "Mechanical properties of fasteners made of carbon steel and alloy steel. Part 1: Bolts, screws and studs with specified property classes—Coarse thread and fine pitch thread." *SS-EN ISO 898-1*, Stockholm, Sweden.

SIS (Swedish Standards Institute). (2009a). "Metallic materials—Tensile testing. Part 1: Method of test at room temperature." *SS-EN ISO 6892-1:2009*, Stockholm, Sweden.

SIS (Swedish Standards Institute). (2009b). "Testing hardened concrete. Part 3: Compressive strength of test specimens." *SS-EN 12390-3:2009*, Stockholm, Sweden.

SIS (Swedish Standards Institute). (2011). "Hexagon head bolts—Product grades A and B." *SS-EN ISO 4014*, Stockholm, Sweden.

Smith, B., Kurama, Y., and McGinnis, M. (2011). "Design and measured behavior of a hybrid precast concrete wall specimen for seismic regions." *J. Struct. Eng.*, 10.1061/(ASCE)ST.1943-541X.0000327, 1052–1062.

Täljsten, B. (2000). "Strengthening of existing concrete structures with carbon fibre fabrics or laminates: Design, material, and execution." *Technical Rep. No. 2000:16*, Luleå Univ. of Technology, Luleå, Sweden.

Tan, K. H. (2002). "Strength enhancement of rectangular reinforced concrete columns using fiber-reinforced polymer." *J. Compos. Constr.*, 10.1061/(ASCE)1090-0268(2002)6:3(175), 175–183.

Tanwongsval, S., Maalej, M., and Paramasivam, P. (2003). "Strengthening of RC wall-like columns with FRP under sustained loading." *Mater. Struct.*, 36(5), 282–290.

Tetta, Z. C., Koutas, L. N., and Bournas, D. A. (2016). "Shear strengthening of full-scale RC T-beams using textile-reinforced mortar and textile-based anchors." *Compos. Part B Eng.*, 95, 225–239.

Todut, C., Dan, D., and Stoian, V. (2014). "Theoretical and experimental study on precast reinforced concrete wall panels subjected to shear force." *Eng. Struct.*, 80, 323–338.

Todut, C., Dan, D., and Stoian, V. (2015). "Numerical and experimental investigation on seismically damaged reinforced concrete wall panels retrofitted with FRP composites." *Compos. Struct.*, 119, 648–665.

Triantafillou, T. C., Choutopoulou, E., Fotaki, E., Skorda, M., Stathopoulou, M., and Karlos, K. (2016). "FRP confinement of wall-like reinforced concrete columns." *Mater. Struct.*, 49(1), 651–664.

Wu, Y.-F., and Wei, Y.-Y. (2010). "Effect of cross-sectional aspect ratio on the strength of CFRP-confined rectangular concrete columns." *Eng. Struct.*, 32(1), 32–45.

Wu, Y.-F., Yun, Y., Wei, Y., and Zhou, Y. (2014). "Effect of predamage on the stress-strain relationship of confined concrete under monotonic loading." *J. Struct. Eng.*, 10.1061/(ASCE)ST.1943-541X.0001015, 04014093.

# Paper IV

## Tests on reinforced concrete slabs with cut-out openings strengthened with fibre-reinforced polymers

Sorin-Codruţ Floruţ; Gabriel Sas; Cosmin Popescu; and Valeriu Stoian

Published in:
*Composites Part B: Engineering*
Vol. 66, 2014
pp. 484-493

Composites: Part B 66 (2014) 484–493

Contents lists available at ScienceDirect

Composites: Part B

journal homepage: www.elsevier.com/locate/compositesb

# Tests on reinforced concrete slabs with cut-out openings strengthened with fibre-reinforced polymers

Sorin-Codruţ Floruţ [a,*], Gabriel Sas [b], Cosmin Popescu [c], Valeriu Stoian [a]

[a] Politehnica University of Timisoara, 2nd T. Lalescu, 300223 Timisoara, Romania
[b] NORUT, Rombaksveien E-6 47, N-8517 Narvik, Norway
[c] Luleå University of Technology, SE-97187, Sweden

ARTICLE INFO

*Article history:*
Received 2 April 2014
Received in revised form 5 June 2014
Accepted 16 June 2014
Available online 22 June 2014

*Keywords:*
A. Carbon fibre
C. Damage mechanics
D. Mechanical testing
Near-surface mounted reinforcement

ABSTRACT

This paper presents the results of experimental investigations on reinforced concrete slabs strengthened using fibre-reinforced polymers (FRP). Eight tests were carried out on four two-way slabs, with and without cut-out openings. Investigations on slabs with cut-outs revealed that the FRP can be placed only around the edges of the cut-out when retrofitting the slabs whereas, in the situation of inserting cut-outs combined with increased demands of capacity, it is necessary to apply FRP components on most of the soffit of the slab. The proposed strengthening system enabled the load and deflection capacities of the FRP-strengthened slabs, in relation to their un-strengthened reference slabs, to be enhanced by up to 121% and 57% for slabs with and without cut-outs respectively.


## 1. Introduction

The load carrying capacity of reinforced concrete (RC) slabs may be compromised for a number of reasons, including design errors, building code changes, structural damage and changes of functional use by creating new openings.

The experimental research presented in this paper deals with the structural rehabilitation of RC two-way slabs, with and without cut-out openings. One method that can be used to increase their load capacity is to apply fibre-reinforced polymers (FRP) as externally bonded (EB) or near surface mounted (NSM) reinforcement. Several guidelines for designing and applying FRPs as strengthening systems for RC structures have been published [1,2]. However, how to use FRPs to strengthen structural elements with cut-out openings is only addressed to a small extent in these guidelines due to a lack of experimental and theoretical investigations on the variations in geometry, materials and loading conditions.

Many researchers [3–10] tested the feasibility of restoring or improving the load capacity of solid slabs by means of EB FRPs. Despite the efficiency of the method, the majority of the retrofitted elements experienced debonding as a failure mode. To solve this challenge, several researchers [11–13] successfully tested different anchorage systems for FRPs applied as EB reinforcement on slabs. Furthermore, plane elements (i.e. RC walls) could also be strengthened using mechanical anchored FRPs thus being efficient in preventing debonding [14]. The NSM technique, which is relatively new compared to EB, has been proven to produce better anchoring behaviour than EB [15]. This technique introduced a new debonding mode, the slip of the reinforcement in the concrete groove. However, this failure mode is preferred to the sudden debonding of EB strips [16].

In the literature, there are several studies of slabs with cut-out openings strengthened with FRP materials [17–25]. Casadei et al. [17] tested one-way slabs with both centrally located openings and openings near the supports, strengthened by carbon FRP (CFRP) laminates. This method has been proved to be effective only for the case with openings in the sagging region. The presence of the openings in the hogging region increased the shear stress in the concrete slab, leading to premature failure [17].

Lower tensile forces in the steel reinforcement accompanied by a more favourable crack distribution were important improvements when using FRP strips for strengthening one-way slabs with a rectangular cut-out in the centre of each slab [18]. Although the method produced an ultimate bearing capacity similar to the one recorded for the control element, the elements failed due to debonding.

In another series of tests, Tan and Zhao [19] found that all the strengthened slabs with symmetric and asymmetric openings that they investigated exhibited the same load capacity as un-strengthened slabs with openings, with some cases being even higher.

* Corresponding author. Tel.: +40 256403942.
*E-mail addresses:* codrut.florut@upt.ro (S.-C. Floruţ), gabriel.sas@norut.no (G. Sas), cosmin.popescu@ltu.se (C. Popescu), valeriu.stoian@upt.ro (V. Stoian).

http://dx.doi.org/10.1016/j.compositesb.2014.06.008
1359-8368/

Flexural failure mode was associated with small-sized openings whereas a new failure pattern with non-orthogonal yield lines initiating from the corners of the cut-out was reported for large-sized openings. The same researchers also proved that CFRP sheets are more effective compared with CFRP plates because of the premature debonding of the latter. In relation to the position of the opening, it was found that specimens with openings placed in the maximum moment zone failed in flexural mode while openings located in the shear zone failed in shear mode [20].

The location of load application and the type of the loading surface was believed to play an important role in determining the failure behaviour [21]. Using a line load configuration induces stress concentrations which can have a negative influence on the location where debonding starts [21].

According to [22], the NSM CFRP strips performed better than the EB CFRP plates when used for strengthening slabs with centred openings due to the greater resistance to debonding. When EB CFRP plates were used together with FRP anchors, the flexural capacity of the slab was fully restored.

Compared to one-way slabs, less research has been carried out on FRP-strengthened two-way RC slabs with cut-out openings. Casadei et al. [23] claimed to be the first to report tests on RC slabs with openings and strengthened with CFRP laminates around the cut-out. The anchorage system prevented the premature debonding of the laminates which yielded into full utilisation of the FRPs. Enochsson et al. [24] tested two-way slabs strengthened with FRP composite materials. The tests revealed that specimens with larger openings have a higher load capacity and stiffness than the ones with smaller openings. Although this contradicted their design method, Enochsson et al. [24] have justified this as "the slabs with the large openings behave closer to a system of four beams than a slab".

Elsayed et al. [25] proved the benefits of using mechanically-fastened EB FRPs over the conventionally applied EB FRPs. The latter provided a lower performance in serviceability compared with the mechanically-fastened technique.

De Lorenzis and Teng [26] concluded that the NSM technique is less prone to debonding, can be pre-stressed more easily and is better protected against fire, chemical and mechanical damage. However, in some cases, it could be more beneficial to use both NSM and EB techniques especially when the concrete cover is limited.

In most of the above mentioned research programs, the cut-outs were created in the centre of the tested slabs and the applied strengthening techniques were either EB or NSM types. In this research, mixed retrofitting solutions (NSM + EB) are tested on two-way RC slabs with cut-out openings located on the sides of the element.

The first objective of the research program was to verify how the cut-out openings influence the loading behaviour of the slabs. This study also provides relevant information about the influence of the surface and position of the openings on un-strengthened slabs loaded with distributed loads on small areas.

The second objective was to investigate whether the FRP strengthening solutions can restore and increase the load capacity of slabs with cut-outs in comparison to that of the full slab and their corresponding unstrengthened slabs with openings, respectively.

## 2. Experimental tests

### 2.1. The test specimens

Four RC two-way concrete slabs were cast. The specimens were designed with a ratio between the clear length and clear width of about 1.55 (see Fig. 1) with dimensions of 2650 × 3950 × 120 mm. The clear span-to-thickness ratio was 20 for the short edge of the slabs. The elements replicate two-way single span simply-supported slabs, designed according to EN1992-1-1 [27]. The top of the slab was reinforced along its contour for constructional reasons only. Reinforcement at the bottom consisted of welded wire meshes made of bars with a diameter of 4 mm, arranged at a spacing of 100 mm in both directions parallel to the edges of the elements. The concrete cover provided for the outermost steel reinforcement bars (i.e. rebar placed parallel to the short edge of the slabs) had a thickness of 15 mm. The steel reinforcement ratios, based on the effective depth on the short and long edges, were 0.117% and 0.127%, respectively. The steel reinforcement ratio, based on total thickness, was 0.105%. Elements with openings were detailed in such a way as to replicate cut-outs sawn into a full element i.e. no additional reinforcement was placed around the edges of the openings.

The first specimen, denoted FS-01, was a full slab and served as the reference. The second slab, RSC-01, had a small opening. Two identical specimens with large openings were cast, designated RLC-01 and RLC-02. Details of their geometries are shown in Figs. 2 and 3.

### 2.2. Material properties

The average cubic compressive strength of concrete ($f_{cm}$) was determined based on 12 cube tests [28] at the time of testing of each slab. Three cubes were tested for each slab. All tests were carried out after 28 days. Tensile tests of the steel reinforcement were carried out on 20 samples based on specifications described in [29]. Five samples were tested for each cast slab, 4 batches in total. The properties determined were the yield stress ($f_{yk}$), tensile strength ($f_t$) and ultimate strain ($\varepsilon_{uk}$). Commercial CFRP products were used for strengthening the slabs. These products consisted of high strength NSM strips, plates and sheets. All the mechanical properties of these materials are shown in Table 1.

### 2.3. Design and detailing of the CFRP strengthening

The CFRP components were bonded to the soffit of the slabs in two directions. The CFRP components parallel to the short edge of the specimens were installed using the NSM technique and those on the direction parallel to the long edge of the slabs were installed using the EB technique.

The required amount of CFRP was determined using the following procedure. For specimen FS-01-FRP (the full slab), the capable tensile force of steel reinforcement was matched to that of the CFRP components to be installed. The strengthening for specimen RLC-02-FRP was similarly designed, with the only difference being that the NSM bars intercepted by the cut-out opening were placed in the immediate vicinity of the opening. This design procedure aimed to cover the scenario when a slab is damaged and strengthened to give a higher load capacity. For slabs RSC-01-FRP and RLC-01-FRP, the FRP system was designed so that its tensile capacity equalled that of the steel reinforcement that was removed when the slabs were sawn. This second procedure aimed to test whether the capacity of the slab can be restored to its un-strengthened, undamaged state using FRP. See Fig. 2 for the details and geometrical properties of the applied strengthening.

Strengthened reference specimens have had the suffix FRP added to their nomenclature. For example, RSC-01-FRP refers to a reinforced concrete slab with a Rectangular Small Cut-out which has been strengthened.

### 2.4. Test setup, loading protocol and instrumentation

It was planned to load each slab beyond the point where the tensile reinforcement yielded, then unload, apply the FRP

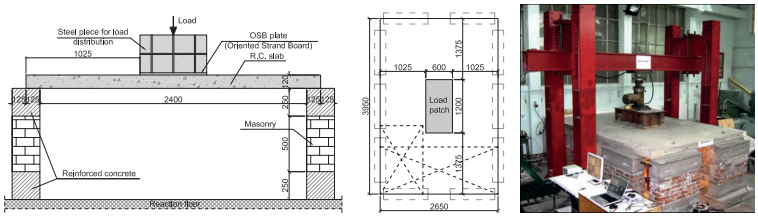


**Fig. 1.** Test setup, top view of the test setup with dimensions of the slab and general overview of the test setup.

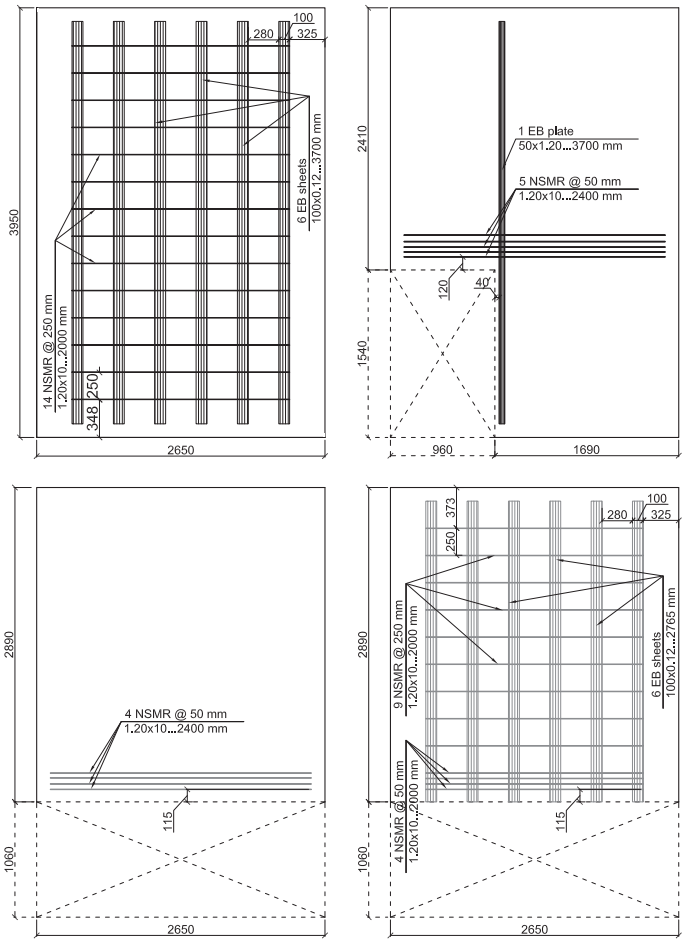


**Fig. 2.** Detailing of the CFRP strengthening systems applied.

strengthening and test again until collapse. In total, this testing regime yielded eight tests performed on four slabs.

The test setup consisted of a 1 m high discontinuous peripheral wall made out of brick masonry and reinforced concrete beams, a rigid loading frame and a hydraulic jack. The load was distributed over a central patch of 600 × 1200 mm through a spatial steel assembly, and was applied in controlled increments of 5 kN. A vertical cross-section through the test setup is shown in Fig. 1. The

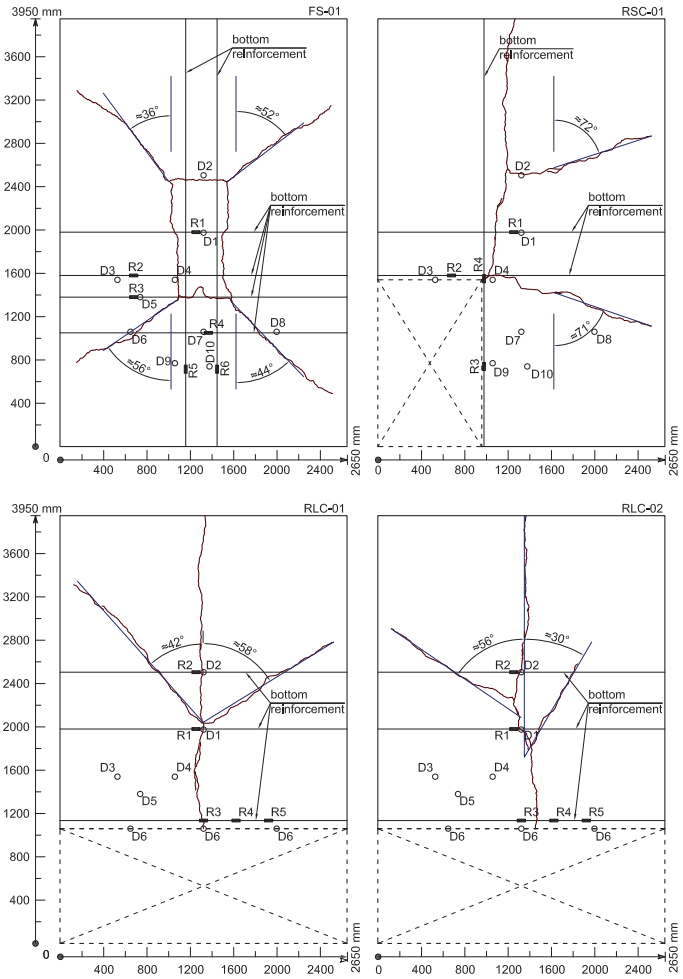


**Fig. 3.** The positioning of the displacement transducers ($D$) and strain gauges installed on the reinforcement ($R$) and the cracking pattern resulting after loading the reference specimens.

**Table 1**
Mechanical properties of the materials.

| | Concrete | | Reinforcement | | NSM | | Plates | | Sheets | |
|---|---|---|---|---|---|---|---|---|---|---|
| Element | $f_{cm}$ (MPa) | $f_{yk}$ (MPa) | $f_t$ (MPa) | $\varepsilon_{uk}$ (%) | $E_{FRP}$ (GPa) | $\varepsilon_{FRP}$ (%) | $E_{FRP}$ (GPa) | $\varepsilon_{FRP}$ (%) | $E_{FRP}$ (GPa) | $\varepsilon_{FRP}$ (%) |
| FS-01(-FRP) | 65 | 596.7 | 665.7 | 2.7 | 165 | 1.7 | – | – | 231 | 1.7 |
| RSC-01(-FRP) | 62 | 537.2 | 616.8 | 2.4 | 165 | 1.7 | 165 | 1.7 | – | – |
| RLC-01(-FRP) | 66 | 546.1 | 624.8 | 3.4 | 165 | 1.7 | – | – | – | – |
| RLC-02(-FRP) | 62 | 548.3 | 616.8 | 3.1 | 165 | 1.7 | – | – | 231 | 1.7 |

position of the load patch (i.e. the centre of the full slab) was maintained throughout all 8 tests, regardless of the geometry of slabs with cut-outs; even if asymmetrical, it provided an un-favourable type of loading for all specimens. All slabs were pre-cracked and the loading was stopped to avoid total collapse when the maximum recorded vertical deflection reached the allowable deflection (i.e. $L/250 = 9.6$ mm) according to EN1992-1-1 [27].

The slabs were laid on a layer of fresh mortar, which permitted horizontal settling under their own weight. The supporting area had a width of 125 mm. This type of support prevented

gravitational displacements but allowed the uplift of the corners and edges of the slabs. Ten displacement transducers were installed to measure the deflection of the slabs, as shown in Fig. 3. The location of the transducers was fixed for all 8 tests. However, between tests, some were removed as they would be located inside the area of a cut-out opening. For each specimen, 4–6 strain gauges were installed on the bottom steel reinforcement, located as shown in Fig. 3. Strain gauges were also installed on the FRPs to monitor the strain at debonding; their positions are highlighted in Fig. 4. The locations of the displacement transducers are similar to the ones used for the reference tests. Due to space limitations, only some selected deflections and strain measurements are presented here, thus for further details, see [30].

## 3. Results and discussions

### 3.1. Tests on reference slabs

The results of the tests are shown in Table 2. Fig. 5 shows graphs of the load displacement response recorded for all tests. The full slab (FS-01) developed the highest load capacity while the slabs with the largest openings (RLC-01 & 02) had the lowest capacity. The crack pattern of the full slab (FS-01) developed along the yield lines and under the loading area (Fig. 3). The cracks under the loading area indicate punching failure of the slab under the loading surface, see Fig. 6. The crack pattern of the slab with small-sized opening (RSC-01) initiated at the re-entrant corner of the cut-out

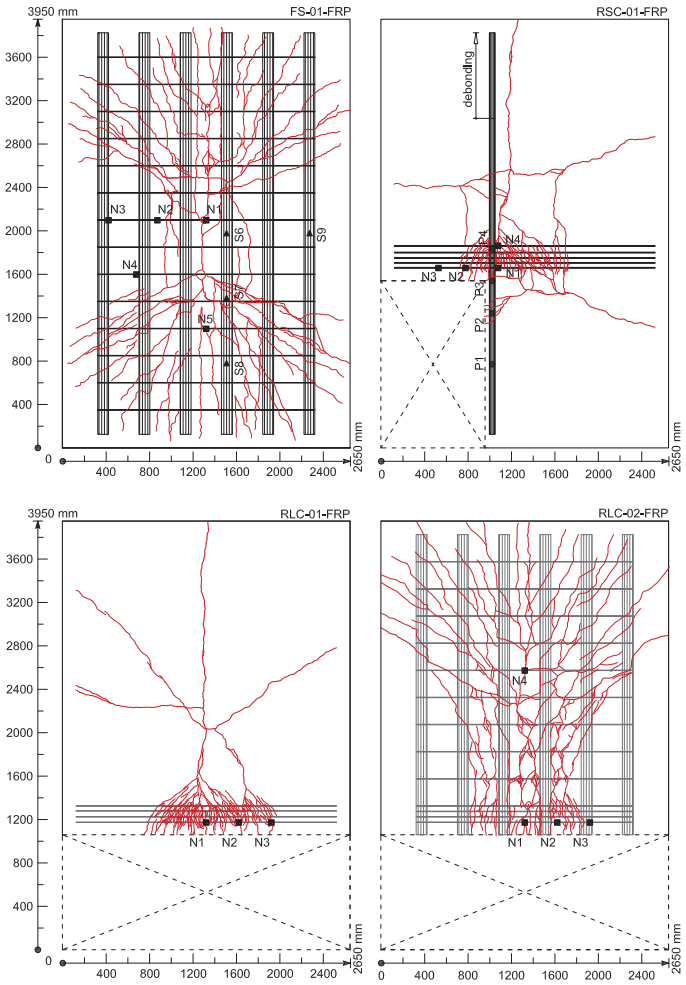


**Fig. 4.** The positioning of the strain gauges installed on the FRP (*N* = NSM, *P* = plates and *S* = sheets) and the cracking pattern resulting after loading the strengthened specimens.

and developed in a direction quasi-parallel to the long edge of the specimen (Fig. 3).

The slabs with large openings, RLC-01 & 02, had identical geometries; however, the ultimate capacity was different. A 10% higher capacity in the favour of the former was recorded. The origin of this difference was identified after testing. Due to a test procedure error with slab RLC-02, the outermost steel reinforcement was placed along its length, while for all other slabs, the outermost steel reinforcement was placed along their short side. This misplacement decreased the internal lever arm of the structural reinforcement, thus reducing its capacity. By creating the two types of cut-outs in the three slabs, the slabs' area decreased to 86.71% (by creating the small cut-out) and to 74.74% (by creating large cut-outs) of the total area of the full slab. Both the size and location of the cut-out opening influenced the load capacity. Although the area of RLC-01 is 10% smaller than RSC-01, the ultimate loads are relatively similar. The elastic limit was reached when at least one strain gauge indicated a value of the strain ($\varepsilon_y$) presented in Table 2. No tension stiffening effect was accounted for in the evaluation of these strains.

### 3.2. Tests on strengthened/retrofitted specimens

All strengthened slabs were tested to failure after the epoxy resin had cured for at least seven days. Fig. 5 shows the load displacement responses of all four strengthened slabs with dashed lines; the results are shown in Table 2. The strains measured in the FRP sheets and NSM bars are not given because the primary failure mode of the strengthening was rupture of the FRPs. The authors consider that plots of these values do not provide any useful information. However, the strains recorded on FRP plate are reported in Fig. 7. The slab FS-01-FRP showed extensive deformation capacity and increased strength compared to the reference specimen. The capacity increased up to 57% compared to the reference specimen. Numerous new small cracks appeared during testing due to better stress redistribution enabled by the FRP (see Fig. 4). It is interesting to note that, after strengthening, two new major cracks had formed, starting from cracks opened during the test on the un-strengthened slab. Failure occurred through rupturing of the FRPs intercepted by the major cracks.

The FRP strengthening system applied on the slab with a small opening (RSC-01-FRP) restored the load capacity to its initial value. A mixed failure mode was recorded for this specimen. First, the EB plate failed due to debonding at the far end of the slab (Fig. 8), then the NSM bars failed due to rupturing near to the corner of the cut-out opening. In the area where CFRP were installed, the crack concentration increased compared to the un-strengthened slab. The main cracks, which caused the slab's failure, are identical to those opened as a result of the test on the un-strengthened slab.

The test on the retrofitted slab with a large opening (RLC-01-FRP) exhibited virtually identical strength and deformation capacity as the un-strengthened reference specimen. All NSM FRP strips failed due to fibre rupture in their central area, corresponding to the location of the major crack. The failure was brittle, ending in a total collapse of the slab, see Fig. 9. In the area where NSM were mounted, the crack density was greater than that of the un-strengthened slab (see Fig. 4). New main cracks opened as a result of the test on the un-strengthened slab.

The second slab with a large opening strengthened with FRP (RLC-02-FRP) failed when all the CFRP strengthening components experienced fibre rupture. The FRP enabled stress redistribution over the entire soffit of the slab; hence, numerous small cracks similar to the slab FS-01-FRP developed. Slab RLC-02-FRP developed the highest ultimate capacity relative to its effective area (22.14 kN/m$^2$), higher even than the full specimen FS-01-FRP (20.95 kN/m$^2$). This behaviour is in accordance with the results reported by Enochsson et al. [24].

### 3.3. Test predictions by yield line theory

#### 3.3.1. The yield line theory

The yield line theory was presented by Ingerslev [31] and further developed by Johansen [32] and Wood and Jones [33]. This method predicts the load at which the flexural capacity of slabs is reached using the rigid plastic theory in accordance to the upper bound theorem. The procedure employs the use of predefined crack patterns (yield lines) [33]. Different layout patterns of the yield lines can be assumed resulting in several upper bound solutions. For design purposed the minor value is chosen. The failure load can be calculated using two different techniques: (1) the virtual-work method and (2) the equilibrium method. The virtual-work method assumes that at collapse the work done due to a virtual imposed displacement is equal to the internal work dissipated along the yield lines [33]. As an alternative, the equilibrium method differs from the work method "in that the equilibrium of each of the rigid regions is considered" [33]. The two techniques yield the same results; therefore here the capacity of the slabs was computed using the virtual work method only (Eq. (1)).

$$\sum \left[ \iint q\delta dxdy \right]_{\text{each region}} = \sum \left[ \theta_n \int m_b ds \right]_{\text{each yield line}} \tag{1}$$

The left-hand side of Eq. (1) represents the external work, with $q$ denoting the load on unit area and $\delta$ the virtual displacement, while the right-hand side represent the internal work with $\theta_n$ denoting the normal rotation of the yield line and $m_b$ the capable moment along the yield line.

The ultimate bending moment along the yield line can be found considering the equilibrium condition shown in Fig. 10:

$$m_b L = (m_x \cdot L \sin\alpha)\sin\alpha + (m_y \cdot L\cos\alpha)\cos\alpha \tag{2}$$

$$m_b = m_x \sin^2\alpha + m_y \cos^2\alpha \tag{3}$$

**Table 2**
Test results.

| Element | Load (kN) | Cracking load (kN) | $S$ (%) | $R$ (%) | $F$ (kN/m$^2$) | MD (mm) | $\varepsilon_y$ (%) | FY (kN) |
|---|---|---|---|---|---|---|---|---|
| FS-01 | 118 | NA | 100 | 100 | 13.4 | 10.3 (D1) | 0.269 | 46.75 (R1) |
| RSC-01 | 87 | 65 | 87 | 73 | 11.3 | 11.4 (D4) | 0.273 | NA |
| RLC-01 | 75 | 60 | 75 | 63 | 11.3 | 9.6 (D7) | 0.274 | 61.75 (R3) |
| RLC-02 | 67 | 55 | 75 | 57 | 10.1 | 9 (D7) | 0.298 | 61.5 (R1) |
| FS-01-FRP | 186 | – | 100 | 100 | 20.9 | 45 (D1) | – | – |
| RSC-01-FRP | 86 | – | 87 | 46 | 11.1 | 33 (D1, D2, D4) | – | – |
| RLC-01-FRP | 75 | – | 75 | 40 | 11.2 | 8.5 (D7) | – | – |
| RLC-02-FRP | 147 | – | 75 | 79 | 22.2 | 63.2 (D1) | – | – |

$S$ = ratio, expressed in%, between the surface of one specimen with an opening and that of the full slab. $R$ = ratio, expressed in%, between the load of one specimen with an opening and that of the full slab. $F$ = normalised load at the surface of one specimen. $D$ = displacement at maximum load. MD = maximum displacement at maximum load, with the transducers that recorded the values given in parentheses. FY = First yielding load with the gauges that recorded the values given in parentheses.

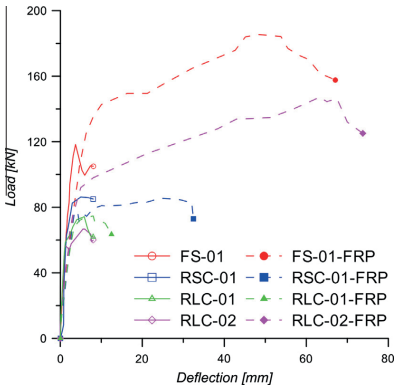


**Fig. 5.** Load displacement diagrams for all tested slabs.

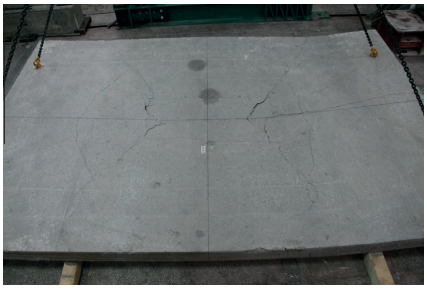

**Fig. 6.** Failure of the specimen FS-01.

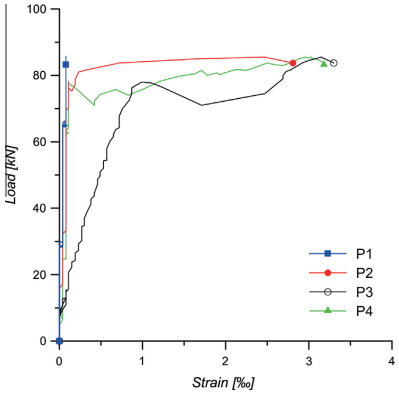


**Fig. 7.** Strains on FRP plate for specimen RSC-01-FRP.

where $m_x$, $m_y$ are the moment capacities per unit width in the $x$- and $y$-directions, respectively, calculated according to [27]:

$$m_{x,y} = A_{sx,sy} \cdot f_{yk} \cdot 0.9d \tag{4}$$

where $A_{sx}$, $A_{sy}$ are the areas of the reinforcement per unit width and $d$ is the effective depth.

**Fig. 8.** Detail of the debonding failure taken after the end of the test on specimen RSC-01-FRP.

**Fig. 9.** Total collapse of the specimen RLC-01-FRP after testing.

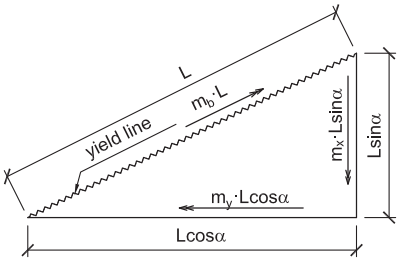


**Fig. 10.** Evaluation of the bending moment along the yield line.

If the slab is isotropically reinforced (i.e. $m_x = m_y$), Eq. (3) reduces to $m_b = m_x = m_y$. In the present study, due to differences in effective depths along the two axes, the $m_x$ and $m_y$ moments are slightly different. For simplicity these differences were disregard in these calculations.

The angle between axis of rotation of each region and yield line determines the slope of the yield line. For a full slab these yield lines intersects the corners at 45°. Due to symmetry along the longitudinal axis, the same assumptions can be made for the slab with large cut outs. It was shown by Kennedy and Goodchild [34] that assuming 45° will produce only a 3% error compared with theoretically determined angle.

For slabs with asymmetric openings, different yield line patterns can be assumed, depending on the opening size and position,

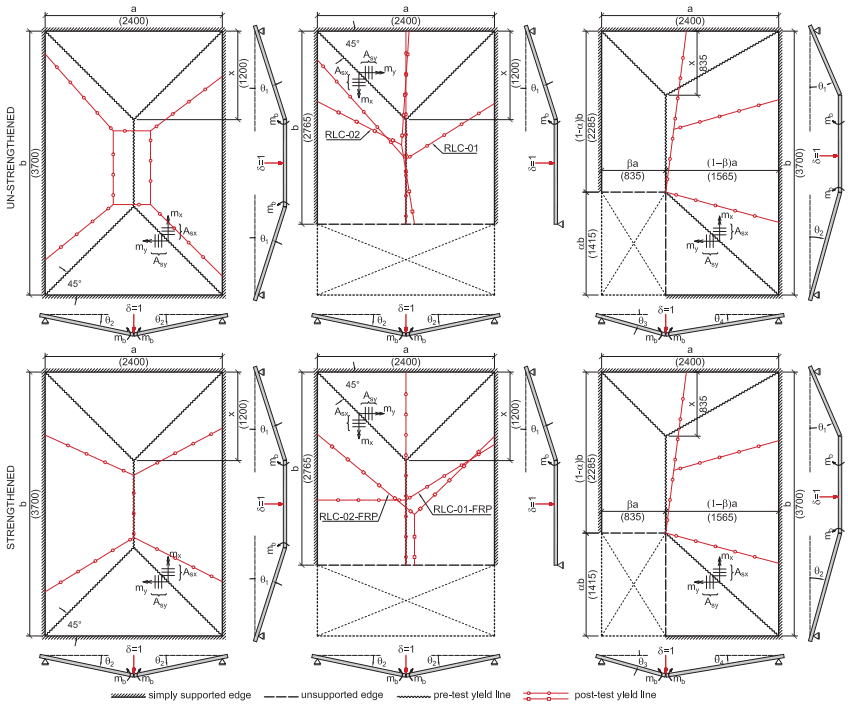


**Fig. 11.** Pre and post-test yield line patterns for both strengthened and unstrengthened slabs.

as noted by Park and Gamble [35]. For slabs with openings at corners, Park and Gamble [35] proposed different possible yield line patterns that are most likely to occur function of the opening size. The equation for finding the ultimate load of each pattern type includes several unknown terms (i.e. $\alpha$, $\beta$, $x$) which define the theoretical positions of the yield lines. The exact values for these terms are determined by differentiating the constitutive equations and finding the maximum value for $\partial q/\partial\alpha = 0$, $\partial q/\partial\beta = 0$, $\partial q/\partial x = 0$. This mathematical procedure is laborious due to nonlinearity of the equations. Moreover, Wood and Jones [33] suggested that such a technique may not always be used due to discontinuity in the slab boundaries. In this study the layout of the yield lines are assumed to start from the re-entrant corner of the cut-out opening.

The failure load per unit area was derived from Eq. (1) for each slab. Due to space limitations only the final solution will be stated as follows: Eq. (5) – ultimate uniformly distributed load/unit area for a full slab; Eq. (6) – ultimate uniformly distributed load/unit area for slab with small cut-out opening; Eq. (7) – ultimate uniformly distributed load/unit area for slab with large cut-out opening.

$$q = \frac{2 \cdot m_b\left(\frac{a}{x} + \frac{2b}{a}\right)}{\frac{2ax}{3} + \frac{a(b-2x)}{2}} \tag{5}$$

$$q = \frac{m_b \cdot \left(\frac{a}{x} + \frac{1-\beta}{\alpha} \cdot \frac{a}{b} + \frac{1-\alpha}{\beta} \cdot \frac{b}{a} + \frac{1}{1-\beta} \cdot \frac{b}{a}\right)}{\left[\frac{ax(2\beta-1)}{6} + ab(1-\beta)\left(\frac{\alpha}{3} + \frac{1-\alpha}{2}\right)\right]} \tag{6}$$

$$q = \frac{6 \cdot m_b\left(\frac{a}{x} + \frac{4b}{a}\right)}{a(3b-x)} \tag{7}$$

In this study two different approaches were used: (1) pre-tests predictions: the yield line theory was applied assuming the theoretical distribution of the yield lines (“pre-test yield lines” in Fig. 11) and (2) post-tests predictions: the yield line theory was applied to the real crack pattern observed on the tested slabs (“post-test yield lines” in Fig. 11). All slabs were simply supported along their contour, therefore only positive yield lines have developed.

### 3.3.2. Pre-test predictions

The following assumptions were made for pre-test predictions:

(a) the resisting moment of the un-strengthened slabs was evaluated assuming that the steel reinforcement intersected by the yield lines is yielding, the value of the yield stress, $f_{yk}$, was assumed as in Table 1
(b) the FRP reinforcement around openings was uniformly distributed over the entire surface of the slab
(c) the resisting moment of the FRP-strengthened slabs was evaluated assuming only the strength contribution of the FRP strengthening. The steel reinforcement, considered already yielded, is neglected. The yield stress, $f_{yk}$, was replaced in Eq. (4) with the strength of FRP corresponding to its rupture strain (i.e. 1.7% for all FRP components)

**Table 3**
Comparison of the ultimate load with analytical predictions.

| Test | Slab area ($m^2$) | Test results | | Yield line predictions | | | | | |
|---|---|---|---|---|---|---|---|---|---|
| | | | | Pre-tests predictions | | Accuracy | Post-tests predictions | | Accuracy |
| | | $q$ (kN/$m^2$) | $P_{u,test}$ (kN) | $q$ (kN/$m^2$) | $P_{u,pred}$ (kN) | $\frac{P_{u,test}}{P_{u,pred}}$ | $q$ (kN/$m^2$) | $P_{u,pred}$ (kN) | $\frac{P_{u,test}}{P_{u,pred}}$ |
| FS-01 | 8.88 | 13.29 | 118 | 20.38 | 181 | 0.65 | 13.74 | 122 | 0.97 |
| RSC-01 | 7.70 | 11.30 | 87 | 23.50 | 181 | 0.48 | 11.69 | 90 | 0.97 |
| RLC-01 | 6.64 | 11.29 | 75 | 14.91 | 99 | 0.76 | 9.34 | 62 | 1.2 |
| RLC-02 | 6.64 | 10.09 | 67 | 14.31 | 95 | 0.71 | 9.04 | 60 | 1.11 |
| FS-01-FRP | 8.88 | 20.95 | 186 | 24.32 | 216 | 0.86 | 20.27 | 180 | 1.03 |
| RSC-01-FRP | 7.70 | 11.17 | 86 | 14.55 | 112 | 0.77 | 10.65 | 82 | 1.05 |
| RLC-01-FRP | 6.64 | 11.29 | 75 | 11.75 | 78 | 0.96 | 12.95 | 86 | 0.87 |
| RLC-02-FRP | 6.64 | 22.14 | 147 | 23.49 | 156 | 0.94 | 20.63 | 137 | 1.07 |
| Average | | | | | | 0.77 | | | 1.03 |
| Standard deviation | | | | | | 0.16 | | | 0.10 |

Using this approach the capacities of the slabs predicted by yield line theory are overestimated compared to those from tests, see Table 3. These predictions are not accurate because the crack pattern observed in tests did not developed according to the one assumed in the yield line theory. The reason of these deviations lies in the load strategy adopted. The loading system was not able to simulate a uniformly distributed load over the entire surface. Under high loads the slabs partially lifted from the supports, therefore changing the stress distribution in the slab towards the supports, and consequently the cracking pattern.

*3.3.3. Post-test predictions*

The assumptions presented above are valid for this approach also. However for specimen RSC-01-FRP the value of the yield stress was computed using the debonding strain; recall that this strengthening system failed by debonding, see Fig. 8. For this specimen debonding occurred at the far end of the slab where strain gauges were not installed (see Figs. 4 and 7). Simple to more complex models can be used for the evaluation of the bond strength [36–38]. D'Antino and Pellegrino [36] reviewed the performance of several bond models. That work did not indicate any model to predict accurately the strains at debonding. Therefore here the Fib Bulletin 14 [1] formulation was used to estimate the strain at debonding; the bond strain resulted is 0.8‰.

The ultimate capacity of both strengthened and un-strengthened slabs were calculated using the yield lines observed from tests (Fig. 11). Table 3 shows that the average ratio between experimental values and those predicted based on the real crack pattern are more accurate than those predicted by theoretically assumed ones. For all elements, the predicted values were within the acceptable 10% limit [35] except for slab RLC-01 being however, on the conservative side.

## 4. Conclusions

The research presented in this paper addressed issues regarding the strengthening of damaged two-way RC slabs with cut-out openings created on their sides. The following conclusions were drawn based on observations from the experimental tests:

- The tests showed that the load capacity of slabs with cut-out openings is not directly proportional to the reduction in their area. Reducing the effective area of a solid slab, by cutting out small and large openings, to 87% and 75% can decrease the resistance to 73%, 63% and 57% respectively. Note that the last two values refer to slabs with the same opening size. However, the smaller internal lever arm of the primary reinforcement diminished the capacity of the slab exhibiting the later value.
- The results for slabs RSC-01-FRP and RLC-01-FRP showed that using a quantity of FRP equivalent to the steel reinforcement removed by sawing the cut-out, the capacity of the slab can be restored fully, even when damaged prior to strengthening.
- In order to restore and increase the capacity beyond the design value of the un-strengthened slab, the strengthening system was designed to replace the reinforcement in the slab. Tests on slabs FS-01-FRP and RLC-02-FRP showed an increase in ultimate capacity of up to 57% and 121% respectively, compared to the values recorded during the tests on the un-strengthened specimens FS-01 and RLC-02 respectively. Slab RLC-02-FRP had the highest ultimate capacity relative to its effective area.
- The tests have also shown that debonding problems can be avoided by using the NSM technique. In all tests, the strengthening systems primarily failed due to rupture. The debonding of the FRP plate used in the test RSC-01-FRP was due to a secondary failure mode, since it occurred at the far end of the slab. It is unclear to the authors whether the loading system used produced a favourable effect on the bonding properties; this research subject needs further investigation.
- Because of their superior mechanical properties compared to steel reinforcement, the FRPs enabled better stress redistribution and, consequently, a more uniform cracking distribution. The new formed major cracks show that this behaviour was due to the un-damaged part of the steel reinforcement that had yielded during the control testing.
- One practical problem in applying the yield-line method is that designers must consider a large number of failure mechanisms to ensure that the lowest collapse load is found. This procedure implies lengthy calculations and skilled engineering to ensure that the right collapse mechanism is chosen, especially in cases like slabs with openings, were the general assumptions are not fully applicable. In this respect, analytical pre-tests predictions lead to un-conservative values whereas for post-tests prediction indicated a good approximation. However, for design purposes it is not common to carry out laboratory investigations. Perhaps numerical analysis could be a tool to overcome this challenge.
- This study tested four types of strengthening configurations using high strength FRP. How different strengthening configurations and different FRP material properties might influence the capacity of slabs with cut-out openings is a subject for future work.

## Acknowledgements

The first and last authors would like to acknowledge The Romanian Ministry of Education and Research; the research work has

been partly funded through the CEEX and CNCSIS programs of the National University Research Council of Romania. The second and third authors would like to acknowledge The Research Council of Norway and Development Fund of the Swedish Construction Industry (SBUF) for financing their work within this project.

## References

[1] Fib Bulletin 14. Externally bonded FRP reinforcement for RC structures. Lausanne: international federation for structural concrete; 2001.
[2] ACI 440.2R-08. Guide for the design and construction of externally bonded FRP systems for strengthening concrete structures. Farmington Hills: American Concrete Institute; 2008.
[3] Shahawy MA, Beitelman T, Arockiasamy M, Sowrirajan R. Experimental investigation on structural repair and strengthening of damaged prestressed concrete slabs utilizing externally bonded carbon laminates. Compos Part B – Eng 1996;27(3–4):217–24.
[4] Limam O, Foret G, Ehrlacher A. RC two-way slabs strengthened with CFRP strips: experimental study and a limit analysis approach. Compos Struct 2003;60(4):467–71.
[5] Mosallam AS, Mosalam KM. Strengthening of two-way concrete slabs with FRP composite laminates. Constr Build Mater 2003;17(1):43–54.
[6] Arduini M, Nanni A, Romagnolo M. Performance of one-way reinforced concrete slabs with externally bonded fiber-reinforced polymer strengthening. ACI Struct J 2004;101(2):193–201.
[7] Ebead U, Marzouk H. Fiber-reinforced polymer strengthening of two-way slabs. ACI Struct J 2004;101(5):650–9.
[8] Shahrooz BM, Boy S. Retrofit of a three-span slab bridge with fiber reinforced polymer systems; testing and rating. J Compos Constr 2004;8(3):241–7.
[9] Kim YJ, Longworth JM, Wight RG, Green MF. Flexure of two-way slabs strengthened with prestressed or nonprestressed CFRP sheets. J Compos Constr 2008;12(4):366–74.
[10] Mosallam A, Reda Taha MM, Kim JJ, Nasr A. Strength and ductility of RC slabs strengthened with hybrid high-performance composite retrofit system. Eng Struct 2012;36(9803):70–80.
[11] Teng JG, Lam L, Chan W, Wang J. Retrofitting of deficient RC cantilever slabs using GFRP strips. J Compos Constr 2000;4(2):75–84.
[12] El Maaddawy T, Soudki K. Strengthening of reinforced concrete slabs with mechanically-anchored unbonded FRP system. Constr Build Mater 2008;22(4):444–55.
[13] Smith ST, Hu S, Kim SJ, Seracino R. FRP-strengthened RC slabs anchored with FRP anchors. Eng Struct 2011;33(4):1075–87.
[14] Dan D. Experimental tests on seismically damaged composite steel concrete walls retrofitted with CFRP composites. Eng Struct 2012;45:338–48.
[15] Everaldo B, Joaquim António Oliveira B, Paulo BL. Efficient strengthening technique to increase the flexural resistance of existing RC slabs. J Compos Constr 2008;12(2):149–59.
[16] Foret G, Limam O. Experimental and numerical analysis of RC two-way slabs strengthened with NSM CFRP rods. Constr Build Mater 2008;22(10):2025–30.
[17] Casadei P, Ibell TJ, Nanni A. Experimental results of one-way slabs with openings strengthened with CFRP laminates. In: Proceedings of proceedings, fibre-reinforced polymer reinforcement for concrete structures, FRPRCS – 6. Singapore Conference 8–10 July, Conference 2003. p. 1097–106.
[18] Vasquez A, Karbhari VM. Fiber-reinforced polymer composite strengthening of concrete slabs with cutouts. ACI Struct J 2003;100(5):665–73.
[19] Tan KH, Zhao H. Strengthening of openings in one-way reinforced-concrete sabs using carbon fiber-reinforced polymer systems. J Compos Constr 2004;8(5):393–402.
[20] Özgür A, Nalan K, Onur A. Strengthening of one way RC slab with opening using CFRP strips. Constr Build Mater 2013;48(10):883–93.
[21] Smith ST, Kim SJ. Strengthening of one-way spanning RC slabs with cutouts using FRP composites. Constr Build Mater 2009;23(4):1578–90.
[22] Seliem HM, Seracino R, Sumner EA, Smith ST. Case study on the restoration of flexural capacity of continuous one-way RC slabs with cutouts. J Compos Constr 2011;15(6):992–8.
[23] Casadei P, Nanni A, Ibell TJ. Experiments on two-way RC slabs with openings strengthened with CFRP laminates. In: Proceedings of advancing with composites, PLAST 2003. Milan, Italy, Conference 7–9 May, Conference 2003.
[24] Enochsson O, Lundqvist J, Taljsten B, Rusinowski P, Olofsson T. CFRP strengthened openings in two-way concrete slabs – an experimental and numerical study. Constr Build Mater 2007;21(4):810–26.
[25] Elsayed WE, Ebead UA, Neale KW. Mechanically fastened FRP-strengthened two-way concrete slabs with and without cutouts. J Compos Constr 2009;13(3):198–207.
[26] De Lorenzis L, Teng JG. Near-surface mounted FRP reinforcement: an emerging technique for strengthening structures. Compos Part B – Eng 2007;38(2):119–43.
[27] EN 1992-1-1. Eurocode 2: design of concrete structures – Part 1–1: general rules and rules for buildings. Brussels: COMITÉ EUROPÉEN DE NORMALISATION; 2004.
[28] SR EN 12390-1-4. Testing hardened concrete – Parts 1–4. 2002.
[29] SR EN 10002-1. Metallic materials – tensile testing – Part 1: method of test at ambient temperature. 2002.
[30] Floruț SC. Performance study of elements strengthened with FRP composite materials subjected to flexure (in Romanian), PhD Thesis. Ed. Politehnica – Timisoara: Politehnica University of Timisoara; 2011.
[31] Ingerslev A. The strength of rectangular slabs. J Inst Struct Eng 1923;1(1):3–14.
[32] Johansen KW. Yield line theory. London: Cement and Concrete Association; 1962.
[33] Wood RH, Jones LL. Yield-line analysis of slabs: Thames & Hudson. London: Chatto & Windus; 1967.
[34] Kennedy G, Goodchild CH. Practical yield line design. Camberley, Surrey: The Concrete Centre; 2004.
[35] Park R, Gamble WL. Reinforce concrete slabs. 2nd ed. John Wiley & Sons, Inc.; 2000.
[36] D'Antino T, Pellegrino C. Bond between FRP composites and concrete: assessment of design procedures and analytical models. Compos Part B: Eng 2014;60:440–56.
[37] Sas G, Carolin A, Täljsten B. A model for predicting the shear bearing capacity of FRP-strengthened beams. Mech Compos Mater 2008;44(3):245–56.
[38] Caggiano A, Martinelli E, Faella C. A fully-analytical approach for modelling the response of FRP plates bonded to a brittle substrate. Int J Solids Struct 2012;49(17):2291–300.

# Paper V

**Assessment of RC walls with cut-out openings strengthened by FRP using a rigid-plastic approach**

Cosmin Popescu; Jacob W. Schmidt; Per Goltermann; and Gabriel Sas

Submitted to:
*Engineering Structures*
August 2016
pp. 1-20

# Assessment of RC walls with cut-out openings strengthened by FRP using a rigid-plastic approach

**Cosmin Popescu**[a,*]; **Jacob W. Schmidt**[b]; **Per Goltermann**[b]; and **Gabriel Sas**[c]

[a] Northern Research Institute – NORUT, Rombaksveien E6-47, N-8517 Narvik, Norway

[b] Technical Univ. of Denmark, Dept. of Civil Engineering, Building 118, DK-2800 Kgs. Lyngby, Denmark

[c] Luleå Univ. of Technology, Dept. of Civil, Environmental and Natural Resources Engineering, SE-97187, Luleå, Sweden

* Corresponding author. Tel.: +46 702375433.
E-mail addresses: cosmin.popescu@norut.no (C. Popescu), jws@byg.dtu.dk (J.W. Schmidt), pg@byg.dtu.dk (P. Goltermann), gabriel.sas@ltu.se (G. Sas)

## Abstract

Building refurbishment works frequently require the cutting of new openings in concrete walls. The addition of new openings weakens the overall response of such elements, so they usually require strengthening. However, current design codes offer little guidance on strengthening walls with openings, and less still on the use of non-metallic reinforcements such as FRP (Fibre reinforced polymers) to ensure sufficient capacity. This paper proposes a new procedure based on limit analysis theory for evaluating the ultimate load of walls with cut-out openings that have been strengthened with FRPs. The approach is verified against transverse (out-of-plane) and axial (in-plane) loading. These loading types result in different failure mechanisms: transverse loading leads to failure due to yielding/rupture of the steel reinforcement while axial loading leads to failure by concrete crushing. Predictions made using the new method agree closely with experimental results.

**Author keywords**: Walls with openings, Eccentric axial loading, Transverse loading, Concrete plasticity, Effectiveness factor, Strengthening, Fibre-reinforced polymers

## 1. Introduction

Precast concrete walls are commonly used as load-bearing elements for low- to mid-rise structures. The widespread popularity of such elements is due to their efficient construction and design flexibility. Openings for doors and/or windows can be readily accommodated by carefully considering the effects of their presence during the design stage and addressing any weaknesses they may introduce by specifying appropriate reinforcement detailing around their edges. However, problems frequently arise when such structures are refurbished and new openings (i.e. cut-out openings) are introduced to facilitate changes in role, for example when apartment buildings are converted into office spaces. These openings introduce weaknesses that can reduce the wall's overall performance in terms of flexural and/or axial strength, stiffness, and energy dissipation. Consequently, repairs (defined here as actions that fully or partially restore the structure's load-carrying capacity) using fibre-reinforced polymers (FRP) are often required. However, before a repair method can be used with confidence, it is necessary to have reliable information on the degree to which the un-strengthened wall has been weakened.

Although there have been many experimental studies on the behaviour of reinforced concrete (RC)

walls, the performance of RC walls with openings has not been investigated in the same depth. The few studies that have been published in this area [1-6] have focused on structural walls subjected to seismic forces; but equally important, are also those designed for non-seismic applications, i.e. walls that must primarily withstand axial compression loads, which are much less studied. The literature on the behaviour of axially loaded walls was recently reviewed by Popescu et al. [7]. It was concluded that most reported tests have focused on the behaviour of one-way walls [8-13], i.e. walls restrained along the top and bottom edges developing a uniaxial curvature. Fewer tests have been conducted on walls under two-way action [11, 14-16], i.e. walls restrained along all edges developing a biaxial curvature, and walls with openings [17-20].

Efforts have also been made to develop design models capable of predicting the axial capacity of such elements. Most such models are empirical and calibrated using data from limited numbers of one-way and two-way action tests, with loading eccentricities of up to one sixth of the wall's thickness. These design models take into account the contribution of the reinforcement [9, 12, 16], high-strength concrete and increasing slenderness [21], material nonlinearities [13, 22, 23], and the presence of the opening [17, 18, 24]. Major design codes such as EN1992-1-1 [25], ACI 318 [26] and AS3600 [27] also offer design models. These models were initially developed for one-way walls but restraining factors were subsequently introduced into the European [25] and Australian [27] design codes on the basis of German work [28]. These restraining factors were added to reduce the wall's effective height based on the boundary conditions and to thereby account for the effects of restraining the lateral edges (i.e. two-way action).

After reviewing existing design methods against a database covering 253 tests on both one- and two-way walls under axial loading, with and without openings, [7], it was found that "design models established in design codes provide the most conservative results, while those proposed in other studies [13, 16, 17, 29] showed a certain level of non-conservatism". Moreover, we were only able to identify a single study on the strengthening of axially loaded concrete walls with cut-out openings using carbon-FRP (CFRP) in the literature [20]. Unfortunately, this study only considered one-way walls, and so the associated design model is only valid for such walls.

Because empirical models have certain shortcomings (for example, they rely on coefficients obtained by curve-fitting using data from a specific experimental setup), their application in practical contexts is likely to give rise to considerable scatter on both the safe and unsafe sides. Therefore, there is a clear need for a theory-based method that can describe biaxial effects on panels restrained on all sides and also account for the effects of openings and the contributions of FRP strengthening materials. This manuscript describes the development of such a general analytical method based on limit analysis and concrete plasticity. Experiments conducted by the authors at Luleå University of Technology and the Technical University of Denmark provided the model's foundations, and the results of these studies are briefly summarized here.

## 2. Overview of the experimental tests

During service, RC walls must withstand various kinds of loads, including (1) gravitational loads parallel to the mid-surface at a given eccentricity due to construction errors; (2) horizontal out-of-plane forces due to wind loads; (3) handling, transportation and erection loads, and potentially (4) accidental

loads such as seismic or blast loads. Loads of the first two classes are usually the governing load cases for structures erected in non-seismic regions and are therefore the focus of this study (Figure 1). The results of experiments on two-way walls under lateral (out-of-plane) bending [30] and under eccentric uniaxial compression [31, 32] will be briefly summarized in this section. Both experimental programmes include walls with symmetric openings that replicate solid walls with sawn cut-outs, i.e. no additional reinforcement was placed around the edges or corners of the openings. An overview of the main properties of the tested walls is given in Table 1.

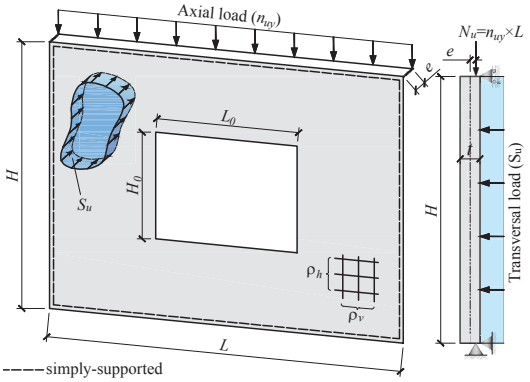


**Figure 1.** Wall specimen used as a reference in analytical evaluation: geometry and loading

**Table 1.** Summary of tested specimens

| Wall | $L$ (m) | $H$ (m) | $t$ (m) | $L_0$ (m) | $H_0$ [a] (m) | $f_c$ [b] (MPa) | $\rho_h$ (%) | $\rho_v$ (%) | $f_y$ (MPa) | $f_u$ (MPa) | $\delta_{peak}$ [c] (mm) | $S_{exp}$ (kN/m$^2$) | $N_{exp}$ (kN) |
|---|---|---|---|---|---|---|---|---|---|---|---|---|---|
| *Walls under transversal load* | | | | | | | | | | | | | |
| A | 4.0 | 2.6 | 0.1 | - | - | 49.7 | 0.196 | 0.190 | 600 | 662 | 81.81 | 21.2 | - |
| B | | | | - | - | 49.7 | 0.196 | 0.190 | 600 | 662 | 73.08 | 21.8 | |
| C | | | | 1.3 | 1.0 | 49.7 | 0.196 | 0.190 | 600 | 662 | 125.19 | 15.3 | |
| D | | | | 1.3 | 1.0 | 49.7 | 0.196 | 0.190 | 600 | 662 | 109.51 | 17.0 | |
| E | | | | 1.3 | 1.0 | 49.7 | 0.136 | 0.133 | 651 | 701 | 115.85 | 11.0 | |
| F | | | | 1.3 | 1.0 | 49.7 | 0.136 | 0.133 | 651 | 701 | 108.74 | 12.3 | |
| *Loads under eccentric axial load* | | | | | | | | | | | | | |
| I-C | 1.8 | 1.35 | 0.06 | - | - | 62.8 | 0.315 | 0.327 | 632 | 693 | 18.96 | - | 2363 |
| I-S | | | | 0.45 | 1.05 | 62.8 | 0.315 | 0.327 | 632 | 693 | 26.67 | | 1500 |
| I-L | | | | 0.90 | 1.05 | 62.8 | 0.315 | 0.327 | 632 | 693 | 11.18 | | 1180 |
| II-S | | | | 0.45 | 1.05 | 62.8 | 0.315 | 0.327 | 632 | 693 | 22.35 | | 2241 |
| II-L | | | | 0.90 | 1.05 | 62.8 | 0.315 | 0.327 | 632 | 693 | 5.84 | | 1497 |
| III-S1 | | | | 0.45 | 1.05 | 64.4 | 0.315 | 0.327 | 632 | 693 | 21.73 | | 2178 |
| III-S2 | | | | 0.45 | 1.05 | 64.4 | 0.315 | 0.327 | 632 | 693 | 17.41 | | 2009 |
| III-L1 | | | | 0.90 | 1.05 | 64.4 | 0.315 | 0.327 | 632 | 693 | 12.34 | | 1334 |
| III-L2 | | | | 0.90 | 1.05 | 64.4 | 0.315 | 0.327 | 632 | 693 | 7.31 | | 1482 |

[a] Heights of window- and door-type openings in walls under transverse and axial loading, respectively.
[b] Mean compressive strength determined based on cylinder and cube tests for walls under transverse and axial loading, respectively. A conversion factor of 0.83 is used in later calculations to convert the cube compressive strength into cylinder compressive strength.
[c] Maximum out-of-plane displacements at peak load: measurements in the mid-point location for solid walls and at the opening edge for specimens with openings.

### 2.1. Transversally loaded walls

An experimental program was conducted in which six full-scale lightly reinforced concrete walls (4 m × 2.6 m × 0.1 m) were subjected to uniform transverse loading. The applied force was fully distributed on the wall surface using airbags that react against a backing steel frame. The walls' vertical and horizontal edges were simply supported, i.e. restrained against translation while allowing rotation. No vertical pre-compression other than their own weight was added to the tested specimens. Parameters varied across the tested specimens include the reinforcement ratio and the presence of a window opening. The reinforcement consisted of a single wire mesh (ϕ5/150 or ϕ6/150) offset from the mid-surface towards the tension side of the wall in order to achieve a concrete cover of about 30 mm.

### 2.2. Axially loaded walls

Half-scale walls designed to represent typical wall panels in residential buildings with and without cut-out openings (1.8 m × 1.35 m × 0.06 m), were constructed for testing to failure. The walls were tested in two-way action and subjected to axial loading with low eccentricity along the weak axis ($1/6^{th}$ of the wall's thickness) to represent imperfections due to thickness variation and misalignment of the panels during the construction process. The test matrix can be divided into three stages, designated I-III. Three specimens were loaded to failure in stage I: a solid wall (I-C), a wall with a "small" symmetric single door opening (I-S), and a panel with a "large" symmetric double door opening (I-L). In stage II, two specimens [one with a small opening (II-S) and one with a large opening (II-L)] were first precracked and then strengthened with CFRP before being tested to failure. In stage III, duplicated specimens with openings of each size were strengthened with the FRP system in an uncracked state and then loaded to failure. It should be noted that "small" and "large" are used here as convenient designations rather than as clearly delimited terms with specific thresholds and implications.

All specimens were reinforced with welded wire fabric (ϕ5/100) placed centrally in a single layer. Uniaxial U-shaped CFRP sheets covering the entire wall's surface and fixed in place with mechanical anchorages were used for strength enhancement. The anchorages were prestressed with a torque estimated from the clamp load as 75% of the proof load as specified in SS-EN ISO 898-1 [33]. The material properties of the FRP system are given in Table 2.

**Table 2.** Characteristics of the CFRP and its adhesive

| Property | Epoxy adhesive (StoPox LH) | CFRP sheets (StoFRP IMS300 C300) |
|---|---|---|
| Layer thickness, $t_{frp}$ (mm) | - | 0.17 |
| Tensile strength, $f_{frp}$ (MPa) | >60 | >5500 |
| Elastic modulus, $E_{frp}$ (GPa) | 2 | 290 |
| Elongation at breack, $\varepsilon_{frp}$ (%) | 3 | 1.9 |

The strengthening system was designed in accordance with the FRP-confinement design model proposed by Lam and Teng [34]. An estimate of the required thickness of the FRP jacket was obtained by arranging the mechanical anchorages in a configuration that would create vertical strips with cross-sectional aspect ratio that was limited to 2:1 (60 x 120 $mm^2$ as shown in Figure 2). The addition of the

FRP layers would increase the concrete's compressive strength up to the value ($f_{cc}$) needed to bring the strengthened wall's load bearing capacity up to that of the original solid wall. Two and three FRP layers were used to strengthen the specimens with small and large openings, respectively.

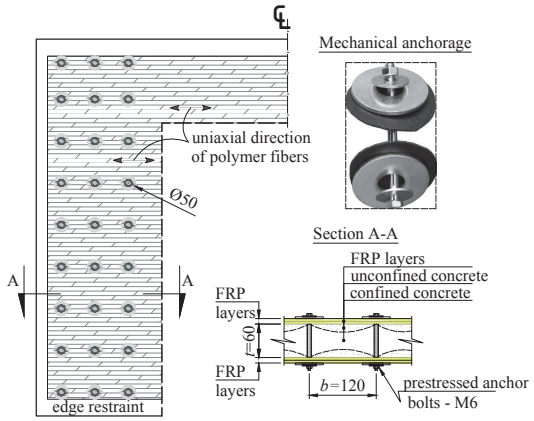


**Figure 2.** FRP-strengthening details

## 3. Design for ultimate strength and comparison with tests

### 3.1. Failure mechanism

The failure mechanism of walls under transverse loads is virtually identical to that of a slab unless the contribution of vertical loads is very important. Bailey and Toh [35] showed that two distinct failure modes can occur for transversally loaded slabs depending on the reinforcement ratio. This parameter is defined by the ultimate tensile force of the reinforcement relative to the compressive force of the concrete across the thickness of the slab [35], and is computed using an expression with the following form:

$$\rho = \frac{1}{2}\left[\left(\frac{f_{u,x}A_{s,x}}{0.8f_c d_x}\right)+\left(\frac{f_{u,y}A_{s,y}}{0.8f_c d_y}\right)\right] \quad (1)$$

Bailey's experimental observations yielded a threshold value for the parameter ρ, which delineates the transition point from failure due to reinforcement fracture ($\rho < 0.08$) and failure due to concrete crushing ($\rho > 0.08$). However, this threshold is only valid for square plates; further tests are required to define a suitable threshold value for rectangular plates. For the specimens tested in this work, the reinforcement ratio calculated according to Eq. (1) is 0.05 for transversally loaded walls. In the case of solid walls, the mechanism of failure involved the formation of cracks extending from approximately the centre of the wall towards the corners at an angle of approximately 45° to the floor; in walls with openings, failure occurred via the formation of diagonal cracks extending from the corners of the opening to the closest corner of the wall as shown in Figure 3a. The experimental results indicated that the reinforcement fractured along the yield lines, confirming Bailey's conclusions. The failure mechanism is ductile, and the associated displacements are large (see Table 1).

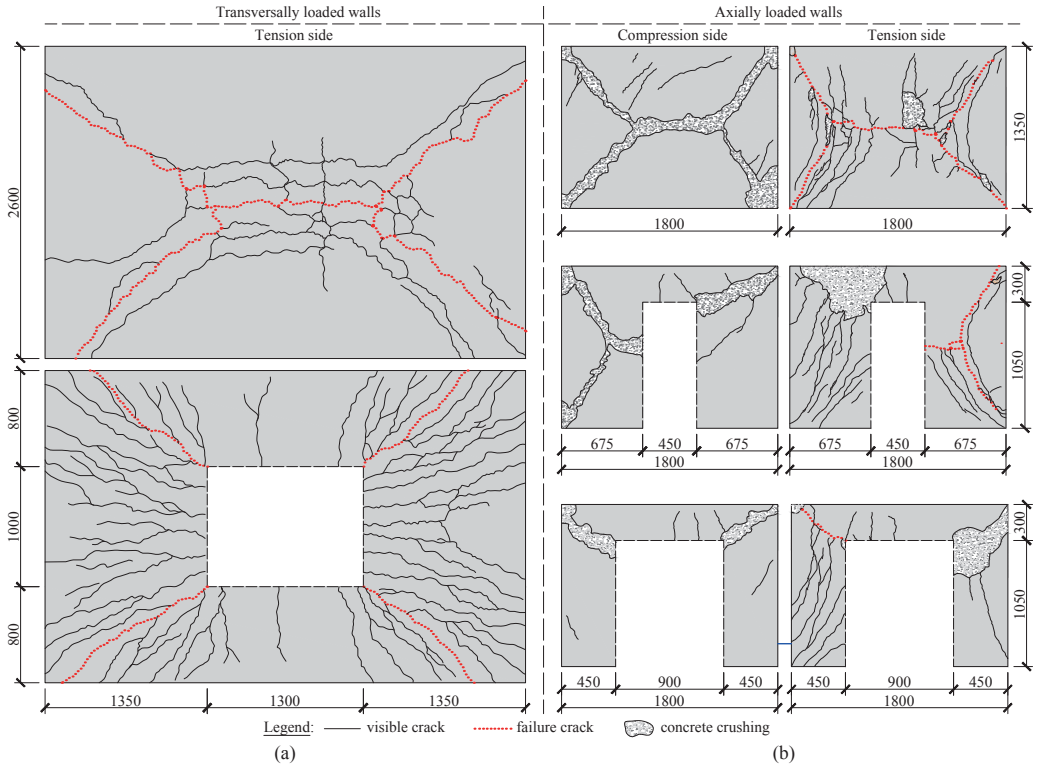


**Figure 3.** Typical crack patterns for walls under: (a) lateral (out-of-plane) bending and (b) eccentric uniaxial compression

Crack propagation is significantly influenced by the dominant load (transverse vs. axial loading), but the crack pattern at the ultimate load was independent of the loading strategy, as illustrated in Figure 3b. The failure process for walls under eccentric axial loads started from the corners of the wall – the concrete initially cracked on the tension side of the wall, with subsequent concrete crushing on the compression side along the major cracks. This mechanism is brittle, and the associated displacements are relatively small (see Table 1). Double curvature in both the horizontal and vertical directions of the walls was observed in the experiments. This indicates that, in contrast to the typical assumptions of design codes, the lateral restraints make the problem three-dimensional rather than one-dimensional. The addition of CFRP (for strengthened walls) did not appear to change the position of the yield lines prior to failure. After that point, as seen in Figure 4 the failure became localized along the bottom of the piers due to crushing of the concrete, which caused the covering CFRP mesh to be torn away from the wall.

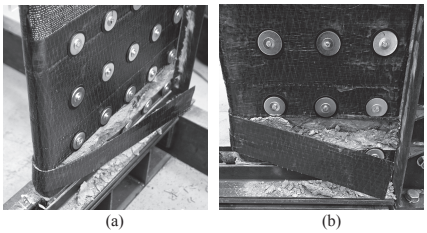


**Figure 4.** Typical failure modes of the FRP-strengthened specimens: (a) wall with a small opening and (b) wall with a large opening

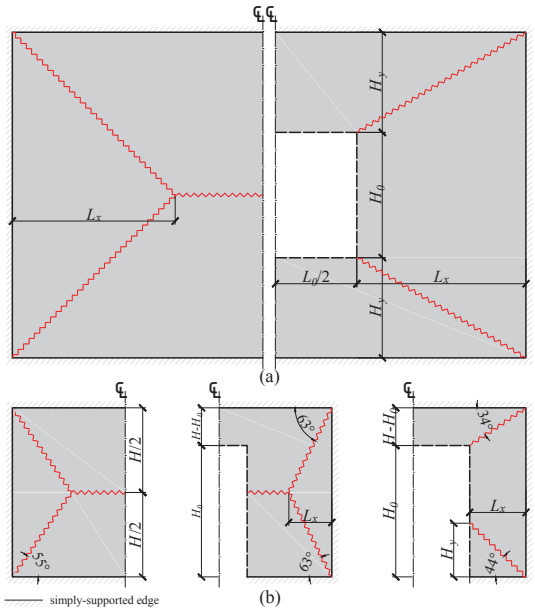


**Figure 5.** Failure mechanisms for walls under (a) transverse loading; (b) axial loading

The major cracks shown in Figure 3 define the geometrical models (yield lines) related to the corresponding failure mechanisms. Figure 5a shows the yield lines adopted for walls under transverse loading; those for walls under axial loading are illustrated in Figure 5b.

### 3.2. **Yield conditions**

This section describes the yield conditions for all of the constituent materials included in the analysis, i.e. concrete, steel reinforcement and FRP. Qualitative depictions of the real and idealized stress-strain laws for each material are presented in Figure 6. However, the basic theorem of limit analysis implies that materials exhibit perfect plasticity with idealized failure criteria as shown in Figure 6. Elastic displacements are neglected, which implies rigid behaviour until the plastic plateau is reached.

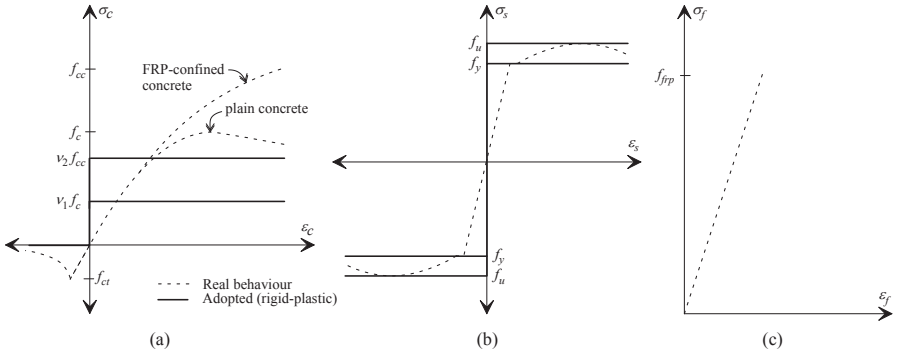


**Figure 6.** Yield conditions for: (a) concrete; (b) metallic reinforcement and (c) FRP

### 3.2.1. *Concrete*

The concrete is assumed to behave according to the modified Coulomb criterion with tensile strength accounted for using a zero tensile cut-off but otherwise neglected (see Figure 6a). The ultimate strength of concrete under uniaxial stress state must be reduced to an equivalent plastic compressive strength using an effectiveness factor $\nu < 1$ because of the material's brittleness and the influence of transverse strains on the concrete's strength [36]. According to the fib Model Code 2010 [36], the effectiveness factor can be expressed as the product of $\eta_{fc}$ and $\eta_{\varepsilon}$ – strength reduction factors reflecting the brittleness of concrete and the influence of transverse cracking, respectively.

$$\nu_1 = \eta_{fc} \cdot \eta_{\varepsilon} \tag{2}$$

where $\eta_{fc}$ is defined as:

$$\eta_{fc} = \left( \frac{f_{c0}}{f_c} \right)^{1/3} \leq 1.0 \tag{3}$$

with $f_{c0}$=30 MPa, and $\eta_{\varepsilon}$=0.55 for compression bands with reinforcement running obliquely to the direction of compression.

### 3.2.2. *Steel reinforcement*

The steel reinforcement was also assumed to behave in a rigid-plastic manner in both tension and compression, as shown in Figure 6b. Two values for the plastic plateau were selected, representing two different cases. In the first case, the plateau corresponds to the yielding point reached in uniaxial tensile tests on reinforcement coupons (see Table 1). In the second case, the plastic plateau is defined as the tensile strength reached in uniaxial tensile tests on reinforcement coupons (see Table 1). The reason for using the tensile strength as the plastic plateau rather than the yield strength of the material will be discussed later.

### 3.2.3. *Fibre-reinforced polymers*

The real behaviour of the non-metallic reinforcement, i.e. CFRP, is linear elastic, with no plasticity or softening branch (Figure 6c). Consequently, the assumption of rigid-plastic behaviour becomes questionable. In an attempt to account for the contribution of FRP in strengthened slabs with openings, Florut et al. [37] used the strength corresponding to the debonding strain as observed in experimental tests. An alternative procedure proposed in this paper is to update the concrete model using an enhanced confined compressive strength ($f_{cc}$) due to FRP-confinement. The procedure is based on the following expressions, as discussed previously [34]:

$$f_{cc} = \left( 1 + k_1 k_{s1} \frac{f_l}{f_c} \right) f_c \tag{4}$$

where $k_1$=3.3 is the confinement effectiveness coefficient, $k_{s1}$ is a parameter used to account for the effect of the non-uniformity of confinement according to Eq. (5), and $f_l$ is the confining pressure defined as in Eq. (6).

$$k_{s1} = \left(\frac{b}{t}\right)^2 \frac{A_e}{A_c} \tag{5}$$

$$f_l = \frac{2 f_{frp} n_{layers} t_{frp}}{\sqrt{b^2 + h^2}} \tag{6}$$

and,

$$\frac{A_e}{A_c} = \frac{1 - \left[(b/h)(h-2R)^2 + (h/b)(b-2R)^2\right]/3A_g - \rho_{sc}}{1 - \rho_{sc}} \tag{7}$$

where $b$ and $h$ are width and height of the cross-section, respectively, $A_e$ is effective confinement area, $A_c$ is the total area of the cross-section, $R$ is the corner radius, $r_{sc}$ is the cross-sectional area proportion of longitudinal steel, and $A_g$ is the gross area of the column section with rounded corners.

The abovementioned model is valid only for pure axial loads, but the specimens in this work were loaded with small eccentricities to simulate the effects of the imperfections that occur in normal construction practices. Therefore, the effectiveness factor should incorporate an additional parameter to account for eccentricity and slenderness effects. The impact of these effects is demonstrated by the difference between the strain readings obtained on the tension (e.g. F1-T, see Figure 7) and compression (e.g. F1-C, see Figure 7) sides of the specimens, as shown in Figure 7. To illustrate this point, we present ultimate strain readings for specimens II-L (Figure 7a) and II-S (Figure 7b).

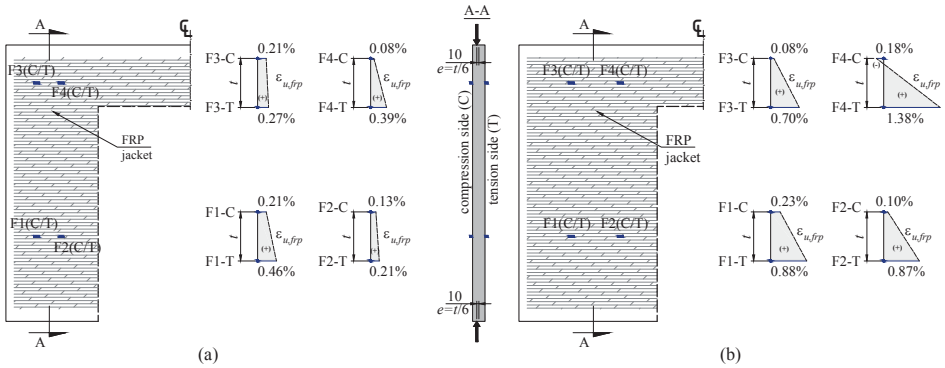


**Figure 7.** Strain gauge locations (on polymer fibres) and ultimate strain readings for: (a) wall with large opening; (b) wall with small opening

The transformation factor from non-uniform confinement to uniform confinement was calculated as the ratio between the average and maximum strain at each measurement point according to Eq. (8):

$$\eta_{\varepsilon,frp} = \frac{\varepsilon_{avg}}{\varepsilon_{u,frp-max}} \leq 1.0 \tag{8}$$

where,

$$\varepsilon_{avg} = \frac{\varepsilon_{u,frp-max} + \varepsilon_{u,frp-min}}{2} \tag{9}$$

It should be noted that these values are locally measured strains that may be affected by stress concentrations or being offset from the maximum values of the strain path. Therefore, the transformation factor due to eccentricity was averaged over the points F1-F4 for all specimens tested, yielding a value of approximately 0.65. The new expression for the effectiveness factor was then defined by Eq. (10).

$$\nu_2 = \eta_{fc} \cdot \eta_{\varepsilon} \cdot \left( \eta_{\varepsilon,frp} \cdot \Delta f \right) \tag{10}$$

with $\Delta f$ – the increase in compressive strength from unconfined to FRP-confined concrete.

Unlike the term $\eta_{\varepsilon,frp}$, the other two terms in Eq. (10) are calculated in the same way as for un-strengthened walls. The difference is that the compressive strength is replaced with the confined compressive strength in Eq. (3) and the effect of transverse strain is conservatively treated as being the same. However, the addition of extra reinforcement (i.e. FRP) means that transverse strains are unlikely to produce the same internal damage in concrete. It would therefore be useful to further calibrate the model in future studies.

### 3.3. **Limit analysis approach**

The limit analysis theory for slabs (i.e. the yield line method) has been extensively investigated in recent decades. However, there are only a few published examples of its use to predict the ultimate capacity of plain or lightly-reinforced elements with limited ductility. Such elements are typically strengthened with a single layer of reinforcing material, which is used to control cracks formed due to creep, shrinkage and erection/transportation loads. Because of their limited plasticity, the applicability of the limit analysis approach could potentially be questioned. However, it may be relevant in cases where the walls are predominantly subject to out-of-plane bending. The method was first described by Ingerslev [38] and further developed by Johansen [39]. The analysis is performed by means of "virtual work" or using the "equilibrium method". In this paper the virtual work method is used, in which a possible plastic collapse mechanism occurs along predefined yield lines as shown schematically in Figure 5. Usually, multiple collapse mechanisms are tested and the yield line solution is defined as the solution with the lowest load at failure (in assessments) or the highest moments (during design processes). The process in this work was simplified by considering only the collapse mechanism observed in the tests, which involves the formation of wide cracks (fracture lines) as shown in Figure 3. These fracture lines indicate the positions of the positive yield lines that divide the plates into rigid disks and thereby dissipate energy. The method assumes that the work dissipated along the yield lines (i.e. the internal work) is equal to the work done by the applied loads (i.e. the external work). This assumption yields a work equation of the following form:

$$\sum \left( \iint S_u \delta dx dy \right)_{\text{each region}} = \sum \left( \int m_b \theta ds \right)_{\text{each yield line}} \tag{11}$$

where the integrals on the left- and right-hand sides represent the external and internal work, respectively, with $S_u$ denoting the uniformly distributed load per unit area, $\delta$ the virtual displacement, $m_b$ the bending moment, and $\theta$ the rotation of the region about its axis of rotation. Equation (11) represents the classical solution valid for plates loaded perpendicular to the elements' mid-plane. In walls where vertical forces will affect the external work and the corresponding strength components, the out-of-plane loads may be

accompanied by in-plane loads. A diagram used to develop a work equation applicable to such situations is presented in Figure 8.

The work equation now becomes:

$$\sum\left(\iint S_u \delta dxdy\right)_{\text{each region}} - \int\left(n_{ux,uy}\delta dx, y\right)_{\text{each boundary}} = \sum\left(\int m_b \theta ds\right)_{\text{each yield line}} \tag{12}$$

where $n_{ux}$, $n_{uy}$ is the uniform in-plane compressive force per unit length applied in the $x$- (horizontal) and $y$- (vertical) directions, respectively. To compare the predicted loads to the available experimental data, these compressive forces are applied eccentric to the mid-plane of the wall along its weak axis while forces acting in the $x$-direction are assumed to be non-existent. Depending on their magnitude, these compressive forces can either favourably contribute to the wall's capacity or govern its ultimate failure. Thus, two cases are investigated in the current study: (1) $n_{uy} << S_u$, corresponding to dominant transverse loads, and (2) $n_{uy} >> S_u$, corresponding to dominant in-plane vertical loads.

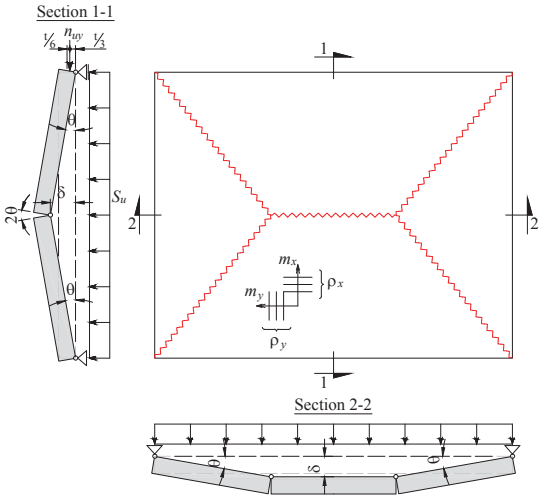


**Figure 8.** Yield-line pattern for a simply supported wall under in- and out-of-plane loads

### 3.4. **Case I: Dominant transverse loads**

Practical examples of such loadings include wind loads, blasts, snow avalanches, and lateral earth pressure. Such loadings are typically unlikely to occur; where they do occur frequently in mid-rise concrete structures (as may be the case for, e.g., wind loads), they are unlikely to become dominant. In addition to the uniformly distributed loads acting perpendicularly to the wall mid-plane, the walls may be subjected to other loads such as gravitational loads. These are expected to increase their ultimate capacity due to the favourable contribution of non-negligible and constant gravitational loads. However, in cases where the axial load derives solely from the self-weight, the additional contribution tends to be small. In previous investigations on masonry walls [40], it was found that self-weight accounted for less than 10% of the ultimate load in simply supported walls, so the self-weight contribution was disregarded when comparing theoretical predictions to experimental data.

The external and internal work can be obtained using Eq. (12) and used to derive a failure load, leading to the following expressions:

- for the solid wall

$$S_u = \frac{2m_b\left(H/L_x + 2L/H\right)}{\left[\left(L/2 - L_x/3\right)\right]H} \tag{13}$$

- for the wall with opening

$$S_u = \frac{4m_b\left(H_y/L_x + L_x/H_y\right)}{\left(\frac{4}{3}L_xH_y + H_0L_x + L_0H_y + H_0L_0\right)} \tag{14}$$

The unknown term, $L_x$, defines the theoretically correct position of the inclined yield lines. For the solid walls the exact solution was found by differentiating equation (13) over the term $L_x$, $\partial S_u/\partial L_x = 0$, that is,

$$\frac{12m_b\left[4H^2L_x - 3HL + 4L\left(L_x\right)^2\right]}{\left(L_x\right)^2\left(-2L_x + 3L\right)^2 H} = 0 \tag{15}$$

which leads to a quadratic solution for $L_x$ with the following positive root:

$$L_x = \frac{1}{2}\frac{\left(-H + \sqrt{H^2 + 3L^2}\right)H}{L} \tag{16}$$

Solving Eq. (16) provides the slope of the yield line, which is predicted to intersect with the corners of the wall at 40°; this is consistent with the average angle observed experimentally in the crack patterns at failure. Openings, when present, tend to attract yield lines [41]. Thus, in specimens with openings, the yield lines of a solid wall are interrupted by cracks connecting the corners of the wall to the closest corner of the opening, as shown in Figure 5a.

The reinforcement contributes to the internal work. It is accounted for in the work equation by first considering the equilibrium condition shown in Figure 9 to determine the bending moment $m_b$.

$$m_bL = \left(m_x \cdot L\sin\alpha\right)\sin\alpha + \left(m_y \cdot L\cos\alpha\right)\cos\alpha \tag{17}$$

$$m_b = m_x\sin^2\alpha + m_y\cos^2\alpha \tag{18}$$

where $m_x$, $m_y$ are the moment capacities per unit width in the $x$- and $y$-directions, respectively, expressed as follows:

$$m_{x,y} = \left(1 - \frac{1}{2}\frac{A_{sx,sy}f_y}{sdf_c}\right)\frac{dA_sf_y}{s} \tag{19}$$

where $A_{sx}$, $A_{sy}$ are the areas of the reinforcement per unit width in the $x$- and $y$-directions, respectively, $f_y$ is the yield strength of the reinforcement, $d$ is the effective depth, and $s$ is the reinforcement spacing. In the isotropic case (i.e. $m_x = m_y$), Eq. (18) reduces to $m_b = m_x = m_y$. For simplicity, the minor differences in the effective depths along the principal directions of the reinforcement are neglected in the following calculations.

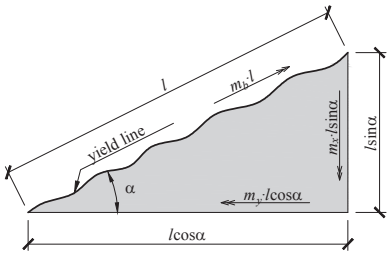


**Figure 9.** Bending moment along a yield line

The failure capacities predicted by yield line analysis are given in Table 3. These predictions underestimate the capacity in all cases; the average ratio of the theoretically and experimentally determined capacities was 0.85. This may be because the inclusion of lightly reinforced specimens in the tests resulted in some large deflections at failure (see Table 1) with rupture of the steel reinforcement, which limits the applicability of the rigid-plastic approach. The method is most useful when the maximum deflection recorded at failure does not exceed half wall's thickness, or more precisely, 0.42× the wall's thickness based on the expression of Wang et al. [42] (Eq. 20).

$$w_0 = \sqrt{\frac{0.1 f_y}{E_s} \cdot \frac{3L^2}{8}} \tag{20}$$

Better predictions could be obtained by considering two hidden capacities: (1) strain hardening of the reinforcement, and (2) tensile membrane action (TMA) due to large deflections. While the former only requires updating the yield condition (refer to Figure 6b), i.e. substituting the yield strength with the ultimate strength of the reinforcement, the latter approach would require a more advanced analysis that takes into account the effect of changes in geometry. For plates with a central deflection, $w$, greater than $w_0$, Wang et al. [42] proposed a model that explicitly considers the TMA by including in the equilibrium equation the vertical component that develops in the reinforcement. The use of TMA is usually neglected in common cases on the basis of lower bound theory and only considered when design is performed against accidental loads, e.g. structures subjected to fire [43]. Consequently, the underprediction of the experimentally measured capacities was addressed by considering the effects of reinforcement strain hardening. Improved predictions taking this factor into account are presented in Table 3.

**Table 3.** Experimental ultimate transverse loads and yield line predictions obtained with and without consideration of the effects of strain hardening

| Wall | Ultimate transverse load (kN/m$^2$) | | | | |
|---|---|---|---|---|---|
| | Experimental ($S_{exp}$) | Predicted ($S_u$) | | | |
| | | No strain hardening | Accuracy $S_u/S_{exp}$ | Strain hardening | Accuracy $S_u/S_{exp}$ |
| A | 21.2 | 18.37 | 0.87 | 20.23 | 0.95 |
| B | 21.8 | 18.37 | 0.84 | 20.23 | 0.93 |
| C | 15.3 | 13.24 | 0.87 | 14.59 | 0.95 |
| D | 17.0 | 13.24 | 0.78 | 14.59 | 0.86 |
| E | 11.0 | 10.10 | 0.92 | 10.86 | 0.99 |
| F | 12.3 | 10.10 | 0.82 | 10.86 | 0.88 |
| Average | | | 0.85 | | 0.93 |
| CoV (%) | | | 5.50 | | 5.20 |

### 3.5. Case II: Dominant in-plane vertical loads

In cases where the walls are part of a structure with regular floor plans that carry mainly axial loads, the main contribution to the ultimate capacity comes from the concrete in compression (compressive membrane action - CMA) and the reinforcement. There are few publications in the literature describing experimental studies that could shed light on the real contribution of reinforcing materials to the ultimate capacity when applied in a single layer. Moreover, design codes usually neglect the contribution of reinforcement for lightly-reinforced elements where the main purpose of reinforcement is to control cracking due to creep, shrinkage and erection/transportation loads. Given the limited understanding of these issues and the lack of relevant experimental data, the contribution from the reinforcement in such cases was neglected.

Because of the small displacements of the element at failure, a compressive membrane effect develops that depends solely on the concrete's plasticity. This effect can be attributed to the in-plane restraints provided by the vertical edge supports. The membrane moment can be determined by considering a horizontally restrained unreinforced one-way strip that is transversally loaded by two symmetrical line loads as proposed by Nielsen [41]. By considering the maximum deflection exhibited by the experimentally studied walls before undergoing plastic collapse ($\delta_{peak}$) as presented in Table 1, the membrane moment can be expressed as:

$$m_c = \frac{1}{4} f_c \left(t - \delta_{peak}\right)^2 \tag{21}$$

The derivation of this equation has been presented elsewhere [41] and, for the sake of brevity, will not be reproduced here. The compressive strength of concrete in Eq. (21) is modified by the effectiveness factors calculated according to Eqs. (2) and (10) for unstrengthened walls and walls strengthened with FRP, respectively.

As in the case of transversally loaded walls, the work done by the external loads must be balanced by the virtual internal work. As suggested by Nielsen [41], the internal work is determined by replacing the bending moment $m_b$ in the usual yield line solution with the membrane moment $m_c$. The determination of exact solutions for the inclined yield lines are in this case cumbersome; in this work, such solutions were obtained by considering experimental evidence in the first case, and subsequently validated using advanced computational simulations (Fig. 10).

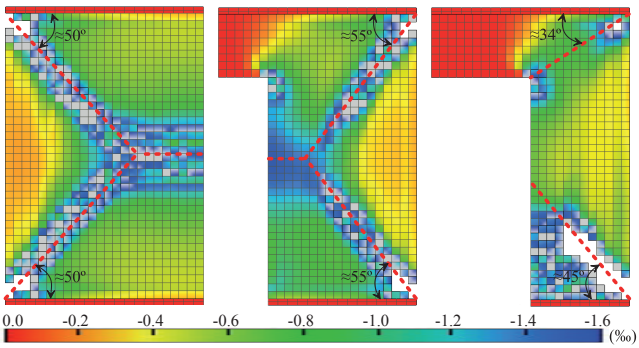


**Figure 10.** Predicting the inclination of the yield lines based on the principal plastic strains in the concrete

Results obtained based on a three-dimensional nonlinear finite element model [44] implemented using ATENA-Science [45] are illustrated in Figure 10. The figure shows the calculated principal plastic strains in concrete on the compression side at failure to support the validity of the plastic mechanism adopted in Figure 5b and the close agreement between predictions based on this mechanism and the experimental observations. No further results based on the computer simulations will be presented in this paper because they have already been described in a separate publication [44]. At ultimate, the magnitude of the principal plastic strains in concrete were capped at a predefined level during post-processing to highlight the possible plastic mechanism. For ease of visualisation, finite elements with strains above this threshold value (50% of the ultimate compressive strain in the concrete, where $e_{cu}$=3.2‰) are not displayed. A median line is then drawn through the crushing band, indicating the yield line's inclination. The angles predicted were in close agreement with the experimental observations. The external and internal work for the different kinds of axially loaded walls can be computed using the following expressions:

**External work**

$$W_E = \begin{cases} \frac{t}{3} n_{uy} L(\theta_1 + \theta_2) & \rightarrow \text{solid wall} \\ \frac{t}{3} n_{uy} \frac{L - L_0}{2}(\theta_1 + \theta_2) & \rightarrow \text{small opening} \\ \frac{t}{3} n_{uy} L_x(\theta_1 + \theta_2) & \rightarrow \text{large opening} \end{cases} \tag{22}$$

**Internal work**

$$W_I = \begin{cases} m_c L(\theta_1 + \theta_2) + 2m_c H\varphi & \rightarrow \text{solid wall} \\ m_c \frac{L - L_0}{2}(\theta_1 + \theta_2) + m_c H\varphi & \rightarrow \text{small opening} \\ m_c L_x(\theta_1 + \theta_2) + m_c H\varphi & \rightarrow \text{large opening} \end{cases} \tag{23}$$

where for the solid wall $\theta_1 = \theta_2 = 2\delta / H$ and $\varphi = \delta / L_x$; for the wall with small opening $\theta_1 = \theta_2 = 2\delta / H$ and $\varphi = \delta / L_x$; and for the wall with large opening $\theta_1 = \delta / H_y$; $\theta_2 = \delta / (H - H_0)$ and $\varphi = \delta / L_x$.

Equating the internal and external work done gives the following expressions for the uniform in-plane compressive force per unit length:

- For the solid wall

$$n_{uy} = \frac{3m_c H\left(\frac{2L}{H} + \frac{H}{L_x}\right)}{2tL} \tag{24}$$

- For the wall with small opening

$$n_{uy} = \frac{3m_c H\left[\frac{2(L - L_0)}{H} + \frac{H}{L_x}\right]}{2t(L - L_0)} \tag{25}$$

- For the wall with large opening

$$n_{uy} = \frac{3m_c\left(\frac{H}{L_x}+\frac{L_x}{H_y}+\frac{L_x}{H-H_0}\right)}{tL_x\left[\frac{H_y+H-H_0}{H_y\left(H-H_0\right)}\right]} \tag{27}$$

The predicted ultimate axial load is calculated according to Eq. (27):

$$N_u = n_{uy}\left(L-L_0\right) \tag{27}$$

The test results are summarized in Table 4, together with the failure loads predicted by the yield-line method. Although the average ratio of experimental to predicted loads was conservative in most cases, the ratios for the FRP-strengthened walls were somewhat un-conservative. It should be noted that the predicted values were evaluated using a safety factor of 1; in practical applications, the safety factor should be optimized carefully.

**Table 4.** Comparison of the measured ultimate axial loads and yield line predictions

| Wall | Ultimate axial load (kN) | | Accuracy |
|---|---|---|---|
| | Experimental ($N_{exp}$) | Predicted ($N_u$) | $N_{exp}/N_u$ |
| I-C | 2363 | 1872 | 1.26 |
| I-S | 1500 | 1325 | 1.13 |
| I-L | 1180 | 1046 | 1.13 |
| II-S | 2241 | 1942 | 1.15 |
| II-L | 1497 | 1596 | 0.95 |
| III-S1 | 2178 | 2034 | 1.07 |
| III-S2 | 2009 | 2520 | 0.80 |
| III-L1 | 1334 | 1230 | 1.08 |
| III-L2 | 1482 | 1504 | 0.99 |
| Average | | | 1.06 |
| CoV (%) | | | 12.7 |

## 4. Concluding Remarks

Design codes treat walls reinforced with minimal amounts of reinforcing material as being unreinforced and model their ultimate capacity using empirical expressions that assume uniaxial behaviour. As demonstrated by a literature review conducted by the authors of this work, this approach yields very conservative results. Studies on the failure mechanisms of such elements have shown that their lateral restraints transform the failure problem from a one-dimensional problem into a three-dimensional problem (plate mechanism). Additionally, existing design codes offer limited guidance in situations where new openings need to be cut into an existing wall, or where there is a need to apply strengthening using externally bonded reinforcement (i.e. FRP). There is a need for more rigorous treatment of these cases because their inadequate description in current design codes often leads to uncertainties in the design/assessment process.

The paper uses the limit analysis approach to evaluate the failure loads of in- and out-of-plane loaded RC walls with and without openings. The predictions obtained using this approach agree well

with experimental data for walls subject to dominant out-of-plane bending. Reasonably good agreement was also achieved for walls under gravitational loads, although some of the predictions in these cases were on the un-safe side because the compressive struts are the main strength component in walls under axial loads (a more complex phenomenon). In order to account for the effects of transverse strains and material brittleness, the calculated strength must be modified using an appropriate effectiveness factor.

The problem of estimating the elements' strength becomes more complicated if they are strengthened with FRP because the reinforcing fibres exhibit linear-elastic behaviour with no plasticity. As such, their behaviour cannot be described using the plasticity theory. We therefore propose an alternative approach whereby the yield criteria of the concrete are updated based on the confined compressive strength due to FRP-confinement. However, because slender elements and load imperfections are usually encountered in practice, the confinement is generally non-uniform, which limits the effectiveness of the FRP. An effectiveness factor intended to account for these additional effects was computed based on the experimental observations. However, because this factor was determined using experimental data for only six strengthened walls, further work will be required to validate it. In addition, studies could be conducted on walls strengthened with bi- or multi-axial fibres to increase the reliability of the proposed procedure and make it practically useful in assessments.

## Notation

| | | | |
|---|---|---|---|
| $A_{sx}$, $A_{sy}$ | areas of the reinforcement per unit width in the x- and y-directions, respectively | $m_c$ | membrane moment |
| $E_{frp}$ | elastic modulus of FRP | $m_x$, $m_y$ | moment capacities per unit width in the x- and y-directions, respectively |
| $E_s$ | elastic modulus of reinforcement | $n_{laryers}$ | number of FRP layers |
| $H$ | height of the wall | $n_{ux}$, $n_{uy}$ | uniform in-plane compressive force per unit length applied in the x- and y-direction, respectively |
| $H_0$ | height of the cut-out opening | $s$ | reinforcement spacing |
| $L$ | length of the wall | $t$ | thickness of the wall |
| $L_0$ | length of the cut-out opening | $t_{frp}$ | thickness of a FRP layer |
| $L_x$, $L_y$ | projection of the yield lines onto its axis of rotation in both orthogonal directions | $w$, $w_0$ | experimental/theoretical displacement at the formation of yield-line pattern |
| $N_{exp}$, $N_u$ | experimental/predicted ultimate load for walls under axial loading | $\alpha$ | yield line's inclination relative to the reinforcement |
| $R$ | corner radius | $\delta$ | virtual displacement |
| $S_{exp}$, $S_u$ | experimental/predicted ultimate load for walls under transverse loading | $\delta_{peak}$ | out-of-plane displacements at peak load |
| $W_E$ | external work | $\varepsilon_{avg}$ | average strain on FRP between measurements on the tension and compression side |
| $W_I$ | internal work | $\varepsilon_{cu}$ | ultimate compressive strain in concrete |
| $b$ | width of the virtual cross-section | $\varepsilon_{frp}$ | elongation at break of FRP |
| $d$ | effective depth | $\varepsilon_{u,frp\text{-}max}$, $\varepsilon_{u,frp\text{-}min}$ | maximum/minimum strain registered on FRP on a specific location |
| $f_c$ | compressive strength of unconfined concrete | $\eta_{fc}$ | factor accounting for brittleness of concrete |
| $f_{cc}$ | compressive strength of confined concrete | $\eta_\varepsilon$ | factor accounting for influence of transverse cracking |
| $f_{c0}$ | default value of compressive strength | $\eta_{\varepsilon,frp}$ | factor accounting for non-uniform confinement |
| $f_{ct}$ | tensile strength of concrete | $\nu_1$, $\nu_2$ | effectiveness factor |
| $f_{frp}$ | tensile strength of FRP | $\theta$, $\varphi$ | angle of disk rotation |

| | | | |
|---|---|---|---|
| $f_l$ | confining pressure | $\rho_h / \rho_v$ | horizontal/vertical reinforcement ratio |
| $f_y$ | yield strength of reinforcement | $\rho_{sc}$ | cross-sectional area ratio of longitudinal steel |
| $f_u$ | tensile strength of reinforcement | $\sigma_c / \varepsilon_c$ | stress/strain in concrete |
| $h$ | height of the virtual cross-section | $\sigma_s / \varepsilon_s$ | stress/strain in steel reinforcement |
| $k_1$ | confinement effectiveness coefficient | $\sigma_f / \varepsilon_f$ | stress/strain in FRP |


## Acknowledgements

The authors would like to acknowledge the Research Council of Norway (RFF), Development Fund of the Swedish Construction Industry (SBUF) and Skanska for financing the work in this project. The authors wish to thank Tech. Lic. Niklas Bagge from Luleå University of Technology for helpful discussions and suggestions. The authors would also like to thank the Swedish branch of Nordea bank for financial support of Cosmin Popescu during an external stay at the Technical University of Denmark.


## References


[1] Ali A, Wight J. RC Structural Walls with Staggered Door Openings. J Struct Eng 1991; 117(5):1514 31.

[2] Taylor CP. Design of slender reinforced concrete walls with openings. ACI Struct J 1998; 95(4):420-33.

[3] Wang J, Sakashita M, Kono S, Tanaka H. Shear behaviour of reinforced concrete structural walls with eccentric openings under cyclic loading: experimental study. Struct Des Tall Spec 2012; 21(9):669-81.

[4] Todut C, Dan D, Stoian V. Theoretical and experimental study on precast reinforced concrete wall panels subjected to shear force. Eng Struct 2014; 80:323-38.

[5] Mosoarca M. Failure analysis of RC shear walls with staggered openings under seismic loads. Eng Fail Anal 2014; 41:48-64.

[6] Mosallam AS, Nasr A. Structural performance of RC shear walls with post-construction openings strengthened with FRP composite laminates. Compos Part B-Eng 2016; *In Press*.

[7] Popescu C, Sas G, Blanksvärd T, Täljsten B. Concrete walls weakened by openings as compression members: A review. Eng Struct 2015; 89:172-90.

[8] Pillai SU, Parthasarathy CV. Ultimate strength and design of concrete walls. Build Environ 1977; 12(1):25-9.

[9] Saheb M, Desayi P. Ultimate strength of RC wall panels in one-way in-plane action. J Struct Eng 1989; 115(10):2617-30.

[10] Fragomeni S. Design of Normal and High Strength Reinforced Concrete Walls [PhD Thesis]. Melbourne, Australia: Univ. of Melbourne; 1995.

[11] Doh JH. Experimental and Theoretical Studies of Normal and High Strength Concrete Wall Panels [PhD Thesis]. Gold Coast, Australia: Griffith Univ.; 2002.

[12] Ganesan N, Indira PV, Santhakumar A. Prediction of ultimate strength of reinforced geopolymer concrete wall panels in one-way action. Constr Build Mater 2013; 48:91-7.

[13] Robinson G, Palmeri A, Austin S. Design methodologies for one way spanning eccentrically loaded

minimally or centrally reinforced pre-cast RC panels. Eng Struct 2013; 56:1945-56.
[14] Swartz SE, Rosebraugh VH, Rogacki SA. A method for determining the buckling strength of concrete panels. Exp Mech 1974; 14(4):138-44.
[15] Sanjayan JG. Load capacity of slender high-strength concrete walls with side supports. ACI Struct J 1999; 96(4):571-6.
[16] Saheb M, Desayi P. Ultimate Strength of R.C. Wall Panels in Two-Way In-Plane Action. J Struct Eng 1990; 116(5):1384-402.
[17] Saheb M, Desayi P. Ultimate strength of RC wall panels with openings. J Struct Eng 1990; 116(6):1565-78.
[18] Doh JH, Fragomeni S. Ultimate load formula for reinforced concrete wall panels with openings. Adv Struct Eng 2006; 9(1):103-15.
[19] Lee D-J. Experimental and theoretical study of normal and high strength concrete wall panels with openings [PhD Thesis]. Gold Coast, Australia: Griffith Univ.; 2008.
[20] Mohammed B, Ean LW, Malek MA. One way RC wall panels with openings strengthened with CFRP. Constr Build Mater 2013; 40:575-83.
[21] Doh J, Fragomeni S. Evaluation of experimental work on concrete walls in one-way and two-way action. Austr J Struct Eng 2005; 6(1):37–52.
[22] Aghayere AO, MacGregor JG. Analysis of concrete plates under combined in-plane and transverse loads. ACI Struct J 1990; 87(5):539-47.
[23] Hegger J, Dressen T, Will N. Load-bearing capacity of plain concrete walls. Mag Concrete Res 2009; 61(3):173-82.
[24] Guan H, Cooper C, Lee D-J. Ultimate strength analysis of normal and high strength concrete wall panels with varying opening configurations. Eng Struct 2010; 32(5):1341-55.
[25] EN1992-1-1. Design of concrete structures – Part 1–1: General rules and rules for buildings. Brussels, Belgium: CEN (European Committee for Standardization); 2004.
[26] ACI 318. Building code requirements for structural concrete and commentary Farmington Hills, MI: American Concrete Institute (ACI); 2011.
[27] AS3600. Concrete structures. Sydney, Australia: Standards Australia; 2009.
[28] DIN 1045. Reinforced concrete structures: Design and construction. Berlin: DIN (Deutsches Institut für Normung); 1988.
[29] Ganesan N, Indira PV, Rajendra Prasad S. Strength and Behavior of SFRSCC and SFRC Wall Panels under One-Way In-Plane Action. In: Parra-Montesinos G, Reinhardt H, Naaman AE, editors. High Performance Fiber Reinforced Cement Composites 6: Springer Netherlands; 2012. p. 279-86.
[30] Sadiki M, Reenberg AM. Tværbelastede vægelementer [Master thesis]. Lyngby, Denmark: Technical Univ. of Denmark; 2013.
[31] Popescu C, Sas G, Sabau C, Blanksvärd T. Effect of cut-out openings on the axial strength of concrete walls. J Struct Eng 2016; 142(11), 04016100.
[32] Popescu C, Sas G, Blanksvärd T, Täljsten B. Concrete walls with cut-out openings strengthened by FRP-confinement. J Compos Constr 2016; *E-pub ahead of print*.
[33] SS-EN ISO 898-1. Mechanical properties of fasteners made of carbon steel and alloy steel - Part 1:

Bolts, screws and studs with specified property classes - Coarse thread and fine pitch thread (ISO 898-1:2013). Stockholm, Sweden: Swedish Standards Institute (SIS); 2013.

[34] Lam L, Teng JG. Design-Oriented Stress-Strain Model for FRP-Confined Concrete in Rectangular Columns. J Reinf Plast Comp 2003; 22(13):1149-86.

[35] Bailey CG, Toh WS. Small-scale concrete slab tests at ambient and elevated temperatures. Eng Struct 2007; 29(10):2775-91.

[36] fib Model Code 2010. fib Model Code 2010 for Concrete Structures. Lausanne, Switzerland: Fédération Internationale du Béton; 2013.

[37] Florut S-C, Sas G, Popescu C, Stoian V. Tests on reinforced concrete slabs with cut-out openings strengthened with fibre-reinforced polymers. Compos Part B-Eng 2014; 66C:484–93.

[38] Ingerslev A. The strength of rectangular slabs. J Inst Struct Eng 1923; 1(1):3–14.

[39] Johansen KW. Yield line theory. London: Cement and Concrete Association; 1962.

[40] Hansen LZ. Unreinforced Masonry Walls Transversely and Axially Loaded [PhD Thesis]. Lyngby, Denmark: Technical Univ. of Denmark; 2004.

[41] Nielsen MP. Limit analysis and concrete plasticity, Second Edition. Boca Raton, FL: CRC Press; 1999.

[42] Wang Y, Dong Y-L, Yuan G-L, Zou C-Y. New Failure Criterion to Determine the Load Carrying Capacity of Two-Way Reinforced Concrete Slabs. Adv Struct Eng 2015; 18(2):221-36.

[43] Bailey CG, Toh WS, Chan BM. Simplified and Advanced Analysis of Membrane Action of Concrete Slabs. ACI Struct J 2008; 105(1):30-40.

[44] Popescu C, Sas G. The Development of an Experimental Program through Design of Experiments and FEM Analysis: A Preliminary Study. Nord Concrete Res 2014; 51:14.

[45] Cervenka Consulting Ltd. ATENA - Advanced Tool for Engineering Nonlinear Analysis. Prague, Czech Republic 2015.

## About the author

Cosmin Popescu (born October 21, 1987) grew up in Rovinari, a small coal mining town in Gorj County, Oltenia, Romania. He is married to Adriana and together they have a son, Albert, now 5 months old. Cosmin moved to Timisoara in 2006 for university studies in civil/structural engineering at Politehnica University of Timisoara. He obtained a Bachelor and Master diploma (Dipl. ing) in 2010 and 2012, respectively. In 2010, after completing his bachelor studies, he joined an engineering firm (Arhitim s.r.l.) where he carried out structural design, analysis, and detailing for various industrial, as well as residential, facilities. In 2013, he enrolled in a Ph.D. programme in structural engineering at Luleå University of Technology (LTU). The Ph.D. programme was jointly managed under a cooperative agreement between the Northern Research Institute – Norut Narvik and LTU. While at LTU, Cosmin was involved in teaching activities in Building Materials and Concrete Structures, as well as supervising Master degree projects in structural engineering. Cosmin's research covers topics related to structural engineering with a specialisation in assessment and strengthening of concrete structures.

Department of Civil, Environmental and Natural Resources Engineering
Division of Structural and Fire Engineering

---

ISSN 1402-1544
ISBN 978-91-7583-794-9 (print)
ISBN 978-91-7583-795-6 (pdf)

Luleå University of Technology 2017

LULEÅ
UNIVERSITY
OF TECHNOLOGY